Nils Ryden

Surface Wave Testing of Pavements

2004

Surface Wave Testing of Pavements

Nils Rydèn

Department of Engineering Geology
Lund Institute of Technology, Lund University

In cooperation with
Kansas Geological Survey
University of Kansas

Doctoral Thesis
2004

ISRN LUTVDG/TVTG-1015-SE
ISBN 91-973406-4-2

Surface Wave Testing of Pavements

Nils Rydén

Doctoral Thesis

Department of Engineering Geology
Lund Institute of Technology
Lund University

in cooperation with
Kansas Geological Survey
University of Kansas

Lund 2004

Printed by KFS AB, Lund 2004

Papers

Paper I. Ryden, N., Park, C. B., Ulriksen, P. and Miller, R. D., 2004, Multimodal approach to seismic pavement testing, *Journal of Geotechnical and Geoenvironmental Engineering*, ASCE, Vol. 130, No. 6, pp 636-645.

Paper II. Ryden, N., Park, C.B., Ulriksen, P., and Miller R.D., 2003, Lamb wave analysis for non-destructive testing of concrete plate structures, Proceedings of the Symposium on the Application of Geophysics to Engineering and Environmental Problems (SAGEEP 2003), San Antonio, TX, April 6-10, INF03.

Paper III. Ryden, N., and Park, C.B., 2004, Surface waves in inversely dispersive media, Accepted for publication in: *Near Surface Geophysics*.

Paper IV. Ryden, N., and Lowe, M., 2004, Guided wave propagation in three-layer pavement structures, Submitted for publication to: *Journal of the Acoustical Society of America*.

Paper V. Ryden, N., and Park, C.B., 2004, Inversion of surface waves using phase velocity spectra, Submitted for publication to: *Geophysics*.

Related papers

Ekdahl, U., Bengtsson, P.E., and Ryden, N., 2004, A new framework for analytical pavement design based on systematic control during construction work, Proceedings of the 14th Nordic Geotechnical Meeting (NGM 2004), Ystad, Sweden, May 19-21.

Ryden, N., Park, C.B., and Ulriksen, P., 2004, A framework for inversion of wavefield spectra in seismic non-destructive testing of pavements, Accepted for publication, 2nd International Conference on Site Characterization (ISC-2), Porto, Portugal, Sep 19-22.

Ivanov, J., Miller, R.D., Park C.B., Ryden, N., 2003, Seismic search for underground anomalies, Expanded Abstract, Society of Exploration Geophysicists, NSG3.2.

Ryden, N., Park, C.B., Ulriksen, P., and Miller R.D., 2002, Branching of dispersion curve in surface wave testing of pavements, Proceedings of the Symposium on the Application of Geophysics to Engineering and Environmental Problems (SAGEEP 2002), Las Vegas, NV, February 10-14, 12SEI7.

Ryden, N., Ulriksen, P., Park, C.B., and Miller R.D., 2002, Portable seismic acquisition system (PSAS) for pavement MASW, Proceedings of the Symposium on the Application of Geophysics to Engineering and Environmental Problems (SAGEEP 2002), Las Vegas, NV, February 10-14, 13IDA7.

Park, C.B., Ryden, N., Miller, R.D., and Ulriksen, P., 2002, Time break correction in multichannel simulation with one receiver (MSOR), Proceedings of the Symposium on the Application of Geophysics to Engineering and Environmental Problems (SAGEEP 2002), Las Vegas, NV, February 10-14, 12SEI3.

Ryden, N.R., Jeppsson, J., and Park, C.B., 2002, Destructive and non-destructive assessment of concrete structures, Proceedings of the XVIII Symposium on Nordic Concrete Research, Helsingor, Denmark, June 12-14, pp 153-156.

Park, C.B., Ryden, N., Westerhoff, R., and Miller, R.D., 2002, Lamb waves observed during MASW surveys, Expanded Abstract, Society of Exploration Geophysicists, Salt Lake City, Utah, 2002.

Ryden, N., Park, C.B., Ulriksen, P., Ekdahl, U., and Miller, R.D., 2002, Multichannel analysis of seismic waves for layer moduli evaluation of pavements, Proceedings of the BCRA 2002, Lissabon, Portugal.

Ryden, N., Ulriksen, P., Park, C.B., Miller, R.D., Xia, J., and Ivanov, J., 2001, High frequency MASW for non-destructive testing of pavements-accelerometer approach, Proceedings of the Symposium on the Application of Geophysics to Engineering and Environmental Problems (SAGEEP 2001), Denver, Colorado, RBA-5.

Park, C.B., Ivanov, J., Miller, R.D., Xia, J., Ryden, N., 2001, Seismic investigation of pavements by MASW method-geophone approach, Proceedings of the Symposium on the Application of Geophysics to Engineering and Environmental Problems (SAGEEP 2001), Denver, Colorado, RBA-6.

Park, C.B., Miller, R.D., Xia, J., Ivanov, J., Ryden, N., 2001, Multichannel analysis of surface waves (MASW) for pavement: Feasibility test, Proceedings of the 5th SEGJ International Symposium 2001, Tokyo, Japan.

Acknowledgements

Ulf Ekdahl initiated this project and I am very thankful for all the support and help he has given me. I would also like to give my most sincere appreciation to Dr. Choon Park at the Kansas Geological Survey and Associate Prof. Peter Ulriksen for all the assistance, guidance and excellent supervising they have given me.

This project is part of the Swedish Infrastructure Program "Road-Bridge-Tunnel" and is financed by the Swedish Association for Innovation Systems (VINNOVA), Peab, Lund University, the Swedish National Road Administration (Vägverket), and the Development Fund of the Swedish Construction Industry (SBUF), and they are all acknowledged for the financing.

Special thanks to Peter Jonsson for all the time he spent helping me. Sincere thanks also to my other supervisors during the project; Per-Evert Bengtsson, Dr. Mats Svensson, Prof. Leif Bjelm, and Dr. Bo S Malmborg. I would also like to thank all other colleagues at the Department in Lund, especially Martin Holmén for assistance with Labview, Roger Wisén and Per Lindh for computer assistance. The rest of the group at Foundation Technology, and all others who have helped me at Peab. Bengt Bengtsson for his expertise and fine work on the trigger device.

I would like to express a sincere appreciation for all the hospitality and help I have received during my visits to Kansas Geological Survey (KGS), Section Chief Richard Miller, Prof. Daniel Merriam, Dr. Jianghai Xia, Dr. Julian Ivanov, Mary Brohammer and of course to the only one who can repair an electronic melt-down faster than I can make it happen, Brett Bennett.

I would like to thank Dr. Michael Lowe, Prof. Peter Cawley, and all the rest of the non-destructive testing group at the Department of Mechanical Engineering, Imperial College, for all the excellent help, inspiration, and hospitality they have given me during my visits to London.

I am also very grateful to: Dr. Anders Bodare for fruitful discussions and help with the transfer matrix method. Prof. Nenad Gucunski for his help and hospitality during my visit to Rutgers University. Prof. Soheil Nazarian and Dr. Deren Yuan at the University of Texas at El Paso for the hospitality they showed me during my visit to El Paso and for the help and guidance along the way. Wayne Marsey at Hughes Technical Center in Atlantic City for inviting me to the National Airport Pavement Test Facility.

Dr. Jonas Brunskog, Dr. Joakim Jeppsson, Lennart Dahl, Dr. Adam O'Neill, and Dr. Claudio Strobbia, Dr. Per Ullidtz, Prof. Richard Vidale, Dr. Marwan Aouad, Prof. Sebastiano Foti, and Prof. Giovanni Cascante, have all been helping me with various parts of this work and their help is greatly appreciated.

And last but foremost I thank my family and friends.

Notation

Notations refer to chapters 1 to 3.

A	Amplitude
A0	Anti-symmetric Lamb wave fundamental mode
D, D	Layer interface matrix (section 3.1.2), distance (section 3.3.2)
d	Thickness
E	Young's modulus
E_{max}	Maximum (or small strain) Young's modulus
E^*	Complex dynamic modulus
E_1	Storage modulus (elastic component)
E_2	Loss modulus (viscous component)
e	Void ratio
f	Frequency, Hz
G	Shear modulus
G_{max}	Maximum (or small strain) shear modulus
G_0	Maximum (or small strain) shear modulus
i	$\sqrt{-1}$
K	Constant (Eq. 54, section 3.2.2)
k, k	Wave number
n	Ratio (V_S/V_P) (Eq. 45, section 3.1.3), constant (Eq. 54, section 3.2.2)
P	Period
S	System matrix
s	Ratio between V_S and V_R (Eq. 45, section 3.1.3)
S0	Symmetric Lamb wave fundamental mode
t	Time
u, u	Displacement
V	Wave propagation velocity (speed)
V_P	Compressional wave velocity
$V_{P\,plate}$	Quasi-longitudinal wave velocity in plates
V_{ph}	Phase velocity
V_R	Rayleigh wave velocity
V_S	Shear wave velocity
x, x	Position
α	Compressional wave velocity (section 3.1.1-3.1.3), constant (section 3.1.4)
α_{plate}	Quasi-longitudinal wave velocity in plates
α_T	Shift factor
β	Shear wave velocity (section 3.1.1-3.1.3), constant (section 3.1.4)
$\Delta\phi$	Phase difference
Δx	Distance increment
ε	Strain
ν	Poisson's ratio

θ	Phase angle of complex E-modulus
λ	Wavelength, Lamé constant (section 3.1.1)
μ	Lamé constant
ρ	Density
ϕ	Helmholtz scalar potential (section 3.1.2), Phase angle (section 3.3.1-3.3.3)
σ	Stress
σ_m	Mean stress
σ_0	Mean stress
ω	Frequency, rad/s
ψ	Helmholtz vector potential

Abbreviations

CSW	Continuous Surface Wave
FFT	Fast Fourier Transform
FWD	Falling Weight Deflectometer
MASW	Multichannel Analysis of Surface Waves
MSOR	Multichannel Simulation with One Receiver
NDT	Non Destructive Testing
PI	Plasticity Index
PSAS	Portable Seismic Acquisition System
SASW	Spectral Analysis of Surface Waves
TRB	Transportation Research Board

Abstract

A novel approach for surface wave testing of pavements is presented. It is a non-destructive testing (NDT) technique that can be used to obtain the thickness and stiffness properties of the different layers in a pavement. With this method structural properties of the pavement can be mapped as a function of time and space, providing a valuable tool in pavement design and management. The technical development is based on a theoretical study of wave propagation in pavement structures and on the reported difficulties experienced with existing methods. A computer based data acquisition system and program for evaluation of layer properties have been developed.

From the theoretical study on wave propagation in pavement structures, it is concluded that the nature of wave propagation has been oversimplified in previous studies. Results show that the measurable wave field at the surface of a pavement structure is dominated by leaky quasi-Lamb waves in the first and second layer. The fundamental anti-symmetric mode of vibration is the dominating mode generated in the stiff top layer. This mode drives the complete system and continuity across the boundaries generates higher order modes in the embedded second layer. The interaction of leaky Lamb waves in the first two layers results in large variations in the excitability and the attenuation, so that only the waves corresponding to certain portions of the dispersion curves are measurable at the pavement surface. These portions of dispersion curves (mode branches) are critical for a refined NDT technique for pavements.

To resolve the different mode branches it is necessary to record the complete wave field on the pavement surface. In this study the multichannel data acquisition method is replaced by multichannel simulation with one receiver (MSOR). This method uses only one accelerometer-receiver and a light hammer-source, to generate a synthetic receiver array. The recorded data is automatically and objectively transformed to a phase velocity spectrum through the multichannel analysis of surface waves (MASW) processing scheme.

The top layer thickness, and stiffness properties are obtained automatically in the field by a Lamb wave analysis of the measured phase velocity spectrum. The inversion of deeper embedded layers is based on the full phase velocity spectrum. The main benefit from the developed inversion procedure is that the raw field data can be automatically processed and inverted without any subjective user input to identify discrete dispersion curves. The viscoelastic properties of the asphalt layer are included to produce the asphalt stiffness as a function of frequency, a mastercurve.

In this study the presented NDT technique is applied to pavements and concrete structures. However, generic findings here may also be useful in other fields. Possible applications are; ultrasonic testing of coated materials and sandwich structures, surface wave soil site characterization, and medical applications.

Table of contents

1 Introduction

1.1 Background

Surface waves are stress waves traveling along the free surface of a material. Most of the energy in these waves is confined to the close vicinity of the surface, similar to waves propagating on the surface of water. The velocity of wave propagation is dependent on the elastic properties of the affected medium. This principle is used in this study, to estimate the stiffness and thickness of the different layers in a pavement construction. With an efficient NDT technique structural properties can be mapped as a function of time and space providing a valuable tool in pavement design and management.

Today the demand for accurate and efficient NDT techniques is greater than ever. Pavements are an important part of the worlds transportation infrastructure and consequently play a significant role in its economy. The annual investment of funds to construct and maintain a viable road system is enormous. The optimum use of these funds is a challenge, which demands the best technology available. The state of the art of pavement design has been very empirical, with trial and error as basis for the decisions. This process does not lend itself to optimization of the financial resources. However, today pavement design is progressively moving from empirical to analytical methods. Analytical methods are the standard engineering procedure for design and analysis of most civil engineering constructions. Theoretical stresses and displacements are calculated from material properties and analyzed in order to predict the final performance of a construction. To successfully implement any analytical pavement design procedure it is essential to develop tools that can measure material properties at each depth in the field, *in-situ*. With such tools pavement material properties can be verified in the field and compared to the required material properties. The most important material properties are those related to the stiffness of the materials, for example Young's modulus (*E*-modulus). A higher *E*-modulus value results in less deformation (strain) for a given load (stress). Consequently there is a need to develop improved NDT techniques for pavement applications. A successful and efficient NDT device for pavements can save money spent on the pavement design and maintenance.

The most widespread NDT method for pavements is the Falling Weight Deflectometer (FWD) (Huang, 1993). The FWD test is based on deflection measurements at the surface resulting from a given dynamic load. This method provides a good estimate of the actual non-linear response of the complete pavement construction at relatively large strain levels (Ullidtz, 1998). Unfortunately, the *E*-modulus is a complicated function of both stress and strain level under this load situation, and it is therefore difficult to obtain fundamental material properties from this type of test. Wave propagation methods affect the materials in their linear elastic region and provide material properties that are not affected by non-linear properties. For example, the *E*-modulus of different materials in different pavement constructions can be compared under the exact same loading condition by using wave propagation based methods. The main result from both

deflection and wave propagation methods is a stiffness modulus as a function of depth profile, see Figure 1.

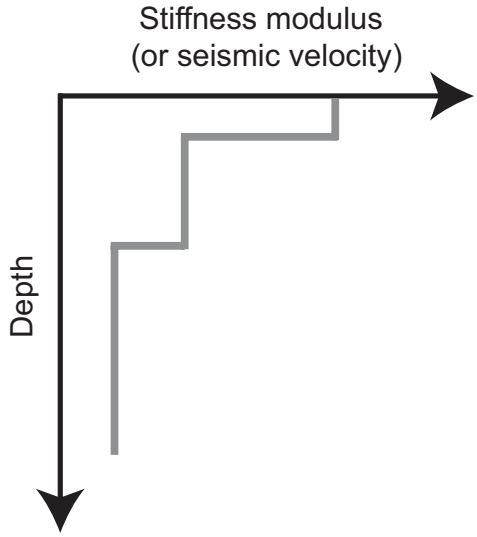

Figure 1. The final result from surface wave or deflection based testing of pavements is a stiffness modulus profile of the test section.

The fundamental principle of using sound "to see" has been successfully utilized in many fields, ranging from medical applications to global seismology. For example, the crust of the earth has been characterized by analyzing surface waves generated from earthquakes. However, surface wave testing of pavements has proved to be a challenging task. The fundamental difficulties encountered can be traced back to the fundamental nature of wave propagation in layered media where the stiffness decreases with depth (such as a pavement system). Sezawa (1938) was first to report on the anomalous behavior of surface waves in this type of layer setting, and his speculative conclusions revealed some of the difficulties to come. From his office at the Earthquake Research Institute in Tokyo, Sezawa (1938) wrote about the possible existence of surface waves in this type of medium:

"…the idea of the probable existence of such waves occurred to me about ten years ago when I was studying the dispersion of Rayleigh-waves, having even gone as far as to present a few results of the investigation at one of the meetings of the Institute, yet owing to there being certain uncertainties about my numerical calculations, I refrained from publishing any part of it."

Professor Gerald Picket at the University of Wisconsin, USA, studied the work finally published by Sezawa and proposed to use surface waves for NDT of pavements (Picket, 1945). In the view of the author, the work presented by his student Richard Vidale, still holds as the finest publication on surface wave testing of pavements (Vidale, 1964). The fundamental difficulties that can be encountered in surface wave testing of pavements were identified by Jones (1962) and Vidale (1964). However, without the availability of

modern computers it was impossible to reveal the complete phenomena of surface wave propagation in pavement systems. Therefore, the problem statement by Vidale (1964) still holds as the problem statement for the theoretical part of the present work:

"Given such a system, it is desired to know what effect the material properties of the layers will have upon the phase velocities measured at the surface, so that from these measurements the properties and depth of each layer may be inferred."

1.2 Objectives

The main objective with this study is to develop an improved non-destructive testing (NDT) technique for pavements utilizing surface waves. This project was initiated with the aim of using seismic measurements for the generation of input parameters in analytical pavement design.

1.3 Methods

This work is based on both reported and experienced (Ryden, 1999) difficulties with existing surface wave methods for NDT of pavements. The progress and developments within this context has been carried out through a combination of field experiments and numerical modeling.

1.4 Limitations

This thesis is focused on the development of a method for surface wave testing of pavements. Extensive evaluation of the method under many different conditions remains to be conducted. Although more than 100 data sets have been collected during the development, only a few detailed case studies are presented in this thesis. The presented technique is based solely on phase velocity measurements. The analysis and data processing is restricted to phase velocities and there is no analysis of damping properties. No other related measurement techniques such as the Impact Echo or Impulse Response method have been studied or utilized.

1 Introduction

2 Summary of papers

The included papers reflect the work in a chronological order. Paper I presents the early field experiments and results with the developed hardware and software components. The fundamental approach of using the complete phase velocity spectrum instead of discrete dispersion curves is outlined. In Paper II the proposed method is applied to non-destructive testing of an old concrete bridge. Paper III presents a detailed theoretical study of the Lamb wave approximation used in Paper I and II. In Paper IV the theoretical study is extended to a three-layer system representing a more realistic pavement structure. This paper reveals some of the previously unexplained phenomena of wave propagation in pavement structures. The results from Paper I-IV have been used to develop an inversion procedure utilizing the complete phase velocity spectrum, which is described in Paper V.

Paper I: Multimodal approach to seismic pavement testing

In this paper a new approach to non-destructive seismic pavement testing is presented. The final version of the measurement system, field set up, and data processing technique is described. Much of the early work in this project was spent on the literature review along with experimental measurements on pavements and concrete slabs. Many ideas and prototypes were disregarded, and the main findings from that period have been summarized in this paper. It is concluded that the nature of wave propagation along the surface of a pavement structure has been oversimplified in earlier techniques. At high frequencies (1-30 kHz) the wavefield is dominated by multiple modes of guided waves following the main trend of Lamb waves in the stiff top layer. At lower frequencies (50-1000 Hz) several branches of dispersion curves are observed in the phase velocity spectrum. Results are verified with both synthetic and real data. At this point, a complete understanding and description of the visible branches at low frequencies was not available and this unexplained phenomenon served as a motivation for further studies.

Paper II: Lamb wave analysis for non-destructive testing of concrete plate structures

Inspired by the results from Paper I, the Lamb wave approximation was tested on an old concrete bridge in Malmoe, Sweden. Measurements were conducted on the two supports of the concrete bridge. The thickness and elastic constants could be evaluated directly in the field. Results from the seismic field test showed good agreement with results obtained from more expensive tests based on core drillings. The paper is included in the thesis because it also contains a practical description of how to calculate theoretical Lamb wave dispersion curves, a parametric study, and the fundamentals about Lamb waves in a free plate. The nature of Lamb wave propagation plays a major part in the overall understanding of wave propagation in pavement structures, and is therefore an important part of the thesis.

Paper III: Surface waves in inversely dispersive media

The Lamb wave approximation at high frequencies is used in both Paper I and II. With this approach it is assumed that the top layer or concrete support can be approximated with a free plate. In reality, the top layer in a pavement structure is in contact with the underlying compacted granular material (base). The influence on the theoretical dispersion curves from this lower velocity material is investigated in this paper. The discrepancy between dispersion curves for a free plate and a plate resting on a lower velocity half-space is theoretically quantified. It is concluded that the error involved in the Lamb wave approximation is less than 10% in the high frequency range. In this paper it is also emphasized that dispersion curves in this type of layering must be calculated in the complex wave number domain. In this layer setting, where the seismic velocity decreases with depth, energy is radiating down towards the lower velocity half-space in proportion to the imaginary part of the wave number. The excitability for each point on the dispersion curves is also calculated. It is shown that both the attenuation due to leakage and the excitability are critical parameters for a correct understanding of wave propagation in this type of layer model. Mode shapes are included in the study to visualize displacements inside the medium. Results of the study show that for inversely dispersive media the Rayleigh wave assumption is not valid, and other types of interface waves and leaky Lamb waves contribute to most of the wavefield.

Paper IV: Guided wave propagation in three-layer pavement structures

In this paper the study from Paper III is extended to include two layers on a half-space with decreasing velocity with depth. This layer setting is used to represent a more realistic pavement structure than the plate on a half-space model used in Paper III. Theoretical dispersion curves are calculated and studied from the same perspective as in Paper III, using attenuation due to leakage and excitability. Here it is shown that the branches of dispersion curves visible in the phase velocity spectrum, observed in Paper I, can be theoretically explained as different mode branches if both leakage and excitability are taken into account. Results show that several difficulties that have been reported with the conventional method can be theoretically explained from these mode branches, i.e. problems related to unwrapping of the measured phase difference and the lack of sensitivity to the layer properties of the second embedded layer. It is concluded, that the observed mode branches at lower frequencies (50-1000 Hz) hold the greatest potential for a refined evaluation technique of all pavement layer properties.

Paper V: Inversion of surface waves using phase velocity spectra

From the results presented in Paper III and IV it can be concluded that the linearized matrix techniques traditionally used for the inversion of surface wave data are not suitable for surface wave testing of pavements. A new approach for the inversion of the complete phase velocity spectrum based on Simulated Annealing is presented in this paper. This technique tries to fit a theoretically calculated complete phase velocity spectrum to the measured replica. The entire procedure of dealing with discrete dispersion curves and partial derivatives is avoided. Furthermore the interference effect

from different modes of propagation is taken into account through modal superposition along the survey line. The viscoelastic properties of the asphalt layer must be properly accounted for in the inversion. By doing this, the frequency dependent stiffness of the asphalt layer, the mastercurve, is obtained directly and there is no need for any empirical relation to get the 30 Hz design modulus value.

2 Summary of papers

3 Field of research

This work stretches over several disciplines of science, including wave propagation theory, inversion theory, pavement engineering, soil mechanics, signal processing, and computer-based data acquisition. All those topics are described elsewhere and the purpose of this chapter is to give a concise review of the fundamental principles of this work. Key topics covered are; wave propagation in layered media, pavement material stiffness properties, and a literature review of surface wave testing of pavements.

3.1 Seismic wave propagation

In this section the fundamentals of seismic/acoustic wave propagation in solids are described. Many derivations are lengthy and text books are recommended for a complete coverage of this theory (Graff, 1975; Ingard, 1988; Cremer and Heckl, 1988; Bedford and Drumheller, 1994). The wave equation, matrix techniques for wave propagation in layered media, and modal dispersion curves are the key issues covered.

3.1.1 Body waves and the wave equation

The wave equation for an isotropic infinite elastic solid is based on Newton's second law, which states that force is equal to mass times acceleration. The acceleration and force can be expressed as partial derivatives of displacement (u) and stress (σ) respectively. Equilibrium in an infinitesimal cubic element of density (ρ) then requires that

$$\rho \frac{\partial^2 u_1}{\partial t^2} = \frac{\partial \sigma_{11}}{\partial x_1} + \frac{\partial \sigma_{12}}{\partial x_2} + \frac{\partial \sigma_{13}}{\partial x_3} \tag{1}$$

$$\rho \frac{\partial^2 u_2}{\partial t^2} = \frac{\partial \sigma_{21}}{\partial x_1} + \frac{\partial \sigma_{22}}{\partial x_2} + \frac{\partial \sigma_{23}}{\partial x_3} \tag{2}$$

$$\rho \frac{\partial^2 u_3}{\partial t^2} = \frac{\partial \sigma_{31}}{\partial x_1} + \frac{\partial \sigma_{32}}{\partial x_2} + \frac{\partial \sigma_{33}}{\partial x_3} \tag{3}$$

for the three coordinates respectively, where $\mathbf{x}(x_1, x_2, x_3)$ represents the Cartesian coordinate system and $\mathbf{u}(u_1, u_2, u_3)$ the corresponding displacements in the three dimensions, t is time, and σ_{11}, σ_{12},…are the different stress components acting on the cube. These stress components can be rewritten in terms of strain and elastic constants by using the linear elastic stress-strain relations (Hooke's law)

$$\sigma_{11} = \lambda\Delta + 2\mu\varepsilon_{11} \qquad \sigma_{22} = \lambda\Delta + 2\mu\varepsilon_{22} \qquad \sigma_{33} = \lambda\Delta + 2\mu\varepsilon_{33} \tag{4}$$

$$\sigma_{12} = \mu\varepsilon_{12} \qquad \sigma_{23} = \mu\varepsilon_{23} \qquad \sigma_{13} = \mu\varepsilon_{13} \tag{5}$$

where λ and μ are Lamé's elastic constants and $\Delta=\varepsilon_{11}+\varepsilon_{22}+\varepsilon_{33}$ is the change in volume of the element. The strain-displacement relations are given by

$$\varepsilon_{11} = \frac{\partial u_1}{\partial x_1} \qquad \varepsilon_{22} = \frac{\partial u_2}{\partial x_2} \qquad \varepsilon_{33} = \frac{\partial u_3}{\partial x_3} \tag{6}$$

$$\varepsilon_{12} = \frac{\partial u_1}{\partial x_2} + \frac{\partial u_2}{\partial x_1} \qquad \varepsilon_{23} = \frac{\partial u_2}{\partial x_3} + \frac{\partial u_3}{\partial x_2} \qquad \varepsilon_{13} = \frac{\partial u_1}{\partial x_3} + \frac{\partial u_3}{\partial x_1} \tag{7}$$

By using the stress-strain (Equation 4-5) and the strain-displacement relations (Equation 6-7) the equations of motion (Equation 1-3) can be expressed by using displacements instead of stresses

$$\rho\frac{\partial^2 u_1}{\partial t^2} = (\lambda+\mu)\frac{\partial}{\partial x_1}\left(\frac{\partial u_1}{\partial x_1} + \frac{\partial u_2}{\partial x_2} + \frac{\partial u_3}{\partial x_3}\right) + \mu\nabla^2 u_1 \tag{8}$$

$$\rho\frac{\partial^2 u_2}{\partial t^2} = (\lambda+\mu)\frac{\partial}{\partial x_2}\left(\frac{\partial u_1}{\partial x_1} + \frac{\partial u_2}{\partial x_2} + \frac{\partial u_3}{\partial x_3}\right) + \mu\nabla^2 u_2 \tag{9}$$

$$\rho\frac{\partial^2 u_3}{\partial t^2} = (\lambda+\mu)\frac{\partial}{\partial x_3}\left(\frac{\partial u_1}{\partial x_1} + \frac{\partial u_2}{\partial x_2} + \frac{\partial u_3}{\partial x_3}\right) + \mu\nabla^2 u_3 \tag{10}$$

These equations are called the displacement equations of motion (a wave equation) and express the balance of linear momentum. This is the most general form of the wave equation, which all elastic oscillations in the interior of a solid must satisfy. Expressed in vector form, Equation 8-10 is reduced to

$$\rho\frac{\partial^2 \mathbf{u}}{\partial t^2} = (\lambda+\mu)\nabla(\nabla\cdot\mathbf{u}) + \mu\nabla^2\mathbf{u} \tag{11}$$

where ∇ is the vector operator

$$\nabla = \left(\frac{\partial}{\partial x_1}, \frac{\partial}{\partial x_2}, \frac{\partial}{\partial x_3}\right) \tag{12}$$

and ∇^2 is the scalar operator

$$\nabla^2 = \left(\frac{\partial^2}{\partial x_1^2} + \frac{\partial^2}{\partial x_2^2} + \frac{\partial^2}{\partial x_3^2} \right) \tag{13}$$

Lamé's constants are usually used in the wave equation but can be replaced by Young's modulus (E) and Poisson's ratio (ν) by using

$$\lambda = \frac{E\nu}{(1+\nu)(1-2\nu)} \tag{14}$$

$$\mu = \frac{E}{2(1+\nu)} \tag{15}$$

The displacement equation of motion cannot be solved directly. Therefore a form of solution must be assumed and checked for suitability by differentiation and substitution. In this case it is assumed that the wavefront is an infinite plane normal to the direction of propagation and the form of solution can be expressed as

$$u_1, u_2, u_3 = Ae^{i(kx_1 - \omega t)} + Be^{i(kx_1 + \omega t)} \tag{16}$$

where k is the wave number and ω is the angular frequency. The first term represents a wave propagating in the positive x_1 direction with amplitude A and the second term represents a wave propagating in the opposite direction with amplitude B. Differentiation of Equation 16 and substituting into Equation 11 yields two possible solutions (eigensolutions) for the velocity of wave propagation in an infinite elastic isotropic medium.

$$V_P = \alpha = \sqrt{\frac{\lambda + 2\mu}{\rho}} = \sqrt{\frac{E(1-\nu)}{\rho(1+\nu)(1-2\nu)}} \tag{17}$$

$$V_S = \beta = \sqrt{\frac{\mu}{\rho}} = \sqrt{\frac{E}{2\rho(1+\nu)}} \tag{18}$$

The first solution (Equation 17) represents the rotational free part of the wavefield, longitudinal also called compression waves (P-waves). These waves are body waves traveling with relatively small particle displacements parallel to the direction of propagation. The longitudinal wave is the fastest traveling wave, hence it is also called primary wave or P-wave. Particle motion of the P-wave is illustrated in Figure 2.

The second solution (Equation 18) represents the divergence free part of the wavefield, shear waves also called transverse waves (S-waves). Shear waves propagate only by shear strain in a direction perpendicular to the direction of propagation. In this case the medium retains its shape rather than volume compared to the P-wave. The speed V_S is given by Equation 18 independently of boundary conditions, i.e. half-space, beam, or

plate. This is because there is no change in volume of an element during wave propagation. Since the shear wave is slower and therefore appears after the compression wave it is called secondary wave or S-wave. The corresponding particle motion of the S-wave is illustrated in Figure 2.

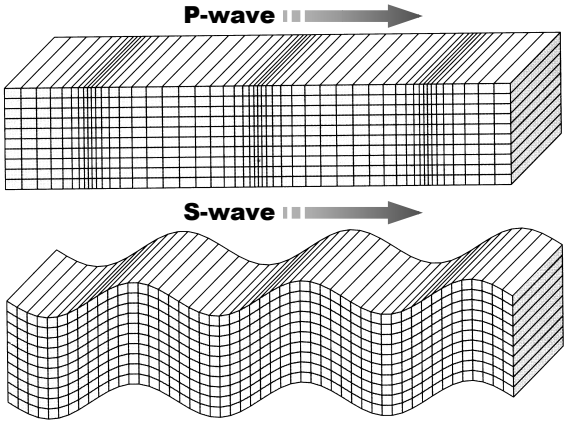

Figure 2. Characteristic motion of body wave propagation, compression wave (P-wave), and shear wave (S-wave), from Shearer (1999).

P- and S-waves are the two fundamental types of waves traveling in an infinite medium. Depending on boundary conditions other types of wave propagation can also develop. Pure P- and S-waves are called body waves or bulk waves. Equation 17 and 18 are often used in material characterization to obtain the elastic constants E and ν from measured or evaluated seismic velocities and the bulk density of the material. However these equations are only valid for plane waves inside a medium that is much larger than the oscillating wavelength. It should be pointed out that in most civil engineering applications appropriate boundary conditions must be taken into account. For example the velocity (speed) of P-wave propagation along a free plate is slightly reduced because of the free boundaries in one dimension. The corresponding quasi-longitudinal wave speed ($V_{P\ plate}$) is slower than V_P in an infinite medium and related to the E, ρ, and ν constants by

$$V_{P\ plate} = \alpha_{\text{plate}} = \sqrt{\frac{E}{\rho\left(1-\nu^2\right)}} \tag{19}$$

3.1.2 Field equations for guided waves in layered media

In this study seismic measurements are conducted on the surface of pavement structures. This implies a quite different situation than the infinite homogeneous medium described above. The free surface and the layering of the pavement structure generate dispersive guided waves and pure P- and S-waves cannot be directly measured from the surface. However, wave propagation in multilayered media with a free surface can be predicted

based on the superposition of pure P- and S-waves within each layer and the appropriate boundary conditions between layers. This theory was first presented by Thomson (1950) and Haskell (1953). Since then a large number of publications have been devoted to matrix techniques for modeling guided waves in multilayered media (Lowe, 1995). Applications of this theory ranges from ultrasonic testing of thin films and coatings (Kuttruff, 1991; Lee and Cheng, 2001) to global seismology (Shearer, 1999). The final equations necessary to predict wave propagation in layered media using the global matrix method (Knopoff, 1964) are given within the papers of this thesis. This section gives some additional background and theory on the derivation of the matrix equations. The approach taken here follows from the paper by Lowe (1995). Other recommended publications on matrix techniques are; Kausel and Roesset (1981), Buchen and Ben-Hador (1996), and Gucunski and Maher (2000).

The P- and S-waves described in the previous section are independent and the total displacement field can be divided into one P- and one S-wave component. In vector form this is done by using Helmholtz method where the scalar function ϕ represents the irrotational part of the wavefield (P-waves) and the vector function $\boldsymbol{\psi}$ represents the divergence free part (S-waves). P-waves or longitudinal waves are here represented with index L and shear waves with index S. The body wave velocities V_P and V_S are given by α and β respectively, which follows the notation used in the matrix equations in the papers of this thesis.

$$\phi = A_{(L)} e^{i(\mathbf{k}\cdot\mathbf{x}-\omega t)} \tag{20}$$

and

$$|\boldsymbol{\psi}| = A_{(S)} e^{i(\mathbf{k}\cdot\mathbf{x}-\omega t)} \tag{21}$$

where $A_{(L)}$ and $A_{(S)}$ are the P- and S-wave amplitudes respectively. In this vector formulation $\mathbf{k}$ is the wave number vector, which is in the direction of propagation. The phase velocity (V_{ph}) is given from

$$V_{ph} = \frac{\omega}{|\mathbf{k}|} \tag{22}$$

The displacement fields (Equation 16) can now be expressed as

$$\mathbf{u}_{(L)} = \nabla\phi \tag{23}$$

$$\mathbf{u}_{(S)} = \nabla \times \boldsymbol{\psi} \tag{24}$$

where $\times$ is the vector cross product. Before proceeding with the matrix equations the model is restricted to the plane of each plate or layer (x_3=0 and u_3=0). It is also assumed that the wavelength is much smaller than the width in the x_3 direction so that the plane

strain assumption is valid. Each layer is thus defined in the x_1 and x_2 direction and the particle motion is described in this plane only, see Figure 3. Wave propagation in multilayered media can now be predicted by superposing P- and S-waves in each layer and by using Snell's law for the interaction of waves between layers. Waves above and below the interface must share the same frequency (ω) and wave number k_1 in the x_1 direction. The k_1 component of the wave number is the projection of the body waves along the layer interface (or horizontal surface) and determines V_{ph} in the x_1 direction. Consequently all field equations describing wave motion anywhere in the layer model contain the factor

$$F = e^{i(k_1 x_1 - \omega t)} \tag{25}$$

which is an invariant of the system. Using Snell's law the k_2 component of partial P- and S-waves traveling in positive (+) and negative (-) x_2 direction can be expressed with k_1 using

$$k_{2(L\pm)} = \pm\sqrt{\frac{\omega^2}{\alpha^2} - k_1^2} \tag{26}$$

$$k_{2(S\pm)} = \pm\sqrt{\frac{\omega^2}{\beta^2} - k_1^2} \tag{27}$$

Positive directions of x_1 and x_2 are shown in Figure 3 along with the partial waves in a four layer model.

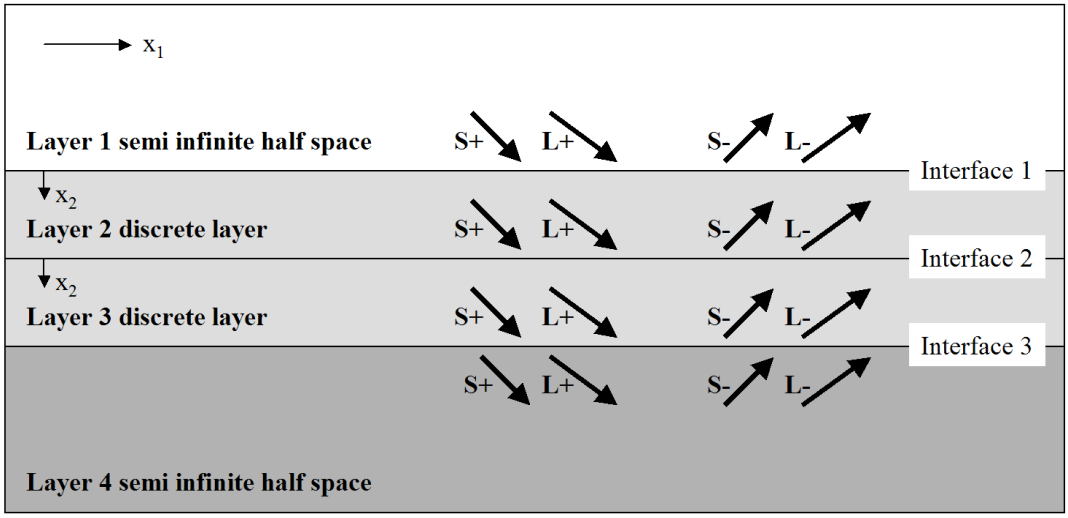

Figure 3. Schematic illustration of the layered model used in the global matrix approach, after Lowe (1995). In surface wave applications the top half-space is modelled as vacuum to represent the free surface.

The total displacements and stresses in a layer can be calculated by superposing these partial bulk waves. Since we are only dealing with wave propagation in the x_1 and x_2 direction it is sufficient to derive expressions for the displacements u_1 and u_2, and the stress components σ_{22} and σ_{12} (normal and shear stress). By using Equations 20-27 these components can be expressed using only the k_1 component of the wave number. For longitudinal waves propagating up (-) and down (+) these expressions are given by

$$u_1 = k_1 A_{(L\pm)} F e^{\pm i\left(\omega^2/\alpha^2 - k_1^2\right)^{1/2} x_2} \tag{28}$$

$$u_2 = \pm\left(\omega^2/\alpha^2 - k_1^2\right)^{1/2} A_{(L\pm)} F e^{\pm i\left(\omega^2/\alpha^2 - k_1^2\right)^{1/2} x_2} \tag{29}$$

$$\sigma_{22} = \left(\omega^2 - 2\beta^2 k_1^2\right) i\rho A_{(L\pm)} F e^{\pm i\left(\omega^2/\alpha^2 - k_1^2\right)^{1/2} x_2} \tag{30}$$

$$\sigma_{12} = \pm 2\beta^2 k_1 \left(\omega^2/\alpha^2 - k_1^2\right)^{1/2} i\rho A_{(L\pm)} F e^{\pm i\left(\omega^2/\alpha^2 - k_1^2\right)^{1/2} x_2} \tag{31}$$

and for shear waves

$$u_1 = \pm\left(\omega^2/\beta^2 - k_1^2\right)^{1/2} A_{(S\pm)} F e^{\pm i\left(\omega^2/\beta^2 - k_1^2\right)^{1/2} x_2} \tag{32}$$

$$u_2 = -k_1 A_{(S\pm)} F e^{\pm i\left(\omega^2/\beta^2 - k_1^2\right)^{1/2} x_2} \tag{33}$$

$$\sigma_{22} = -2\beta^2 k_1 \left(\omega^2/\beta^2 - k_1^2\right)^{1/2} i\rho A_{(S\pm)} F e^{\pm i\left(\omega^2/\beta^2 - k_1^2\right)^{1/2} x_2} \tag{34}$$

$$\sigma_{12} = \left(\omega^2 - 2\beta^2 k_1^2\right) i\rho A_{(S\pm)} F e^{\pm i\left(\omega^2/\beta^2 - k_1^2\right)^{1/2} x_2} \tag{35}$$

The summation of the contribution from the four partial waves for each displacement and stress component can be written in matrix form as

$$\begin{Bmatrix} u_1 \\ u_2 \\ \sigma_{22} \\ \sigma_{12} \end{Bmatrix} = \begin{bmatrix} k_1 g_\alpha & k_1/g_\alpha & C_\beta g_\beta & -C_\beta/g_\beta \\ C_\alpha g_\alpha & -C_\alpha/g_\alpha & -k_1 g_\beta & -k_1/g_\beta \\ i\rho B g_\alpha & i\rho B/g_\alpha & -2i\rho k_1\beta^2 C_\beta g_\beta & 2i\rho k_1\beta^2 C_\beta/g_\beta \\ 2i\rho k_1\beta^2 C_\alpha g_\alpha & -2i\rho k_1\beta^2 C_\alpha/g_\alpha & i\rho B g_\beta & i\rho B/g_\beta \end{bmatrix} \begin{Bmatrix} A_{(L+)} \\ A_{(L-)} \\ A_{(S+)} \\ A_{(S-)} \end{Bmatrix} \tag{36}$$

where the common factor F has been excluded and the following substitutions have been made

$$C_\alpha = \left(\omega^2/\alpha^2 - k_1^2\right)^{1/2} \tag{37}$$

$$C_\beta = \left(\omega^2/\beta^2 - k_1^2\right)^{1/2} \tag{38}$$

$$g_\alpha = e^{i\left(\omega^2/\alpha^2 - k_1^2\right)^{1/2} x_2} \tag{39}$$

$$g_\beta = e^{i\left(\omega^2/\beta^2 - k_1^2\right)^{1/2} x_2} \tag{40}$$

$$B = \omega^2 - 2\beta^2 k_1^2 \tag{41}$$

Equation 34 represents the field matrix ($\mathbf{D_i}$) describing the relationship between the partial wave amplitudes, displacements, and stresses anywhere in a layer (*i*). Displacement and stresses along the upper and lower interface of each layer can now be expressed by setting x_2 equal to zero or the layer thickness depending on which interface is described. The resulting interface matrices $\mathbf{D_{it}}$ and $\mathbf{D_{ib}}$ describe the displacements and stresses at the interface as a function of the partial wave amplitudes (*A*) from above (index *t*) or below (index *b*) the interface. The thickness (*d*) in the x_2 direction of each layer is entered as x_2 into the equations and is zero for the half-space matrices. The interface matrices are slightly simplified by redefining the origin of the bulk waves in each layer to be at their entry to the layer instead of the top of the layer (Lowe, 1995). The interface matrices can then be written as

$$\left[\mathbf{D}_{it}\right] = \begin{bmatrix} k_1 & k_1 g_\alpha & C_\beta & -C_\beta g_\beta \\ C_\alpha & -C_\alpha g_\alpha & -k_1 & -k_1 g_\beta \\ i\rho B & i\rho B g_\alpha & -2i\rho k_1 \beta^2 C_\beta & 2i\rho k_1 \beta^2 C_\beta g_\beta \\ 2i\rho k_1 \beta^2 C_\alpha & -2i\rho k_1 \beta^2 C_\alpha g_\alpha & i\rho B & i\rho B g_\beta \end{bmatrix} \tag{42}$$

$$\left[\mathbf{D}_{ib}\right] = \begin{bmatrix} k_1 g_\alpha & k_1 & C_\beta g_\beta & -C_\beta \\ C_\alpha g_\alpha & -C_\alpha & -k_1 g_\beta & -k_1 \\ i\rho B g_\alpha & i\rho B & -2i\rho k_1 \beta^2 C_\beta g_\beta & 2i\rho k_1 \beta^2 C_\beta \\ 2i\rho k_1 \beta^2 C_\alpha g_\alpha & -2i\rho k_1 \beta^2 C_\alpha & i\rho B g_\beta & i\rho B \end{bmatrix} \tag{43}$$

By satisfying the boundary conditions at each layer interface, multilayered media can be modeled by assembling interface matrices from each layer into one global matrix (**S**), describing the complete layer model. For a layer model with four layers as in Figure 3 the system matrix becomes:

$$\mathbf{S} = \begin{bmatrix} \mathbf{D}_{1b}^{-} & -\mathbf{D}_{2t} & & \\ & \mathbf{D}_{2b} & \mathbf{D}_{3t} & \\ & & \mathbf{D}_{3b} & -\mathbf{D}_{4t}^{+} \end{bmatrix} \tag{44}$$

Each row in **S** represents each interface and each column corresponds to each layer including the two half-spaces. The incoming waves in the half-spaces are defined to be zero, according to the condition for a modal solution that the system is unforced. These waves are thus identified as knowns and therefore the half-space matrices are only four-by-two matrices containing only the outgoing waves. The (-) index on $\mathbf{D}_{1b}$ above represents the outgoing (up) waves in the top half-space (columns two and four in $\mathbf{D}_b$) and the (+) index on $\mathbf{D}_{4t}$ represents outgoing (down) waves in the bottom half-space (columns one and three in $\mathbf{D}_t$). In surface wave applications the top surface is usually free. This can be taken into account by some modifications to the **D** matrix. However, the exact same result can be obtained much more easily, simply by setting the bulk wave velocities, α and β, in the top layer to arbitrary nonzero values and the bulk density to zero (Lowe, 1995). In this way the same matrices can be used for both vacuum and solid half-spaces.

Modal solutions predict the unforced vibrations of the system, i.e. modal dispersion curves. A dispersion curve defines the phase velocities as a function of frequency at which waves can propagate along the x_1 direction. For a given set of layer properties x_2 (through thickness), α, β, and ρ modal solutions can be found at certain combinations of ω and k_1 which satisfies all equations in the field matrix simultaneously, i.e. when the determinant of **S** is zero. Further description on this procedure can be found in Paper III and IV of this thesis. Response solutions at a given frequency and wave number can be obtained with the same matrix formulation. One of the amplitudes is then assigned a unit amplitude and resulting displacements or stresses can be calculated by inverting the field matrix.

3.1.3 Guided waves and dispersion curves

In an infinite, homogeneous, and isotropic medium only body waves exist. However, in layered media other wave types can be generated. These waves are called guided waves and are formed by the interaction of P- and S-waves at the interface between layers. Therefore guided waves carry information on the structural properties (elastic constants and boundary conditions) of the medium. Guided waves propagating along a free surface are called surface waves (Telford et al., 1990). The phase velocity of horizontally propagating guided waves in layered media is frequency dependent, i.e. dispersive. The relation between frequency and phase velocity is defined by a dispersion curve.

Dispersion curves play a central role in this thesis. The presented method is based on measurements of dispersion properties of unknown systems (pavements) from which a corresponding layer model is evaluated. This section is dedicated to explain more about dispersion of guided waves and dispersion curves.

Rayleigh waves represent a special type of guided wave propagating along the surface of a homogenous half-space (Rayleigh, 1885). Rayleigh waves are generated from reflections and mode conversions of body waves at a free surface. The proportions of the partial wave amplitudes are such that both the shear and normal stress cancel out at the

surface satisfying the free boundary condition. At the surface, the particle motion is elliptical and retrograde with respect to the direction of propagation (Telford et al., 1990). The amplitude of the motion decreases exponentially with depth below the surface, see Figure 4.

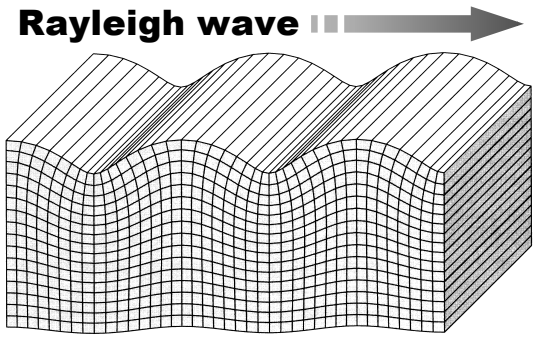

Figure 4. Characteristic motion of Rayleigh wave propagation, from Shearer (1999)

The Rayleigh wave velocity (V_R) is slightly slower than the shear wave velocity. The exact ratio between V_S and V_R ($s=V_S/V_R$) is dependent on the ratio between V_S and V_P ($n=V_S/V_P$), i.e., Poisson's ratio. All velocities must obey the Rayleigh dispersion relation

$$-4s^2\sqrt{s^2-n^2}\sqrt{s^2-1}+\left(1-2s^2\right)^2=0 \tag{45}$$

Lord Rayleigh (Rayleigh, 1885) found a solution to this expression that now describes the Rayleigh wave velocity. By studying Equation 45 it can be found that V_R is only slightly slower than V_S and in practice V_R can be approximated with Equation (46) (Nazarian et al., 1999)

$$V_R = V_S/\left(1.13-0.16\nu\right) \tag{46}$$

Approximately 67% of the induced energy from an impulse source on a homogenous half-space propagates as Rayleigh waves (Richart et al., 1970). Therefore Rayleigh waves show larger amplitudes than the body waves on the surface. Because of geometrical damping, the amplitude of the Rayleigh wave decays with the square root of the distance from the source (Richart et al., 1970). Figure 5 illustrates the particle motion of Rayleigh waves in comparison to P- and S-waves.

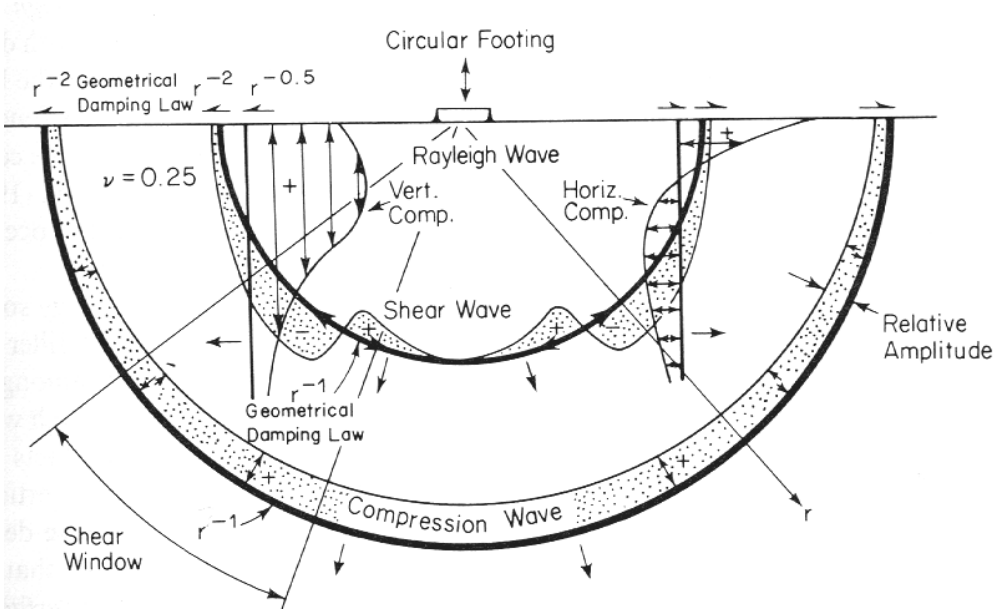

Figure 5. Distribution of seismic waves from a circular footing on a homogeneous, isotropic, elastic half-space. The particle motion is visualised at a distance of approximately 2.5 wavelengths from the source. The different wave types are drawn in proportion to the velocity of each wave, from Richard et al. (1970).

A Rayleigh type of wave travels through a zone that is approximately one wavelength deep (Graff, 1975). Material properties of this zone affect the velocity of the wave propagation. Long wavelengths/low frequencies penetrate deeper. Short wavelengths/high frequencies penetrate a shallow volume close to the surface. Therefore, if the medium is layered with different properties at different depths, different wavelengths (or frequencies) will propagate with a different phase velocity.

An example is used to illustrate dispersion of surface waves in a layered medium. Layer model A represents a three-layer model with a free surface above and a soild half-space below one 0.2 m thick discrete layer. Material properties and boundary conditions for this system are shown in Figure 6.

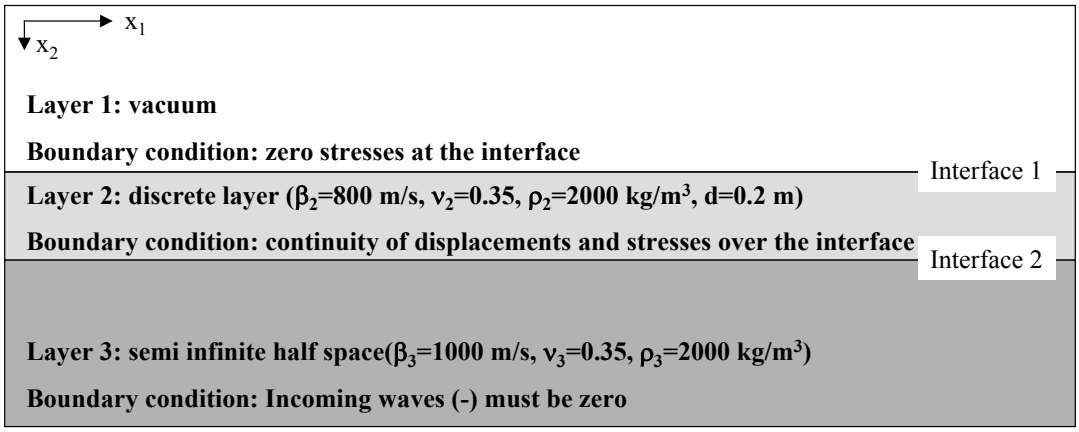

Figure 6. Example layer model A used to illustrate dispersion of surface waves.

Following the global matrix method explained in the previous section this system can be described with the system matrix **S**

$$\mathbf{S} = \begin{bmatrix} D_{1b}^{-} & -D_{2t} & \\ & D_{2b} & D_{3t}^{+} \end{bmatrix} \tag{47}$$

where each row represents each interface and each column represents each layer as described in section 3.1.2. The fundamental mode dispersion curve has been calculated by searching for V_{ph} at different frequencies where the determinant of **S** changes sign, i.e. is close to zero. The resulting roots (V_{ph} and f pairs) can also be plotted as wavelength (λ) versus phase velocity by using

$$\lambda = V_{ph} / f \tag{48}$$

Figure 7a shows the shear wave velocity as a function of depth for the example layer model A. The corresponding dispersion curve is plotted in Figure 7b. At short wavelengths the phase velocity approaches the Rayleigh wave velocity of the low velocity layer close to the surface (V_R=745 m/s) and at longer wavelengths the phase velocity approaches the Rayleigh wave velocity of the lower half-space (V_R=931 m/s). Two wavelengths λ_1=0.19 m and λ_2=0.88 m have been marked as [1] and [2] in Figure 7b. The corresponding vertical displacement component of these two wavelengths has been calculated in Figure 7c. Here it can be seen that the wave motion of the shorter wavelength [1] is concentrated to the shallow low velocity layer and thus mostly affected by the properties of this layer. The longer wavelength [2] penetrates deeper into the higher velocity half-space and the phase velocity is dependent on the material properties of both layers.

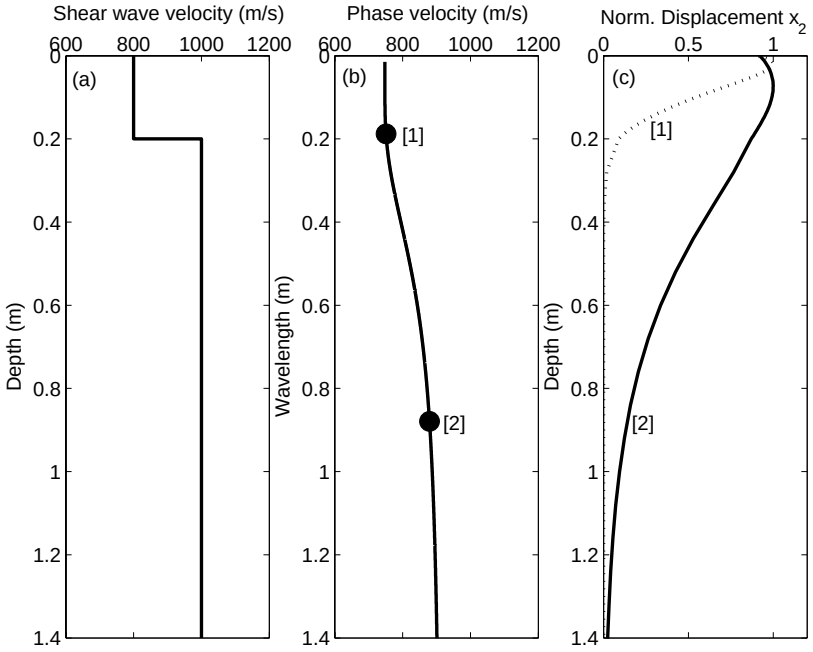

Figure 7. (a) Example layer model showing V_S as a function of depth. (b) shows the corresponding fundamental mode dispersion curve and (c) shows the vertical component of wave motion at two different wavelengths labelled [1] and [2].

For more complicated layer settings it is usually more difficult to directly compare the dispersion curve with the layer model as done in Figure 7 above. In general, dispersion properties of a layered system becomes more complicated when there are large velocity contrasts between layers and/or a decreasing shear wave velocity with depth.

Layer model B is used to show that dispersion of guided waves can also arise from the geometry of the medium. Figure 8 shows a layer model representing a free plate in vacuum. In this case surface waves can develop at both the upper and lower surface forming guided waves where the whole plate is bending. These waves were first studied by Lamb (1917) who found that there are two different types of waves that can propagate in a plate, one symmetrical (S) (also called longitudinal or extensional), and one anti-symmetrical (A) (also called flexural or bending) type of wave.

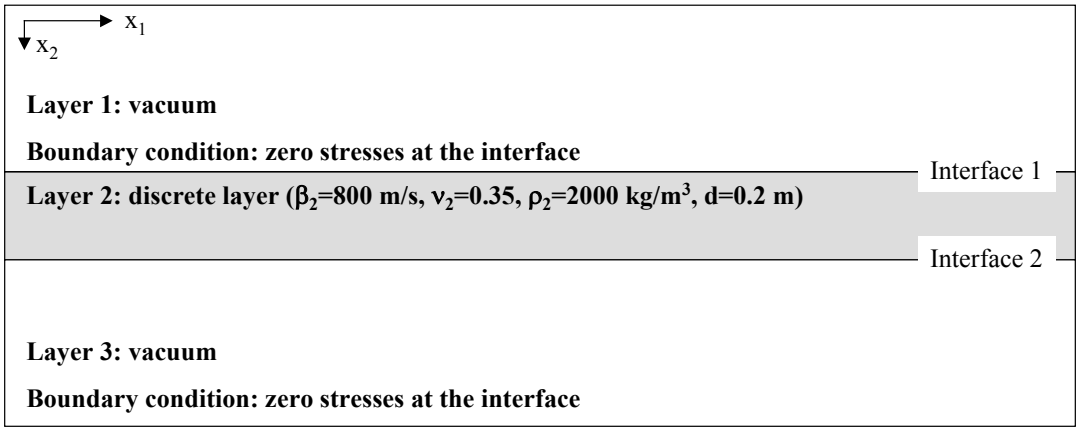

Figure 8. Example layer model B used to illustrate dispersion of guided waves in a free plate.

Fundamental mode Lamb wave dispersion curves from layer model B are plotted in Figure 9. In this example there is no variation in material properties within the plate and the dispersion mechanism is quite different from the surface waves studied in example A above. In this case it is the ratio between wavelength and thickness that makes the phase velocity vary with frequency. The layer is bending as a whole, which is illustrated with mode shapes embedded in Figure 9. At high frequencies (short wavelengths) both the A0 and S0 dispersion curve approaches the Rayleigh wave velocity of the plate. Lamb type of waves play a fundamental part in wave propagation in pavement structures and is further studied within the papers of the thesis.

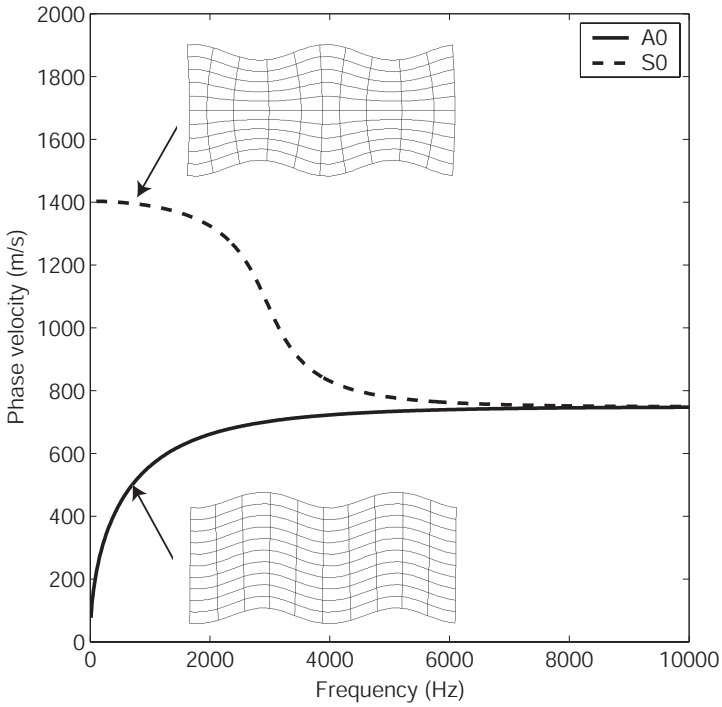

Figure 9. Fundamental mode anti-symmetric (A0) and symmetric (S0) Lamb wave dispersion curves calculated from example layer model B.

Dispersion curves from example layer model A and B have been shown to illustrate the dispersion mechanism in simple systems. It has been shown that dispersion curves of a layered medium are dependent on both the geometry and material properties of the system. These characteristics make guided waves suitable for material characterization of unknown layered systems. In fact, guided waves can be used to measure material properties of embedded layers and areas of structures that are difficult or impossible to access with conventional techniques. For example, buried pipes (Long et al., 2003), thin films and coatings (Lee and Cheng, 2001), and material properties of embedded pavement layers. However, it should be pointed out that dispersion curves of guided waves can become quite complicated in many systems and are rarely as easily described as in the examples above. For example multiple modes of guided waves are often excited and it is not always easy to identify and separate these modes.

Higher modes of propagation play an essential part in the work presented in this thesis. As described earlier, only two modes of wave propagation are possible in an infinite medium, i.e., the P- and S-wave. However, the presence of boundaries and/or layers of different stiffness properties allows for other modes of propagation as exemplified in example A and B. For simplicity only the two fundamental mode dispersion curves (A0 and S0) were presented in example B. However, at a fixed frequency multiple modes can exist, all satisfying the boundary conditions for guided wave propagation. The mode with the lowest phase velocity represents the fundamental mode of propagation. Successively

higher modes propagate with higher phase velocities, i.e., longer wavelengths. Their different number of nodal plains in the thickness direction characterizes higher modes of propagation. The real part of the vertical displacement components of symmetrical Lamb waves (S0-S3) have been plotted in Figure 10. The layer model in example B has been used to calculate the displacement at different depths (mode shape) in the plate. The number of nodal points (zero displacement) increases with increasing mode number.

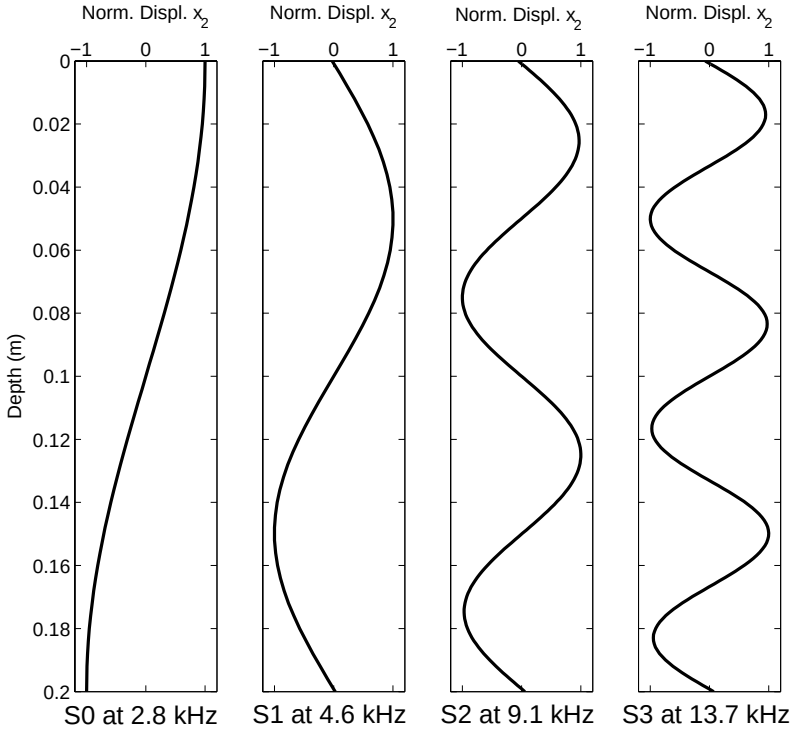

Figure 10. Vertical displacement component (real part) of the fundamental mode (S0) and successive higher modes (S1-S3) of symmetric Lamb waves.

Multiple modes of guided waves can increase the sensitivity of guided wave techniques. All steps from field measurements to evaluation of layer properties can benefit from a good understanding and thorough study on the possible modes that may be excited in each application. Consequently, it is an important part of the development of each new guided wave technique to first study the nature of wave propagation in each specific case (Lowe and Cawley, 1995a; 1995b). Paper III and IV of this thesis are devoted to the theory of guided waves in pavement structures.

3.1.4 Wave propagation in pavement materials

In the theory given above, the wave propagation medium or layer has been modeled as a homogenous continuum. However, it is worth mentioning that in reality pavement materials are particulate materials built up by small particles, gas, and fluid. In concrete and asphalt materials, particles are bonded together with cement or bitumen. Under

operational loads, the state of the particles (orientation and contact) remain fixed and therefore the stiffness of these materials are not dependent on the state of stress within the material. In this sense unbound materials (soils) are more complicated, showing more pronounced non-linear stress dependent stiffness and strength properties with volume change tendencies even under operational load levels (Craig, 1992). The properties of the combined medium of soil are dependent on the forces between the particles and the amount of gas (air) and fluid (water) between the particles.

From a wave propagation point of view it is usually assumed that a particulate material can be modeled as a continuum if the wavelength is significantly larger than the particle size within the medium (Santamarina et al., 2001). Smaller wavelengths will be strongly attenuated from a combination of absorption and scattering (Jacobs and Owino, 2000). Cracks and surface roughness will have a similar effect on wave propagation parameters (Viktorov, 1967; Santamarina and Cascante, 1998; Hévin et al., 1998; Crane, et al., 1997).

Wave propagation speed (V_P and V_S) in soils is dependent on the skeleton stiffness of the particles, porosity, and degree of saturation. The P-wave velocity of propagation is dependent on both the bulk and shear stiffness while the S-wave velocity is only dependent on the shear stiffness (Equations 17 and 18). In saturated soils the bulk modulus of the fluid becomes the dominating parameter for P-wave propagation (Santamarina et al., 2001). In this case the P-wave velocity will give very little or no information on the skeleton stiffness of the particles, which is usually of primary interest in soil mechanics applications. In a soil with a lower degree of saturation both the P- and S-wave velocity of propagation will reflect the skeleton stiffness of the soil. This provides a unique possibility to monitor the undisturbed small strain stiffness of soils by using wave propagation methods. Approximate wave propagation velocities in materials that are relevant for this study are given in Table 1.

Table 1. Approximate velocities of different materials, from (Santamarina et al., 2001; Hall, 2000; Bodare, 1997)

Material	V_S (m/s)	V_P (m/s)	Density (kg/m^3)	Poisson's ratio
Concrete	1300-2800	2000-4600	2400	0.20
Asphalt*	600-2500	1100-4500	2300-2400	0.20-0.40
Pavement base	250-500	350-800	2100-2300	0.10-0.30
Clay, silt	40-300	100-600	1400-2000	0.40-0.50
Clay,silt (saturated)	40-250	1450	1400-2000	0.45-0.50
Sand	100-500	150-1000	1600-2000	0.15-0.35
Sand (saturated)	80-450	1450	2000-2300	0.45-0.50
Till	300-750	600-1500	1800-2300	0.20-0.40
Till (saturated)	250-700	1400-2000	2100-2400	0.45-0.50
Granite, Gneiss	1700-3500	3500-7000	2200-2600	0.20

***Viscoelastic material**

The *in-situ* state of effective stress and void ratio are the dominating factors influencing the skeleton stiffness of particulate materials, hence also the P-wave velocity in

unsaturated conditions and the S-wave velocity in both saturated and unsaturated conditions. The wave propagation velocity can be expressed as a function of the mean effective stress (σ'_0) with a power function as

$$V = \alpha\left(\frac{\sigma'_0}{1\,\text{kPa}}\right)^{\beta} \tag{49}$$

where α and β are empirical coefficients dependent on the contact properties between the particles. The coefficient β can be related to the geometry and contact plane of the particles and α is related to the relative density (void ratio), contact behavior, and fabric changes (Santamarina et al., 2001). Typical values for α and β and the relation between the coefficients are illustrated in Figure 11.

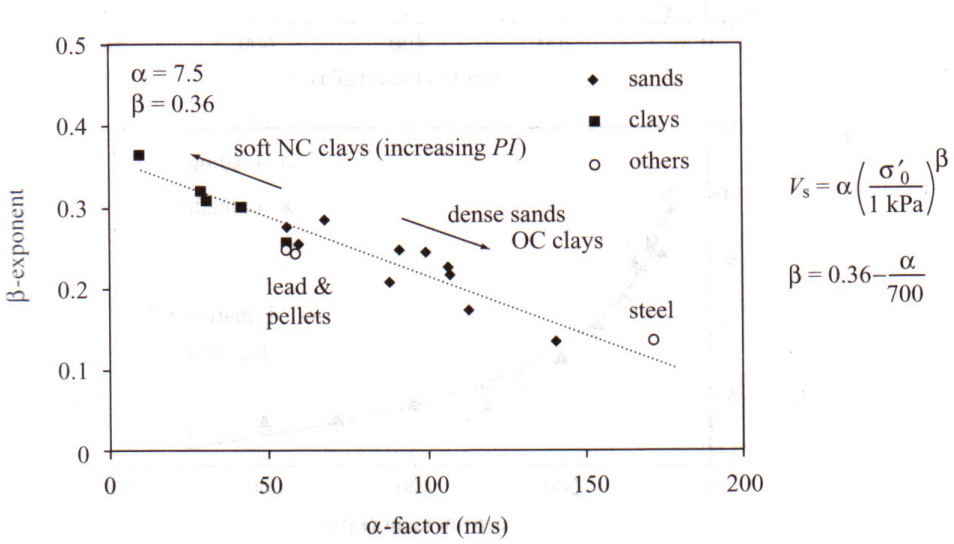

Figure 11. Typical values for α and β, from Santamarina et al., (2001). The proposed relation between α and β is indicated with a dotted line.

The empirical link between wave propagation velocity and the *in-situ* state of stress can be used to estimate the state of stress built up from compaction and soil suction by using seismic measurements in the field (Ekdahl et al., 2004). This assumes that the correct velocity-stress relation (α and β coefficients) has been determined for the specific type of soil and fabric and that the soil is not affected by ageing (cementation between particles) which also increases the small strain stiffness of the soil (Howie et al., 2002).

3.2 Pavement design and materials

The pavement structure consists of several individual layers, see Figure 12. From a bearing capacity point of view, the main purpose of the layers is to distribute traffic loads from vehicles to the underlying natural soil (subgrade). The main design criterion is that stress and strain developing from the traffic load must not exceed the capability of the material anywhere in the construction. Those parameters that have usually been regarded as critical are the strain level on the bottom of the asphalt layer (ε_1) and the strain level on top of the subgrade (ε_2), see Figure 12. However, the pavement construction should also be designed for other requirements like optimal drainage, low temperature cracking, low (or no) frost heave, and high tire friction.

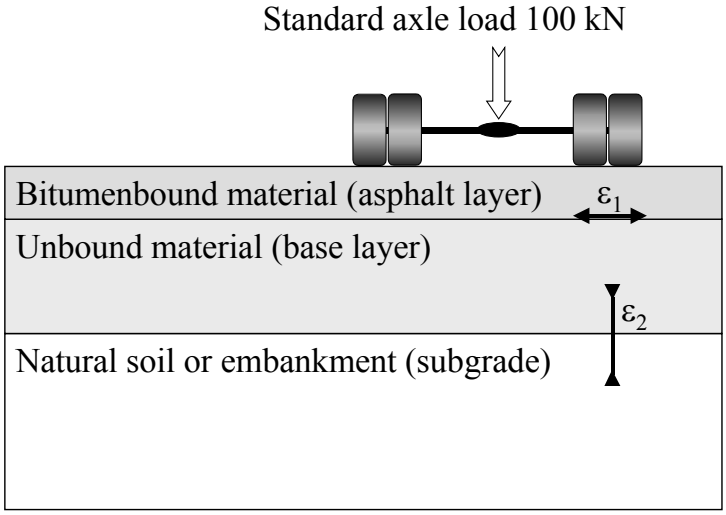

Figure 12. Schematic figure of pavement structure loaded with a standard axle load. Commonly used critical parameters in pavement design are strain level on the bottom of the asphalt layer (ε_1) and strain level on top of the subgrade (ε_2).

Traditionally, pavements have been designed and constructed from handbook-based specifications. These specifications have been more based on experience and empirical relations than on analytical design. Analytical design is the standard engineering procedure for design and analysis of most civil engineering constructions. Theoretical stresses and displacements are calculated from material properties and analysed in order to predict the final performance of a construction. Analytical design is progressively entering the pavement design specifications (Ullidtz, 1998). Among pavement authorities there is a shift towards "functional" contracts in which the contractor is required to take more responsibility for the design, construction, and maintenance of the pavement. Consequently, there is a larger need for analytical pavement design, where the construction can be analyzed and optimized in every single case.

Rehabilitation of existing pavements is becoming an increasing area of pavement engineering. Due to the increase in traffic amount and traffic loads, old pavements need

rehabilitation to maintain safety. A key issue here is to routinely investigate the structural status of the road network. With an efficient NDT technique the structural status can be mapped as a function of time and space providing a valuable tool in pavement design and management. This will become an important issue in order to maintain good quality pavements in an economical and technical efficient manner.

As pointed out in section 3.1.4 pavement materials are built up by particulate materials, with different phases (solid particles, gas, and fluid). Their properties are dependent on interparticle forces and interactions between the phases (Santamarina et al., 2001). Pavement materials are known to exhibit non-linear viscoelastic-plastic behavior, and are generally dependent on strain rate, strain level, stress level, shape of loading pulse, temperature and moisture content (Craig, 1992). The behavior of such materials is challenging to measure, describe, and predict. A certain idealization of the material behavior is inevitable.

Traditionally, pavement materials have been described as isotropic linear elastic. Isotropic linear elastic materials can be described with two individual constants, e.g. Young's modulus (E) and Poisson's ratio (ν). However, it has been shown that pavement models based solely on linear elastic theory are unable to successfully predict actual pavement response (COST 333, 1999). Consequently, more advanced constitutive models are being developed.

A framework for analytical pavement design has been developed by Ekdahl et al., (2004). This method is based on a non-linear elastic material model with a Mohr–Coulomb yield criterion representing a serviceability limit stress boundary. The main idea is that cyclic stresses below this boundary will result in stable behavior of the materials. Both field and laboratory tests are used to measure and validate the material properties used in the analytical design procedure. One of the most important parameters governing both the strength and stiffness of the unbound granular base layer is the *in-situ* isotropic mean effective stress level. The velocity-stress relation introduced in section 3.1.4 is used to estimate the stress level from seismic measurements (Santamarina and Potts, 1994; Santamarina and Cascante, 1996). Non-destructive seismic tests are conducted in the field during construction with the method developed in this thesis. From these tests the dynamic stiffness modulus, Poisson's ratio and thickness of each layer can be controlled directly in the field.

3.2.1 Asphalt

The asphalt layer is a composite material consisting of bitumen and different aggregate fractions (bituminous mix). The pure bitumen phase of the material is usually only 4-7% by weight but has a significant effect on the composite material properties (Nilsson, 2001). Bitumen behaves as an elastic material at low temperatures or short loading times, but at high temperatures or long loading times the behavior is viscous. In the range between these extremes the material is viscoelastic (Nilsson, 2003). Figure 13 shows the effect of loading time and temperature on a bituminous mix.

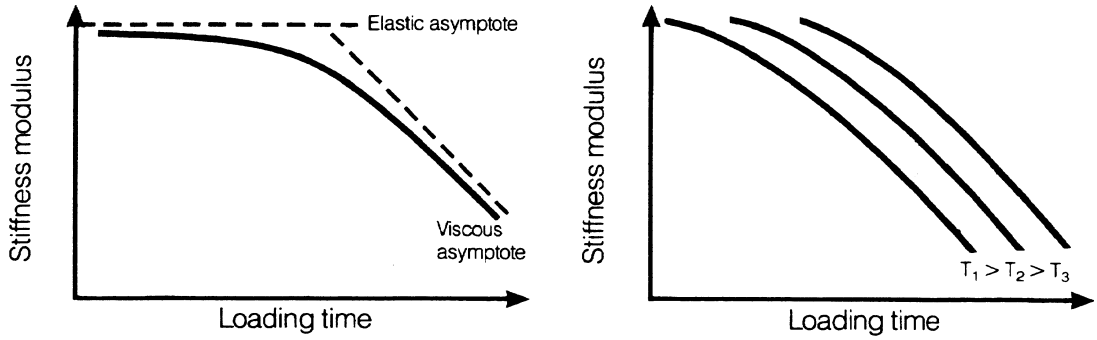

Figure 13. Asphalt stiffness modulus as a function of loading time and temperature. Different temperatures are represented with T1, T2, and T3, from Whiteoak (1990).

Since the asphalt material is viscoelastic the stiffness modulus cannot be defined by a constant. The complex stiffness modulus (E^*), is used to account for the viscous component, see Equation 50 (Ullidtz, 1998). The absolute value of E^* is referred to as the dynamic modulus ($|E^*|$) (Huang, 1993).

$$\left|E^*\right| = \sqrt{E_1^2 + E_2^2} \tag{50}$$

where E_1 is the storage modulus (elastic component), and E_2 is the loss modulus (viscous component). In polar coordinates the relation between the elastic and viscous components is represented by the phase angle (θ). The phase angle is given by taking the argument of the complex modulus according to

$$\tan\theta = \frac{E_2}{E_1} \tag{51}$$

To characterize the asphalt material a number of laboratory tests have been developed. The most versatile test is the frequency sweep test, also referred to as the dynamic modulus test (Huang, 1993). In the frequency sweep test, E^* is determined in a frequency range of 1-30 Hz at a fixed reference temperature. It is possible to expand this range by repeating the test at different temperatures (Nilsson, 2003). At low temperatures (<20° C) the frequency sweep test can be performed all the way down to 0.1 Hz. This technique is based on the principle of time-temperature correspondence, or thermo-rheological simplicity (Lee and Kim, 1998). A linear thermo-rheological material is defined as a material whose temperature changes, alter only the position of the viscoelasticity function referred to a frequency scale but not the general shape of the function (Martincek, 1994). The curve obtained by shifting measurements at different temperatures by a shift factor (α_T) is called master curve (Neifar and Benedetto, 2000), and is illustrated in Figure 14.

Alternatively, the complex shear modulus (G^*) can be determined in a similar way with the Superpave Shear Tester (Shenoy and Romero, 2000).

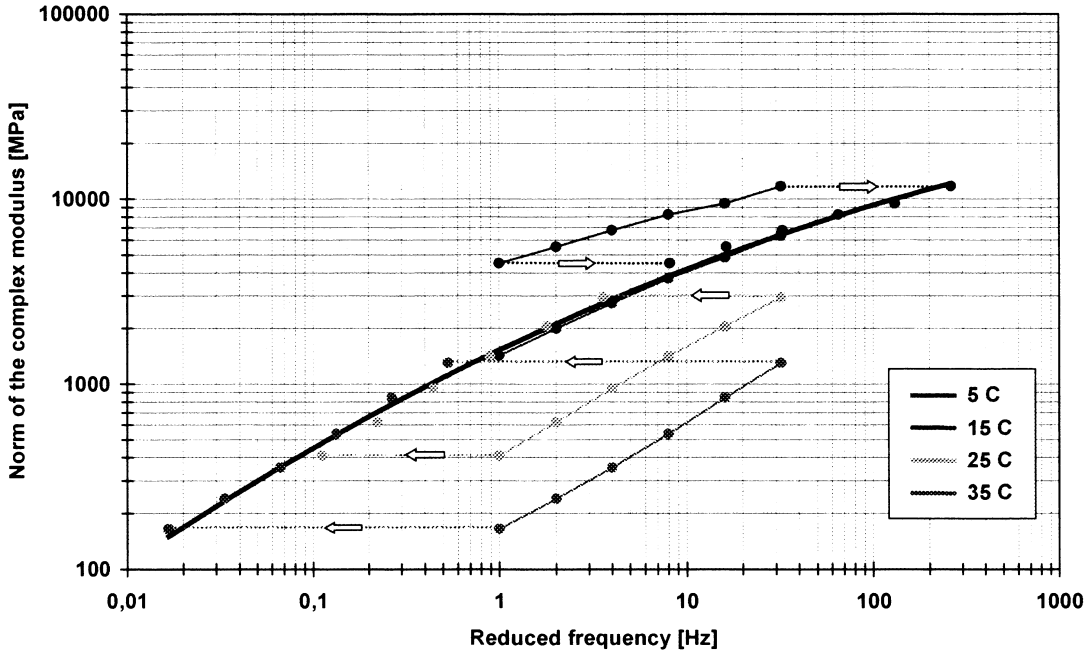

Figure 14. Master curve obtained from frequency sweep tests at different temperatures. The upper curve represents a temperature of 5 degrees. The 15 degrees values are chosen as a reference temperature and higher respectively lower temperature measurements have been horizontally shifted to match the 15 degrees reference curve, from Nilsson (1999).

It should be noted that today there is no method in use which can provide the mastercurve of the asphalt layer directly in the field. The Falling Weight Deflectometer (FWD) test is routinely used for quality control of the complete pavement construction (Ullidtz, 1998). The FWD test is based on deflection measurements at the surface resulting from a given dynamic load. The resulting deflections at different distances from the load are dependent on the thickness and stiffness of all layers in the pavement construction. If layer thicknesses are known, the *E*-modulus of each layer can be estimated from a backcalculation procedure (similar to the inversion of dispersion curves). Results have shown that this technique is more sensitive to the base and the subgrade layers and not very sensitive to the dynamic modulus of a thin asphalt layer (Aouad, 1993; Fonquinos, 1995). Quality control of the asphalt layer is usually based on core samples and laboratory tests.

3.2.2 Base and subgrade

The main purpose with the pavement layers is to spread the loads acting on the surface without exceeding the material capabilities. A granular material with a specified fraction gradation is regularly used as base material. The subgrade material is often the local natural soil or rock. However if the local soil is too soft, and an increased base or asphalt thickness is not enough, it may need to be stabilized (Lindh, 2000) or excavated and replaced by a soil of better quality. Both base and subgrade materials show a complex behavior, i.e. stress-dependency and non-linear stress-strain relationship (Larsson, 1994). The long-term response of the base and the upper part of the subgrade is shown as permanent (plastic) deformation, i.e., rutting at the pavement surface. Predicting this long-term response of pavement materials from physical material parameters is a challenging task and has been the objective of many recent studies, for example (Niekerk et al., 1998) and (Hornych et al., 1998).

Generally both granular and cohesive soils show a similar behavior in terms of stiffness properties. In Figure 15 the soil behavior is divided into three main groups related to the strain level, elastic region at very low strain levels, elasto-plastic in between, and failure at large strain levels.

Shearing strain	10^{-6}	10^{-5}	10^{-4}	10^{-3}	10^{-2}	10^{-1}
Phenomena	Wave propagation, vibrations		Cracks, differential settlement		Slide, compaction liquefaction	
Mechanical characteristics	Elastic		Elasto-plastic		Failure	
Effect of load repetition	◄					►
Effect of loading rate	◄					►
Properties	Shear-modulus, Poisson's ratio, Material damping				Angle of friction, cohesion	
Model of soil behavior	Linear elastic model		Equivalent linear models		Cyclic non-linear models	

Figure 15. Changes in soil behavior and other aspects as a function of shear strain, from Ishihara (1996).

As indicated in Figure 15 and discussed in section 3.1.4 above, wave propagation methods offer dynamic stiffness properties representative for very low strain levels. The most important soil stiffness parameter at low strain levels is the shear modulus (G) (Bodare, 1997; Massarsch, 1999). The shear modulus can be calculated from the shear wave velocity by using

$$G = \rho V_S^2 \tag{52}$$

where ρ is the bulk density of the material. This equation expresses the same relation as given previously in Equation 18. As discussed in section 3.1.4, both the shear modulus and the shear wave velocity is profoundly dependent on the skeleton stiffness (mean effective state of stress) of particulate materials. The general stress and strain dependency of the shear modulus is illustrated in Figure 16. The maximum or initial *G*-modulus is often termed G_{max} or G_0. Tawfiq et al., (2000) proposed to combine seismic and deflection based tests to obtain the curvilinear modulus relation of the base material in pavements, Figure 16.

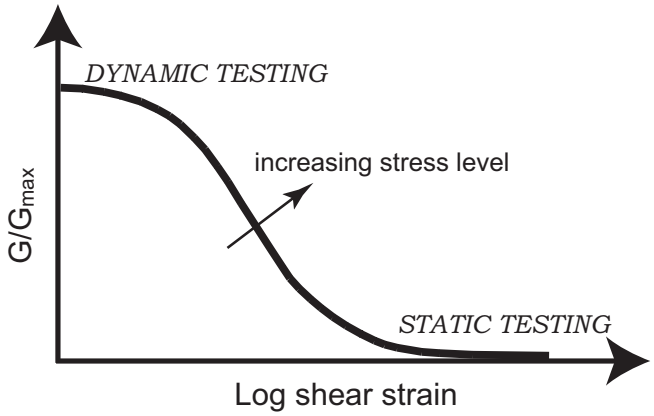

Figure 16. Schematic illustration showing shear modulus stress and strain dependency.

Young's modulus *E* can be determined from the *G* modulus and Poisson's ratio (ν) by using

$$E = 2G(1+\nu) \tag{53}$$

Generally the *E*-modulus follows the same behavior as the *G*-modulus shown in Figure 16. Similar to the velocity-stress relation presented in section 3.1.4 the modulus-stress relation can also be expressed with a power function as

$$E_{\max} = K(\sigma_m)^n \tag{54}$$

here *K* and *n* are empirical material dependent constants similar to α and β in Equation 49. For granular materials the *n* factor has been found to be in the order of 0.5 (Biarez et al., 1999) which corresponds to a β exponent of 0.25, see Figure 11. Based on an extensive number of triaxial tests on both sand and clay, Biarez et al. (1999) proposed that *K* could be expressed as a function of void ratio (*e*) as

$$K = \frac{500}{e} \tag{55}$$

when both E_{max} and σ_m are expressed in MPa. It should be noted that this relation is in close agreement with the results based on wave propagation tests presented by Santamarina et al. (2001).

In a plastic cohesive soil the plasticity index (*PI*) also affects the modulus. Many studies have resulted in material models (constitutive laws), which consider that the modulus is dependent on both stress and strain level, for example (Jamiolkowski et al., 1991; Ishibashi and Zhang, 1993; Ekdahl, 1997; Ekdahl et al., 2004).

When the *E*- or *G*-modulus is determined from field or laboratory tests it is important to relate the measured value to the specific strain and stress level. Different methods usually affect the material in different ways and therefore absolute values from different tests cannot be compared without taking the non-linear stress and strain behavior into account. The G_{max} modulus is often determined from seismic velocity measurements, which can be performed both in the laboratory and in the field.

3.3 Seismic pavement testing, a literature review

The main objective with seismic non-destructive testing (NDT) of pavements is to estimate the unknown structural properties (thickness and stiffness) of the different layers in a pavement construction. With an efficient NDT technique these properties can be mapped as a function of time and space, providing a valuable tool in pavement design and management. Methods based on surface wave propagation hold the potential to provide this information.

Surface wave methods are based on the dispersive nature of surface waves in a layered medium. The basic approach can be divided into two steps, (1) measure an experimental dispersion curve on the pavement surface, and (2) estimate a layer model by matching the measured dispersion curve with a theoretical dispersion curve from a known layer model (inversion). The first step is the most critical part of any surface wave method. Therefore the following review of surface wave testing of pavements is focused on the measured dispersion curve. The second step where a theoretical dispersion curve (as described in section 3.1.3) is iteratively matched with the experimental dispersion curve is only briefly covered. More information about inversion of surface wave dispersion curves can be found elsewhere (Yuan and Nazarian, 1993; Williams and Gucunski, 1995; Tokimatsu, 1997; Xia et al. 1999; 2000b; Beaty et al., 2002).

The dispersion curve shows the phase velocity (V_{ph}) as a function of frequency (*f*). The main objective with surface wave measurements is therefore to measure phase velocities at known frequencies along the pavement surface. Before the established surface wave methods are described, some fundamentals of the measured parameters are given. Here we recall the assumption that a single mode of harmonic plane wave propagation in the x_1 direction can be described with F ($F = Ae^{i\phi} = Ae^{i(k_1 x_1 - \omega t)}$) defined in Equation 25. The amplitude (A) is here included for completeness and it is unity in this example. We study a single frequency component, f=100 Hz ($\omega=2\pi f$), with a phase velocity V_{ph}=200 m/s

($k=\omega/V_{ph}$). Figure 17 shows a three-dimensional (3-D) image of the real component of the wavefield F in space (x_1), time (t), and amplitude (A). The periodicity is given by the wave number (k_1) and angular frequency (ω). The value of F is complex and can be defined with amplitude and phase (ϕ) as shown in the two 2-D time and space projections in Figure 17. The phase of one cycle is defined from $-\pi$ to π and therefore the phase plots wraps around after each period (P) or wavelength (λ). Since we are only interested in the phase velocity along the x_1 direction it is the phase values in this dimension that need to be measured. By measuring the phase difference ($\Delta\phi$) over a known distance (Δx) at a certain frequency, the phase velocity can be calculated as

$$V_{ph} = \frac{\omega \Delta x}{\Delta \phi} \tag{56}$$

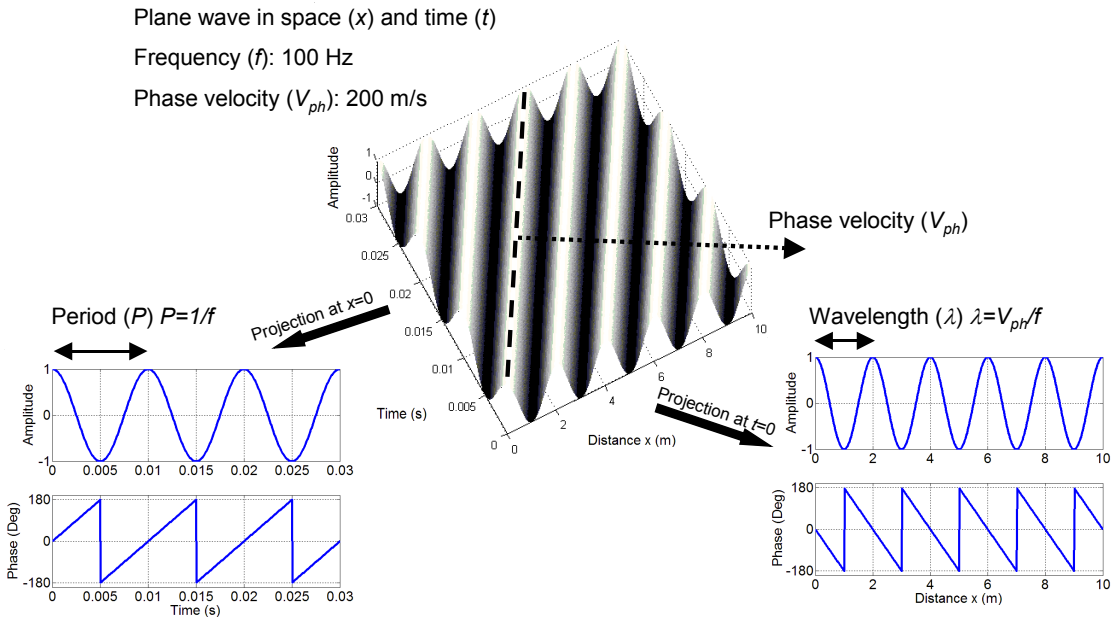

Figure 17. A plane wave in space and time. The phase velocity vector is indicated with an arrow.

3.3.1 The steady state vibration method

The steady state vibration technique, also called the Continous Surface Wave (CSW) method, was the first attempt to map stiffness of the surface layers by measuring surface wave dispersion. The method was developed in the 1950s and 1960s (Van der Poel, 1951; Jones, 1955; 1962). Sezawa (1938a; 1938b) and Pickett (1945) made the theoretical derivation that showed the possibility to map dispersion of surface waves where the stiffness decreases as a function of depth, i.e. pavement profile. However, at this point there were some speculations regarding the nature of surface wave propagation in this type of layered system (Press and Dobrin, 1956). Jones (1962) was first to acknowledge that phase velocities greater than the shear wave velocity of the subgrade represent leaky

waves and must be calculated with a complex wave number. The work by Jones (1962) was refined by Vidale (1964) who studied theoretical dispersion curves from pavement systems in the complex wave number domain. However, without modern computers these studies became limited. Martincek (1994) concluded that even with modern computers it is very difficult to calculate dispersion curves from pavement systems in the complex wave number domain.

The early steady state measuerements on pavement systems were presented by Van der Poel (1951), Heukelom and Foster (1960), Jones (1955; 1958; 1962), and Vidale (1964). In the steady state method, a vibrator is used as a seismic source and one geophone is used as receiver. The geophone is moved progressively away from the vibrator to map wavelengths on the surface with the specified frequency. Originally only successive amplitude maximums as related to the source signal were measured as a function of offset (distance) from the source (Van der Poel, 1951). The length between two maximums corresponds to one wavelength (λ), see Figure 17. This procedure is repeated for different frequencies and Equation 57 is then used to calculate the phase velocity at different frequencies to obtain the complete dispersion curve.

$$V_{ph} = \lambda f \tag{57}$$

In a further development of the method the absolute phase angle was measured at smaller increments from the source for more detailed measurements (Martincek, 1994).

Figure 18 shows the result from early steady state measurements by Heukelum and Foster (1960). In Figure 18a, the measured dispersion curve is divided into three portions which are interpreted to correspond to each layer in the pavement construction. In this example the depth to each layer in the pavement construction has been correlated to the wavelength divided by two. This simplified evaluation technique was used in the early experiments but was later concluded to be a too crude approximation (Jones, 1962; Vidale 1964).

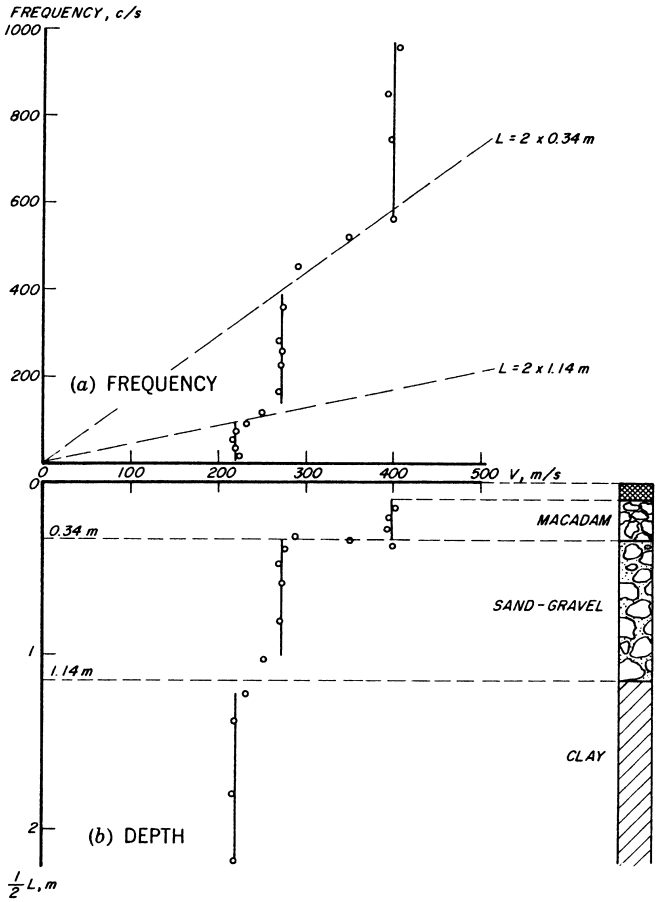

Figure 18. Result from the steady state vibration method on a pavement profile. The depth to each layer interface has been correlated with the wavelength divided by 2, from Heukelum and Foster (1960).

In the early 1980s, the steady state method was improved because of the progress in computer power at that time (Gordon, 1997), and is thereafter mostly referred to as the CSW method. Data acquisition could be performed digitally with several receivers and the measuring process became much faster. The evaluation (inversion) of soil site layer properties was approached with refined theories (Tokimatsu et al., 1991), but the evaluation of pavement layer properties was still regarded as a quite complex issue (Martincek, 1994).

3.3.2 The Spectral Analysis of Surface Waves (SASW) method

Heisey et al. (1982) first introduced the Spectral Analysis of Surface Waves (SASW) method. Since then a lot of research has been conducted, mainly at the University of Texas at Austin (Nazarian et al, 1983; Nazarian, 1984; Nazarian et al., 1987; Rix et al., 1991; Aouad, 1993; Stokoe et al, 1994; Fonquinos, 1995). Hiltunen and Gucunski (1994) presented an "Annotated bibliography on SASW" with 41 SASW abstracts, about half of these publications are focused on pavement testing. As described above the fundamental

approach to measure surface wave phase velocity at different frequencies was already established in the steady state method (Jones, 1955). However the instruments required for real time Fast Fourier Transformation (FFT) had not yet become available. The FFT made it feasible to measure a whole range of frequencies simultaneously. This revolution in digital data acquisition made the SASW method possible (Rix and Santamarina, 2000).

Several publications in recent years have described the SASW method in detail (Aouad, 1993; Stokoe et al., 1994; Stokoe and Santamarina, 2000; Svensson, 2001). The essential elements in the field procedure are the measurement of surface waves between two receivers located a known distance apart on the pavement surface. Figure 19 shows the principle set-up of the experimental arrangement for a SASW test.

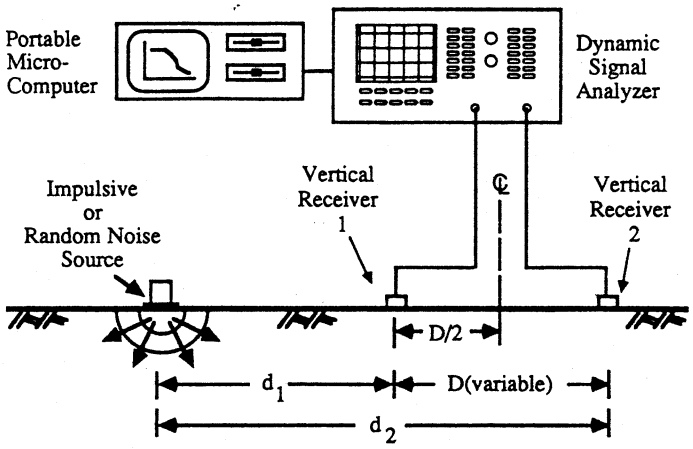

Figure 19. Schematic of experimental arrangement for SASW tests, from Rix et al. (1991).

In the SASW method, the phase difference ($\Delta\phi$) between two receivers is measured for a number of frequencies, by means of a transient impulse applied to the pavement surface, see Figure 19. The phase velocity (V_{ph}) of a specific frequency of surface waves is calculated from the phase difference $\Delta\phi$ and the receiver spacing ($D=\Delta x$) with Equation 56. Therefore, $\Delta\phi$ is the most critical parameter extracted from the measured data because it determines the accuracy of the dispersion curve constructed afterwards. The coherence function is a quality factor, used in the field to verify if the signals recorded at the receivers are descendent from the same source (Santamarina and Fratta, 1998). Good coherence results in a coherence value close to 1.0. Non-coherent noise that enters the measurements results in a lower coherence value. This information is used to judge which frequency span that can be used when the dispersion curve is calculated from the measured phase difference.

Usually there is only a limited range of frequencies at each receiver spacing (D) that can be used for the dispersion curve calculation. This limitation is usually referred to originate from the near- and far-field effect. The SASW method assumes plane surface wave propagation (Figure 17) between the receivers and a smooth continuous dispersion curve that can be determined through the wrapped phase difference spectrum. However,

every surface wave frequency component needs to propagate a certain distance from the source before plane wave propagation can be assumed (Ganji et al., 1998). This near-field effect usually extends about one half wavelength from the source (Stokoe et al., 1994), but is site specific. There is also a far-field effect where high frequency surface waves are contaminated by body waves (Park et al., 1999c). The criteria that sets the limit of frequencies (or wavelengths) that can be used for the dispersion curve calculation from a given set-up geometry is often addressed as the "wavelength filter criteria". Table 2, summarizes different recommended field configurations (according to the denominations in Figure 19) as a function of measured wavelength.

Table 2. Recommendations from different researchers on the SASW set-up according to the wavelength filter criteria. The denominations used are presented in Figure 19, from Ganji et al. (1998).

Reference	(d_1) criteria	(D) criteria
Lysmer (1966)	$2.5\lambda<d_1$	-
Heisey et al. (1982)	$d_1=D$	$0.3333\lambda<D<2\lambda$
Sanchez-Salinero et al. (1987)	$d_1=D$	$2\lambda<D$
Roesset et al. (1989)	$0.5\lambda<d_1<2\lambda$	$0.5d_1<D<d_1$
Gucunski and Woods (1992)	-	$0.5\lambda<D<4\lambda$
Tokimatsu et al. (1991)	$0.25\lambda<d_1+(D/2)$	$0.0625\lambda<D<\lambda$

To calculate the dispersion curve from the measured wrapped phase spectrum the unwrappping process must first be resolved correctly (Al-Hunaidi, 1992). As seen in Figure 20 the measured phase difference is defined as a value between –180 and 180 degrees. When the phase difference becomes larger than 180 or -180 degrees it wraps around. The absolute phase difference for a specific frequency is often more than 180 degrees, i.e. the number of total "wrap arounds" needs to be determined in order to calculate a correct phase velocity.

After the phase unwrapping process has been conducted, the phase velocity at each frequency can be calculated. Figure 21 shows the resulting dispersion curve from the data presented in Figure 20. Heisey's wavelength filter criterion from Table 2 is marked to illustrate the recommended acceptable range of frequencies. Several measurements recorded with different spacing between the receivers are usually necessary to cover all frequencies (or wavelengths) of interest.

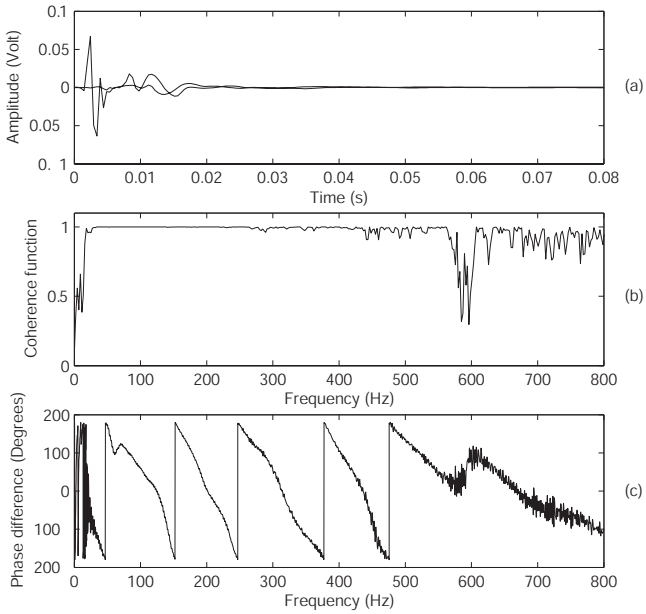

Figure 20. Example from SASW field plots received instantly on site. In (a) time signals from both receivers, (b) the coherence function of the recorded signals, and (c) the wrapped phase of the cross power spectrum. The example is taken from a SASW test on a pavement construction with receiver spacing, D=1.3 meters.

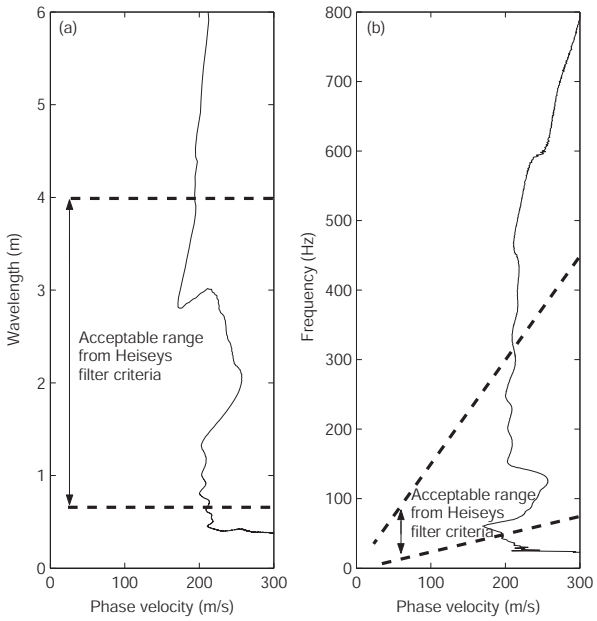

Figure 21. Calculated dispersion curve from data in Figure 20, (a) wavelength domain and (b) frequency domain. Marked line shows the usable range according to the wave filter criteria presented by Heisey et al. (1982).

Finally a compact dispersion curve is constructed from the individual dispersion curves at each receiver spacing. The final dispersion curve assembled in this way has a broader frequency range compared to each individual dispersion curve, which is necessary for the inversion of a shear wave velocity with depth profile. The complete procedure, as presented by Wu et al. (2002), from SASW measurements to an inverted layer model is summarized in Figure 22.

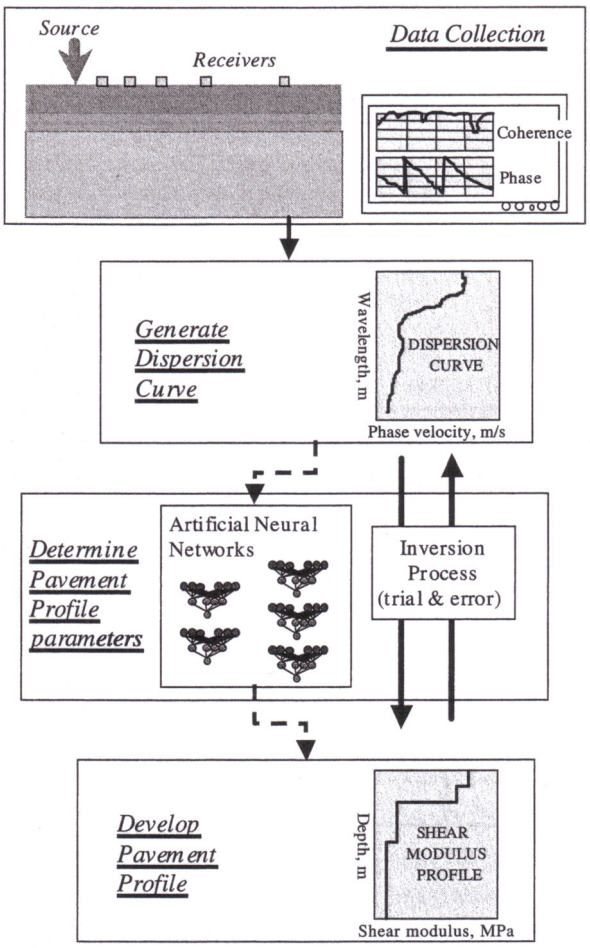

Figure 22. SASW flow chart, from Wu et al., (2002).

The inversion of pavement layer properties from the compact dispersion curve obtained with the SASW method has proved to be a challenging task. The initial procedure was based on a normal mode theoretical dispersion curve as described in section 3.1.3. The difference between the measured and theoretical dispersion curve was first minimized with a manual trial and error procedure (Nazarian, 1984). Hossain and Drnevich (1989) presented an automatic procedure based on a finite difference method to calculate the theoretical dispersion curve and a linearized optimization technique to minimize the difference between the measured and theoretical dispersion curve. A similar method was later presented by Yuan and Nazarian (1993). These techniques are all based on a normal

single mode dispersion curve. However, it was later found that the compact dispersion curve obtained from the SASW test on pavements is actually dependent on the receiver locations and formed by superposition of different modes of propagation (Roesset et al., 1990; Gucunski and Woods, 1992; Tokimatsu et al., 1992). To overcome this problem a new procedure based on a theoretical simulation of the complete test set-up was proposed (Williams and Gucunski, 1995). The main objective with this approach is to implicitly reproduce the same distortions in the theoretical dispersion curve as present in the measured dispersion curve. This technique was first implemented with a neural network to find the best matching theoretical dispersion curve (Williams and Gucunski, 1995; Gucunski et al., 1998; Kim and Kim, 1998; Wu et al., 2002). Al-Hunaidi (1998) used the same procedure in combination with genetic algorithms, and Ganji et al., (1998) used a non-linear matrix based inversion technique for the optimization routine. Recently Rambod and Gucunski (2003) proposed to use simulated annealing to find the best matching theoretical dispersion curve.

3.3.3 Experiences gained from seismic pavement testing

Surface wave measurements have been continuously enhanced and proved to be useful for pavement testing (Aouad, 1993; Yuan et al., 1998; Nazarian et al., 1999). At normal soil sites, where the seismic velocity increases with depth, surface wave methods have proved successful in a number of applications (Matthews et al., 1996; Miller et al., 1999; Stokoe and Santamarina, 2000; Park et al., 1999a). In both soil mechanics (Abbis, 2001) and pavement design (Haegeman, 2002; Abdallah et al., 2003; Ekdahl et al., 2004) material models based on the result of surface wave measurements are starting to develop. However, difficulties with the measuring procedure in seismic pavement testing are still reported. In the millennium paper from the Transportation Research Board (TRB) on the characteristics of pavement sections, it was concluded that seismic wave based testing shows great potential but requires further work by the research community (Scullion et al., 2000).

Much of the work reported in this thesis originates from the reported and experienced difficulties with surface wave testing of pavements (Ryden, 1999). The evaluation of the top layer thickness and stiffness has proved to be most efficient and accurate (Roesset et al., 1990; Akhlaghi and Cogill, 1994). The inversion of deeper embedded layers has been the most challenging part in surface wave testing of pavements (Ganji et al., 1998; Gucunski et al., 2000). Particularly the embedded second layer (base) underneath the asphalt layer has been difficult to resolve (Aouad, 1993; Wu et al., 2002). Reported difficulties and experience gained from the conventional methods are summarized below.

From the pioneer studies on seismic pavement testing, Van der Poel (1951), Heukelum and Foster (1960), and Vidale (1964) concluded that there existed discontinuities in the measurements of surface waves on pavements, manifested in two ways:

- Theoretically it was found that the dispersion curve from pavement profiles was not continuous, but was divided into several branches of dispersion curves.

- For some frequencies it was discovered that the phase velocity along the surface was not constant but sometimes changed from a lower to a higher velocity at a certain offset.

The branching phenomenon was studied by Jones (1962) and Vidale (1964). One of the models studied by Vidale (1964) is presented in Figure 23. This model represents a two-layer object where a higher velocity layer overlies a lower velocity half-space. The dispersion curve is plotted on coordinates normalized with respect to the properties of the first layer. Two branches in the dispersion curve are visible.

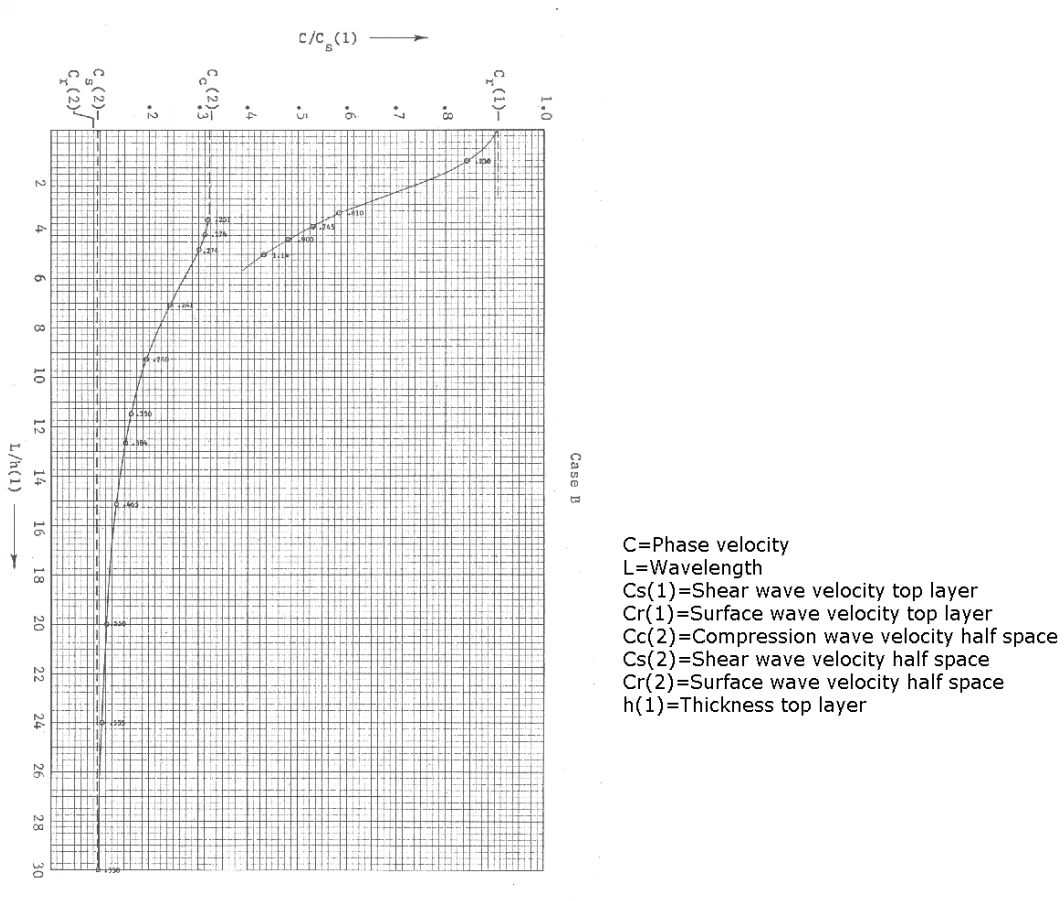

Figure 23. Dispersion curve from a two-layer model where a higher velocity layer overlays a lower velocity half-space. Two branches in the dispersion curve can be seen. The dispersion curve is plotted on coordinates normalized with respect to the properties of the first layer, from Vidale (1964).

The observed change in phase velocity with the offset (distance) from the source is exemplified in Figure 24. Ullidtz (1987) and Martincek (1994) also reported on this phenomenon. The observed change in phase velocity with distance from the source can possibly be explained from the branching phenomenon studied by Vidale (1964). At frequencies where there is an abrupt transition from one phase velocity to another there will be modal interference affecting both the amplitude and phase along the surface.

What is measured at the surface is the dominating phase velocity at that particular offset and frequency.

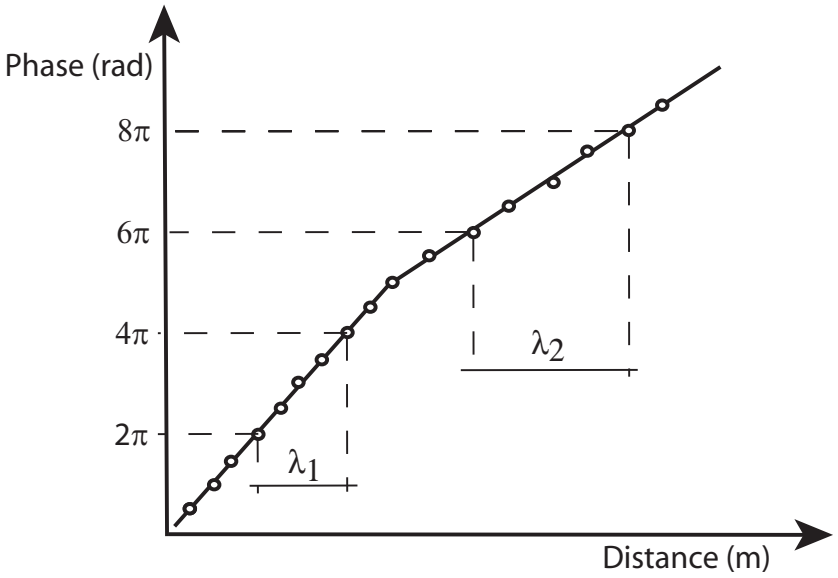

Figure 24. Result from a steady state measurement on a pavement profile. The horizontal axis shows the offset (distance) from the source and the vertical axis shows the phase angle. At one single frequency there are two phase velocities (slope of line) observed, from Martincek (1994).

The early findings exemplified in Figure 23 and Figure 24 was the result of a very detailed analysis of surface wave propagation in pavement structures. Both the theoretical calculations and field measurements were very time consuming which may explain why there was not much published in the 1970's on surface wave testing of pavements. The amount of studies increased significantly in the 1980's after the introduction of the much faster SASW method. However, some of the findings by the pioneers of the steady state method tended to be overlooked in the new studies. Almost all studies were conducted with the SASW approach using only two receivers. If the phase-distance relation is not constant and linear as in Figure 24 it is evident that the phase difference measured between two receivers will be a tricky task.

Several authors have reported on limitations and difficulties related to the two receiver approach methods, at both soil and pavement sites. These problems include the influence of higher modes of surface waves (Rix et al., 1991; Tokimatsu, 1992; Stokoe et al., 1994), variation of phase velocity with distance from the source (Foti, 2000), near- and far-field effects (Fonquinos, 1995), contamination from reflected surface waves (Sheu et al., 1988) see Figure 25, contamination from reflected and direct body waves (Hiltunen and Woods, 1990; Tokimatsu, 1997), non-uniqueness (Ganji et al., 1998), difficulty with phase unwrapping (Al-Hunaidi, 1992), and time consuming testing procedures and data reduction (Hiltunen and Woods, 1990). Several researchers have been studying these limitations. They have proposed a variety of alternatives to minimize these influences.

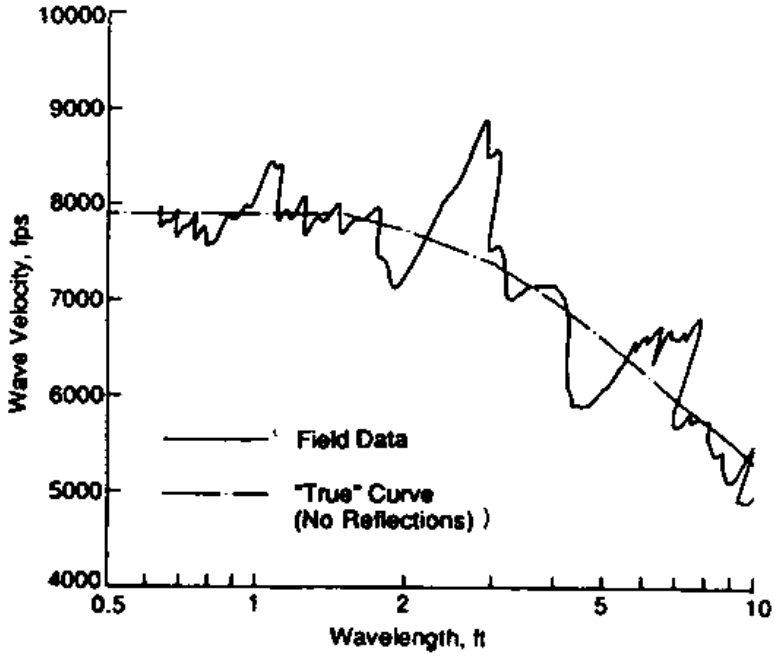

Figure 25. Fluctuations in the measured dispersion curve have been interpreted to originate from reflected surface waves, from Sheu et al. (1988).

The first and most simple solution was to use a phase velocity-wavelength domain filter criterion (Table 2) that maximizes the response from the fundamental mode surface wave (Sanchez-Salinero et al., 1987; Roesset et al., 1990), followed by more sophisticated solutions like numerical simulation of the complete test set-up (Gucunski and Woods, 1992; Ganji et al., 1998) and identification of particle orbits (Tokimatsu et al., 1991). Nazarian and Desai (1993) proposed a method for faster data reduction. All these proposed alternatives improved, to a certain extent, overall performance of the seismic surface wave testing method based on two receiver measurements. However, the seismic phenomena of the pavement system and the distribution between different seismic events were still not clear. The influence of higher modes of surface waves has been a topic of particular speculation.

McMechan and Yedlin (1981) showed that multiple modes of surface waves at a soil site could be resolved by using multichannel data and a two-dimensional (2-D) wavefield transformation technique, the τ-p transformation. Using a 288 channel shot gather at a soil site, Gabriels et al. (1987) successfully separated different modes of surface waves with multichannel measurements and a 2-D Fourier transformation, f-k transformation. At the Kansas Geological Survey (KGS) a method called Multichannel Analysis of Surface Waves (MASW) (Park et al., 1996; 1999c), has been developed. The method utilizes multichannel shot gathers for detailed surface wave analysis. The shot gather is transformed from the offset-time (x-t) domain into the frequency-phase velocity (f-V_{ph}) domain by using a modified version of the τ-p transformation by McMechan and Yedlin

(1981). With this technique fundamental and higher mode dispersion curves from surface waves can be extracted (Park et al., 1998b; 1999b; 2000a; 2001). The MASW transformation technique is described in Paper I of this thesis. Multichannel measurements and 2-D wavefield transformation techniques are now widely utilized in surface wave soil site applications (Zywicki, 1999; Foti, 2000; Beaty et al., 2002; O'Neill, 2003; Strobbia, 2003; Moro et al., 2003; Forbriger, 2003)

The MASW method has so far been applied to geoenvironmental projects to map bedrock surface and find fracture zones where contamination can be spread with ground water (Miller et al., 1999) and (Xia et al., 2000a), locate buried objects under the ground surface (Park et al., 1998a; 1999a), map V_S in water-bottom sediments with underwater MASW (Park et al., 2000b), perform joint analysis of both surface waves and refracted body waves (Ivanov et al., 2000a; 2000b). In this thesis the MASW transformation technique is utilized in surface wave testing of pavements. The idea of using a 2-D wavefield transformation technique in surface wave testing of pavements was originally proposed by Al-Hunaidi and Rainer (1995). However, no field measurements could verify their theory because high frequency multichannel data could not be easily obtained.

The reported difficulties with the SASW method and the development of multichannel surface wave techniques are the seeds for improvements used in the present work.

3 Field of research

4 References

Abbis, C.P., 2001, Deformation of landfill from measurements of shear wave velocity and damping, *Geotechnique,* Vol. 51, No. 6, pp 483-494.

Abdallah, I., Yuan, D., and Nazarian, S., 2003, Validation of software developed for determining design modulus from seismic testing, Research Report 1780-5, Center for Highway Materials Research, the University of Texas at El Paso, TX.

Akhlaghi, B.T., and Cogill, W.H., 1994, Application of the free plate analogy to a single-layered pavement system, *INSIGHT,* Vol. 36, pp 514-518.

Al-Hunaidi, M.O., 1992, Difficulties with phase spectrum unwrapping in spectral analysis of surface waves nondestructive testing of pavements, *Can. Geotech. J.,* Vol. 29, pp 506-511.

Al-Hunaidi, M.O., and Rainer, J.H., 1995, Analysis of multi-mode signals of the SASW method, *Proc 7th Int. Conf. Soil Dynamics and Earthquake Eng.,* pp 259-266.

Al-Hunaidi, M. O., 1998, Evolution-based genetic algorithms for analysis of non-destructive surface wave tests on pavements, *NDT&E International*, Vol. 31, No. 4, pp 273-280.

Aouad, M.F., 1993, Evaluation of Flexible Pavements and Subgrades Using the Spectral-Analysis-of-Surface-Waves (SASW) Method, PhD thesis, Univ. of Texas at Austin, Texas.

Beaty, K.S., Schmitt, D.R. and Sacchi, M., 2002, Simulated annealing inversion of multimode Rayleigh wave dispersion curves for geological structure, *Geophys. J. Int.* Vol. 151, pp 622-631.

Bedford, A., and Drumheller, D.S., 1994, *Introduction to elastic wave propagation*, John Wiley & Sons.

Biarez, J., Liu, H., Gomes Correia, A., and Taibi, S., 1999, *Stress-strain characteristics of soils interesting the serviceability of geotechnical structures, Pre-failure Deformation Characteristics of Geomaterials*, Balkema, Rotterdam, ISBN 90 5809 075 2.

Bodare, A., 1997, Jord och Bergdynamik, Department for soil and rock mechanics, Royal Institute of Technology, Stockholm, Sweden.

Buchen, P.W., and Ben-Hador,R., 1996, Free-mode surface-wave computations, *Geophys. J. Int.*, Vol. 124, pp 869-887.

COST 333, 1999, *Development of new bituminous pavement design method*, EUR 18906.

4 References

Craig, R.F., 1992, *Soil Mechanics*, 5th edition, Chapman and Hall, London, ISBN 0-412-39590-8.

Crane, L.J., Gilchrist, M.D., and Miller, J.J.H., 1997, Analysis of Rayleigh-Lamb wave scattering by a crack in an elastic plate, *Computational Mechanics,* Vol. 19, pp 533-537.

Cremer, L., and Heckl, M., 1988, *Structure-borne sound: Structural vibrations and sound radiation at audio frequencies*, second edition, Springer-Verlag, Berlin.

Ekdahl, U., 1997, Kung Oscars bro, planskild korsning i Lund, Grundläggningsdagen 97, Swedish Geotechnical Society Publication.

Ekdahl, U., Bengtsson, P. E., and Ryden, N., 2004, A new framework for analytical pavement design based on systematic control during construction work, Proceedings of the 14th Nordic Geotechnical Meeting (NGM 2004), Ystad, Sweden, May 19-21.

Fonquinos Mera, R., 1995, Dynamic nondestructive testing of pavements, PhD thesis, Univ. of Texas at Austin, Texas.

Forbriger, T., 2003, Inversion of shallow-seismic wavefields part 1: wavefield transformation, *Geophysical Journal International,* Vol. 153, pp 719-734.

Foti, S., 2000, Multistation methods for geotechnical characterization using surface waves, PhD thesis, Politecnico di Torino, Italy.

Gabriels, P., Snider, R., and Nolet, G., 1987, In situ measurements of shear-wave velocity in sediments with higher-mode Rayleigh waves, *Geophys. Prospecting,* Vol. 35, pp 187-196.

Ganji, V., Gucunski, N., and Nazarian, S., 1998, Automated inversion procedure for spectral analysis of surface waves, *J. Geotech. Engrg.,* ASCE, Vol. 124, No. 8, pp 757-770.

Gordon, M.A., 1997, Application of field seismic geophysics to the measurement of geotechnical stiffness parameters, PhD thesis, Univ. of Surrey, UK.

Graff, K.E., 1975, *Wave motion in elastic solids*. Oxford University Press, London.

Gucunski, N., and Woods, R.D., 1992, Numerical simulation of the SASW test, *Soil Dyn. and Earthquake Engrg. J.,* Vol. 11, No. 4, pp 213-227.

Gucunski, N., Krstic, V., and Maher, M.H., 1998, Backcalculation of pavement profiles from the SASW test by neural networks, Chapter 8 in *Artificial Neural Networks for Civil Engineers: Advanced Features and Applications*, I. Flood and N. Kartam Eds., ASCE, pp 191-222.

4 References

Gucunski, N., and Maher, A., 2000, Evaluation of the dynamic response of pavements and other layered systems using the stiffness matrix approach, Proceedings 79th Annual Meeting, Transportation Research Board, Washington D.C. Paper No. 00-0134.

Haegeman, W., 2002, In situ assessment of stiffness of a road sand embankment, Proceedings of the BCRA 2002, Lissabon, Portugal. pp 629-635.

Hall, L., 2000, Simulations and analyses of train-induced ground vibrations, Ph.D. thesis, Royal Institute of Technology, Stockholm, Sweden.

Haskell, N. A. 1953, The dispersion of surface waves on multilayered media, *Bull. Seismological Soc. of Am.,* Vol. 43, No. 1, pp 17-34.

Heisey, J.S., Stokoe II, K.H., and Meyer, A.H., 1982, Moduli of pavement systems from Spectral Analysis of Surface Waves, *Transp. Res. Rec*., 852, Washington D.C, pp 22-31.

Heukelom, W., and Foster, C.R., 1960, Dynamic testing of pavements, *Journal of the Soil Mechanics and Foundations division*, ASCE, Vol. 86, No. SM1, Part 1, pp 2368-2372.

Hévin, G., Abraham, O., Pedersen, H.A., and Campillo, M., 1998, Characterization of surface cracks with Rayleigh waves: a numerical model, *NDT&E International,* Vol. 31, No. 4, pp 289-297.

Hiltunen, D.R., and Woods, R.D., 1990, Variables affecting the testing of pavements by the surface wave method, *Transp. Res. Rec*., 1260, pp 42-52.

Hiltunen, D.R., and Gucunski, N., 1994, Annotated bibliography on SASW, in Geophysical characterization of sites. ISSMFE Technical Committee #10, edited by R.D. Woods, Oxford Publishers, New Delhi.

Hornych, P., Kazai, A., and Piau, J.M., 1998, Study of the resilient behaviour of unbound granular materials, Proceedings of the 5th International Conference on the Bearing Capacity of Roads and Airfields (BCRA), Trondheim, Norway, pp 1277-1287.

Hossain, M.M., and Drnevich, V.P., 1989, Numerical and optimization techniques applied to surface waves for backcalculation of layer moduli, In ASTM special technical publication 1026, Nondestructive testing of pavements and backcalculation of moduli, Editors Bush III, A.J., and Baladi, G.Y., pp 649-669.

Howie, J.A., Shozen, T., and Vaid, Y.P., 2002, Effect of ageing on stiffness of very loose sand, *Canadian Geotechnical Journal,* Vol. 39, pp 149-156.

Huang, Y.H., 1993, *Pavement analysis and design*, Prentice Hall, New Jersey, ISBN 0-13-655275-7.

4 References

Ingard, K.U., 1988, *Fundamentals of waves and oscillations*, Cambridge University Press, ISBN 0 521 32734 2.

Ishibashi, I., and Zhang, X., 1993, Unified dynamic shear moduli and damping ratios of sand and clay, *Soils and Foundations*, Vol. 33, No. 1, pp 182-191.

Ishihara, K., 1996, *Soil behavior in earthquake geotechnics*, Clarendon Press, Oxford, UK.

Ivanov, J., Park, C.B., Miller, R.D., Xia, J., Hunter, J.A., Good, R.L., and Burns, R.A., 2000a, Joint analysis of surface-wave and refraction events from river-bottom sediments: Technical program with biographies, SEG 70th Annual Meeting, Calgary, Alberta, Canada, pp 1307-1310.

Ivanov, J., Park, C.B., Miller, R.D. and, Xia, J., 2000b, Mapping poisson's ratio of unconsolidated materials from a joint analysis of surface-wave and refraction events, Proceedings of the Symposium on the Application of Geophysics to Engineering and Environmental Problems (SAGEEP 2000), Washington D.C, February 20-24.

Jacobs, L.J., and Owino, J.O., 2000, Effect of aggregate size on attenuation of Rayleigh surface waves in cement-based materials, *Journal of Engineering Mechanics,* Vol. 126, No. 11, pp 1124-1130.

Jamiolkowski, M., Leroueil, S., and Lo Presti, D.C.F., 1991, Design parameters from theory to practise, GEO-COAST 91, Yokohama, pp 877-916.

Jones, R., 1955, A vibration method for measuring the thickness of concrete road slabs in situ, *Magazine of Concrete Research,* Vol. 7, No. 20, pp 97-102.

Jones, R., 1958, In-situ measurement of the dynamic properties of soil by vibration methods, *Géotechnique*, Vol. 8, pp 1-21.

Jones, R., 1962, Surface wave technique for measuring the elastic properties and thickness of roads: Theoretical development, *British Journal of Applied Physics*, Vol. 13, pp 21-29.

Kausel, E., and Roesset, J. M., 1981, Stiffness matrices for layered soils, *Bulletin of the Seismological Society of America*, Vol.71, pp 1743-1761.

Kim, Y., and Kim, Y.R., 1998, Prediction of layer moduli from FWD and surface wave measurements using artificial neural network, Transportation Research Board, 77th Annual Meeting, Washington D.C.

Knopoff, L., 1964, A matrix method for elastic wave problems, *Bulletin of the Seismological Society of America*, Vol. 54, pp 431-438.

4 References

Kuttruff, H., 1991, *Ultrasonics fundamentals and applications,* Elsevier Applied Science, New York.

Lamb, H., 1917, On waves in an elastic plate, *Proc. Roy. Soc. A.*, Vol. 93, pp 114-130.

Larsson, R., 1994, Deformationsegenskaper i jord, Report B 1994:6, Department of Geotechnical Engineering, Chalmers University of Technology, Sweden.

Lee, H.J. and Kim, Y.R., 1998, Viscoelastic constitutive model for asphalt concrete under cyclic loading, *Journal of Engineering Mechanics*, ASCE, Vol. 124, No. 1, pp 32-39.

Lee, Y.C., and Cheng, S.W., 2001, Measuring Lamb wave dispersion curves of a bi-layered plate and its application on material characterization of coating, *IEEE Trans. Ultrason. Ferroelect. Freq. Contr.* Vol. 48, No. 3, pp 830-837.

Lindh, P., 2000, Soil stabilisation of fine-grained till soils: The effect of lime and hydraulic binders on strength and compaction properties, Licentiate thesis, Lund Institute of Technology, Lund University, Sweden.

Long, R., Cawley, P., and Lowe, M., 2003, Acoustic wave propagation in buried iron water pipes, *Proc. R. Soc. Lond. A*, Vol. 459, pp 2749-2770.

Lowe, M.J.S., 1995, Matrix techniques for modeling ultrasonic waves in multilayered media, *IEEE Transactions on Ultrasonics, Ferroelectrics, and Frequency Control*, Vol. 42, pp 525-542.

Lowe, M.J.S., and Cawley, P., 1995a, Comparison of the modal properties of a stiff layer embedded in a solid medium with the minima of the plane-wave reflection coefficient, *J. Acoust. Soc. Am.*, Vol. 97, No. 3, pp 1625-1637.

Lowe, M.J.S., and Cawley, P., 1995b, The influence of the modal properties of a stiff layer embedded in a solid medium on the field generated in the layer by a finite-sized transducer, *J. Acoust. Soc. Am.*, Vol. 97, No. 3, pp 1638-1649.

Martincek, G., 1994, *Dynamics of pavement structures*, E & FN Spon and Ister Science Press, Slovak Republic.

Massarsch, K.R., 1999, Seismic field measurements applied to static geotechnical problems, Proceedings of the Environmental and Engineering Geophysical Society (EEGS), Se1.

Matthews, M.C., Hope, V.S., and Clayton, R.I., 1996, The use of surface waves in the determination of ground stiffness profiles, *Proc. Instn. Geotech. Engng.* Vol. 119, Apr., pp 84-95.

4 References

McMechan, G., and Yedlin, M.J., 1981, Analysis of dispersive waves by wave field transformation, *Geophysics*, Vol. 46, No. 6, pp 869-874.

Miller, R.D., Xia, J., Park, C.B., and Ivanov, J.M., 1999, Multichannel analysis of surface waves to map bedrock, Kansas Geological Survey, *The Leading Edge*, December, pp 1392-1396.

Moro, G. D., Pipan, M., Forte, E., Finetti, I., 2003, Determination of Rayleigh wave dispersion curves for near surface applications in unconsolidated sediments, Expanded Abstract, Society of Exploration Geophysicists. 1247-1250.

Nazarian, S., Stokoe II, K.H., and Hudson, W.R., 1983, Use of spectral analysis of surface waves method for determination of moduli and thicknesses of pavement systems, *Transp. Res. Rec*. 930, Washington DC, pp 38-45.

Nazarian, S., 1984, In situ determination of soil deposits and pavement systems by spectral analysis of surface waves method. PhD thesis, Univ. of Texas at Austin, Texas.

Nazarian, S., Stokoe, II K.H., Briggs, R.C., and Rogers, R., 1987, Determination of pavement layer thicknesses and moduli by SASW method, *Transp. Res. Rec*. 1196, Washington DC, pp 133-150.

Nazarian, S., and Desai, M.R., 1993, Automated surface wave method: field testing. *J. Geotech. Engrg.*, ASCE, Vol. 119, No. 7, pp 1094-1111.

Nazarian, S., Yuan, D., and Tandon, V., 1999, Structural Field Testing of Flexible Pavement Layers with Seismic Methods for Quality Control, *Transp. Res. Rec*., 1654, pp 50-60.

Neifar, M., Benedetto, H. D., 2000, Thermo-viscoplastic law for bituminous mixes, *Journal of Road Materials and Pavement Design.* Vol. 1, No. 2, pp 71-95.

Niekerk, A.A., Houben, L.J.M., and Molenaar, A.A.A., 1998, Estimation of mechanical behaviour of unbound road building materials from physical material properties, Proceedings of the 5th International Conference on the Bearing Capacity of Roads and Airfields (BCRA), Trondheim, Norway, pp 1221-1223.

Nilsson, R., 2003, Fatigue of asphalt mixes – theory of viscoelasticity and continuum damage mechanics applied to uniaxial fatigue data from laboratory tests, PhD thesis, Univ. of Lund, Sweden.

Nilsson, R.N., 1999, A viscoelastic approach to flexible pavement design, Licentiate thesis, Royal Institute of Technology, Division of Highway Engineering, Stockholm, Sweden.

4 References

Nilsson, R.N., 2001, Viscoelastic pavement analysis using veroad, Ph.D. thesis, Royal Institute of Technology, Division of Highway Engineering, Stockholm, Sweden.

O'Neill, A., 2003, Full-waveform reflectivity for modelling, inversion and appraisal of seismic surface wave dispersion in shallow site investigations, Ph.D. thesis, The University of Western Australia, Australia.

Park, C.B., Miller, R.D., and Xia, J., 1996, Multi-channel analysis of surface waves using Vibroseis (MASWV), Kansas Geological Survey, 66th Ann. Internat. Mtg. Soc. Expl.Geophys., Expanded Abstracts, pp 68-71.

Park, C.B., Miller, R.D., and Xia, J., 1998a, Ground roll as a tool to image near-surface anomaly, Kansas Geological Survey, 68th Ann. Internat. Mtg. Soc. Expl.Geophys., Expanded Abstracts, pp 874-877.

Park, C.B., Miller, R.D., and Xia, J., 1998b, Imaging dispersion curves of surface waves on multi-channel record, Kansas Geological Survey, 68th Ann. Internat. Mtg. Soc. Expl.Geophys., Expanded Abstracts, pp 1377-1380.

Park, C.B., Miller, R.D., and Xia, J., 1999a, Detection of near-surface voids using surface wave, Proceedings of the Symposium on the Application of Geophysics to Engineering and Environmental Problems (SAGEEP 1999), Oakland, CA, March 14-18, pp 281-286.

Park, C.B., Miller, R.D., and Xia, J., 1999b, Multimodal analysis of high frequency surface waves, Proceedings of the Symposium on the Application of Geophysics to Engineering and Environmental Problems (SAGEEP 1999), Oakland, CA, March 14-18, pp 115-121.

Park, C.B., Miller, R.D., and Xia, J., 1999c, Multichannel analysis of surface waves, Kansas Geological Survey, *Geophysics*, Vol 64, No 3, pp 800-808.

Park, C.B., Miller, R.D., and Xia, J., 2000a, Detection of higher mode surface waves over unconsolidated sediments by the MASW method, Proceedings of the Symposium on the Application of Geophysics to Engineering and Environmental Problems (SAGEEP 2000), Washington D.C, February 20-24, pp 1-9.

Park, C.B., Miller, R.D., Xia, J., Ivanov, J., Hunter, J.A., Good, R.L., and Burns, R.A., 2000b, Multichannel analysis of underwater surface waves near Vancouver, B.C., Canada: Technical program with biographies, SEG 70th Annual Meeting, Calgary, Alberta, Canada, pp 1303-1306.

Park, C.B., Miller, R.D., and Xia, J., 2001, Offset and resolution of dispersion curve in multichannel analysis of surface waves (MASW), Proceedings of the Symposium on the Application of Geophysics to Engineering and Environmental Problems (SAGEEP 2001), Denver, Colorado, March 4-7.

4 References

Pickett, G., 1945, Dynamic testing of pavements, *Journal of the American Concrete Institute,* Vol. 16, No. 5, pp 473-489.

Press, F., and Dobrin, M. B., 1956, Seismic wave studies over a high-speed surface layer, *Geophysics*, Vol. 21, No. 2, pp 285-298.

Rambod, H., and Gucunski, N., 2003, Inversion of SASW dispersion curve using numerical simulation, Proceedings of the Symposium on the Application of Geophysics to Engineering and Environmental Problems (SAGEEP 2003), San Antonio, Texas, SUR-01.

Rayleigh, Lord, 1885, On waves propagated along the plane surface of an elastic solid, *London Mathematical Soc. Proc.*, Vol 17, pp 4-11.

Richart, F.E., Hall, J.R., and Woods, R.D., 1970, *Vibrations of soils and foundations*, Prentice-Hall Inc, Englewood Cliffs, New Jersey.

Rix, G.J., Stokoe II, K. H., and Roesset, J.M., 1991, Experimental study of factors affecting the Spectral Analysis of Surface Waves method, Research report 1123-5, Center for Transportation Research, The University of Texas at Austin.

Rix, G.J., and Santamarina, J.C., 2000, Signals and inversion in geotechnical site characterization, EEGS Shortcourse, Symposium on the Application of Geophysics to Engineering and Environmental Problems (SAGEEP 2000), Washington D.C, February 24.

Roesset, J.M., Chang, D.W., Stokoe II, K.H., and Auoad, M., 1990, Modulus and thickness of the pavement surface layer from SASW tests, *Transp. Res. Rec*., 1260, pp 53-63.

Ryden, N., 1999, SASW as a tool for non destructive testing of pavements, MSc thesis, Univ. of Lund, Sweden.

Santamarina, J.C., and Potts, B., 1994, On the image of stress changes in particulate media: an experimental study, *Can. Geotech. J.,* Vol 31, pp 215-222.

Santamarina, J.C., and Cascante, G., 1996, Stress anisotropy and wave propagation: a micromechanical view, *Can. Geotech. J.,* Vol 33, pp 770-782.

Santamarina, J.C., and Cascante, G., 1998, Effect on surface roughness on wave propagation parameters, *Geotechnique,* Vol. 48, No. 1, pp 129-136.

Santamarina, J.C., and Fratta, D., 1998, *Introduction to discrete signals and inverse problems in civil engineering*, Georgia Institute of Technology, ISBN 0-7844-0311-2.

4 References

Santamarina, J.C., Klein, K.A., and Fam, M.A., 2001, *Soils and waves*, John Wiley & Sons, New York, ISBN 0-471-49058-X.

Sanchez-Salinero, I., Roesset, J. M., Shao, K. Y., Stokoe, K. H., and Rix, G. J., 1987, Analytical evaluation of variables affecting surface wave testing of pavements, *Transp. Res. Rec*., 1136, pp 86-95.

Scullion, T., Uzan, J., Nazarian, S., and Briggs, B., 2000, Future directions in characterizing strength and deformation properties of pavement layers, Tansportation Research Board (TRB), Millenium paper from the Committee on Strength and Deformation Characteristics of Pavement Sections.

Sezawa, K., 1938a, Anomalous dispersion of elastic surface waves, *Proc. Imp. Acad*, Vol. 14, pp 246-249.

Sezawa, K., 1938b, Anomalous dispersion of elastic surface waves II, *Bull. Earthq. Res. Inst.*, Vol. 16, pp 225-233.

Shearer, P.M., 1999, *Introduction to seismology*, Cambridge University Press, UK, ISBN 0-521-66953-7.

Shenoy, A., and Romero, P., 2000, Specification parameter for asphalt mixtures using frequency sweep data from the Superpave shear tester, *Journal of Road Materials and Pavement Design.* Vol. 1, No. 1, pp 75-96.

Sheu, J.C., Stokoe II, K.H., and Roesset, J.M., 1988, Effect of Reflected Waves in SASW Testing of Pavements, *Transp. Res. Rec*., 1196, pp 51-61.

Stokoe II, K.H., Wright, S.G., Bay, J.A., and Roesset, J.M., 1994, Characterization of geotechnical sites by SASW method, in Geophysical characterization of sites. ISSMFE Technical Committee #10, edited by R.D. Woods, Oxford Publishers, New Delhi.

Stokoe II, K.H., and Santamarina, J.C., 2000, Seismic-wave-based testing in geotechnical engineering, Proceedings of the GeoEng 2000. Melbourne, Australia.

Strobbia, C., 2003, Surface wave methods: acquisition, processing and inversion, Ph.D. thesis, Politecnico di Torino, Italy.

Svensson, M., 2001, Application of the SASW-technique in geotechnical in-situ testing, Ph.D. Thesis, LTH, Lund University, Sweden, ISRN LUTVDG/TVGT-1009-SE.

Tawfiq, K., Sobanjo, J., and Armaghani, J., 2000, Curvilinear behavior of base layer moduli from deflection and seismic methods, *Transp. Res. Rec.,* 1716, pp 55-63.

Telford, W.M., Geldart, L.P., and Scheriff, R.E., 1990, *Applied Geophysics*, 2nd edition, Cambridge University Press, Cambridge, ISBN 0-521-32693-1.

Thomson, W.T., 1950, Transmission of elastic waves through a stratified solid medium, *Journal of Applied Physics*, Vol. 21, pp 89-93.

Tokimatsu, K., Kuwayama, S., Tamura, S., and Miyadera, Y., 1991, Vs determination from steady state Rayleigh wave method, *Soils and Found*, Vol. 31, No. 2, pp 153-163.

Tokimatsu, K., Tamura, S., and Kojima, H., 1992, Effects of multiple modes on Rayleigh wave dispersion characteristics*, J. Geotech. Engrg.,* ASCE, Vol. 118, No. 10, pp 1529-1543.

Tokimatsu, K., 1997. Geotechnical site characterization using surface waves, *Earthquake geotechnical engineering*, Ishihara (ed.), Balkema, Rotterdam.

Ullidtz, P., 1987, *Pavement Analysis*, Developments in Civil Engineering, Vol. 19, Elsevier, ISBN 0-444-42817-8.

Ullidtz, P., 1998, *Modelling flexible pavement response and performance*, Polyteknisk Forlag, Lyngby, Copenhagen, ISBN 87-502-0805-5.

Van der Pol, C., 1951, Dynamic testing of road constructions, *J. appl. Chem.,* Vol. 1, July, pp 281-290.

Vidale, R.F., 1964, The dispersion of stress waves in layered media overlaying a half space of lesser acoustic rigidity, Ph.D. Thesis, Univ. of Wisconsin.

Viktorov, I.A., 1967, *Rayleigh and Lamb waves*, Plenum Press, New York.

Williams, T.P., and Gucunski, N., 1995, Neural networks for backcalculation of moduli from SASW test, *J. Comp. In Civ. Engrg,* ASCE, Vol. 9, No. 1, pp 1-8.

Whiteoak, D., 1990, *The Shell bitumen handbook*, Shell bitumen, UK.

Wu, H., Wang, I., Abdallah, I., and Nazarian, S., 2002, A rapid approach to interpretation of SASW results, Proceedings of the 6th BCRA Conference 2002, Lisbon, Portugal. T8.18.

Xia, J., Miller, R.D., and Park, C.B., 1999, Estimation of near-surface shear-wave velocity by inversion of Rayleigh waves, Kansas Geological Survey, *Geophysics*, Vol. 64, No. 3, pp 691-700.

Xia, J., Miller, R.D., Park, C.B., and Ivanov, J., 2000a, Construction of 2-D vertical shear-wave velocity field by the Multichannel Analysis of Surface Wave technique, Proceedings of the Symposium on the Application of Geophysics to Engineering and Environmental Problems (SAGEEP 2000), Washington D.C, February 20-24, pp 1197-1206.

Xia, J., Miller, R.D., and Park, C.B., 2000b, Advantages of calculating shear-wave velocity from surface waves with higher modes: Technical program with biographies, SEG 70th Annual Meeting, Calgary, Alberta, Canada, pp 1295-1298.

Yuan, D., and Nazarian, S., 1993, Rapid determination of layer properties from surface wave method, *Transp. Res. Rec*., 1377, pp 159-166.

Yuan, D., Nazarian, S., Chen, F., and Hugo, 1998, Use of seismic pavement analyser in monitoring degradation of flexible pavements under Texas Mobile Load Simulator (a case study), Transportation Research Board, Paper No. 981523, Washington DC.

Zywicki, D.J., 1999, Advanced signal processing methods applied to engineering analysis of seismic surface waves, Ph.D. thesis. Georgia Institute of Technology.

Paper I

Multimodal Approach to Seismic Pavement Testing

Nils Ryden[1]; Choon B. Park[2]; Peter Ulriksen[3]; and Richard D. Miller[4]

Abstract: A multimodal approach to nondestructive seismic pavement testing is described. The presented approach is based on multichannel analysis of all types of seismic waves propagating along the surface of the pavement. The multichannel data acquisition method is replaced by multichannel simulation with one receiver. This method uses only one accelerometer-receiver and a light hammer-source, to generate a synthetic receiver array. This data acquisition technique is made possible through careful triggering of the source and results in such simplification of the technique that it is made generally available. Multiple dispersion curves are automatically and objectively extracted using the multichannel analysis of surface waves processing scheme, which is described. Resulting dispersion curves in the high frequency range match with theoretical Lamb waves in a free plate. At lower frequencies there are several branches of dispersion curves corresponding to the lower layers of different stiffness in the pavement system. The observed behavior of multimodal dispersion curves is in agreement with theory, which has been validated through both numerical modeling and the transfer matrix method, by solving for complex wave numbers.

DOI: 10.1061/(ASCE)1090-0241(2004)130:6(636)

CE Database subject headings: Seismic tests; Nondestructive tests; Surface waves; Rayleigh waves; Pavements; Dispersion.

Introduction

Mechanistic and analytical models are the basis of modern pavement design. A prerequisite for using these models is that material properties, such as Young's modulus (E-modulus) and Poisson's ratio (ν), can be measured and validated in the field. Seismic nondestructive testing of pavements is of particular interest because of its ability to measure fundamental low strain physical properties, i.e., seismic velocities, by affecting a representative volume of the material in a nondestructive manner. Surface wave testing utilizes the dispersive nature of surface waves in a layered medium to evaluate elastic stiffness properties of the different layers. The complete procedure can be divided into three phases: (1) data collection at the surface; (2) evaluation of the experimental dispersion curve; and (3) evaluation of the shear wave velocity (V_S) with depth profile from the experimental dispersion curve, i.e., inversion.

The most established surface wave approach, the spectral analysis of surface wave (SASW) method (Heisey et al. 1982), is based on evaluation of phase velocity measurements between two receivers. This method is faster than the earlier steady state approach (Van der Pol 1951), with the limitation that only one phase velocity can be evaluated at each frequency. SASW measurements have been continuously enhanced and have proved to be useful for pavement testing (Nazarian 1984; Aouad 1993; Nazarian et al. 1999). However, several writers have reported on limitations and difficulties related to surface wave measurements based on the two-receiver approach, especially at pavement sites. Most of these difficulties are reported to originate from the influence of higher modes of propagation (Hiltunen and Woods 1990; Rix et al. 1991; Al-Hunaidi 1992; Tokimatsu et al. 1992; Stokoe et al. 1994; Al-Hunaidi and Rainer 1995; Ganji et al. 1998; Ryden 1999). Several researchers have also proposed on a variety of alternatives to handle the influence of higher modes (Sanchez-Salinero et al. 1987; Gucunski and Woods 1992; Al-Hunaidi 1998; Ganji et al. 1998; Gucunski et al. 2000). All these proposed alternatives improved the overall performance of the seismic surface wave testing method based on the two-receiver approach. However, the limitation remains that only one phase velocity can be evaluated at each frequency. The SASW method cannot separate different modes of propagation over a pavement system and thus measures a superposition of all propagating waves at the specific receiver locations. This superposed effect, often termed apparent phase velocity or pseudophase velocity, changes with offset (distance) (Zywicki 1999) and has forced the evaluation of the data to take into account the position of the receivers and the superposition of different modes for the inversion of experimental dispersion curves. An alternative procedure, so far only performed at soil sites, is to delineate different modes of propagation in the measurements, and use theoretically calculated multiple mode dispersion curves for the inversion (Xia et al. 2000; Valentina et al. 2002).

It is the aim of this paper to propose a new approach in seismic pavement testing where the different modes of propagation are separated, thereby potentially clarifying some of the noted difficulties with the SASW method applied to pavement testing. This new approach is based on the multichannel analysis of surface wave (MASW) data processing technique (Park et al. 1998, 1999;

[1]Graduate Student, Dept. of Engineering Geology, Lund Univ., P. O. Box 118, SE-22100 Lund, Sweden. E-mail: nils.ryden@tg.lth.se

[2]Assistant Scientist, Geophysics, Kansas Geological Survey, Univ. of Kansas, 1930 Constant Avenue, Lawrence, KS 66047-3726. E-mail: park@kgs.ku.edu

[3]Associate Professor, Dept. of Engineering Geology, Lund Univ., P. O. Box 118, SE-22100 Lund, Sweden. E-mail: peter.ulriksen@tg.lth.se

[4]Associate Scientist, Geophysics, Section Chief, Kansas Geological Survey, Univ. of Kansas, 1930 Constant Avenue, Lawrence, KS 66047-3726. E-mail: rmiller@kgs.ku.edu

Note. Discussion open until November 1, 2004. Separate discussions must be submitted for individual papers. To extend the closing date by one month, a written request must be filed with the ASCE Managing Editor. The manuscript for this paper was submitted for review and possible publication on August 24, 2001; approved on August 6, 2003. This paper is part of the ***Journal of Geotechnical and Geoenvironmental Engineering***, Vol. 130, No. 6, June 1, 2004. ©ASCE, ISSN 1090-0241/2004/6-636–645/$18.00.

2001), and the multichannel simulation with one receiver (MSOR) method (Ryden et al. 2001) of data acquisition. The nature of multimode dispersion curves in a pavement system is first studied from a theoretical point of view. Key aspects of the field procedure MSOR and the MASW processing technique are presented to describe how multimode dispersion curves can be extracted from multichannel data. Finally the proposed approach is described along with a case study.

Wave Propagation in Pavement Systems

In surface wave testing of pavements, the experimental dispersion curve is often interpreted to represent Rayleigh waves. However, free Rayleigh waves can only propagate at phase velocities slower than the shear wave velocity of the half-space (Thrower 1965). Phase velocities violating this condition are leaking modes and are not free surface waves (Buchen and Ben-Hador 1996). These leaking modes are all guided plate waves formed by the superposition of reflected compression (P) and shear (S) waves within each layer. Thus, the Rayleigh wave is only one of several types of guided dispersive waves propagating in a pavement structure that may be measured at the surface and used for material characterization.

Early work with the steady state method applied to pavements showed that measured phase velocities in the high frequency range corresponds to the fundamental mode of antisymmetric ($A0$) Lamb wave propagation in a free plate (Jones 1955; Vidale 1964; Jones and Thrower 1965). Martincek (1994) verified that the Lamb wave solution was valid from the shortest measurable wavelengths up to wavelengths of six to seven times the thickness of the top layer. Early studies also reported on more than one phase velocity propagating at certain frequencies (Van der Pol 1951; Jones 1955; Heukelom and Foster 1960), thereby indicating the presence of higher modes of propagation. In the work by Jones (1962) and Vidale (1964) it was theoretically revealed that dispersion curves from pavement sites are not continuous with frequency or wavelength, also pointed out by Yuan and Nazarian (1993). Vidale (1964) concluded that there exist as many branches of dispersion curves as there are layers in the construction.

In the case of a free plate, Lamb (1917) derived a dispersion equation where the quasi-longitudinal wave (longitudinal wave in plates), the bending wave, and the Rayleigh wave are all included, termed free Lamb waves. Free Lamb waves propagating in the plane of a free plate are only possible for certain combinations of frequency (f) and phase velocity (c) corresponding to standing waves in the thickness (h) direction. Possible combinations are given by the dispersion relation:

$$\frac{\tan\left(\beta\frac{h}{2}\right)}{\tan\left(\alpha\frac{h}{2}\right)}=-\left[\frac{4\alpha\beta k^2}{(k^2-\beta^2)^2}\right]^{\pm 1} \tag{1}$$

where

$$\alpha^2=\frac{\omega^2}{V_P^2}-k^2 \tag{2}$$

$$\beta^2=\frac{\omega^2}{V_S^2}-k^2 \tag{3}$$

The $\pm$ sign on the right-hand term of Eq. (1) represents, symmetric ($+$), and antisymmetric ($-$), type of wave propagation with respect to the midplane of the plate, see Fig. 1(b). Material stiffness properties are given by V_S and V_P. Using the angular frequency ($\omega=2\pi f$), and the wave number ($k=\omega/c$), a root searching technique has to be used to calculate dispersion curves for a given plate (Graff 1975). In Fig. 1(a) the symmetrical and antisymmetrical modes of wave propagation has been derived from Eq. (1) with a V_S/V_P ratio corresponding to a Poisson's ratio of 0.35, given by

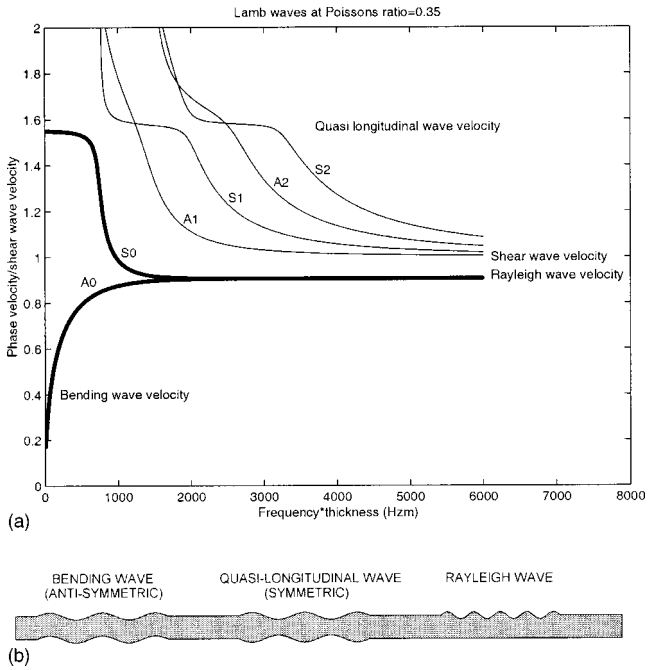

Fig. 1. (a) Lamb wave dispersion curves in free plate. In (b), particle motion is illustrated for pure form of different type of Lamb waves.

$$\nu=\frac{0.5(V_P/V_S)^2-1}{(V_P/V_S)^2-1} \tag{4}$$

It should be noted that the phase velocity and frequency axes can be normalized with respect to the shear wave velocity and the thickness of the plate for a given Poisson's ratio. The different types of wave propagation are indicated on the dispersion curves and the fundamental mode particle motion is indicated on the plate below the dispersion curves [Fig. 1(b)]. Higher modes of symmetrical and antisymmetrical wave motion develop at their respective cutoff frequency (Graff 1975), which is related to the plate thickness.

The theory given above is only valid for a free plate. However as stated above several researchers have reported that the Lamb wave solution of the top layer only, is valid for a layered pavement up to wavelengths of six to seven times the thickness of the top layer. Theoretical dispersion curves for a layered elastic medium are usually calculated with a matrix formulation based on wave propagation theory. The most widely used formulation is the transfer matrix method (Thomson 1950; Haskell 1953). The derivation of the problem and some aspects on numerical implementations are discussed in the literature (Thrower 1965; Dunkin 1965; Kausel and Roesset 1981; Lowe 1995) and are thus omitted here. The wave number that makes the value of the determinant of the global matrix (assembled from all layer matrixes) vanish is searched for each frequency. Generally only the real part of the wave number (k_r) that makes the real part of the determinant vanish is solved in the traditional SASW inversion procedure (Stokoe et al. 1994).

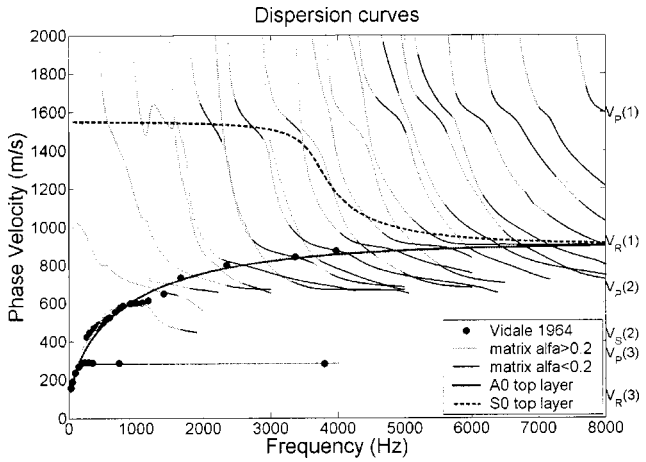

Fig. 2. Theoretical dispersion curves derived from transfer matrix method by solving for both real and complex part of wave number. Fundamental modes of Lamb waves for free plate with properties as of top layer (from Table 1) are plotted with thicker solid and dotted lines.

In pavement structures the wave number is only purely real at phase velocities slower than the shear wave velocity of the half-space, representing free Rayleigh wave propagation. At higher phase velocities the wave number contains a small imaginary part (k_j), representing leaky modes. The ratio α given by

$$\alpha = \frac{2\pi k_j}{k_r} \tag{5}$$

represents an extra attenuation factor unique for systems where the velocity decreases with depth or for a plate in water (Vidale 1964). Modes with a small imaginary part of the wave number are termed leaky modes because energy is radiated to the coupling medium in proportion to α (Lowe 1995). Solving for both the real and the imaginary part of the wave number is computationally demanding but cannot be ignored when theoretical dispersion curves for pavement systems are calculated.

In Fig. 2 dispersion curves have been calculated from the layer model in Table 1 by solving for both the real and the imaginary part of the wave number. A theoretical pavement structure studied by Vidale (1964) has been used for comparison purposes (see Table 1). Black lines represent poles where $\alpha < 0.2$ and gray lines represent poles where $\alpha > 0.2$. As α increases, the wave changes from propagating to oscillatory motion. The points calculated by Vidale (1964) using a different matrix formulation are presented as solid circles in Fig. 2. It is shown that there exist many different modes of dispersion curves. As indicated in Fig. 2, there are several asymptotic trends of phase velocities corresponding to seismic velocities in the theoretical layer model (Table 1). The fundamental modes of symmetrical ($S0$) and antisymmetrical ($A0$) free Lamb waves are plotted as dotted and solid thicker lines to illustrate how higher modes with lower attenuation ($\alpha < 0.2$) follow the trend of Lamb waves. The number of modes increases with frequency and the complexity of finding and calculating all modes can become large. A complete description of this procedure is not possible within this paper and will be addressed in future publications.

Multichannel Recording and its Simulation

The multichannel method, in general, aims at a maximized discrimination of signal against various types of noise based on unique two-dimensional (2D) patterns of seismic waves in time-offset (t-x), frequency-offset (f-x), or frequency-wave number (f-k) domain (Yilmaz 1987). True multichannel data acquisition deploys multiple receivers placed on top of a medium surface with an equal spacing along a linear survey line. Each receiver is connected to a common multichannel recording instrument (seismograph) where a separate channel is dedicated to recording signals from each receiver. The multichannel method is a pattern-recognition method that can delineate the complexity of seismic characteristics through the coherency measurement in velocity and attenuation of different types of seismic waves (e.g., multimodal surface waves, various types of body waves, and a wide range of ambient noise). In addition to this advantage in the effectiveness of signal extraction, it also provides a redundancy in measurement through the field procedure.

A true multichannel survey requires an expensive and bulky multichannel (e.g., 48-channel) recording device and many receivers deployed simultaneously in a small area. However, in seismic pavement testing, where the survey dimension is microscopic in comparison to the conventional exploration survey, this would indicate a formidable survey expense and also an inconvenient field procedure with many components and complicated wiring deployed in a small area. Instead, the multichannel recording can be simulated with only one receiver and a single-channel recording device: multichannel simulation with one receiver (MSOR) (Ryden et al. 2001). There are two alternative approaches to this simulation. One is to fix the source point and move the receiver point consecutively by the same amount of distance along a preset survey line after obtaining a single-channel measurement at one point. The other approach is to fix the receiver point and move the source point in the same way [Fig. 3(a)]. Then a simulated multichannel record is constructed by compiling all individual seismic traces in the acquired order. In any case, a horizontally traveling seismic wave will appear on the record with its arrival pattern following a linear trend whose slope gives the velocity of the wave [Fig. 3(b)]. Either of these two alternatives will give a result identical to that obtained through the true multichannel method provided the following conditions are met:

1. There is no significant lateral change in the thickness of each layer that is assumed to be homogeneous within the surveyed distance; and
2. There is no significant inconsistency in triggering.

Table 1. Theoretical Pavement Profile Representing Case EB12 Studied by Vidale (1964)

Layer	Thickness (m)	Poisson's ratio	Density (kg/m^3)	V_S (m/s)	V_P (m/s)	V_R (m/s)
1	0.2	0.167	2000	1000	1581	906
2	0.4	0.167	2000	419	663	378
3	∞ (matrix)	0.450	2000	96	318	91
	15.4 (fast Lagrangian analysis of continua)					

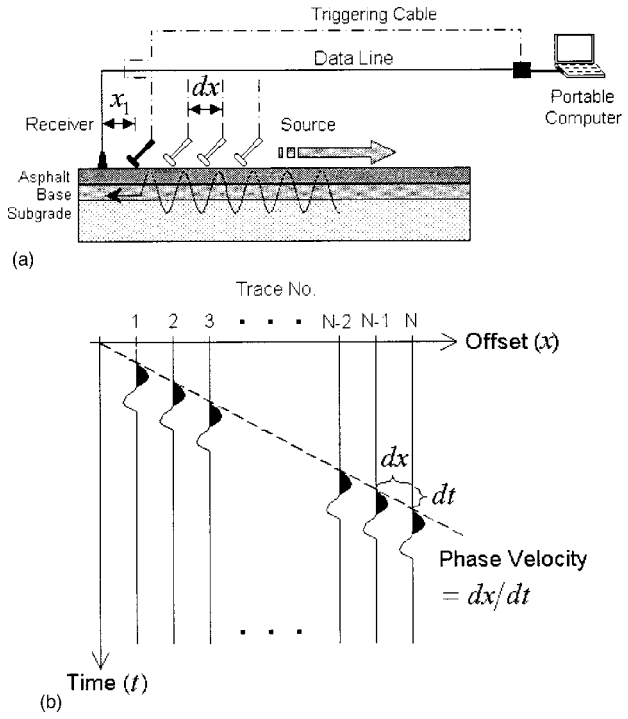

Fig. 3. (a) Schematics illustrating multichannel simulation with one receiver survey with fixed receiver and moving source. In (b), true (or simulated) multichannel record is schematically illustrated.

In practice, the first assumption is usually met to a sufficient extent in pavement testing, and the second is related to the precision of the triggering mechanism. The latter can be readily noticed once a compiled record is displayed, and in addition, a remedial processing technique is available to compensate for the inconsistency to a certain degree (Park et al. 2002). Considering a greater difficulty in ensuring a satisfactory coupling between receiver and medium surface in the case of the receiver-moving approach, the source-moving approach is utilized in this study. A simulated multichannel record is referred to as an MSOR record, or simply a record.

In this study, the data acquisition system was triggered with an accelerometer attached on the impact source. By using a comparator circuit the system is triggered at a preselected level of the accelerometer signal. Only one high frequency source, a 0.22 kg carpenter hammer, has been used to cover all frequencies of interest. To improve source coupling and the precision of the source point, a steel spike has been used as a source-coupling device. An accelerometer with a natural resonance frequency of 30 kHz was used as the receiver and was attached to the pavement with sticky grease.

The data acquisition system consists of a portable computer equipped with a PC-card, source, receiver, and external signal conditioning. This configuration is called the portable seismic acquisition system (PSAS) (Ryden et al. 2002). A PC-card from Measurement Computing, Middleboro, Mass. (PC-CARD DAS-16/16-AO), has been used. This card has a single-channel sample rate of 200 kSa/s with a 16-bit dynamic range. With the PSAS system the MSOR method is implemented efficiently because data are streamed directly to the computer and all impacts can be generated with intervals only fractions of a second apart. The PSAS system was developed at the department of Geotechnology, Lund University, and is further described in Ryden et al. (2002).

Phase Velocity Analysis Scheme

Here, the dispersion analysis scheme as normally adopted in the MASW method is described. More detailed description can be found in Park et al. (1998; 2001). A N-channel record mr_N is defined as an array of N traces collected by one of the aforementioned acquisition methods: $mr_N = r_i$ $(i=1,2,\ldots,N)$ with its frequency-domain representation of $MR_N(\omega)=R_i(\omega)=FFT[r_i]$ $(i=1,2,\ldots,N)$. Then, $R_i(\omega)$ can be written as a product of amplitude, $A_i(\omega)$, and phase, $P_i(\omega)$, terms: $R_i(\omega)=A_i(\omega)P_i(\omega)$. $A_i(\omega)$ changes with both offset (i) and angular frequency (ω) due to spherical divergence, attenuation, and the source spectrum characteristics. $P_i(\omega)$ is the term that is determined by phase velocity (c) of each frequency

$$P_i(\omega)=e^{-j\Phi_i(\omega)} \tag{6}$$

where

$$\Phi_i(\omega)=\omega x_i/c=\omega\{x_1+(i-1)dx\}/c \tag{7}$$

Consider one specific frequency (e.g., 10 kHz) of $R_i(\omega)$. Its time-domain representation will be an array of sinusoid curves of the same angular frequency, but with different amplitude and phase. Since the amplitude does not contain any information linked to phase velocity, $R_i(\omega)$ can be normalized without loss of significant information

$$R_{i,\text{norm}}(\omega)=R_i(\omega)/|R_i(\omega)|=P_i(\omega) \tag{8}$$

Fig. 4(a) shows an array of normalized sinusoid curves for an arbitrary frequency of 10 kHz propagating at another arbitrary phase velocity of 1,420 m/s. Sinusoid curves in the figure have the same phase along a slope (S_0) of the phase velocity, whereas they have a different phase along the slopes of other phase velocities, as indicated in the figure. Therefore, if the curves are summed together within a finite time length (e.g., one period) along the slope S_0, then it will give another sinusoid curve of finite length whose amplitude (A_S) is N. On the other hand, A_S will be smaller than N if the summation is performed along other slopes. This principle is the key element of the dispersion analysis employed in the MASW method. In practice the summation can be performed in a scanning manner along many different slopes specified by different phase velocities changing by small increments (e.g., 5 m/s) within a given range (e.g., 100–5,000 m/s). The result of each summation as represented by amplitude (A_S) of summed sinusoid curves can be then displayed in a 2D format (i.e., phase velocity versus A_S). In this 2D scanned curve, the phase velocity that gives the maximum amplitude $(A_{S,\max})$ will be the correct value being sought [Fig. 4(b)]. As illustrated in Fig. 4(b), the 2D scanned curve has one main lobe with a peak amplitude $A_{S,\max}$ and many side lobes on both sides. It is the sharpness of this main lobe that affects the resolution and accuracy of the analyzed dispersion relationship. In Park et al. (2001) a detailed parametric examination of the scanning method on its resolution in response to change in such parameters as N, c, dx, and ω is presented. Generally the sharpness of the peak A_S increases with N, and this means that more traces will ensure higher resolution in the determination of a phase velocity. This effect is illustrated in Fig. 4(b) for N values of 2, 20, and 80 traces. A_S has been normalized with respect to N so that the peak value is one in all three cases.

The aforementioned summation operation can actually be accomplished in the frequency domain

$$A_s(c_T)=e^{-j\delta_{1,T}}R_{1,\text{norm}}(\omega)+e^{-j\delta_{2,T}}R_{2,\text{norm}}(\omega)+\cdots+e^{-j\delta_{N,T}}R_{N,\text{norm}}(\omega) \tag{9}$$

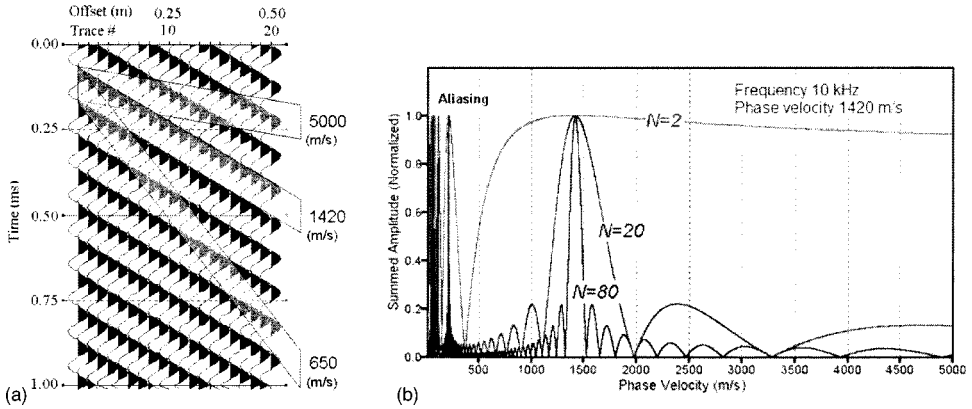

Fig. 4. (a) Synthetic record where single-frequency (10 kHz) component of seismic wave is displayed with phase velocity of 1,420 m/s, and (b) corresponding summed amplitude curves for different number of traces (N).

where

$$\delta_{i,T}=\omega[\{x_1+(i-1)dx\}/c_T] \tag{10}$$

This is a phase term that increases with offset (distance) (x) and determined by a testing phase velocity (c_T) within a scanning range. $A_S(c_T)$ is a complex number whose absolute value ($|A_S(c_T)|$) is the same as the amplitude (A_S) of summed sinusoid wave in time domain previously explained.

When seismic wave propagation invokes multimodal characteristics (like inclusion of higher modes) or includes different types of waves (like body and surface waves together), a multiple number of phase velocities can exist at the same frequency. This multiphase-velocity case can be treated as a linear superposition of individual single-phase-velocity cases. For example, if there exists a fundamental mode ($M0$) [Fig. 5(a)] and one higher mode ($M1$) [Fig. 5(b)] at the same frequency with different phase velocities and amplitudes, the measured wavefield then would be the same as a superposition [Fig. 5(c)] of the two separate records [Figs. 5(a) and (b)]. This means that if the phase-velocity scanning is applied to this multimodal record, the resulting scanned curve will be the same as a superposition [Fig. 5(e)] of the two individual scanned curves [Fig. 5(d)] obtained from each single-mode record. Park et al. (2001) shows that in this case, however, the superposition involves a scaling term determined by the relative energy partitioning between the two modes. Therefore, two main lobes appear with different peak amplitudes. This is additional information that would be critical for the study of energy partitioning between different modes or different types of seismic waves along the survey line. To identify dispersion curves, all 2D curves at different frequencies are assembled to a 3D image showing the energy distribution as a function of phase velocity and frequency. This is illustrated with a numerical modeling example in the next section.

Numerical Test

A numerical example is presented to show that the phase velocity analysis scheme can delineate multiple wave propagation modes in pavements. For comparison purposes we study the same theoretical layer model presented earlier and used by Vidale (1964) (Table 1).

The computer code FLAC (fast Lagrangian analysis of continua) (Itasca 2000) has been used in the numerical study. FLAC is a commercially available 2D explicit finite difference code. The program utilizes a time-marching method to solve the equation of motion. The nature of the problem was assumed to be axisymmetric with a linear elastic material model; i.e., no material damping was introduced. The upper horizontal axis of the model is free of any constraint so that surface waves can develop along the surface. The horizontal bottom and right side of the model has viscous boundary conditions in order to absorb as much energy as possible, thereby minimizing reflections from the edges. A finite difference mesh of cells (800×800) was set up. Internally FLAC divides each cell into four triangular subcells (Itasca 2000). Cell size (0.005×0.005 m) was set up following recommendations by Kuhlemeyer and Lysmer (1973). They showed that for accurate modeling of wave propagation the cell size should be ten times smaller than the wavelength modeled. A Ricker wavelet was applied as a velocity history in the upper left corner of the model (at zero offset). The Ricker wavelet had a 100% bandwidth and a 700 Hz center frequency. The pulse is truncated where the envelope falls 60 dB below the peak amplitude. Time step (5 μs) was set up according to the recommendations of Zerwer et al. (2002).

Vertical acceleration histories on the surface at incremental offsets (0–8 m) from the source were extracted from the FLAC model. These histories were combined into a multichannel record as normally results from MSOR measurements. When this record is analyzed by the scanning method and the scanned results are displayed in a 3D format, the pattern of main lobes creates a gray scale image of dispersion curves (Fig. 6). This type of display will be informative for identifying different modes (or types) of seismic waves.

There are several branches of dispersion curves visible in Fig. 6. As expected, almost all branches and modes of dispersion curves match with dispersion curves derived with the matrix formulation (solving for complex wave numbers) (compare Fig. 6 with Fig. 2). This theoretically confirms the ability of the presented phase velocity analysis scheme to delineate multiple dispersion curves from a pavement site, provided a multichannel record has been measured or simulated with the MSOR technique. Dispersion curves corresponding to free Lamb waves calculated from the properties of the top layer only are also plotted in the dispersion curve image. This illustrates how the overall trend of all branches follow the $A0$ Lamb wave dispersion curve of the top layer only. It should also be noted that the image of dispersion curves is obtained automatically and objectively from the multichannel record without going through any filtering of

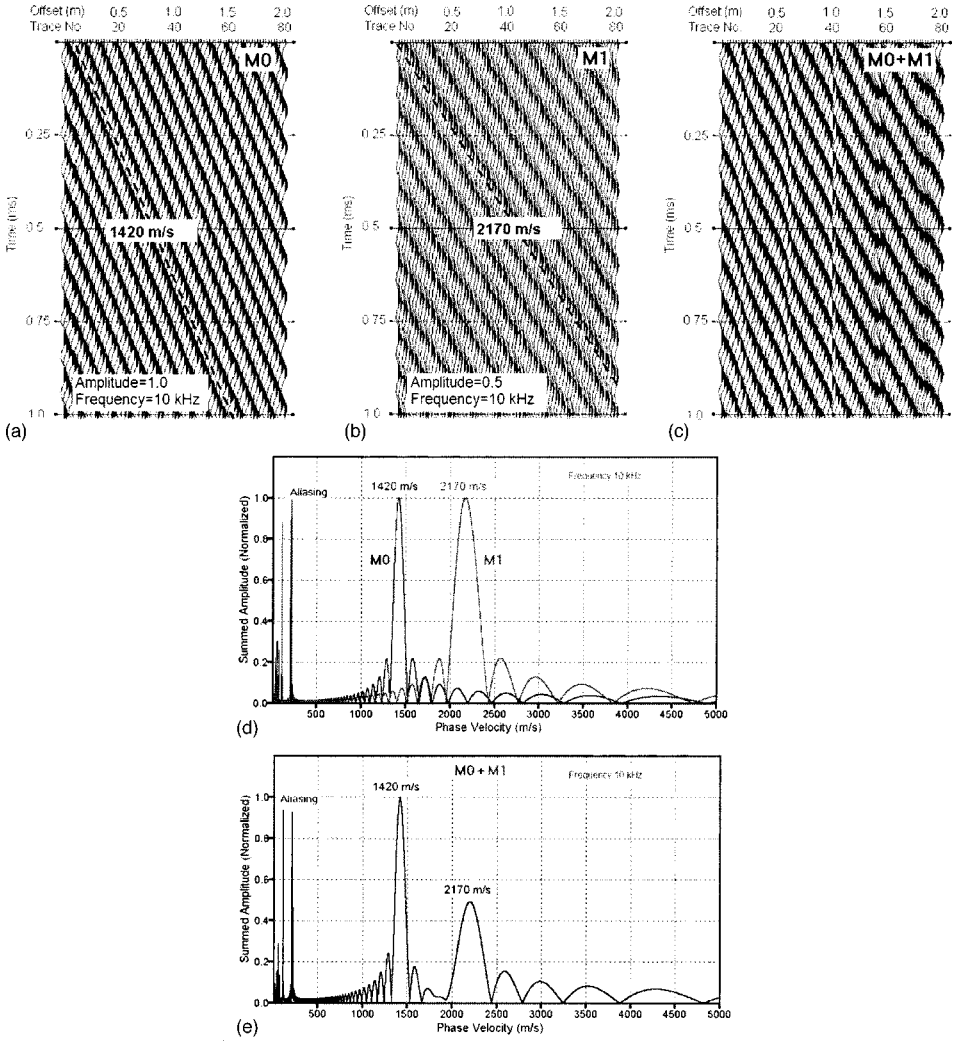

Fig. 5. Synthetic records that model single-frequency (10 kHz) component (a) of fundamental mode ($M0$) with phase velocity of 1,420 m/s, (b) of higher mode ($M1$) with phase velocity of 2,170 m/s and with a relative energy only half that of fundamental mode, and (c) of both modes ($M0$ and $M1$) propagating simultaneously. Phase velocity scanning curves obtained from records in (a) and (b) are displayed in (d) and same curve obtained from the multimodal record of (c) is displayed in (e).

near and far field effects and without problems of phase unwrapping.

Field Test

MSOR measurements were conducted at the Denmark Technical University (DTU) at the testing facility for the Danish Road Testing Machine. Several full-scale pavement constructions have been built and tested here in an enclosed climate controlled chamber (Zhang and Macdonald 2001). The complete pavement construction inside the testing facility is 20 m long, 2.5 m wide, and 2 m thick. This test site was chosen to obtain the best possible controlled environment where temperature and layering are well defined. The given layering at the DTU test site is presented in Table 2.

Following the MSOR method, one accelerometer was located at zero offset. The PSAS was set to 200 kHz sample rate. While keeping the accelerometer at zero offset and by changing the impact points of the hammer from offset 0.025 to 2.0 m with 0.025 m impact separation, data were collected with 40 ms record

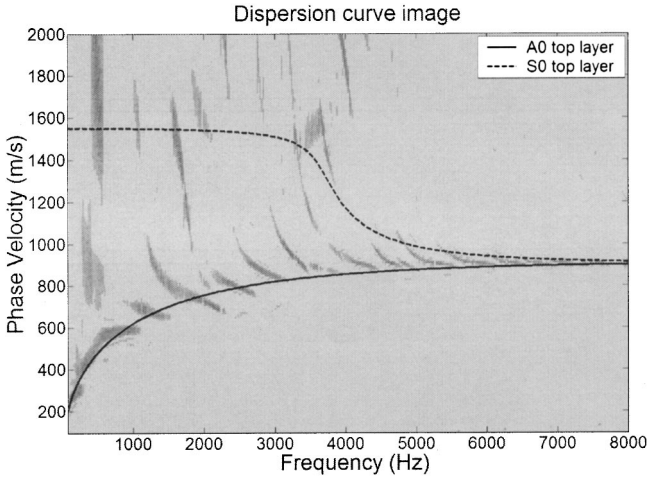

Fig. 6. Frequency-phase velocity image, created from presented phase velocity analysis scheme and synthetic data obtained from numerical modeling of pavement profile in Table 1

Table 2. Layering at Denmark Technical University Test Site

Layer	Thickness (m)
Asphalt 1 (high porosity)	0.036
Asphalt 2 (low porosity)	0.084
Base (granular material)	0.140
Subgrade (clay till)	1.376
Drainage layer (sand)	0.181
Concrete	0.250
Natural soil	~10.000

length using the equipment described earlier. At each offset five impacts were made with the spike kept in a fixed position. The asphalt temperature was 20°C.

The resulting multichannel record in offset-time domain is presented in Fig. 7. Each trace represents a stack of the last four signals from each impact point (offset). The first stroke at each impact point is only used to stabilize the source point. The main wave fronts seen in Fig. 7 are low frequency (about 1 kHz) surface waves. Fig. 8 shows the corresponding amplitude spectrum of the complete multichannel record. Beyond 0.7 m offset there is no significant energy at high frequencies (>5 kHz).

As an intermediate step toward the transformation to the 3D frequency-phase velocity image, the multichannel record in Fig. 7 is plotted in single frequency format at 5,800 Hz [Fig. 9(a)]. At this frequency two main patterns (phase velocities) can be identified, indicated with straight lines in the figure. From the offset (horizontal axis) and the time (vertical axis) the phase velocity of each line (pattern) is calculated to 1,338 and 2,705 m/s, respectively. It should be observed that although the energy above 5 kHz is very low at far offsets (>0.7 m) in the amplitude spectrum presented in Fig. 8, there is still a coherent phase velocity pattern in Fig. 9(a) extending all the way to 2.0 m offset when the data is plotted in multichannel format. If there were only random noise in this frequency range at offsets larger than 0.7 m there should not be any coherency in the phase velocity pattern. Applying the presented phase velocity analysis scheme at the same frequency clearly identifies the two-phase velocities [Fig. 9(b)].

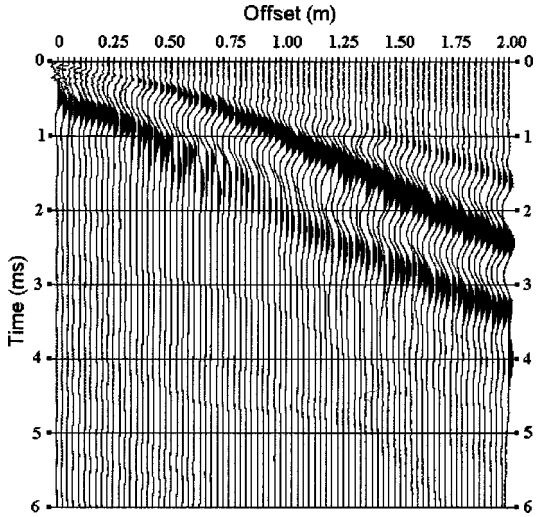

Fig. 7. Compiled multichannel record obtained from multichannel simulation with one receiver measurements at Denmark Technical University test site

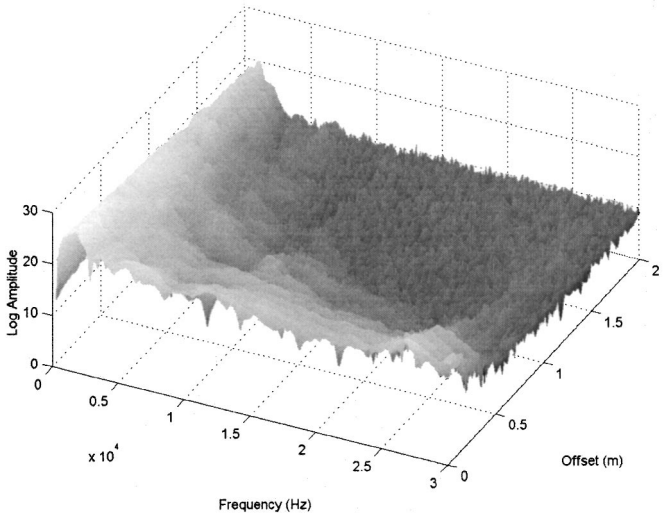

Fig. 8. 3D amplitude spectrum from recorded data at Denmark Technical University test site

In Fig. 10 the full record is automatically transformed to the frequency-phase velocity domain by using the presented phase velocity scheme of the MASW wavefield transformation method (Park et al. 1998, 2001). The phase velocity image shows phase velocity dispersion up to 28 kHz above which the surface waves are spatially aliased due to the distance between impact points.

In Fig. 10 the theoretical fundamental mode dispersion curves of antisymmetric ($A0$) and symmetric ($S0$) Lamb waves [Eq. (1)] are plotted on top of the phase velocity contour curves. An almost perfect match is obtained for the given thickness of 0.120 m (Table 2), with a Poisson's ratio of 0.35 and a shear wave velocity of 1,611 m/s. By assuming or measuring the bulk density (ρ), the low strain shear modulus (G) can be calculated using

$$G = \rho V_S^2 \tag{11}$$

and the low strain Young's modulus, E, can also be determined by using

$$E = 2G(1+\nu) \tag{12}$$

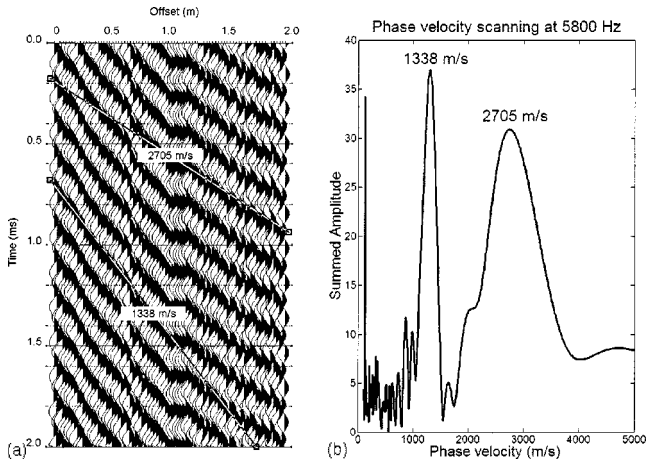

Fig. 9. (a) Single-frequency (5,800 Hz) display of data in Fig. 7 showing two different slopes (phase velocities) at same frequency. In (b), two velocities are identified as peaks in 2D scanned amplitude curve.

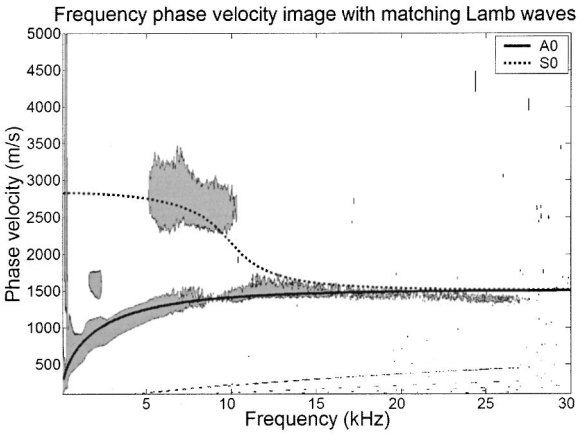

Fig. 10. Frequency-phase velocity image of Denmark Technical University data presented as contour plot at summed amplitude of 25 [compare with Fig. 9(b)]. Theoretical free Lamb wave dispersion curves have been matched to experimental data.

Setting the asphalt bulk density to 2,400 kg/m^3, the dynamic E modulus of the asphalt layer is calculated to 16.8 GPa. This modulus is only representative for the temperature and frequency during the measurement (i.e., 20°C and 15 kHz). The representative frequency 15 kHz is here taken from the part where the matching $A0$ dispersion curve is approaching a constant velocity.

At frequencies higher than 15 kHz the measured phase velocity is decreasing as in the case of normal Rayleigh wave dispersion where the velocity increases with depth. This can be explained from the higher porosity (lower stiffness) of the thin top asphalt layer (Table 2). To resolve the stiffness of this thin layer, frequencies higher than 28 kHz should have been measured.

In Fig. 11 the phase velocity image is plotted in a larger scale centered around 750 m/s and 1750 Hz, and is now presented with contour curves at a higher summed amplitude level. There are three different branches of dispersion curves visible in the image. Cutoff frequencies and abruptly changing phase velocities separate the branches. This correlates with the predicted theory presented by Vidale (1964), where each branch corresponds to each layer in the pavement. In Fig. 11 the different branches (i.e., layers), are marked 1 subgrade, 2 base, and 3 asphalt layer (start of the $A0$ mode).

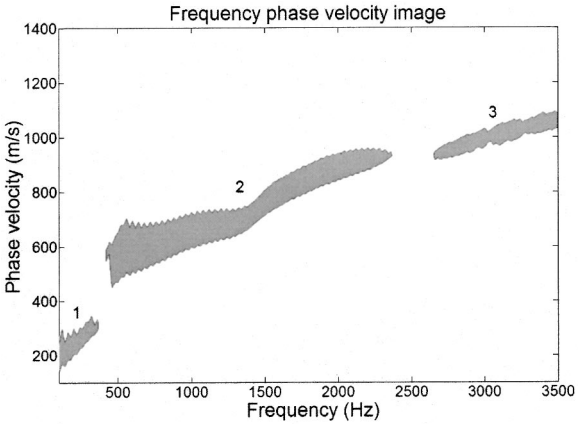

Fig. 11. Frequency-phase velocity image (contour curves at summed amplitude of 35) displayed in smaller frequency and phase velocity range

Discussion

A multimodal approach to nondestructive seismic pavement testing has been described. In summary, the most critical factors for a successful simulation of a true multichannel shot gather on a pavement surface are (1) no significant lateral change in the thickness of each layer that is assumed to be homogeneous within the surveyed distance; (2) accurate triggering; and (3) minimized source-related discontinuities in waveform and statics.

Multiple dispersion curves are automatically and objectively extracted using the presented phase velocity analysis scheme of the MASW method. This processing scheme reduces the analysis time and the risk for operator-related errors in the conventional data reduction and phase unwrapping process. There is no need for any wavelength filter criteria or multiple sources to extract all frequencies of interest. The reported difficulties with extracting correct dispersion curves from phase velocity measurements between two receivers are thus avoided.

Resulting dispersion curves in the high frequency range match with theoretical Lamb waves in a free plate. At lower frequencies there are several branches of dispersion curves corresponding to each layer of different stiffness in the pavement system. The observed behavior of multimodal dispersion curves is in agreement with theory, which has been validated through both numerical modeling and the transfer matrix method, by solving for complex wave numbers. Results indicate that dispersion of stress waves in a pavement system cannot be represented with only one average dispersion curve. Especially at low frequencies (50–3,000 Hz) it seems necessary to resolve the different modes of dispersion curves to increase the overall resolution in seismic pavement testing.

At this stage stiffness properties and the thickness of the top pavement layer are evaluated by matching theoretical dispersion curves of symmetrical and antisymmetrical Lamb waves in a free plate. Several researchers have utilized this approach before, but only with the fundamental antisymmetrical mode (Jones 1955; Jones and Thrower 1965; Akhlaghi and Cogill 1994; Martincek 1994). It is believed that with the approach presented the identification of additional higher modes of dispersion curves will be possible, increasing the resolution of the final result.

To further investigate the possibility of a simplified approach for evaluating the stiffness properties of all layers in the pavement construction, we intend to study how measurable branches are related with the material properties of the layered medium, through the analytical matrix approach, numerical finite difference modeling, and field tests with the MSOR method. This is a critical step in the progression toward a refined and efficient seismic nondestructive testing technique for pavements.

Acknowledgments

The writers would like to give their sincere thanks to Peab Sverige AB, VINNOVA, and the Swedish road authority Vägverket, for financing this project, and to Professor Anders Bodare and Dr. Jonas Brunlid for help with the transfer matrix method, Professor Per Ullidtz for the opportunity to use the RTM facility at DTU, and Mary Brohammer for her assistance in the preparation of this manuscript.

Notation

The following symbols are used in this paper:

A = amplitude term;
AO = fundamental mode of antisymmetric Lamb wave;
c = phase velocity;
dx = incremental distance between receiver or source stations;
E = Young's modulus;
f = frequency;
h = thickness;
k = wave number;
MR = multichannel record in frequency domain;
$M0$ = fundamental mode;
$M1$ = first higher mode;
mr = multichannel record in time domain;
N = number of channels;
P = phase term;
R = record in frequency domain;
r = record in time domain;
S = slope;
SO = fundamental mode of symmetric Lamb wave;
t = time;
V_P = compression (longitudinal) wave velocity;
V_R = Rayleigh wave velocity;
V_S = shear (transverse) wave velocity;
x = offset (distance between source and measurement point);
α = attenuation factor;
λ = wavelength;
ν = Poisson's ratio;
ρ = density; and
ω = angular frequency.

Subscripts and Superscripts

a = average value;
i = offset index (channel number);
j = imaginary part;
N = number of channels;
r = real part;
s = slope; and
T = testing (phase velocity).

References

Akhlaghi, B. T., and Cogill, W. H. (1994). "Application of the free plate analogy to a single-layered pavement system." *Insight*, 36(7), 514–518.

Al-Hunaidi, M. O. (1992). "Difficulties with phase spectrum unwrapping in spectral analysis of surface waves nondestructive testing of pavements." *Can. Geotech. J.*, 29, 506–511.

Al-Hunaidi, M. O. (1998). "Evolution-based genetic algorithms for analysis of non-destructive surface wave tests on pavements." *NDT & E Int.*, 31(4), 273–280.

Al-Hunaidi, M. O., and Rainer, J. H. (1995). "Analysis of multi-mode signals of the SASW method." *Proc., 7th Int. Conf. Soil Dynamics and Earthquake Engineering*, Chania, Crete, 259–266.

Aouad, M. F. (1993). "Evaluation of flexible pavements and subgrades using the spectral-analysis-of-surface-waves (SASW) method." PhD thesis, Univ. of Texas at Austin, Tex.

Buchen, P. W., and Ben-Hador, R. (1996). "Free-mode surface-wave computations." *Geophys. J. Int.*, 124, 869–887.

Dunkin, J. W. (1965). "Computation of modal solutions in layered, elastic media at high frequencies." *Bull. Seismol. Soc. Am.*, 55(2), 335–358.

Ganji, V., Gucunski, N., and Nazarian, S. (1998). "Automated inversion procedure for spectral analysis of surface waves." *J. Geotech. Eng.*, 124(8), 757–770.

Graff, K. E. (1975). *Wave motion in elastic solids*, Oxford University Press, London.

Gucunski, N., Abdallah, I. N., and Nazarian, S. (2000). "ANN backcalculation of pavement profiles from the SASW test." *Pavement subgrade unbound materials, and nondestructive testing*, Geotechnical Special Publication, ASCE, New York, No. 98, 31–50.

Gucunski, N., and Woods, R. D. (1992). "Numerical simulation of the SASW test." *Soil Dyn. Earthquake Eng.*, 11(4), 213–227.

Haskell, N. A. (1953). "The dispersion of surface waves on multilayered media." *Bull. Seismol. Soc. Am.*, 43(1), 17–34.

Heisey, J. S., Stokoe, K. H., and Meyer, A. H. (1982). "Moduli of pavement systems from spectral analysis of surface waves." *Transportation Research Record 852*, Transportation Research Board, Washington, D.C., 22–31.

Heukelum, W., and Foster, C. R. (1960). "Dynamic testing of pavements." *J. Struct. Div.*, 86(1), 1–28.

Hiltunen, D. R., and Woods, R. D. (1990). "Variables affecting the testing of pavements by the surface wave method." *Transportation Research Record 1260*, Transportation Research Board, Washington, D.C., 42–52.

Itasca consulting group, Inc. (2000). *Fast Lagrangian analysis of continua, version 4.0*. ICG, Minneapolis.

Jones, R. (1955). "A vibration method for measuring the thickness of concrete road slabs in situ." *Mag. Concrete Res.*, 7(20), 97–102.

Jones, R. (1962). "Surface wave technique for measuring the elastic properties and thickness of roads: Theoretical development." *Br. J. Appl. Phys.*, 13, 21–29.

Jones, R., and Thrower, E. N. (1965). "An analysis of waves in a two-layer composite plate and its application to surface wave propagation experiments on roads." *J. Sound Vib.*, 2(3), 328–335.

Kausel, E., and Roesset, J. M. (1981). "Stiffness matrices for layered soils." *Bull. Seismol. Soc. Am.*, 71, 1743–1761.

Kuhlemeyer, R. L., and Lysmer, J. (1973). "Finite element method accuracy for wave propagation problems." *J. Soil Mech. Found. Div.*, 99(5), 421–427.

Lamb, H. (1917). "On waves in an elastic plate." *Proc. R. Soc. London*, 93, 114–128.

Lowe, M. J. S. (1995). "Matrix techniques for modeling ultrasonic waves in multilayered media." *IEEE Trans. Ultrason. Ferroelectr. Freq. Control*, 42(4), 525–542.

Martincek, G. (1994). *Dynamics of pavement structures*, E&FN Spon and Ister Science Press, Bratislava, Slovak Republic.

Nazarian, S. (1984). "In situ determination of soil deposits and pavement systems by spectral analysis of surface waves method." PhD thesis, Univ. of Texas at Austin, Tex.

Nazarian, S., Yuan, D., and Tandon, V. (1999). "Structural Field Testing of Flexible Pavement Layers with Seismic Methods for Quality Control." *Transportation Research Record 1654*, Transportation Research Board, Washington, D.C., 50–60.

Park, C. B., Miller, R. D., and Xia, J. (1998). "Imaging dispersion curves of surface waves on multi-channel records." *Technical Program with biographies, SEG, 68th Annual Meeting*, New Orleans, Expanded Abstract, Society of Exploration Geophysicists, 1377–1380.

Park, C. B., Miller, R. D., and Xia, J. (1999). "Multichannel analysis of surface waves." *Geophysics*, 64, 800–808.

Park, C. B., Miller, R. D., and Xia, J. (2001). "Offset and resolution of dispersion curve in multichannel analysis of surface waves (MASW)." *Proc. Symp. on the Application of Geophysics and Engineering and Environmental Problems (SAGEEP 2001)*, Environmental and Engineering Geophysical Society, Annual Meeting, Denver, SSM4.

Park, C. B., Ryden, N., Miller, R. D., and Ulriksen, P. (2002). "Time break correction in multichannel simulation with one receiver (MSOR)." *Proc., Symp. on the Application of Geohysics to Engineering and Environmental Problems (SAGEEP 2002)*, Environmental and

Engineering Geophysical Society, Annual Meeting, Las Vegas, 12SE17.
Rix, G. J., Stokoe, K. H., and Roesset, J. M. (1991). ''Experimental study of factors affecting the spectral-analysis-of-surface-waves method.'' *Research Rep. 1123-5*, Center for Transportation Research, The Univ. of Texas at Austin, Austin, Tex.
Ryden, N. (1999). ''SASW as a tool for non destructive testing of pavements.'' MSc thesis, Univ. of Lund, Sweden.
Ryden, N., Ulriksen, P., Park, C. B., and Miller, R. D. (2002). ''Portable seismic acquisition system (PSAS) for pavement MASW.'' *Proc., Symp. on the Application of Geohysics to Engineering and Environmental Problems (SAGEEP 2002)*, Environmental and Engineering Geophysical Society, Annual Meeting, Las Vegas, 13IDA7.
Ryden, N., Ulriksen, P., Park, C. B., Miller, R. D., Xia, J., and Ivanov, J. (2001). ''High frequency MASW for non-destructive testing of pavements-accelerometer approach.'' *Proc., Symp. on the Application of Geohysics to Engineering and Environmental Problems (SAGEEP 2001)*, Environmental and Engineering Geophysical Society, Annual Meeting, Denver, RBA-5.
Sanchez-Salinero, I., Roesset, J. M., Shao, K. Y., Stokoe, K. H., and Rix, G. J. (1987). ''Analytical evaluation of variables affecting surface wave testing of pavements.'' *Transportation Research Record 1136*, Transportation Research Board, Washington, D.C., 86–95.
Stokoe, K. H., Wright, G. W., James, A. B., and Jose, M. R. (1994). ''Characterization of geotechnical sites by SASW method, in Geophysical characterization of sites.'' ISSMFE Technical Committee #10, edited by R. D. Woods, Oxford Publishers, New Delhi, India.
Thomson, W. T. (1950). ''Transmission of elastic waves through a stratified solid medium.'' *J. Appl. Phys.*, 21(1), 89–93.
Thrower, E. N. (1965). ''The computation of the dispersion of elastic waves in layered media.'' *J. Sound Vib.*, 2(3), 210–226.
Tokimatsu, K., Tamura, S., and Kojima, H. (1992). ''Effects of multiple modes on Rayleigh wave dispersion characteristics.'' *J. Geotech. Eng.*, 118(10), 1529–1543.
Valentina, S. L., Claudio, S., and Foti, S. (2002). ''Multimodal interpretation of surface wave data.'' *Proc., 8th European Meeting of Environmental and Engineering Geophysics (EEGS-ES 2002)*, Environmental and Engineering Geophysical Society European Section, Annual Meeting Aveiro, Portugal, 21–25.
Van der Pol, C. (1951). ''Dynamic testing of road constructions.'' *J. Appl. Chem.*, 1 July, 281–290.
Vidale, R. F. (1964). ''The dispersion of stress waves in layered media overlaying a half space of lesser acoustic rigidity.'' PhD thesis, Univ. of Wisconsin, Wis.
Xia, J., Miller, R. D., and Park, C. B. (2000). ''Advantage of calculating shear-wave velocity from surface waves with higher modes.'' SEG 70th Annual Meeting, Calgary, Alta., Canada, Expanded Abstract, Society of Exploration Geophysicist, 1295–1298.
Yilmaz, O. (1987). *Seismic data processing*, Society of Exploration Geophysicists.
Yuan, D., and Nazarian, S. (1993). ''Rapid determination of layer properties from surface wave method.'' *Transportation Research Record 1377*, Transportation Research Board, Washington, D.C., 159–166.
Zerwer, A., Cascante, G., and Hutchinson, J. (2002). ''Parameter estimation in finite element simulations of Rayleigh waves.'' *J. Geotech. Eng.*, 128(3), 250–261.
Zhang, W., and Macdonald, R. A. (2001). ''Models for determining permanent strains in the subgrade and the pavement functional condition.'' *Proc., 20th ARRB Conf., Managing Your Transport Assets*, Road Research Board, Melbourne, Australia.
Zywicki, D. J. (1999). ''Advanced signal processing methods applied to engineering analysis of seismic surface waves.'' PhD thesis, Georgia Institute of Technology, Atlanta.

Paper II

LAMB WAVE ANALYSIS FOR NON-DESTRUCTIVE TESTING OF CONCRETE PLATE STRUCTURES

Nils Ryden, Choon B. Park+, Peter Ulriksen*, and Richard D. Miller+*

**Department of Geotechnology, Lund University, Sweden*

+Kansas Geological Survey, Lawrence, Kansas

Abstract

Multimodal Lamb wave dispersion curves are measured and analyzed to obtain elastic stiffness parameters and thickness of concrete plate structures. With a simple and cost effective field procedure and by utilizing the Multichannel Analysis of Surface Waves (MASW) processing technique, the characteristics of the different modes in experimental Lamb wave dispersion curves can be measured. Lamb waves are guided dispersive waves propagating in plate structures. By matching theoretical Lamb wave dispersion curves with experimental dispersion curves, Young's modulus, Poisson's ratio, and the thickness of the tested structure can be evaluated. A theoretical background with dispersion equations is given along with a practical guide to generate theoretical dispersion curves. Since these pure Lamb wave dispersion curves are only dependent on the plate parameters, the frequency and the phase velocity can be normalized with respect to shear wave velocity and the thickness of the plate. This reduces the calculations during the matching procedure, and one only need to rescale the normalized axis of the dispersion curves to match theoretical and experimental dispersion curves. With a sensitivity analysis we give some recommendations on the matching procedure. The proposed analysis scheme is demonstrated using a case study on a concrete bridge support. Available reference data is in good agreement with the evaluated parameters from the presented analysis scheme.

Introduction

Non-destructive testing (NDT) of civil infrastructures is an important part of maintenance, risk analysis and verification of new structures. Seismic wave based testing techniques have the advantage of measuring fundamental elastic properties (i.e. seismic velocities), by affecting a representable volume in a non-destructive manner. Dynamic Young's modulus (E) and Poisson's ratio (ν) can be directly calculated from measured seismic velocities by using fundamentally correct relationships.

Lamb waves (Lamb, 1917) are guided dispersive waves propagating in free plate structures. By matching theoretical multimodal Lamb wave dispersion curves with experimental ones, shear wave velocity (V_S), Poisson's ratio, and thickness of the tested plate structure can be evaluated. Lamb waves are commonly used in ultrasonic NDT applications including material characterization of elastic plates (Rogers, 1995), viscoelastic plates (Dean, 1989), bonding inspection (Wu and Liu, 1999), coating inspection (Lee and Cheng, 2001), defect inspection (Gilchrist, 1999), and thickness measurements of thin films (Pei et al., 1995).

In NDT of infrastructures Lamb-wave-based testing techniques for concrete slabs and pavements were proposed already in the 1940's. Picket (1945) presented a theoretical analysis on the application of Lamb waves for non-destructive testing of concrete slabs. In the following years several publications reported on this approach and showed promising results (Jones, 1955; Jones 1962; Vidale, 1964; Jones and Thrower, 1965). A key issue for civil engineering applications using Lamb wave testing techniques is whether the free plate boundary conditions are fulfilled. Naturally concrete slabs and pavement

asphalt layers are in contact with granular base or subgrade/fill material. Several researchers have been investigating this question and studies indicate that Lamb waves are the prevailing type of stress waves generated with their dispersion characteristics little different from the pure (traction-free on both sides) Lamb case. This theory seems valid as far as the stiffness of the underlying layer is a fraction of the stiffness of the plate (Jones and Thrower, 1965; Martincek 1994; Ryden et al., 2002b). In early concrete and pavement applications using Lamb waves the measuring technique, the steady-state surface wave method, was time consuming and the analysis scheme was limited to the fundamental anti-symmetric mode of propagation because the method was not utilizing the multichannel recording and analysis concepts.

In this paper a practical approach for NDT of pavements and concrete structures utilizing multiple modes of Lamb wave dispersion curves is presented. Both the measuring procedure and the analysis scheme is described. A complete description of how to calculate theoretical multimodal Lamb wave dispersion curves is given. The main difference from the original approach presented by Jones (1955) is that measurements can now be made in the level of multimodal nature of Lamb waves in which the dispersion of individual modes are identified through a 2D (time and space) wave field transformation. Also, the entire procedure of testing can be finished within a couple of minutes instead of hours and with significantly cheaper equipment. Both measurements and analysis are made on the same portable computer and the recorded data can be evaluated directly in the field to obtain the final result.

Theoretical Lamb wave dispersion curves

Pure Lamb waves are guided dispersive waves propagating in an elastic isotropic plate with traction free boundaries, Figure 1. Lamb waves are formed by interference of multiple reflections and mode conversion of longitudinal waves (P-waves) and shear waves (S-waves) at the free surfaces of the plate (Viktorov, 1967).

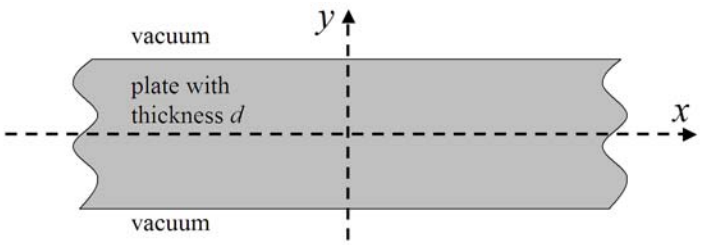

Figure 1. Schematic representation of plate and coordinates.

Lamb waves with particle displacement in both the x- and y-direction actually represents a group of wave types including the bending wave, the Rayleigh wave, and the quasi-longitudinal wave. Lamb (1917) derived the dispersion equation that can handle the transitions between these types of waves. Harmonic wave propagation in the x-direction is only possible for those combinations of frequency (f) and phase velocity (c) corresponding to standing waves in the thickness y-direction. These waves must obey the dispersion equation (Lamb, 1917), from which dispersion curves can be calculated.

$$\frac{\tan\beta\frac{d}{2}}{\tan\alpha\frac{d}{2}} = -\left[\frac{4\alpha\beta k^2}{\left(k^2-\beta^2\right)^2}\right]^{\pm 1} \qquad \text{Eq. 1}$$

where

$$\alpha^2 = \frac{\omega^2}{V_P^2} - k^2 \qquad \text{Eq. 2}$$

$$\beta^2 = \frac{\omega^2}{V_S^2} - k^2 \qquad \text{Eq. 3}$$

The ± sign on the exponent of the right term of equation 1 represents symmetric (+) and anti-symmetric (-) type of wave propagation with respect to the middle of the plate, Figure 2. The other terms are wave number ($k=\omega/c$) where ω is circular frequency ($\omega=2\pi f$); thickness (d); longitudinal wave velocity (V_P); and shear wave velocity (V_S).

Equation 1 represents the dispersion relation for pure Lamb waves with particle motion in both the x- and the y-direction. Although, the equation was derived long ago and looks quite simple, calculating roots for dispersion curve generation can be challenging, especially in some regions of wave number and frequency (Graff, 1975). Therefore further insight into the practical dispersion curve calculation is given next.

The dispersion relation is a transcendental function and it not straightforward to calculate a k value at any given frequency. A root searching technique has to be used to find the right wave numbers at any given frequency. In general roots are complex, but if only propagating waves are studied the imaginary component can be ignored (Achenbach, 1998). In Figure 3 the absolute value of the anti-symmetric function has been plotted as a function of real wave numbers at frequencies of 1 and 10 kHz. In this example the plate thickness is 0.2 m, V_P=1581 m/s, and V_S=1000 m/s. Roots are visible as minima in the absolute function value.

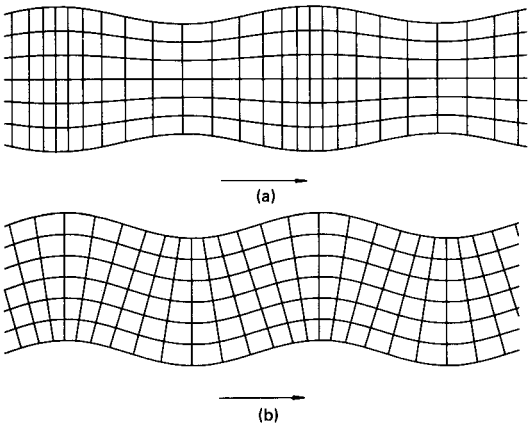

Figure 2. Mode shapes of (a) symmetric and (b) anti-symmetric Lamb wave propagation, from Kuttruff (1991).

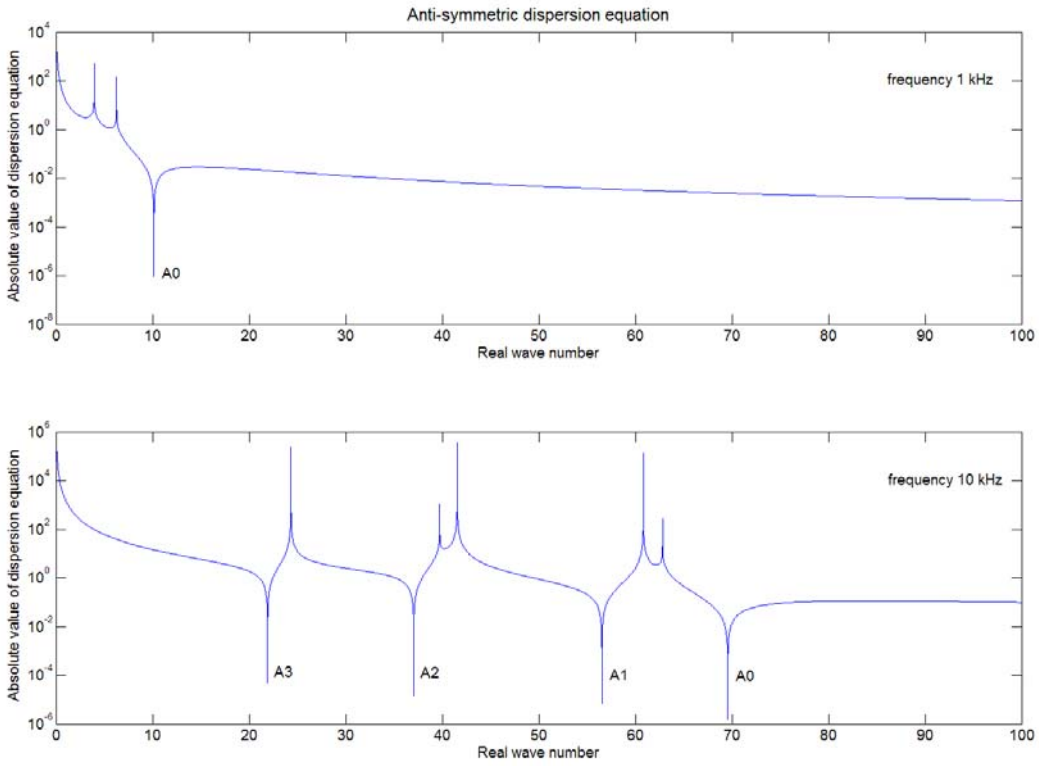

Figure 3. Absolute value of anti-symmetric dispersion equation at 1 kHz (upper) and 10 kHz (lower). Roots of the dispersion equation are visible as minima. The number of roots (at a given frequency) increases with increasing frequency. The anti-symmetric (A) mode numbers are numbered as, A0 fundamental mode, and A1…A3 for higher modes.

By extracting roots over a wide frequency range, dispersion curves of both symmetric (S) and anti-symmteric (A) Lamb waves can be studied. With the material properties given above, dispersion curves have been calculated up to the 2nd higher mode (A2 and S2), see Figure 4. A practicable technique when calculating dispersion curves from Equation 1 is to find the lowest frequency root of each mode first, and then use that root as a starting value. Some kind of minimization technique has to be used to find the exact root iteratively, keeping the frequency fixed and varying the wave number in small increments. When the lowest frequency root (first resonant wave number) at one frequency has been found with sufficient accuracy this wave number can be used as a starting value for the next frequency. This procedure is then repeated over the frequency range of interest.

At the lowest frequencies (here <3 kHz) only the two fundamental modes A0 and S0 exists. In this frequency range the S0 dispersion curve approaches the quasi-longitudinal wave velocity, which is the P-wave velocity along the plate. The A0 dispersion curve approaches the bending wave velocity of the plate: 200 to 400 m/s at these low frequencies. At higher frequencies A0 and S0 approach the Rayleigh wave velocity of the plate. It can be shown analytically that Equation 1 reduces to the Rayleigh wave dispersion equation in a homogeneous half space when the frequency approaches infinity. Practically Rayleigh wave motion develops at about 10 kHz in this example; this is where A0 and S0 merge together at the Rayleigh wave velocity. At these high frequencies and small wavelengths the

finite-thickness plate appears as a semi-infinite medium and wave propagation is limited to the regions closest to the surfaces. Higher modes develop at their respective cut-off frequency, which is related to the thickness of the plate (Graff, 1975). At higher frequencies all higher modes approach the shear wave velocity of the plate. It should also be noted that all symmetric modes have an almost straight part where the phase velocity is close to the quasi-longitudinal wave velocity. All these different types of waves and velocities are indicated on the same dispersion curves in Figure 5. As mentioned earlier, the axis on the dispersion curves can be normalized with respect to the plate properties. In Figure 5 the frequency axis is multiplied with the plate thickness (f*d) and the phase velocity axis is divided by the shear wave velocity of the plate (c/V_S).

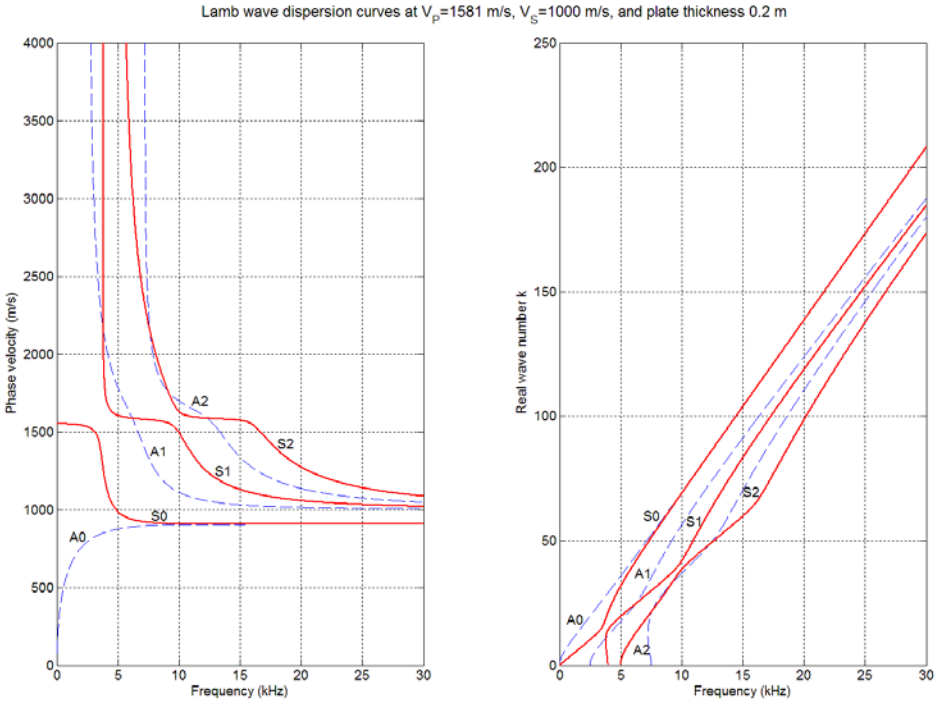

Figure 4. Lamb wave dispersion curves for a free plate with V_P=1581 m/s, V_S=1000 m/s (ν=0.167), and a thickness of 0.2 m. In the frequency-phase velocity domain (left) mode numbers increase upward with higher phase velocities. In the frequency-wave number domain (right) mode number increase downwards with lower wave numbers (compare with Figure 2).

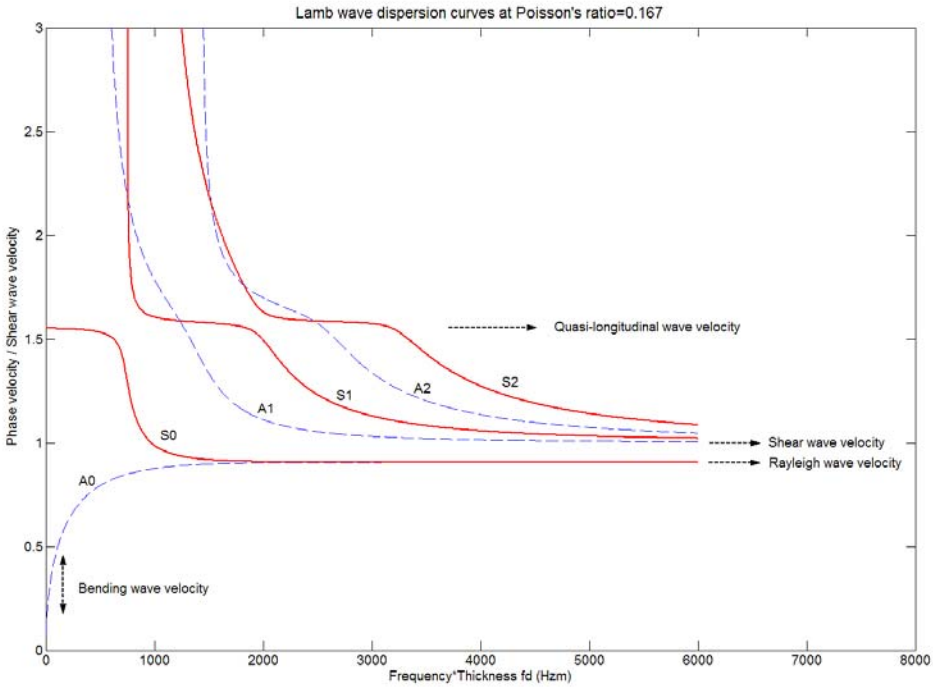

Figure 5. Lamb wave dispersion curves at a Poisson's ratio of 0.167. Axes are normalized with respect to the shear wave velocity and thickness of the plate. The different types of wave propagation are indicated with arrows.

Normalizing the axis with respect to the plate properties (as in Figure 5) significantly reduces computations when experimental dispersion curves are to be matched with theoretical dispersion curves. One only needs to calculate one set of dispersion curves at different Poisson's ratios. These dispersion curves can then be used as a database during the matching procedure. Normalized dispersion curves at fixed Poisson's ratios have been calculated by the authors and can be requested from nils.ryden@tg.lth.se. Very small increments of Poisson's ratio are usually not necessary because the dispersion curves are not very sensitive to changes in Poisson's ratio, which will be illustrated next.

The dispersion equation (Equation 1) is highly non-linear with respect to the plate properties. This implies that different portions of the dispersion curves are not equally sensitive to the plate properties. In Figure 6a-d the effect of a 10% increase in shear wave velocity (Figure 6a), Poisson's ratio (Figure 6b), E-modulus (Figure 6c), and thickness (Figure 6d) are displayed as dotted dispersion curves. The solid reference dispersion curves are the same as those used before. It should be noted that the low frequency range of A0 is not very sensitive to any of the plate properties. Still, this is the mode that has been used most widely in studies on seismic NDT of concrete plate structures and pavements. It is clear from Figure 6 that utilizing higher modes of lamb waves can increase the resolution of the results in terms of thickness and shear wave velocity or E-modulus. It can also be concluded that the Lamb wave dispersion curves are relatively insensitive to changes in Poisson's ratio. Actually there is always a frequency at each dispersion curve that is not affected by Poisson's ratio at all, termed Lamé modes (Graff, 1975). For the comparison on the sensitivity to changes in Poisson's ratio it should, however, be noted that the effect increases slightly with higher Poisson's ratios (here only 0.167).

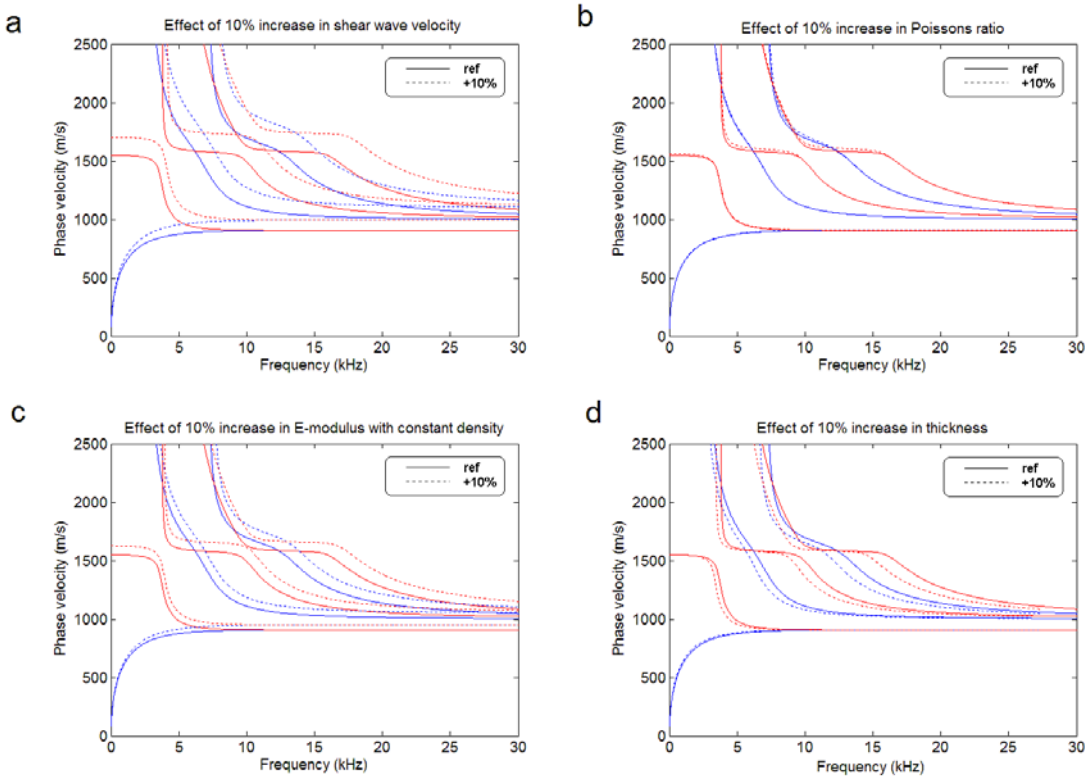

Figure 6. Parametric study on the sensitivity of multimodal Lamb wave dispersion curves on plate properties.

Field method

With a simple and cost effective field procedure and by utilizing the Multichannel Analysis of Surface Waves (MASW) processing technique (Park et al., 1998; Park et al., 1999) experimental Lamb wave dispersion curves can be measured. The multimodal nature of Lamb wave propagation implies that a transient source at the surface will easily generate multiple modes of propagation. Measured time histories along the surface will as a result be composed of a number of superposed modes. Therefore it is important that different modes of Lamb wave propagation can be delineate with a practical and cost effective approach.

The Multichannel Simulation with One Receiver (MSOR) data acquisition technique is used to record data. In the MSOR data acquisition method a multichannel record is obtained with only one receiver. It is fixed at a surface point and receives signals from several hammer impacts at incremental offsets (Ryden et al., 2001). All recorded signals are then compiled to make an equivalent multichannel record for dispersion analysis. The Portable Seismic Acquisition System (PSAS) is used to collect this data (Ryden et al., 2002a). With this system the signal from each impact is automatically streamed to the hard drive of a portable computer and data can be collected with only fractions of a second between the impacts. A schematic description of the field set-up is shown in Figure 7.

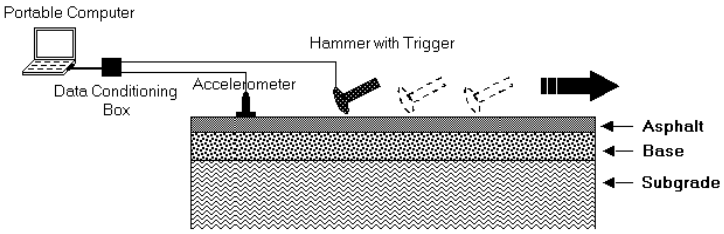

Figure 7. Schematic description of the MSOR measurement set-up.

The resulting multichannel record is automatically and objectively transformed to the frequency-phase velocity domain with the MASW processing technique (Park et al., 1998). With this technique it is possible to extract multimodal dispersion curves from a multichannel (or multichannel equivalent) data set. All coherent phase velocity patterns are mapped with respect to their relative energy level. Therefore the result (phase velocity image) shows how the total seismic energy is distributed between different frequencies and phase velocities. By applying this processing technique on synthetic data (from a finite difference model), multimodal Lamb wave dispersion curves have been observed (Ryden et al., 2002b).

Finally the measured experimental Lamb wave dispersion curves are matched to theoretical dispersion curves. By changing V_S, d, and ν, theoretical Lamb wave dispersion curves are matched manually or automatically to the high frequency dispersion curves in the phase velocity image. This whole procedure can be done in the field in a couple of minutes, provided that normalized dispersion curves have been calculated in advance as described in the previous section. The complete analysis scheme is exemplified next with a case study.

Case study—concrete bridge

Data was collected at an old concrete railroad bridge in Malmoe, Sweden. The investigated concrete bridge was tested along the vertical walls on the south and north supports. This data set has been presented earlier in Ryden et al. (2002c). Along with the non-destructive seismic test, core samples from the same locations were also taken.

Following the MSOR method one accelerometer was located at zero offset (distance). While keeping the accelerometer at zero offset and by changing the impact points of the hammer from offset 0.05 m to 2.00 m with 0.05 m impact separation, data were collected with the PSAS system. A small (0.22 kg) carpenter hammer was used as source. A steel spike was used as a source coupling device to minimize source statics, possible operator related offset errors, and to maximize the bandwidth of the generated stress waves. At each offset 5 impacts were stacked with the spike kept in a fixed position. After the last impact all individual traces are saved in a multichannel format as presented in Figure 8a.

To evaluate phase velocities at each frequency, the time record has been automatically transformed to the frequency-phase velocity domain by using the MASW phase velocity analysis scheme (Park et al., 1998). Several energy crests, which represent different modes of Lamb wave propagation, are visible in the contour plot (Figure 8b).

In Figure 8b the measured data is compared with theoretical Lamb wave dispersion curves corresponding to a 0.43 m thick free plate with a shear wave velocity of 2670 m/s and a Poisson's ratio of 0.15. In this example only the fundamental modes of symmetric and anti-symmetric Lamb waves

have been fully resolved in the measurements. The higher modes S1, S2, A1, and A2 show only week energy in limited parts of the spectrum. Since the higher modes are more sensitive to changes in the material properties (see Figure 6) even these limited parts of the spectrum are useful when matching the measured dispersion curves with the theoretical dispersion curves. The density (ρ), 2400 kg/m3, has no effect on the dispersion curves of pure Lamb waves and is only used to calculate the E-modulus from V_S and ν. The resulting dynamic E-modulus of the concrete support is calculated to 39.4 Gpa (Table 1) from Equation 4.

$$E = 2\rho V_S^2(1+\nu) \qquad \text{Eq. 4}$$

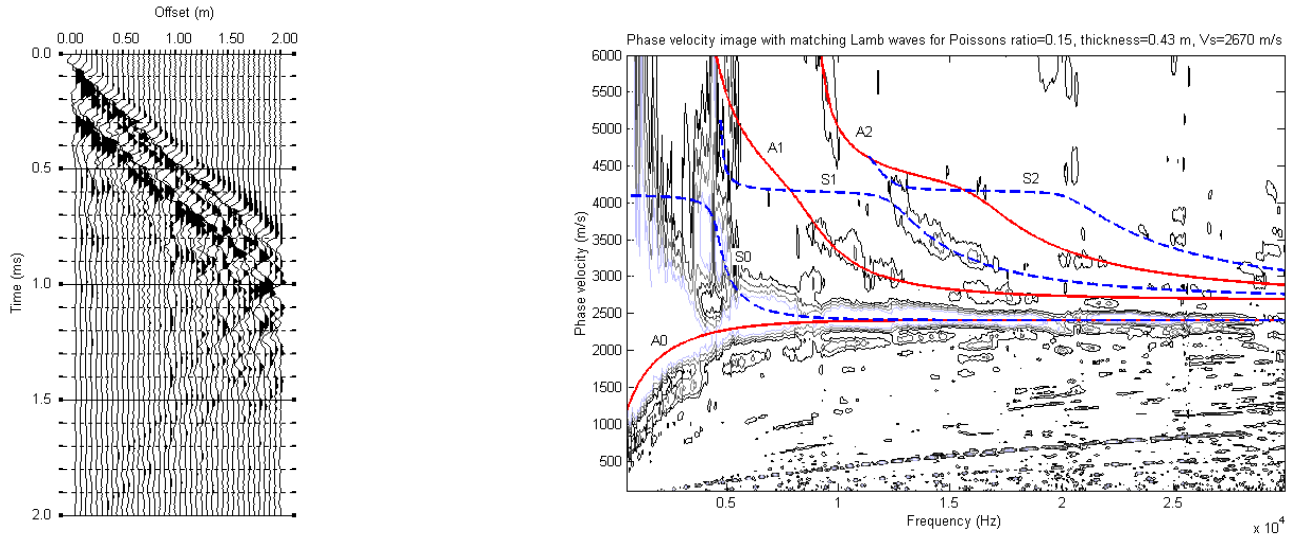

(a) (b)

Figure 8. Result from the seismic field test at the north side of the investigated concrete bridge. In (a) the collected raw data is presented in a multichannel format, (b) shows the corresponding data in the frequency phase velocity domain, as it appears after the MASW transformation method.

The presented result above was collected at the north support of the concrete bridge. The south support was also tested in a similar manner. Alongside the non-destructive seismic tests, core drillings were also conducted at the same locations. The cores were tested with the free-free resonant column method (Richart et al., 1970). A commercially available system, *Grindosonic*, was used for this test. In the free-free resonant test the seismic shear and compression wave velocities are indirectly evaluated from the longitudinal and torsional resonance frequencies of the sample. The resulting E and ν from this laboratory test are presented in Table 1 together with the results from the non-destructive field test.

A comparison of the results shows a slightly higher modulus from the seismic MSOR field test. The discrepancy between the results could to some extent be related to the approximate geometrical correction factors used in the calculation of Young's modulus from the measured resonant frequencies on the drilled cores. In this study the ASTM C1259-94 standard was used to calculate the presented material properties from the free-free resonant test. In Table 1 E and ν are presented both with and without the geometrical correction factor. In the field test pure Lamb wave dispersion curves from a free plate has been used to match the measured dispersion curves. In reality one side of the concrete wall is in contact with soil fill and as mentioned earlier this coupling is not accounted for. Another factor affecting the different methods is the difference in test volume between the two tests.

Table 1. Evaluated dynamic stiffness properties of the tested concrete.

Location	Destructive Grindosonic ASTM correction factors		Destructive Grindosonic No correction factors		Non-destructive MSOR field test	
	E (GPa)	ν	E (GPa)	ν	E (GPa)	ν
South side	40.7	0.18	42.9	0.18	43.6	0.20
North side	37.3	0.15	39.9	0.15	39.4	0.15

Discussion

It is important to remember that pure Lamb wave dispersion curves are only valid strictly for an elastic isotropic plate in vacuum. In this pure case no energy is leaking into the surrounding medium. However, provided that the velocity contrast is large, like soil-concrete, it has been shown by several researchers that Lamb wave dispersion curves are practically not affected by the interface medium (Jones and Thrower, 1965; Martincek, 1994). Based on experimental tests Martincek (1994) concluded that normalized frequencies higher than a *fd* product of 0.15 times the phase velocity ($fd > 0.15c$) are practically not affected by coupling to a lower layer. But, nevertheless, the geometry of the structure should be as close to a free plate as possible. For more complex structures of irregular shape this simplified inversion technique is not possible.

The usefulness of the presented method is related to the simple testing procedure and analysis. Testing in itself is a simple procedure. Approximately 10 minutes were spent on the data collection at 40 different offsets from the receiver, and with the laptop at site the evaluation can be performed immediately. The calculated result can be seen as a mean value for the property of the concrete volume affected by the measured seismic waves. This gives more trustworthy information than the point estimates of the property gained by core drilling. It is also important to remember that the calculated response actually is a mean value based on every hammer blow that is measured. This implies that a standard deviation of the evaluated properties also can be estimated. Since reliability analysis is becoming a more and more common tool for assessment, the variability of the concrete is important. A smaller variability can be used to increase the safety of the structure.

Evaluated dynamic stiffness properties of the concrete can be reduced to static values with known empirical relations (Nagy, 1997). From the static E-modulus it is also possible to estimate the compression strength.

Conclusions

With simple field measurements using one receiver and one source (MSOR) and by utilizing the MASW data processing method, multimodal Lamb wave testing can be performed directly in the field. Measuring shear and compression wave velocity in concrete is common for non-destructive test methods. The unique features that makes this method highly efficient is the simple and cost effective data acquisition and the ability to extract multimode dispersion curves in a robust and objective manner. The case study presented shows good agreement with data from more expensive tests based on core drillings.

In this paper it has also been demonstrated how pure Lamb wave dispersion curves are calculated from the dispersion equation. This can be a tricky task and is therefore described in detail. However dispersion curves for a given Poisson's ratio only need to be calculated once. By normalizing the axis of

the dispersion curves with respect to the shear wave velocity and the thickness of the plate, calculated dispersion curves can be used for any plate with any shear wave velocity and any thickness. Normalized dispersion curves at fixed Poisson's ratios have been calculated by the authors and can be requested from nils.ryden@tg.lth.se.

Acknowledgements

The financial support from Peab AB, VINNOVA, and the Swedish Road Administration is greatly appreciated. We also give our sincere acknowledgements to Dr. Jonas Brunskog at Engineering Acoustics, and Lic. Eng. Joakim Jeppsson at Structural Engineering, Lund University, for their contribution. We thank Mary Brohammer for her assistance in preparation of this manuscript.

References

1. ASTM (1994), "Standard test methods for dynamic Young's modulus, shear modulus, and Poisson's ratio for advanced ceramics by impulse excitation of vibration", Standard C1259-94, *Annual Book of ASTM Standards*, Vol. 15.02.
2. Achenbach, J.D., (1998), "Lamb waves as thickness vibration superimposed on a membrane carrier wave", *J. Acoust. Soc. Am.*, Vol. 103, Nr. 5 May, pp 2283-2286.
3. Dean, G.D. (1989), "Use of plate bending waves for elastic property determination of polymers", *Composites*, Vol. 20, Nr. 6 November, pp 575-582.
4. Gilchrist, M.D. (1999), "Attenuation of ultrasonic Rayleigh-Lamb waves by small horizontal defects in thin aluminium plates", *International Journal of Mechanical Sciences,* Vol. 41, pp 581-594.
5. Graff, K.E. (1975), *Wave motion in elastic solids*. Oxford University Press, London.
6. Jones, R., (1955), "A vibration method for measuring the thickness of concrete road slabs in situ", *Magazine of Concrete Research*, July, pp 97-102.
7. Jones R. (1962), "Surface wave technique for measuring the elastic properties and thickness of roads; Theoretical development", *British Journal of Applied Physics*, Vol. 13.
8. Jones, R. and Thrower, E.N. (1965), "Effect of interfacial contact on the propagation of flexural waves along a composite plate", *J. Sound Vib.*, Vol. 2, Nr. 2, pp 167-174.
9. Kuttruff, H. (1991), *Ultrasonics fundamentals and applications*, Elsevier Applied Science, New York.
10. Lamb, H. (1917), "On waves in an elastic plate", Proceedings of the Royal Society, London, pp 114-128.
11. Lee, Y.C., and Cheng, S.W. (2001), "Measuring Lamb wave dispersion curves of a bi-layered plate and its application on material characterization of coating", *IEEE Transactions on Ultrasonics*, Ferroelectrics, and Frequency Control, Vol. 48, No. 3, May.
12. Martincek, G. (1994), *Dynamics of pavement structures*, E & FN Spon and Ister Science Press, Slovak Republic.
13. Nagy, A. (1997), "Determination of E-modulus of young concrete with nondestructive method", *Journal of Materials in Civil Engineering*, ASCE, Vol. 9, Nr. 1 Feb, pp 15-20.
14. Park, C.B., Miller, R.D., and Xia, J. (1999), "Multichannel analysis of surface waves", Kansas Geological Survey, *Geophysics*, Vol 64, No 3, pp 800-808.
15. Park, C.B., Miller, R.D., and Xia, J. (1998), "Imaging dispersion curves of surface waves on multi-channel record", Kansas Geological Survey, 68th Ann. Internat. Mtg. Soc. Expl.Geophys., Expanded Abstracts, pp 1377-1380.

16. Pei, J., Degertekin, L., Khuri-Yakub, B.T., and Saraswat, K. (1995), "In situ thin film measurement with acoustic Lamb waves", *Appl. Phys. Lett.*, Vol. 66, Nr. 17 April, pp 2177-2179.
17. Picket, G. (1945), "Dynamic testing of pavements", *Journal of the American concrete institute*, Vol. 16, Nr. 5 April, pp 473-489.
18. Richart, F.E., Woods, R.D., and Hall, J.R. (1970), *Vibrations of Soils and Foundations*, Prentice-Hall, Inc., Englewood Cliffs, New Jersey.
19. Rogers, W.P. (1995), "Elastic property measurement using Rayleigh-Lamb waves", *Res Nondestr Eval*, Vol 6, pp 185-208.
20. Ryden, N., Ulriksen, P., Park, C.B., and Miller R.D. (2002a), "Portable seismic acquisition system for pavement MASW", Proceedings of the Symposium on the Application of Geophysics to Engineering and Environmental Problems (SAGEEP 2002), Las Vegas, NV, February 10-14, 2002.
21. Ryden, N., Park, C.B., Ulriksen, P., and Miller R.D. (2002b), "Branching of dispersion curve in surface wave testing of pavements", Proceedings of the Symposium on the Application of Geophysics to Engineering and Environmental Problems (SAGEEP 2002), Las Vegas, NV, February 10-14, 2002.
22. Ryden, N.R., Jeppsson, J., and Park, C.B. (2002c), "Destructive and non-destructive assessment of concrete structures", Proceedings of the XVIII Symposium on Nordic Concrete Research, Helsingor, Denmark, June 12-14, pp 153-156.
23. Ryden, N., Ulriksen, P., Park, C.B., Miller, R.D., Xia, J., and Ivanov, J. (2001), "High frequency MASW for non-destructive testing of pavements-accelerometer approach". Proceedings of the SAGEEP 2001, Denver, Colorado, RBA-5.
24. Vidale, R.F. (1964), "The dispersion of stress waves in layered media overlaying a half space of lesser acoustic rigidity", Ph.D. Thesis, Univ. of Wisconsin.
25. Viktorov, I. A. (1967). *Rayleigh and Lamb waves*. Plenum Press, New York.
26. Wu, T.T. and Liu, Y.H. (1999), "Inverse determination of thickness and elastic properties of bonding layer using laser-generated surface waves", *Ultrasonics,* Vol 37, pp 23-30.

Paper III

Near Surface Geophysics, 2004, 187-197

Surface waves in inversely dispersive media

N. Ryden[1*] and C.B. Park[2]

[1] *Lund University, Sweden, Department of Geotechnology, Lund institute of Technology, Box 118, S-221 00, Lund, Sweden*

[2] *Kansas Geological Survey, Kansas University, USA*

Received January 2004, revision accepted August 2004

ABSTRACT

The dispersion of surface waves in inversely dispersive media where the shear-wave velocity decreases with depth is studied. Theoretical dispersion curves are calculated in the complex wavenumber domain. Excitability and attenuation due to leakage are calculated for each point on the dispersion curves. These additional parameters are critical for a correct understanding of the dispersion properties of surface waves. Mode shapes are included in the study to visualize displacements inside the medium. The results of the study show that, for inversely dispersive media, the Rayleigh-wave assumption is not valid, and other types of interface waves and leaky Lamb waves contribute to the surface wavefield. They also show that, in this case, true theoretical dispersion curves can be approximated by Lamb-wave dispersion curves for a free plate in a vacuum, provided that the stiffness contrast between the top layer and the underlying half-space is large, and also that the shear-wave velocity of the stiff layer is greater than the compressional-wave velocity in the underlying media. The error in the phase velocity resulting from this approximation is investigated and it is shown that the error does not exceed 5% for the fundamental antisymmetric Lamb-wave dispersion curve. Because of the numerical simplicity of calculating its theoretical dispersion curves, the Lamb-wave approximation can provide an effective evaluation method to resolve the thickness and elastic parameters of the stiff top layer. This is exemplified using a set of field data.

INTRODUCTION

Surface-wave methods have become popular in near-surface site characterization and in non-destructive testing of pavements and concrete structures (Nazarian 1984; Park *et al*. 1999; Xia *et al*. 1999; Stokoe and Santamarina 2000). The dispersive nature of surface waves in a layered medium is utilized to estimate a shear-wave velocity (i.e. stiffness) profile of the test site. The complete testing procedure can be divided into three basic steps: (1) generation and measurement of surface waves in the field; (2) data processing and extraction of an experimental dispersion curve; (3) inversion of the experimental dispersion curve to obtain an estimated shear-wave velocity with depth profile.

The same basic principles of surface-wave propagation are often assumed, regardless of the medium investigated. It is usually assumed that Rayleigh waves are the prevailing type of waves generated, with a depth penetration of about one wavelength (Viktorov 1967). However, it has been reported that this assumption holds strictly only at sites where the stiffness increases smoothly as a function of depth (Foti 2000). At sites with a velocity reversal (i.e. stiffness decreases with depth), the nature of surface-wave propagation has been reported as more complicated than at sites with normal dispersion. Several studies have indicated that a measured dispersion curve where the phase velocity increases with frequency, i.e. inverse dispersion, is actually built up by small portions of higher modes (Gucunski and Woods 1992; Tokimatzu *et al*. 1992; Forbriger 2003; Foti *et al*. 2003; Ryden *et al*. 2004). In extreme cases where the stiffness ratio between the top and lower layers is large, it has been shown that the inverse trend of the dispersion curve matches that of pure Lamb waves generated by the stiff top layer only (Jones 1955; Jones and Thrower 1965; Akhlaghi and Cogill 1994; Martincek 1994; Ryden *et al*. 2003). A similar trend of the dispersion has also been observed at certain soil sites where an inverse velocity setting existed close to the surface (Park *et al*. 2002). Martincek (1994) concluded from experimental results on pavements that the Lamb-wave approximation was valid for all wavelengths smaller than five times the thickness of the stiff top layer. Similar results have been reported by other investigators (e.g. Jones 1962; Akhlaghi and Cogill 1994; Ryden *et al*. 2003). All these studies reached an implicit conclusion that if the stiffness contrast is sufficiently large, the Lamb-wave approximation can be used for a simple evaluation of the thickness and the elastic properties of the stiff top layer. However, mainly because of the numerical difficulties involved in calculating normal-mode dispersion curves for an inversely dispersive layer model, the discrepancy between the Lamb-wave and the true dispersion curves has not been quantified. One of the two purposes of this paper is to investigate the exact error involved in the Lamb-wave approximation in order to

* nils.ryden@tg.lth.se

develop a refined but still simple evaluation of the stiff top layer. The difference between pure Lamb-wave dispersion curves for a free plate and the exact solution including the influence of a lower-velocity half-space is studied in detail. The practicality of the Lamb-wave approximation for the evaluation of a stiff top layer is exemplified using a set of field data.

The other purpose is to investigate the propagation characteristics of surface waves in inversely dispersive media. To illustrate the main differences from the Rayleigh-wave dispersion, mode shapes, excitability and leakage are also calculated along with the dispersion curves. The excitability coefficient and the amount of attenuation due to leakage can give further information on which mode will dominate surface displacements. It is also shown that solving only for the real part of the wavenumber will not give the correct phase velocity when wave propagation is leaky. A numerical example with one layer on a half-space is used to explain these characteristics.

LAMB WAVES IN A FREE PLATE

Free Lamb waves are guided dispersive waves propagating in an elastic isotropic plate with traction-free boundary conditions at the top and bottom of the plate. Lamb waves are formed by interference of multiple reflections and mode conversion of compressional waves (P-waves) and shear waves (S-waves) at the two boundaries of the plate (Viktorov 1967). Lamb waves actually represent a group of wave types that include the bending wave, the Rayleigh wave and the quasi-compressional wave. Lamb (1917) derived the dispersion equation that can handle the transitions between these types of waves. Harmonic wave propagation in the x-direction is only possible for those combinations of frequency f and phase velocity V that correspond to standing waves in the thickness y-direction. These waves must obey the dispersion relationship (Lamb 1917) from which dispersion curves can be calculated, i.e.

$$\frac{\tan C_S \dfrac{d}{2}}{\tan C_P \dfrac{d}{2}} = -\left[\frac{4C_P C_S k_x^2}{\left(k_x^2 - C_S^2\right)^2}\right]^{\pm 1}, \qquad (1)$$

where

$$C_P = (\omega^2 / V_P^2 - k_x^2)^{1/2}, \qquad (2)$$

$$f(f,k) = \det[\mathbf{S}] = 0. \qquad (3)$$

The ± sign on the exponent of the right-hand term of (1) represents symmetric (+) and antisymmetric (–) types of wave propagation with respect to the middle of the plate. The other terms are wavenumber $k=\omega/V$, where ω denotes angular frequency, given by $\omega=2\pi f$; thickness d; compressional-wave velocity V_P; and shear-wave velocity V_S. The dispersion relationship (1) is a transcendental function and it is not straightforward to calculate a k value at any given frequency. Some practical considerations for dispersion-curve calculations with (1) are discussed in Ryden *et al*. (2003).

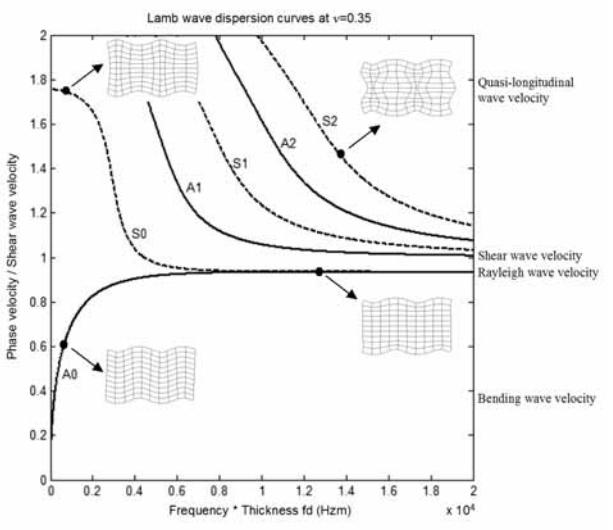

FIGURE 1
Lamb waves for a free plate with a Poisson's ratio of 0.35. Axes are normalized with respect to the plate thickness and shear-wave velocity. Mode shapes are plotted at different modes and frequencies to illustrate the particle motion and the different types of waves included in the Lamb-wave definition.

In Fig. 1, the first three modes of antisymmetric (A) and symmetric (S) dispersion curves have been calculated for a Poisson's ratio ν of 0.35. Because the dispersion curves are only dependent on the thickness and elastic constants of the plate, the dispersion curves can be normalized with respect to the plate properties. In Fig. 1, the frequency axis is multiplied by the plate thickness ($f*d$) and the phase velocity axis is divided by the shear-wave velocity of the plate (V/V_S). At the lowest frequencies (<3 kHz-m), only the two fundamental modes, A0 and S0, exist. In this frequency range, the S0 dispersion curve approaches the quasi-compressional-wave velocity, which is the P-wave velocity along the plate. The A0 dispersion curve approaches the bending-wave velocity of the plate at these low frequencies. At higher frequencies, A0 and S0 approach the Rayleigh-wave velocity of the plate. In practice, in this example, Rayleigh-wave motion develops at about 10 kHz-m; it is where the A0 and S0 curves merge together, at the Rayleigh-wave velocity of the plate. At these high frequencies (and small wavelengths), the finite-thickness plate appears as a semi-infinite medium and wave propagation is limited to the regions closest to the surfaces. Higher modes develop at their respective cut-off frequencies, which are related to the thickness of the plate (Graff 1975). At higher frequencies, all higher modes approach the shear-wave velocity of the plate. All these different types of waves and velocities are indicated on the right-hand y-axes in Fig. 1.

The Lamb-wave dispersion equation is highly non-linear with

respect to the plate properties. This implies that different portions of the dispersion curves are not equally sensitive to the plate properties. In general, higher modes are more sensitive to the plate properties than the fundamental modes, and a change in shear-wave velocity or thickness is dominant over a change in Poisson's ratio (Ryden *et al*. 2003).

WAVE PROPAGATION MODEL FOR A LAYERED MEDIUM

Theoretical dispersion curves for a layered elastic medium can be calculated with a matrix formulation based on wave-propagation theory. In this study, the global matrix method proposed by Knopoff (1964) is used. Each layer, including the half-spaces, is represented by a layer matrix $\mathbf{D}_i$ where stresses σ and displacements u are expressed as a function of the material properties: V_P, V_S, d, the bulk density ρ of each layer, and ω and k. By satisfying the boundary conditions at each layer interface, all layer matrices are assembled in a system matrix **S** describing the complete layer model. Each point on a dispersion curve represents a solution to **S** where all boundary conditions are satisfied simultaneously. For modal solutions to exist, **S** must be singular, i.e. its determinant must be zero. The dispersion equation or characteristic equation then becomes

$$f(f,k) = \det[\mathbf{S}] = 0\,. \tag{4}$$

The global matrix approach can handle leaky waves (complex wavenumbers) without modification and remains stable for high frequencies and large thickness values (Lowe 1995). The complete derivation of all equations can be found in Knopoff (1964), Randall (1967) and Lowe (1995). Here, only the final matrix equations as given by Lowe (1995) are presented. The basic principle is to define one matrix $\boldsymbol{D}_t$ for the top interface and one matrix $\boldsymbol{D}_b$ for the bottom interface of each layer. The interface matrix describes the displacements and stresses at the interface as a function of the partial wave amplitudes A from above (index t) or below (index b) the interface. The thickness d in the y-direction of each layer is entered as y in the equations for dispersion-curve calculations and is zero for the half-space matrices. The partial waves A are divided into compressional waves (P) and shear waves (S). The (+) and (–) indices denote partial waves travelling down (+) and up (–) from the interface (Fig. 2). Thus, we have

$$\begin{Bmatrix} u_x \\ u_y \\ \sigma_{yy} \\ \sigma_{xy} \end{Bmatrix} = [\mathbf{D}_i] * \begin{Bmatrix} A_{(P+)} \\ A_{(P-)} \\ A_{(S+)} \\ A_{(S-)} \end{Bmatrix}, \tag{5}$$

where

$$[\mathbf{D}_{it}] = \begin{bmatrix} k_x & k_x g_P & C_S & -C_S g_S \\ C_P & -C_P g_P & -k_x & -k_x g_S \\ i\rho B & i\rho B g_P & -2i\rho k_x V_S^2 C_S & 2i\rho k_x V_S^2 C_S g_S \\ 2i\rho k_x V_S^2 C_P & -2i\rho k_x V_S^2 C_P g_P & i\rho B & i\rho B g_S \end{bmatrix}, \tag{6}$$

$$[\mathbf{D}_{ib}] = \begin{bmatrix} k_x g_P & k_x & C_S g_S & -C_S \\ C_P g_P & -C_P & -k_x g_S & -k_x \\ i\rho B g_P & i\rho B & -2i\rho k_x V_S^2 C_S g_S & 2i\rho k_x V_S^2 C_S \\ 2i\rho k_x V_S^2 C_P g_P & -2i\rho k_x V_S^2 C_P & i\rho B g_S & i\rho B \end{bmatrix}, \tag{7}$$

and

$$g_P = e^{iC_P y}\,, \tag{8}$$

$$g_S = e^{iC_S y}\,, \tag{9}$$

$$B = \omega^2 - 2V_S^2 k_x^2\,. \tag{10}$$

When the four-by-four matrices, $\mathbf{D}_{ib}$ and $\mathbf{D}_{it}$ (i=1...n), have been calculated for each layer, they are assembled to obtain the global matrix **S** so that stresses and displacements become continuous over the interfaces. For a layer model with four layers as in Fig. 2, the system matrix then becomes

$$\mathbf{S} = \begin{bmatrix} \mathbf{D}_{1b}^{-} & -\mathbf{D}_{2t} & & \\ & \mathbf{D}_{2b} & \mathbf{D}_{3t} & \\ & & \mathbf{D}_{3b} & -\mathbf{D}_{4t}^{+} \end{bmatrix}. \tag{11}$$

Each row in **S** above represents each interface and each column corresponds to each layer including the two half-spaces. The incoming waves in the half-spaces are identified as known parameters and therefore the half-space matrices are four-by-two matrices containing only the outgoing waves. The (–) index on $\mathbf{D}_{1b}$ above represents the outgoing waves in the top half-space (columns 2 and 4 in $\mathbf{D}_b$) and the (+) index on $\mathbf{D}_{4t}$ represents downgoing waves in the bottom half-space (columns 1 and 3 in

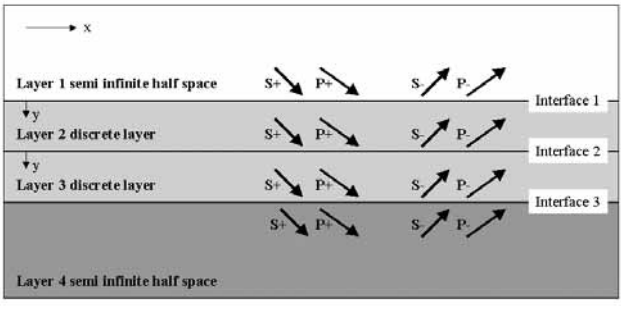

FIGURE 2
Schematic illustration of the layered model used in the global matrix approach, after Lowe (1995). The example shows four layers as they are named in the matrix notation. Only the embedded layers, layers 2 and 3, are discrete layers. Layers 1 and 4 are semi-infinite half-spaces.

$\mathbf{D}_t$). In surface-wave applications, the top surface is usually free. This requires some modifications to the matrix **D**. However, exactly the same result can be obtained by setting the bulk-wave velocities V_P and V_S to arbitrary non-zero values and the bulk density to zero (Lowe 1995). In this way, the same matrices can be used for both vacuum and solid half-spaces.

SOLVING FOR COMPLEX WAVENUMBERS

The wavenumber that makes the value of the determinant of **S** vanish is searched for, for each frequency. Only the real part, k_r, of the wavenumber that makes the real part of the determinant vanish is solved for in some studies on surface-wave propagation (Roësset *et al*. 1991; Stokoe *et al*. 1994). Strictly, the modal solution must be searched for in the complex wavenumber domain, when the phase velocity becomes greater than the shear-wave velocity in the lower half-space. In this case, the particle motion no longer decreases exponentially with depth, violating the condition for true Rayleigh waves (Aki and Richards 1980). Energy radiates down towards the lower half-space, resulting in attenuation of the wave along the surface in the *x*-direction (Vidale 1964), although all materials are purely elastic. Since the phase velocities of higher modes are greater than that of the fundamental mode, this issue becomes even more important for the calculation of higher-mode dispersion curves. Variious alternatives have been proposed to avoid the calculation of complex wavenumbers. One alternative has been to set the properties of the half-space to those of a vacuum so that no energy can leak out from the system (Roësset *et al*. 1991). In another approximate approach, the imaginary part of the determinant is ignored (Stokoe *et al*. 1994). But in most publications the problem with complex wavenumbers is avoided by setting the half-space equal to the highest velocity of the system (Nazarain 1984; Gucunski and Woods 1992; Foti 2000).

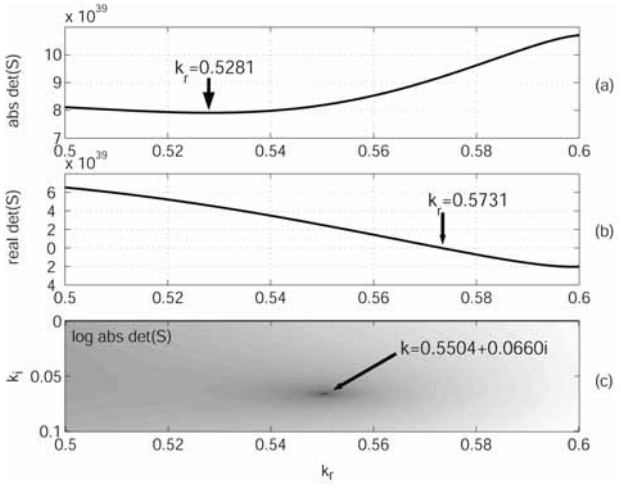

FIGURE 3

Resulting wavenumber if the root of the dispersion equation is searched for in (a) minima of absolute value of the determinant along the real wavenumber axis, (b) real value sign change along the real wavenumber axis, and (c) minima of absolute value in the complex wavenumber domain.

When the phase velocity becomes higher than V_S in the lower half-space, the propagating wave in the *x*-direction becomes leaky and the modal solution must be traced in the complex wavenumber domain. This adds one more dimension to the already complicated problem of finding solutions to equation (4). In this study, the dispersion curve software '*Disperse*' from Imperial College (Pavlakovic *et al*. 1997; Disperse 2001) has been used to trace most of the dispersion curves in the complex wavenumber domain. The Nelder-Mead simplex (direct search) method, as implemented in the function *fminsearch* in *Matlab*, has also proved useful for tracing dispersion curves in the complex wavenumber domain. Instead of searching for a sign change of the real value of the determinant of **S**, a minimum of the absolute value of the determinant is used. In Fig. 3, the modal solution at 200 Hz of one of the dispersion curves used in the subsequent example (V_{S2}=3000 m/s), is illustrated in different domains. In Fig. 3(a), in which the absolute value of the determinant is plotted as a function of k_r, a minimum can be found at k_r=0.5281, corresponding to a phase velocity of 2380 m/s. In Fig. 3(b) only the real part of the determinant is plotted as a function of k_r. A change in sign can be found at k_r=0.5731, corresponding to a phase velocity of 2193 m/s. The exact solution in the complex wavenumber domain is shown as a minimum of the absolute value of the determinant in Fig. 3(c). The exact solution can be found at k=0.5504+0.0660i. The real part of the wavenumber corresponds to a phase velocity of 2283 m/s along the surface in the *x*-direction. This is the exact phase velocity at 200 Hz that should be used when the dispersion curve is plotted. The simplified approaches used in Figs 3(a) and 3(b) result in an erroneous dispersion curve, in this case with an error in the phase velocity at 200 Hz of about 100 m/s.

DEFINITION OF CALCULATED PARAMETERS

Theoretical dispersion curves are usually presented as phase velocity V (V= ω/k_r) plotted as a function of frequency f or wavelength λ, for each mode of propagation. This form of presentation shows all possible combinations of k_r and f of the complete layer system. However, this display does not give any information on those portions of different modes that will be measurable at the surface. All modes calculated from the dispersion equation are usually defined as Rayleigh-wave modes. However, the solution of the matrix equations will give dispersion curves representing any type of guided wave with particle motion in the *x*- and *y*-directions, such as interface waves and plate waves. Some of the calculated k and f pairs will represent other types of guided waves and leaky waves that will not be measurable at the surface. Therefore, we suggest that multiple normal-mode dispersion curves utilized for the inversion of surface-wave data should include the excitability at the surface and the leakage along the surface in the *x*-direction, for each point on the dispersion curve.

This additional information can be helpful for the interpretation of multimodal dispersion curves and can reduce the risk of mode misidentification (Socco *et al*. 2002), resulting in erroneous final results (Zhang and Chan 2003). Including information about amplitude ratios between modes has been proposed in other publications (Gucunski and Woods 1992; Tokimatzu *et al*. 1992; Ganji *et al*. 1998; Hunaidi 1998; Foti 2000), usually for the purpose of calculating an apparent dispersion curve where the complete measurement set-up is taken into account. It should be noted that in this study the locations of the receivers are not taken into account. The mode shape, excitability and leakage of each mode, as used in this study, are defined below.

Mode shape

The mode shape shows how displacement or stress varies as a function of depth y, and can be used to study which layer or layers are affected by a particular mode and frequency. The mode shape is also calculated for a few wavelengths in the direction of propagation x (see example in Fig. 9), although the distribution is known to be sinusoidal. A root of the dispersion equation must first be calculated. This gives a wavenumber k and frequency f pair, representing a modal solution. Then one of the bulk-wave amplitudes A can be set to unity and the other partial wave amplitudes can be calculated relative to the assumed value of unity. The system matrix **S** is then multiplied by the vector **A,** containing all partial wave amplitudes, to obtain the stresses and displacements in the (u,σ) vector of equation (5).

Excitability

The excitability E of a particular mode at a particular frequency is defined as the ratio of displacement of that mode to applied force, when both quantities are measured at the same location and direction (Wilcox *et al*. 2002). A harmonic vertical point force at the surface with a certain frequency will excite different modes along the surface to various degrees. With the global matrix method it will not require much additional computation time to derive the excitability of each point on each dispersion curve. The vertical displacement u_y at the surface is calculated with the same procedure as for the mode shapes from the system matrix. The excitability can then be calculated as

$$E \propto u^2 f \,. \tag{12}$$

Leakage

The attenuation due to leakage of modes is calculated from the ratio between the imaginary k_i and real k_r parts of the wavenumber that arises when the phase velocity exceeds the shear-wave velocity in the lower half-space. Points on a dispersion curve with a large imaginary part of the wavenumber are therefore not likely to appear in measured surface-wave data. This additional information should be helpful in identifying portions of modes that should be compared in the inversion process of surface-wave data. The attenuation coefficient κ is defined as

$$\kappa = \frac{2\pi k_i}{k_r}, \tag{13}$$

where the unit of κ is nepers per wavelength, so that a wave of unit amplitude is reduced to an amplitude of $e^{-\kappa}$ after travelling one wavelength. It should be noted that leakage causes additional attenuation of geometric spreading and material damping.

COMPARING LAMB WAVES WITH NORMAL MODES IN LAYERED MEDIA

A three-layer model (one discrete layer and two semi-infinite half-spaces) is used to study theoretical dispersion curves in inversely dispersive sites and to quantify the discrepancy between these dispersion curves compared to the Lamb-wave dispersion curves for a free plate. Here, the practical value of the additional parameters, *excitability* and *leakage*, defined above, will also be demonstrated. The reference layer model is shown in Fig. 4. The first layer is set to be a vacuum, to represent the trac-

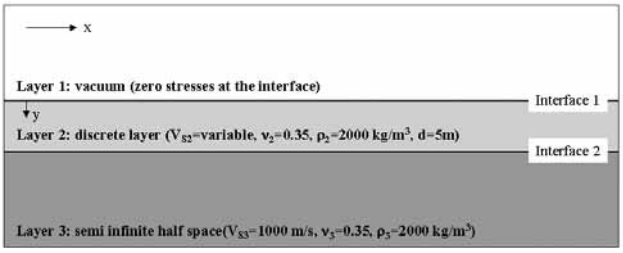

FIGURE 4

Layer model used in the numerical study. All layer properties are kept fixed except for the shear-wave velocity in the second layer.

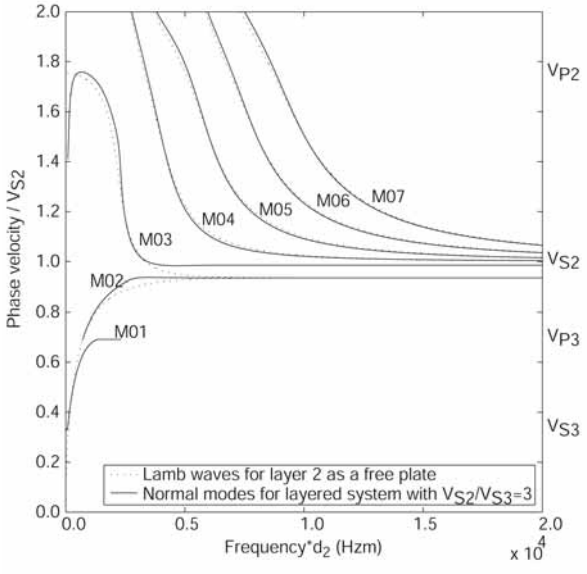

FIGURE 5

A comparison between free Lamb waves (from Fig. 1) and normal modes for the layered model. Axes are normalized with respect to the thickness and shear-wave velocity of the second layer. Bulk-wave velocities of the layered model are indicated on the left-hand y-axis.

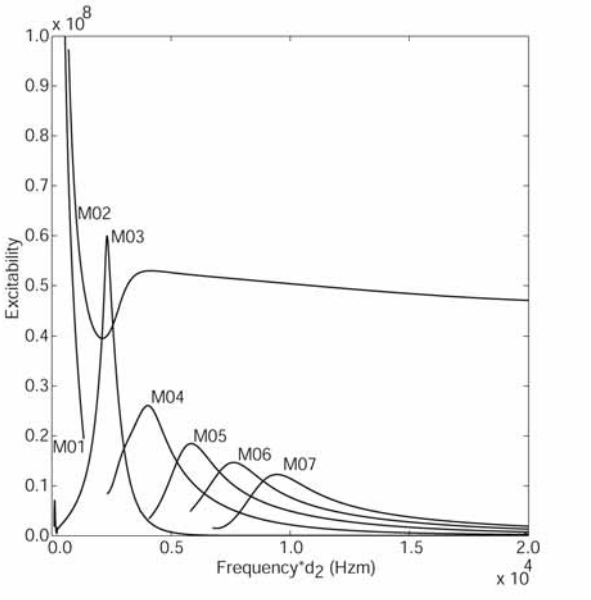

FIGURE 6
Excitability corresponding to the normal-mode dispersion curves in Fig. 5.

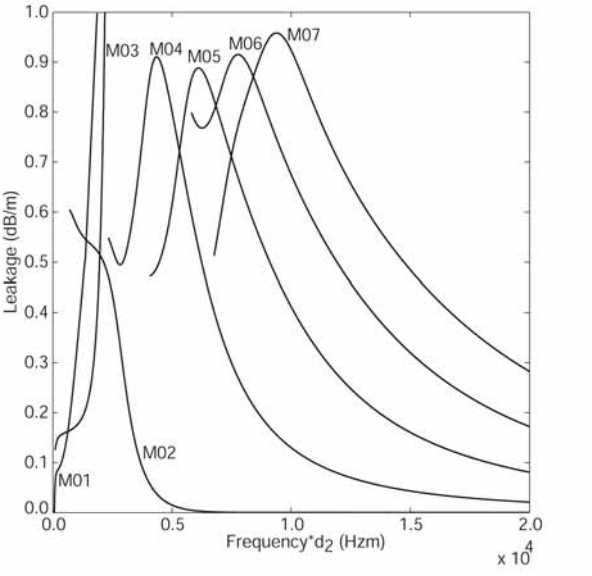

FIGURE 7
Leakage corresponding to the normal-mode dispersion curves in Fig. 5.

tion-free top surface of the second layer. The second layer is set at a thickness of 5 m with a variable shear-wave velocity between 1000 m/s and 4000 m/s.

All Lamb-wave modes from Fig. 1 are first plotted, together with normal modes for the layered model, at a fixed V_{S2}=3000 m/s (see Fig. 5). Solid lines represent normal modes calculated from equation (4) (i.e. the exact solution), and dotted lines represents Lamb-wave dispersion curves for a free plate with V_S=3000 m/s, ν=0.35 and d=5 m. In general, most of the normal modes match quite well with the Lamb-wave dispersion curves for the free plate, especially for the higher modes M04 – M07. For the layered model, the fundamental mode M01 and the first higher mode M02 are closest to the A0 Lamb-wave dispersion curve. The discontinuity along the A0 trend created by the M01 and M02 dispersion curves has been studied in early publications (Jones 1962; Vidale 1964). The M03 mode follows the S0 Lamb-wave dispersion curve, the main difference being that the high-frequency asymptotic trend in phase velocities does not approach the Rayleigh-wave velocity but the shear-wave velocity of the second layer.

In Fig. 6, the corresponding excitability coefficient in the vertical direction at the surface is plotted for each mode of the layered model. The excitability shows that the M02 mode will dominate surface displacements in most of the frequency range. Only in a very narrow frequency band from 2100 to 2600 Hz-m does the M03 mode show a higher excitability than the M02 mode. At the lowest frequencies, only the M01 mode exists and will therefore dominate surface displacements for the lowest frequencies. All higher modes, M04 – M07, exhibit a fairly low excitability and will therefore probably not be observable at the surface. Furthermore all higher modes display a higher attenuation (Fig. 7) due to leakage and will therefore be more attenuated compared to the strong M01 and M02 modes.

From the results above it can be concluded that, for surface-wave applications on a stiff layer supported by softer material, the M01, M02 and M03 modes are of most interest for further investigation. This is due to their dominant excitability and low leakage wave propagation characteristics. In the following sections, these modes will be studied as a function of the stiffness ratio between the second and third layers in the reference model (Fig. 4).

The fundamental mode M01

All fundamental mode (M01) dispersion curves for V_{S2}=1000 – 4000 m/s are plotted in Fig. 8(a). The phase velocity of the fundamental mode is initially the Rayleigh-wave velocity of the lower half-space (931 m/s) at the lowest frequencies and approaches the Rayleigh-wave velocity of the second layer as long as the condition $V_{S2}<V_{P3}$ is satisfied (this is similar to normally dispersive sites). When V_{S2} becomes higher than V_{P3}, which is kept fixed at 2082 m/s, the phase velocity becomes limited by V_{P3} and the wave converts into a leaky interface wave travelling at the interface between the second and third layers. As the wave transforms to an interface wave, the excitability at the surface decreases (Fig. 8b) and the leakage increases (Fig. 8c). Therefore this straight portion of the dispersion curve at a phase velocity equal to V_{P3} will probably not be measurable at the surface. Figure 8(c) shows that the leakage (i.e. the imaginary part of the wavenumber) is zero when $V<V_{S3}$, as expected. When V becomes higher than V_{S3}, the wave becomes leaky. However it should be noted that the leakage approaches zero again for M01 modes at V_{S2}<1600 m/s, corresponding to free interface waves

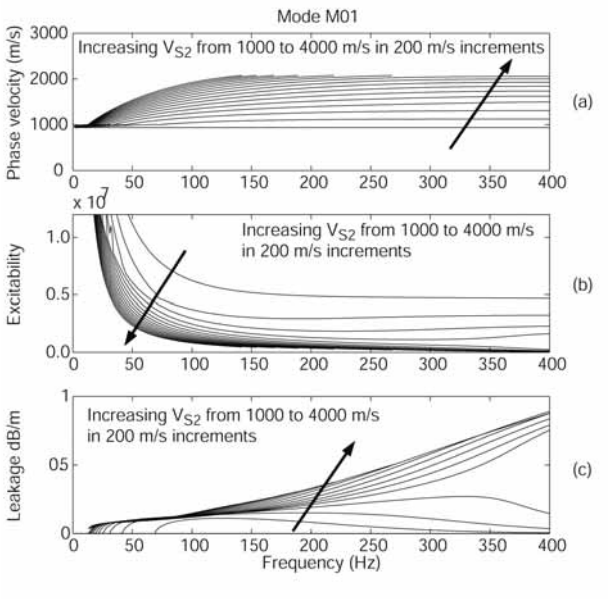

FIGURE 8

(a) Dispersion curves of the M01 mode for different shear-wave velocities of the second layer, i.e. different stiffness ratios between layers 2 and 3. (b) The corresponding excitability coefficient is plotted for the same dispersion curves. (c) The attenuation due to leakage for all M01 modes.

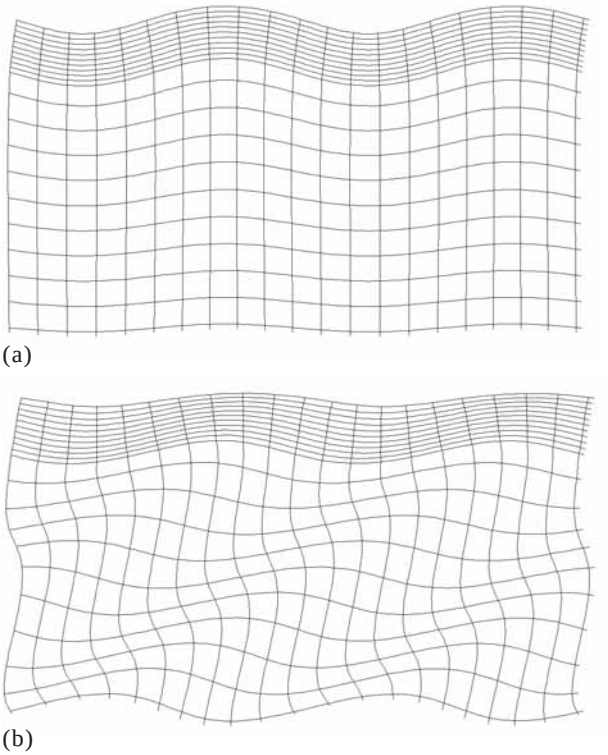

FIGURE 9

Mode shapes at (a) low frequencies where the particle motion approaches the Rayleigh-wave motion. At higher frequencies (b) the M01 mode becomes leaky and energy radiates down into the lower velocity half-space.

(Stonely 1924). At these frequencies the excitability at the surface is very low (Fig. 8b) because the wave is concentrated at the interface between layers 2 and 3 and the particle motion at the free surface tends to zero. As long as the condition $V_{S2} > V_{P3}$ is fulfilled (as for most concrete or asphalt surface-wave applications), the limiting phase velocities of the M01 mode could therefore potentially be used to estimate both V_P and V_S of the lower-velocity underlying media in a simple manner.

Two different characteristic mode shapes are shown in Fig. 9. In Fig. 9(a), the mode shape for the $V < V_{S3}$ case is displayed. Under this condition, particle motion is similar to Rayleigh-wave propagation and there is no leakage. Figure 9(b) shows the mode shape at higher phase velocities ($V > V_{S3}$) where there is leakage. It can be seen in Fig. 9(b) that there is now a vertical oscillating component of particle motion and energy radiates down into the lower half-space.

The first higher mode M02

In Fig. 10, the first higher-mode (M02) dispersion curve for V_{S2}=2200–4000 m/s is plotted. The phase velocity is initially at the compressional-wave velocity of the lower half-space and increases with frequency up to the Rayleigh-wave velocity of the second layer. This behaviour at high frequencies is very similar to the A0 Lamb-wave dispersion curve in Fig. 1. In this case, the leakage decreases and approaches zero when the wavelength becomes smaller than the thickness of the layer (5 m). At these high frequencies and short wavelengths, the wave propagation is again similar to Rayleigh-wave propagation and the discrete layer acts as a semi-infinite half-space.

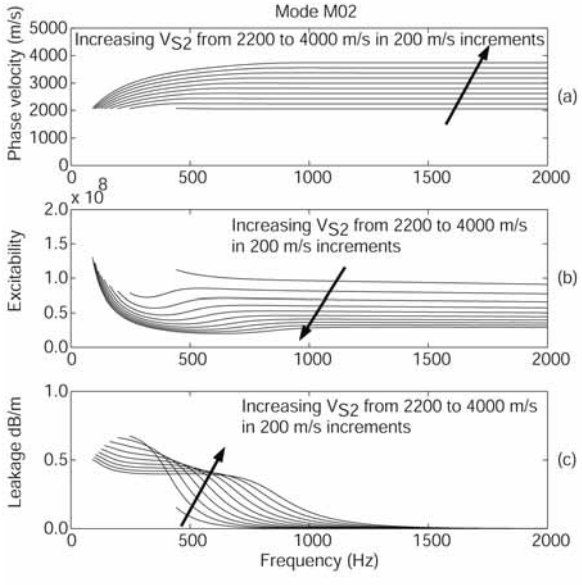

FIGURE 10

(a) Dispersion curves of the M02 mode for V_{S2}=2200–4000 m/s. (b) The corresponding excitability coefficient is plotted for the same dispersion curves. (c) The attenuation due to leakage for all M02 modes.

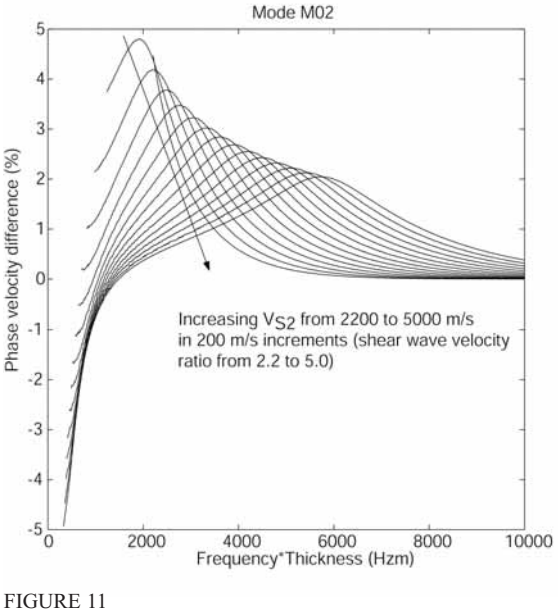

FIGURE 11

The difference between the M02 mode and the A0 Lamb-wave mode calculated with the same free-plate properties as for the second layer in Fig. 4. The largest discrepancy in phase velocities is about 5% for the lowest stiffness ratio of 2.2 between the shear-wave velocities of the second and third layers.

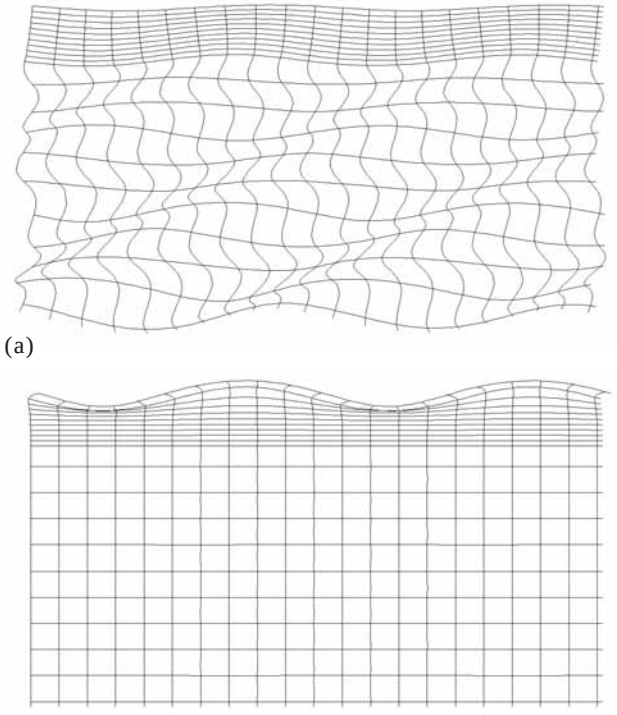

FIGURE 12

(a) Mode shapes at low frequencies where the M02 mode is leaky and energy radiates down into the lower velocity half-space. (b) At higher frequencies the M02 mode shape approaches the Rayleigh-wave motion and is concentrated at the free surface.

To study the Lamb-wave approximation in detail, true Lamb-wave dispersion curves are compared to the exact solutions, including the influence of a lower-velocity half-space calculated above. Figure 11 shows the difference in phase velocities between A0 and M02 as a function of frequency and stiffness ratio. It can be seen that the discrepancy in phase velocities does not exceed 5% at the lowest shear-wave velocity ratio. As the stiffness ratio increases, the difference in phase velocities decreases and should tend to zero at an infinite stiffness contrast.

The mode shapes of the M02 mode at low and high frequencies have been calculated (Figs 12a and 12b). In the low-frequency range (Fig. 12a) and as long as $V_{S2} > V_{P3}$, wave propagation is leaky (see Fig. 10c) and energy radiates down into the lower half-space. At higher frequencies, the particle motion approaches the Rayleigh-wave mode shape again (Fig. 12b).

The second higher mode M03

The second higher-mode (M03) dispersion curve is plotted in a similar format (Fig. 13) with different stiffness ratios between the second and third layers. As shown in Fig. 5, the M03 mode follows the same trend as the S0 Lamb-wave dispersion curve. The main difference is in the asymptotic phase velocity at high frequencies, which here approaches V_{S2} instead of the Rayleigh-wave velocity. The excitability (Fig. 13b) shows one distinct peak at a constant wavelength close to the resonant frequency of

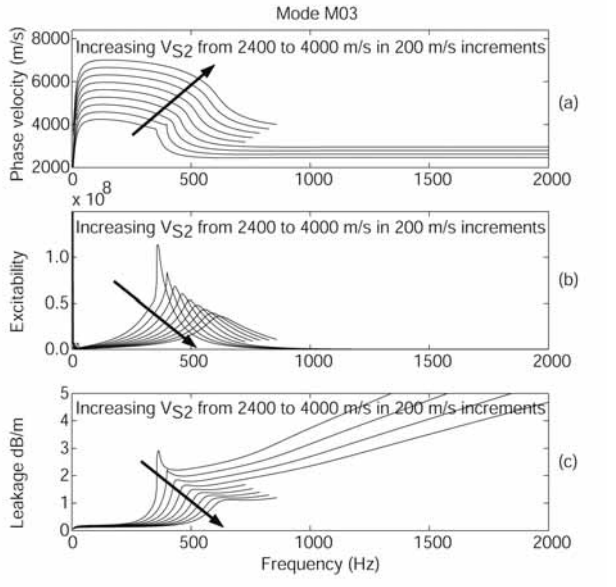

FIGURE 13

(a) Dispersion curves of the M03 mode for V_{S2}=2400–4000 m/s. Not all dispersion curves have been traced in the full frequency range because of numerical difficulties when the phase velocity is equal to one of the bulk-wave velocities in the model. (b) The corresponding excitability coefficient is plotted for the same dispersion curves. (c) The attenuation due to leakage for all M03 modes.

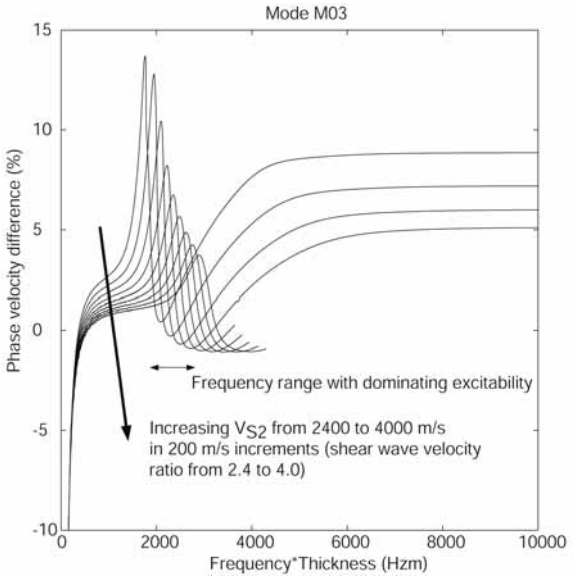

FIGURE 14
The difference between the M03 mode and the S0 Lamb-wave mode calculated with the same free-plate properties as for the second layer in Fig. 4. See text for description.

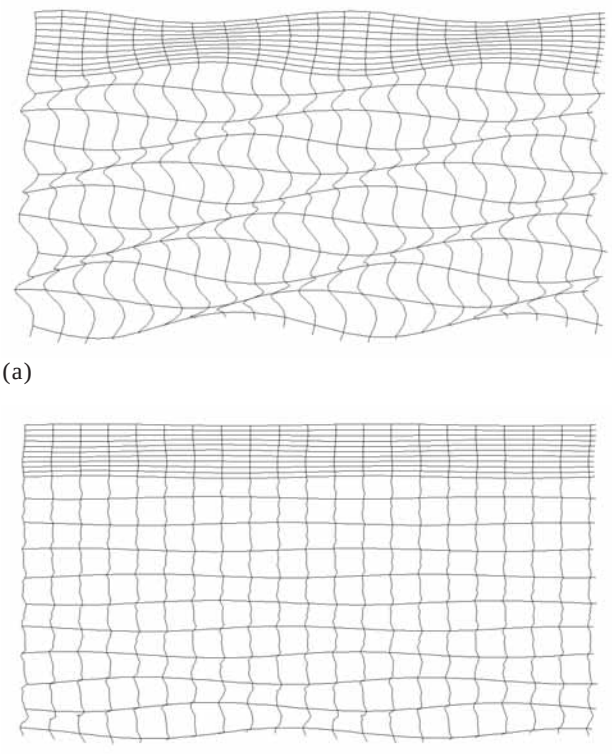

FIGURE 15
Mode shapes at (a) low frequencies, (b) at higher frequencies. See text for description.

the second layer. At frequencies above the peak excitability, the M03 mode is strongly attenuated by leakage (Fig. 13c).

Figure 14 shows the difference in phase velocities of S0 and M03 as a function of frequency and stiffness ratio. The discrepancy in phase velocities has a highest value of 14% for the lowest stiffness contrast (2.4) between the shear-wave velocities of the second and third layers, and decreases to about 3% for a shear-wave velocity ratio of 4. The frequency range with dominant excitability (Fig. 13b) is indicated by an arrow. In practice, this is the only part of the M03 mode that can be excited with a vertical point source at the surface, corresponding to a maximum deviation of about 10%.

Two typical mode shapes of the M03 dispersion curve were calculated (Fig. 15). In the lower frequency range (Fig. 15a), M03 mode particle motion in the stiff layer looks very similar to the characteristic mode shape of the S0 Lamb wave (Fig. 1). There is strong leakage because the phase velocity is higher than the shear-wave velocity of the lower half-space. In the higher frequency range (Fig. 15b) where M03 is leaky, there is almost no particle motion at the surface.

FIELD EXAMPLE

A field example is presented to illustrate the practical usefulness of the above results for a simple evaluation of the stiff top layer at inversely dispersive sites. The exact solution of the multilayered structure (complex wavenumbers) is avoided here by using the free-plate Lamb-wave approximation. Data was collected at a flexible pavement where the asphalt thickness was known to be 0.12 m. Data acquisition was performed with the portable seismic acquisition system (PSAS) (Ryden *et al*. 2002) using only one receiver and a synthetic source array (Ryden *et al*. 2001). The station separation was 0.05 m and data was collected with a total offset range of 2 m. All traces were compiled in a multichannel record shown in Fig. 16(a). The wavefield transformation technique, used in the multichannel analysis of surface waves (MASW) method (Park *et al*. 1998, 1999), was used to transform the collected data to the phase-velocity–frequency domain. Figure 16(b) shows the resulting phase velocity spectrum (overtone image).

The Lamb-wave dispersion curves for a free plate with V_S=2100 m/s, ν=0.35 and d=0.12 m are plotted on top of the overtone image (Fig. 16b). There is a fairly good match between most of the visible energy in the overtone image and the A0 Lamb-wave dispersion curve, for the given thickness and a realistic shear-wave velocity, representative of the asphalt stiffness at high frequencies. It can also be seen that there is a good match between the frequency range of the S0 mode with dominant excitability and the visible high amplitudes in the overtone image at about 14 kHz. In this case, this is also the velocity that can be evaluated in the time domain from the first arrivals. However, because these waves are actually dispersive, the analysis should preferably be conducted in the frequency domain.

In this example, Lamb-wave dispersion curves were matched

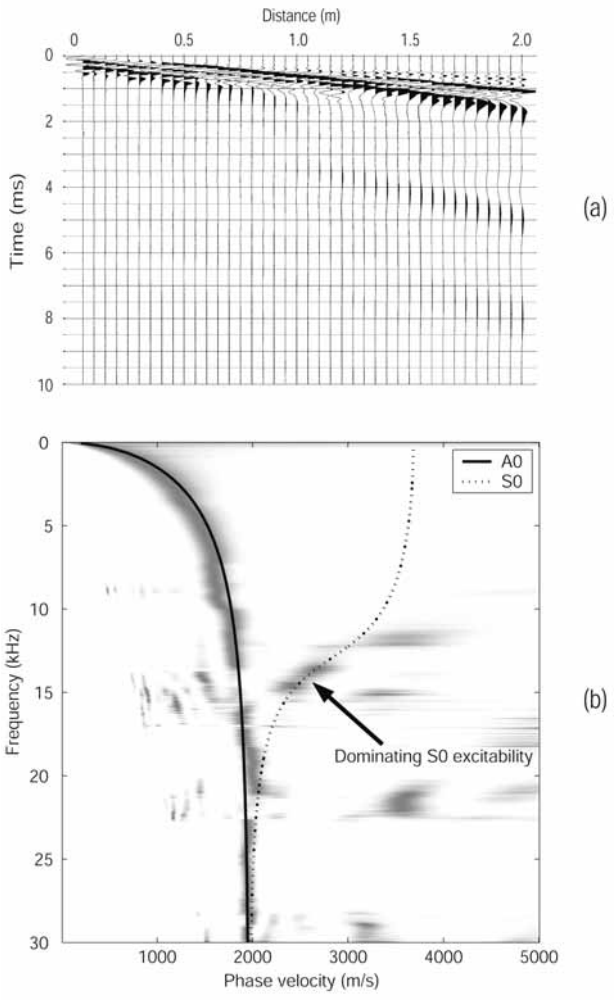

FIGURE 16

(a) Recorded data in the time domain from a flexible pavement with a 0.12 m stiff asphalt layer. (b) The corresponding phase-velocity spectrum from the collected data. The A0 and S0 Lamb-wave dispersion curves, corresponding to V_S=2100 m/s, ν=0.35 and d=0.12, are plotted on top of the grey-scale amplitude spectrum. There is a good match between the Lamb-wave dispersion curves and the measured data and, as predicted from the excitability of the S0 dispersion curve, this mode only shows up in a very narrow frequency band.

with the phase-velocity spectrum by a manual trial-and-error approach. However, it should be possible to implement any automatic optimization routine for this matching process.

CONCLUSIONS

Inverse dispersion of surface waves was studied using a synthetic layer model. It was emphasized that dispersion curves must be traced in the complex wavenumber domain whenever there is leaky wave propagation (i.e. when the phase velocity becomes higher than the shear-wave velocity of the lower half-space). The amount of leakage and the excitability of different modes can provide critical information that can be used to interpret measured data and reduce the risk of possible misidentification of different modes of dispersion curves.

Lamb-wave dispersion curves for a free plate in a vacuum can represent the reality sufficiently closely only if the stiffness contrast between the top layer and the underlying half-space is large. The resulting error in phase velocity in this case was investigated. It was concluded that the error in phase velocity does not exceed 5% if the fundamental antisymmetric Lamb-wave dispersion curve is used as an approximate theoretical dispersion curve, with the restriction that the shear-wave velocity of the stiff layer is greater than the compressional-wave velocity in the underlying media. The reported results are based on a constant Poisson's ratio of 0.35 and a limited range of parameters and are, therefore, strictly only valid for this case.

Lamb-wave dispersion curves are easier to calculate and can therefore, in practice, be used for the evaluation of the thickness and shear-wave velocity of a stiff top layer. The practical usefulness of this approach has been demonstrated with a field data example from a flexible pavement construction.

ACKNOWLEDGEMENTS

We thank Peab Sverige AB, VINNOVA, and the Swedish National Road Administration, for financing this project. We also thank Dr. Peter Ulriksen, Lund University, and Dr. Mike Lowe and Professor Peter Cawley at Imperial College for their assistance. The help from Mary Brohammer with the preparation of this manuscript is also greatly appreciated.

REFERENCES

Akhlaghi B.T. and Cogill W.H. 1994. Application of the free plate analogy to a single-layered pavement system. *INSIGHT* **36**, 514–518.

Aki K. and Richards P.G. 1980. *Quantitative Seismology: Theory and Methods*. W.H. Freeman & Co.

Disperse. 2001. A system for generating dispersion curves. User's manual version 2.0.11. Software version 2.0.15e. Guided Ultrasonics, London.

Forbriger T. 2003. Inversion of shallow-seismic wavefields part 1: wavefield transformation. *Geophysical Journal International* **153**, 719–734.

Foti S. 2000. *Multistation methods for geotechnical characterization using surface waves*. PhD thesis, Politecnico di Torino, Italy.

Foti S., Sambuelli L., Socco V.L. and Strobbia C. 2003. Experiments of joint acquisition of seismic refraction and surface wave data. *Near Surface Geophysics* **1**, 119–129.

Ganji V., Gucunski N. and Nazarian S. 1998. Automated inversion procedure for spectral analysis of surface waves. *Journal of Geotechnical and Geoenvironmental Engineering, ASCE* **124**, 757–770.

Graff K.E. 1975. *Wave Motion in Elastic Solids*. Oxford University Press.

Gucunski N. and Woods R.D. 1992. Numerical simulation of the SASW test. *Soil Dynamics and Earthquake Engineering* **11**, 213–227.

Hunaidi O. 1998. Evolution-based genetic algorithms for analysis of non-destructive surface wave tests on pavements. *NDT&E International* **31**, 273–280.

Jones R. 1955. A vibration method for measuring the thickness of concrete road slabs in situ. *Magazine of Concrete Research*, 97–102.

Jones R. 1962. Surface wave technique for measuring the elastic proper-

ties and thickness of roads: theoretical development. *British Journal of Applied Physics* **13**, 21–29.

Jones R. and Thrower E.N. 1965. An analysis of waves in a two-layer composite plate and its application to surface wave propagation experiments on roads. *Journal of Sound and Vibration* **2**, 328–335.

Knopoff L. 1964. A matrix method for elastic wave problems. *Bulletin of the Seismological Society of America* **54**, 431–438.

Lamb H. 1917. On waves in an elastic plate. *Proceedings of the Royal Society* **93**, 114–128.

Lowe M.J.S. 1995. Matrix techniques for modeling ultrasonic waves in multilayered media. *IEEE Transactions on Ultrasonics, Ferroelectrics, and Frequency Control* **42**, 525–542.

Martincek G. 1994. *Dynamics of Pavement Structures*. E&FN Spon and Ister Science Press.

Nazarian S. 1984. *In situ determination of soil deposits and pavement systems by spectral analysis of surface waves method*. PhD thesis, University of Texas at Austin, Texas.

Park C.B., Miller R.D. and Xia J. 1998. Imaging dispersion curves of surface waves on multi-channel records. 68th SEG Meeting, New Orleans, USA, Expanded Abstracts, 1377–1380.

Park C.B., Miller R.D. and Xia J. 1999. Multichannel analysis of surface waves. *Geophysics* **64**, 800–808.

Park C.B., Ryden N., Westerhoff R. and Miller R.D. 2002. Lamb waves observed during MASW surveys. 72nd SEG Meeting, Salt Lake City, USA, Expanded Abstracts, 1400–1403.

Pavlakovic B., Lowe M., Alleyne D. and Cawley P. 1997. Disperse: a general purpose program for creating dispersion curves. *Review of Progress in Quantitative NDE* **16**, 185–192.

Randall M.J. 1967. Fast programs for layered half-space problems. *Bulletin of the Seismological Society of America* **57**, 1299–1315.

Roësset J.M., Chang D.W. and Stokoe K. 1991. Comparison of 2-D and 3-D models for analysis of surface wave tests. 1st International Conference on Soil Dynamics and Earthquake Engineering, Karlsruhe, Germany, Expanded Abstracts, 111–126.

Ryden N., Park C.B., Ulriksen P. and Miller R.D. 2003. Lamb wave analysis for non-destructive testing of concrete plate structures. Proceedings of the Symposium on the Application of Geophysics to Engineering and Environmental Problems (SAGEEP 2003), San Antonio, TX, CD-Rom.

Ryden N., Park C.B., Ulriksen P. and Miller R.D. 2004. Multimodal approach to seismic pavement testing. *Journal of Geotechnical and Geoenvironmental Engineering, ASCE* **130**, 636–645.

Ryden N., Ulriksen P., Park C.B. and Miller R.D. 2002. Portable seismic acquisition system (PSAS) for pavement MASW. Proceedings of the Symposium on the Application of Geophysics to Engineering and Environmental Problems (SAGEEP 2002), Las Vegas, NV, 13IDA7.

Ryden N., Ulriksen P., Park C.B., Miller R.D., Xia J. and Ivanov J. 2001. High frequency MASW for non-destructive testing of pavements-accelerometer approach. Proceedings of the Symposium on the Application of Geophysics to Engineering and Environmental Problems (SAGEEP 2001), Denver, Colorado, RBA-5.

Socco L.V., Strobbia C. and Foti S. 2002. Multimodal interpretation of surface wave data. Proceedings of the 8th Meeting of the Environmental and Engineering Geophysics Society European Section, Aveiro, Portugal, CD-Rom.

Stokoe II K.H. and Santamarina J.C. 2000. Seismic-wave-based testing in geotechnical engineering. Proceedings of the GeoEng 2000 Meeting, Melbourne, Australia.

Stokoe K.H., Wright G.W., James A.B. and Jose M.R. 1994. Characterization of geotechnical sites by SASW method. In: *Geophysical Characterization of Sites* (ed. R.D. Woods). ISSMFE Technical Committee #10, Oxford Publishers, New Delhi.

Stoneley R. 1924. Elastic waves at the surface of separation of two solids. *Proceedings of the Royal Society* **106**, 416–428.

Tokimatsu K., Tamura S. and Kojima H. 1992. Effects of multiple modes on Rayleigh wave dispersion characteristics. *Journal of Geotechnical and Geoenvironmental Engineering, ASCE* **118**, 1529–1543.

Vidale R.F. 1964. *The dispersion of stress waves in layered media overlaying a half-space of lesser acoustic rigidity*. PhD thesis, University of Wisconsin.

Viktorov I.A. 1967. *Rayleigh and Lamb waves*. Plenum Press, New York.

Wilcox P., Evans M., Diligent O., Lowe M. and Cawley P. 2002. Dispersion and excitability of guided acoustic waves in isotropic beams with arbitrary cross section. *Review of Progress in Quantitative NDE* **21**, 203–210.

Xia J., Miller R.D. and Park C.B. 1999. Estimation of near-surface shear-wave velocity by inversion of Rayleigh wave. *Geophysics* **64**, 691–700.

Zhang S.X. and Chan L.S. 2003. Possible effects of misidentified mode number on Rayleigh wave inversion. *Journal of Applied Geophysics* **53**, 17–29.

Paper IV

Guided wave propagation in three-layer pavement structures

Nils Ryden[a)]
Department of Engineering Geology, Lund Institute of Technology, Lund University, Box 118, S-221 00, Sweden

Michael J. S. Lowe
Department of Mechanical Engineering, Imperial College, London SW7 2AZ, United Kingdom

(Received 10 March 2004; revised 25 August 2004; accepted 26 August 2004)

A study on guided waves in a layered half-space with large velocity contrasts and a decreasing velocity with depth is presented. Multiple mode dispersion curves are calculated in the complex wave number domain, taking into consideration the attenuation caused by leakage into the underlying half-space. The excitability of the modes by a vertical point force on the surface is also calculated. Results show that the measurable wave field at the surface of a pavement structure is dominated by leaky quasi-Lamb waves in the top and second layers. The fundamental antisymmetric mode of vibration is the dominating mode generated in the stiff top layer. This mode drives the complete system and continuity across the boundaries generates higher order modes in the embedded second layer. The interaction of leaky Lamb waves in the first two layers results in large variations in the excitability and the attenuation, so that only the waves corresponding to certain portions of the dispersion curves are measurable remote from the source at the pavement surface. It is concluded that these portions of dispersion curves can be individually resolved in practice, by using multichannel processing techniques. This holds the potential for a refined nondestructive testing technique for pavements.
[DOI: 10.1121/1.1808223]

PACS numbers: 43.35.Pt, 43.35.Cg, 43.40.Le [YHB] Pages: 2902–2913

I. INTRODUCTION

Guided waves are used in a broad range of applications ranging from global seismology to acoustic microscopy. These waves are formed by the interaction of longitudinal (α) and shear (β) bulk waves and the geometry of the medium. Consequently guided waves carry information on the structural properties (thickness, bonding, and elastic constants) of the medium. New applications using guided waves are continuously being developed and often each new application calls for a detailed analysis on the nature of wave propagation in each specific case (Lowe and Cawley, 1995a; b; Long *et al.*, 2003; Lefeuvre *et al.*, 1998).

The theoretical basis of wave propagation in a layered elastic half-space using matrix methods was introduced by Thomson (1950) and Haskell (1953). Since then a large number of studies on wave propagation in layered systems have been presented; see for example (Lowe, 1995). However, there are only a limited number of studies on guided waves in a multi-layered medium with large velocity contrasts and a decreasing velocity with depth (Picket, 1945; Jones, 1962; Vidale, 1964; Zhang and Lu, 2003). This case is of specific interest in acoustic nondestructive testing of pavements and is the motivation and focus for the work presented here. Another application that falls into this category is ultrasonic testing of some types of coated materials (Shuvalov and Every, 2002) and sandwich structures (Lefeuvre *et al.*, 2000), and it is possible that the generic findings here may also be useful in those fields.

Related studies have dealt with the case of one stiff (fast) layer on a lower velocity half-space (Press and Dobrin, 1956; Jones, 1962; Lefeuvre *et al.*, 1998; Cheng *et al.*, 2001; Ryden and Park, 2004). Yapura and Kinra (1995) investigated dispersion curves and mode shapes for a fluid–solid bilayer. Guided waves trapped in an embedded lower velocity layer have been studied by Parra and Xu (1994), and the opposite case with one embedded higher velocity layer by Lowe and Cawley (1995a, b). Dispersion curves of a bilayered plate were investigated by Jones and Thrower (1965), Laperre and Thys (1993), Lee and Cheng (2001), and Simonetti (2004). Similar studies on multilayered plates have been presented by Cheng *et al.* (2001) and Shull *et al.* (1994). To the author's knowledge, there are no studies on a three-layered half-space with large velocity contrasts and decreasing velocity with depth, where multiple modes of guided waves have been studied in the complex wave number domain.

It is the main purpose of this paper to study guided waves in this specific layer setting. Results should be applicable to any such layered system, but here the main emphasis is towards nondestructive testing of pavements. The present three-layer system represents an extension to a more realistic pavement structure from the two-layer system investigated by Ryden and Park (2004). Some background on surface wave testing of pavements is first presented. In the subsequent sections dispersion curves traced in the complex wave number domain along with leakage, excitability, and mode shapes are studied. A numerical example with two layers on a half-space is used to explain these characteristics. Practical

[a)]Electronic mail: nils.ryden@tg.lth.se

consequences from these results related to the application to nondestructive testing of pavements are also discussed.

II. BACKGROUND ON SURFACE WAVE TESTING OF PAVEMENTS

Nondestructive testing of civil engineering structures is useful in maintenance planning of old constructions and verification of material properties in new constructions. The determination of thickness and stiffness of each layer in a pavement construction are typical objectives. Surface wave methods in civil engineering applications are based on the dispersive nature of surface waves in a layered medium. This is used to estimate a shear wave velocity, i.e., stiffness-profile of the test site. The traditional testing procedure can be divided into three basic steps: (1) generation and measurement of stress waves in the field; (2) data processing and extraction of a measured dispersion curve; and (3) inversion of the measured dispersion curve to obtain an estimated shear wave velocity with depth profile.

The same basic principles of surface wave propagation are often assumed, regardless of the investigated medium. It is usually assumed that Rayleigh waves are the prevailing type of wave measured, with a depth penetration from the surface related to the wavelength (λ). In surface wave testing of pavements the measured dispersion curve is usually calculated directly from the wrapped phase difference between two receivers on the surface (Heisey *et al.*, 1982; Nazarian, 1984; Stokoe *et al.*, 1994). This apparently continuous dispersion curve ($\sim$30–30 000 Hz) is then used for the evaluation of layer properties through an iterative inversion procedure (Ganji *et al.*, 1998; Hunaidi, 1998; Xia *et al.*, 1999; Gucunski *et al.*, 2000; Wu *et al.*, 2002). This technique has proved to be most effective for the evaluation of the shear wave velocity in the top (asphalt) and bottom (subgrade) layer (Roesset *et al.*, 1990; Aouad, 1993). The properties of the embedded (base) layer have been more difficult to resolve (Aouad, 1993; Foinquinos *et al.*, 1995). However, the potential of evaluating deeper embedded layers in a nondestructive manner has always been one of the main motivations for surface wave testing of pavements. It is mainly the inclusion of higher modes that has been assumed to be the main source of the experienced difficulties (Aouad, 1993; Foinquinos *et al.*, 1995; Roesset *et al.*, 1990).

To resolve multiple modes of propagation, multichannel measurements and two-dimensional wave field transformation techniques have been introduced in near surface site characterization (Gabriels *et al.*, 1987; Park *et al.*, 1999; Foti, 2000; Forbriger, 2003; O'Neill, 2003; Beaty and Smith, 2003). These methods require more data to be collected in the field but are capable of resolving different modes of propagation in the typical soil site frequency range of 5 to 80 Hz. In an attempt to collect higher frequency multichannel equivalent data on a pavement structure, Ryden *et al.* (2001) proposed to use a synthetic array with only one accelerometer and a small hammer. The measured wave field spectrum obtained from this approach came out to be more complicated than expected (Ryden *et al.*, 2002). Abraham *et al.* (2000) and Inazaki and Xinglin (2003) presented similar data and also concluded that the observed dispersion curves in the phase velocity spectrum could not be readily evaluated.

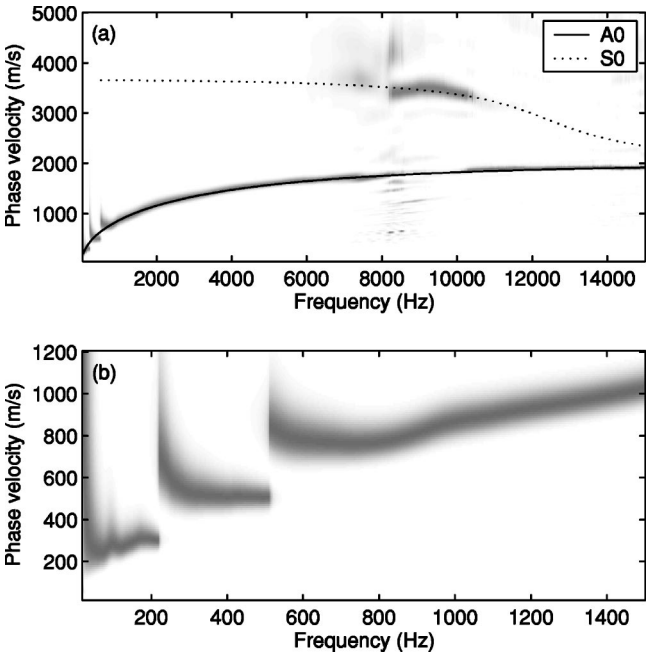

FIG. 1. (a) Gray shading corresponds to the measured phase velocity spectrum from a three-layer pavement construction. Predicted Lamb wave dispersion curves from the top layer as a free plate are superposed as solid (A0) and dotted (S0) lines. (b) The same measured data set displayed in a lower frequency and phase velocity range showing branches of dispersion curves.

Figures 1(a) and (b) shows such a typical measured phase velocity spectrum obtained from the wave field transformation technique presented by Park *et al.* (1998; 1999). The data set was collected over a three-layer pavement structure with 100 equally spaced stations from 0.05 to 5.00 m. The main trend of the data in Fig. 1(a) matches with the dispersion curve of the fundamental antisymmetric (A0) Lamb wave mode (Lamb, 1917) which would be predicted to propagate in the top layer only if it was detached from the others. In other words, the stiff top layer behaves quite independently of the layers beneath it. This characteristic trend was observed already in the early work on surface wave testing of pavements (Jones, 1955, 1962; Vidale, 1964; Jones and Thrower, 1965) and provides a practical technique to estimate both the shear wave velocity (β) and the thickness (d) of the stiff top layer. However, this approach has only been utilized in a few recent studies on surface wave testing of pavements (Akhlaghi and Cogill, 1994; Martincek, 1994). In Ryden *et al.* (2004) the free plate approach for the top layer was extended to include the symmetric (S0) mode since a portion of this mode can be observed in the measured phase velocity spectrum, for example between 8 and 10 kHz in Fig. 1(a). Martincek (1994) concluded from experimental results on pavements that the Lamb wave approximation was valid for all wavelengths smaller than five times the thickness of the stiff top layer. From a theoretical study on the influence of a lower velocity half-space Ryden and Park (2004) quantified the theoretical deviation involved in the free plate approximation to be less than 10%. This approximate approach holds as long as β in the top layer is higher

than α in the underlying medium (Jones and Thrower, 1965), i.e., for a large stiffness contrast. In the other case where β in the top layer is not higher than α in the lower velocity half-space (but still higher than β in the half-space) the cutoff frequency of the second mode occurs at a higher frequency (Zinin *et al.*, 1997). All the studies above made an implicit conclusion that the wave field generated from a vertical point source at the surface of a pavement system is dominated by Lamb type of waves in the stiff top layer.

In Fig. 1(b) the measured phase velocity spectrum is plotted in a lower frequency and phase velocity range. Several branches of dispersion curves are visible, limited by cutoff frequencies and abruptly changing phase velocities. A similar pattern was observed by Gucunski and Woods (1992) and Tokimatsu *et al.* (1992) in numerical modeling of surface wave measurements over a layer model with an embedded low velocity layer. They concluded that the observed discontinuities were created by mode jumping between successively higher modes. This phenomenon was later emphasized by other researchers too (Foti *et al.*, 2003; O'Neill, 2003; Zhang and Lu, 2003), but no studies have focused on the explanation of this behavior. Furthermore, in all these studies, the velocity of the bottom half-space was always set to be the highest velocity of the system in order to avoid tracing dispersion curves in the complex wave number domain.

III. WAVE PROPAGATION MODEL

The global matrix method proposed by Knopoff (1964) and implemented as described by Lowe (1995) is used to predict theoretical dispersion curves in this study. The wave propagation model can handle leaky waves (complex wave numbers) without modification and remains stable for high frequencies and large thickness values (Lowe, 1995). A system matrix (**S**) is assembled from all layer interface matrices ($\mathbf{D}_i$) describing the displacement and stress fields associated with harmonic wave propagation along the multilayered structure. In each layer interface matrix, stresses (σ) and displacements (u) are expressed as a function of the material properties; α, β, d, bulk density (ρ) of the layer, circular frequency (ω), and wave number (k). Each point on a dispersion curve represents a solution to **S** where all boundary conditions are satisfied simultaneously. The dispersion equation or characteristic equation then becomes

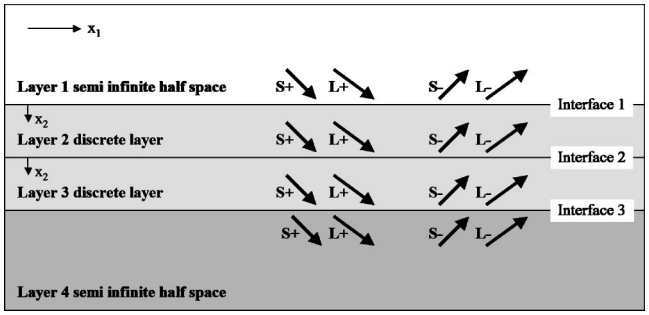

FIG. 2. Schematic illustration of the layered model used in the global matrix approach, after Lowe (1995).

$$f(\omega,k)=\det[\mathbf{S}]=0. \tag{1}$$

More details on the wave propagation model can be found in Knopoff (1964), Randall (1967), or Lowe (1995). Here only the final matrix equations as given by Lowe (1995) are presented. Each layer is represented with one matrix for the top interface ($\mathbf{D}_t$) and one matrix for the bottom interface ($\mathbf{D}_b$). The interface matrix describes the displacements and stresses at the interface as a function of the partial wave amplitudes (A) from above (index t) or below (index b) the interface. The thickness (d) in the x_2 direction of each layer is entered as x_2 into the equations for dispersion curve calculations and is zero for the half-space matrices. The partial waves A are divided into longitudinal waves (L) and shear waves (S). The $(+)$ and $(-)$ indices denote partial waves traveling down $(+)$ and up $(-)$ from the interface (see Fig. 2). The interface matrices are

$$\begin{Bmatrix} u_1 \\ u_2 \\ \sigma_{22} \\ \sigma_{12} \end{Bmatrix} = [\mathbf{D}_i] * \begin{Bmatrix} A_{(L+)} \\ A_{(L-)} \\ A_{(S+)} \\ A_{(S-)} \end{Bmatrix}, \tag{2}$$

where

$$[\mathbf{D}_{it}] = \begin{bmatrix} k_1 & k_1 g_\alpha & C_\beta & -C_\beta g_\beta \\ C_\alpha & -C_\alpha g_\alpha & -k_1 & -k_1 g_\beta \\ i\rho B & i\rho B g_\alpha & -2i\rho k_1 \beta^2 C_\beta & 2i\rho k_1 \beta^2 C_\beta g_\beta \\ 2i\rho k_1 \beta^2 C_\alpha & -2i\rho k_1 \beta^2 C_\alpha g_\alpha & i\rho B & i\rho B g_\beta \end{bmatrix}, \tag{3}$$

$$[\mathbf{D}_{ib}] = \begin{bmatrix} k_1 g_\alpha & k_1 & C_\beta g_\beta & -C_\beta \\ C_\alpha g_\alpha & -C_\alpha & -k_1 g_\beta & -k_1 \\ i\rho B g_\alpha & i\rho B & -2i\rho k_1 \beta^2 C_\beta g_\beta & 2i\rho k_1 \beta^2 C_\beta \\ 2i\rho k_1 \beta^2 C_\alpha g_\alpha & -2i\rho k_1 \beta^2 C_\alpha & i\rho B g_\beta & i\rho B \end{bmatrix} \tag{4}$$

and

$$g_\alpha = e^{iC_\alpha x_2}, \quad g_\beta = e^{iC_\beta x_2}, \tag{5}$$

$$C_\alpha = (\omega^2/\alpha^2 - k_1^2)^{1/2}, \quad C_\beta = (\omega^2/\beta^2 - k_1^2)^{1/2}, \tag{6}$$

$$B = \omega^2 - 2\beta^2 k_1^2. \tag{7}$$

When the four-by-four $\mathbf{D}_{ib}$ and $\mathbf{D}_{it}$, $(i=1,...,n)$ matrices have been calculated for each layer they are assembled to obtain the global **S** matrix so that stresses and displacements become continuous over the interfaces. For a layer model with four layers as in Fig. 2 the system matrix then becomes

$$\mathbf{S} = \begin{bmatrix} \mathbf{D}_{1b}^- & -\mathbf{D}_{2t} & & \\ & \mathbf{D}_{2b} & \mathbf{D}_{3t} & \\ & & \mathbf{D}_{3b} & -\mathbf{D}_{4t}^+ \end{bmatrix}. \tag{8}$$

The $(-)$ index on $\mathbf{D}_{1b}$ above represents the outgoing (up) waves in the top half-space (columns two and four in $\mathbf{D}_b$) and the $(+)$ index on $\mathbf{D}_{4t}$ represents outgoing (down) waves in the bottom half-space (columns one and three in $\mathbf{D}_t$). These half-space matrices are only four-by-two matrices given that the incoming waves in the half-spaces are zero for unforced modal solutions. A free surface can be modeled by some modifications to the **D** matrix. However, exactly the same result can be obtained much more easily simply by setting the bulk wave velocities α and β in the top layer to arbitrary nonzero values and the bulk density to zero (Lowe, 1995). In this way the same matrices can be used for both vacuum and solid half-spaces.

A. Dispersion curves in the complex wave number domain

The dispersion curves are found by numerical searches for the ω-k pairs that make the value of the determinant of **S** vanish in Eq. (1). These modal solutions must be searched in the complex wave number domain in any part of the solution space where the phase velocity (corresponding to the real part of the wave number) becomes greater than the shear wave velocity in the lower half-space. Thus the numerical solution is in three variables: ω, k_{real} and $k_{\text{imaginary}}$. For such complex solutions the particle motion does not decrease exponentially with depth. Instead energy radiates down into the lower half-space, resulting in attenuation of the wave along the surface in the x_1 direction (Vidale, 1964), even though all materials are purely elastic. In this study the dispersion curve software ''Disperse'' developed at Imperial College (Pavlakovic *et al.*, 1997; Disperse, 2001) has been used to trace the dispersion curves in the complex wave number domain.

B. Excitability and leakage

The solution of the matrix equations gives dispersion curves representing any type of guided wave which may exist with particle motion in the x_1 and x_2 directions; these include modes such as interface waves and plate waves which may not always be measurable at the surface. Therefore it is useful to calculate some more information to help the interpretation of the waves which are actually detected in the measurements. The key information here is the excitability (E) at the surface and the leakage (κ) along the x_1 direction. The excitability indicates the extent to which each mode is excited when the surface force is applied; the leakage indicates how quickly the amplitude of the signal attenuates with the distance from the source. Both of these quantities differ for the different modes and also for different locations along each dispersion curve.

TABLE I. Reference layer model representing a flexible pavement construction.

Layer	β (m/s)	α (m/s)	ρ (kg/m^3)	Thickness (m)
1	1400	2914	2000	0.20
2	500	1041	2000	0.60
3	100	208	2000	∞

The excitability (E) of a particular mode at a particular frequency is defined as the ratio of displacement of that mode to the applied force when both quantities are measured at the same location and direction (Wilcox *et al.*, 2004). A harmonic vertical point force at the surface with a certain frequency will excite different modes along the surface to various degrees. The vertical displacement (u_2) from a vertical unit amplitude load at the surface is used to calculate the excitability as

$$E \propto u^2 f. \tag{9}$$

The attenuation due to the leakage of modes is calculated from the ratio between the imaginary part (k_i) and the real part (k_r) of the wave number. This is nonzero when the phase velocity exceeds the shear wave velocity in the lower half-space. Points on a dispersion curve with a large imaginary part of the wave number have large attenuation and are therefore not likely to appear in measured surface wave data. The attenuation coefficient (κ) is defined as

$$\kappa = \frac{2\pi k_i}{k_r}, \tag{10}$$

where κ is in nepers per wavelength, so that a wave of unit amplitude is reduced to an amplitude of $e^{-\kappa}$ after traveling one wavelength.

IV. ANALYSIS OF A THREE-LAYER REFERENCE MODEL

The same reference model, representing a flexible pavement construction with a relative stiff and thick base layer, is used throughout this study. The bulk wave velocities decrease with depth. All parameters are defined as elastic, homogenous, and isotropic. The thickness and elastic constants of each layer are given in Table I. Material attenuation is not included in the model. However, the dominating mechanism for loss of energy, leakage, is included. Thus the model correctly accounts for the effect of attenuation on experimental measurements, though a little underestimated.

A. Dispersion curves over a broad frequency range

The dispersion curves for all modes are first presented in the full frequency range that is normally utilized in pavement testing (Fig. 3). Within this frequency range there are more than 100 possible modes of propagation. The curves are

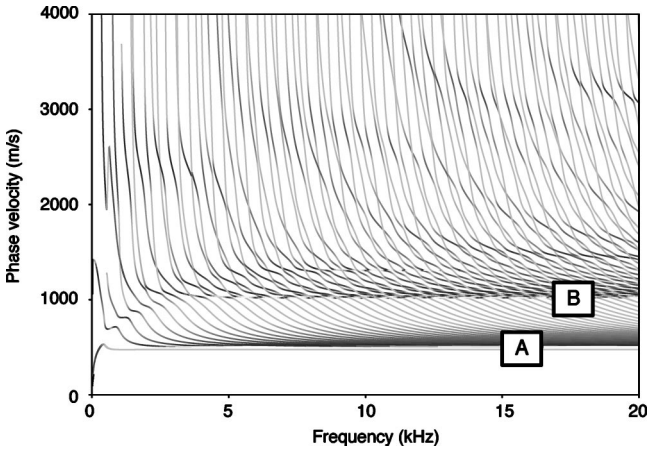

FIG. 3. Predicted dispersion curves from the three-layer reference model (Table I). Dark portions correspond to low attenuation due to leakage.

gray-scale coded with respect to the amount of attenuation due to leakage (from 0 to 0.55 np/m). Black points on each dispersion curve correspond to portions with low leakage in the x_1 direction. It is immediately evident from this figure that the full spectrum of modes is considerably more complex than the measured phase velocity spectrum presented in Fig. 1(a) and than what is normally presented from surface wave testing of pavements.

In order to explain the main trends of all the dispersion curves in Fig. 3, a two-layer model is first used for comparison purposes. The embedded second layer in the reference model (Table I) is excluded, so that the model consists only of the stiff surface layer on the half-space. The resulting dispersion curves are plotted in Fig. 4. For this reduced system there are only nine possible modes of propagation within the same frequency range as in Fig. 3. It should be noted how the overall trend of the black portions in Fig. 3 matches with the individual dispersion curves in Fig. 4. This comparison bears for all but the two lowest phase velocity trends (labeled A and B in Fig. 3), which are related to interface waves in the three-layer model (Stoneley, 1924). The overall trend of the first three modes in Fig. 4 (labeled 1–3) also matches fairly well with the measured phase velocity spectrum in Fig. 1(a). The second mode in Fig. 4 is closely linked

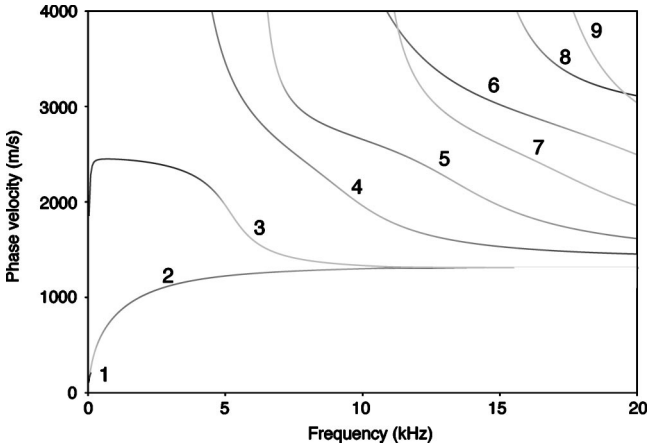

FIG. 4. Predicted dispersion curves from a two-layer model where the second layer from the reference model (Table I) has been excluded.

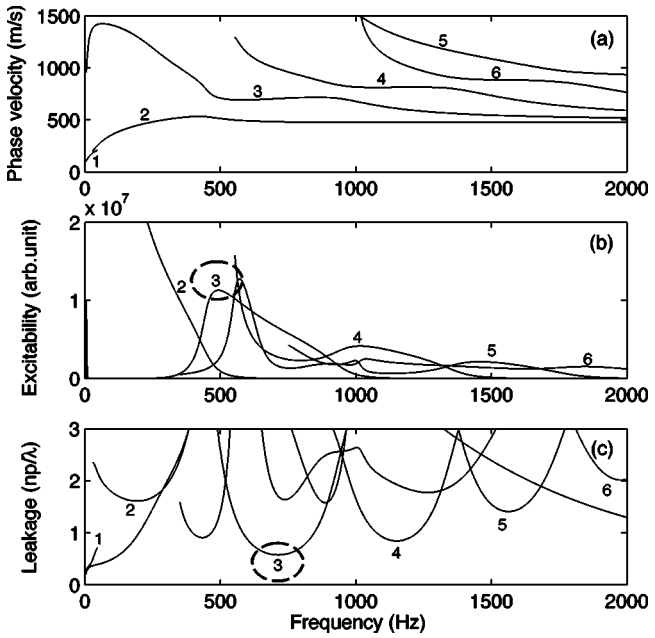

FIG. 5. (a) The first six modes from Fig. 3 with corresponding (b) excitability and (c) leakage.

to the antisymmetric Lamb wave mode (A0) in a free plate and is the dominating mode over most of the frequency range in this type of two-layer system (Ryden and Park, 2004).

Let us consider the trend of this mode (mode 2 in Fig. 4) in comparison to all the modes in Fig. 3 more closely. By following the individual higher modes in Fig. 3 from low to high frequencies it can be observed that all modes exhibit a terracelike portion close to phase velocities of the second mode in the two-layer system. At these terracelike portions the mode is less dispersive (straighter horizontally aligned dispersion curve) and less leaky (darker gray). This kind of terracelike behavior has been observed in other studies on bilayered plates (Yapura and Kinra, 1995; Simonetti, 2004). The general trend of the dispersion curves of the dominating layer seems to break up into small branches of dispersion curves in the three-layer model. At higher frequencies (>2 kHz) all individual modes of the three-layer system merge together and form the overall trend of the dispersion curves of the two-layer system. This indicates that the general trend of the observed wave field spectrum in Fig. 1(a) is mainly formed by the properties of the top and the bottom layer. However, at low frequencies (<2 kHz) branches of dispersion curves are more separated, revealing the presence of the embedded second layer in the three-layer model. This indicates that the observed branches of dispersion curves in Fig. 1(b) are the key features that can be used to estimate the properties of the complete three-layer pavement system. Therefore the following sections will be focused on these measurable branches at lower frequencies.

B. Branches of dispersion curves at lower frequencies

The first six modes from Fig. 3 are plotted in Fig. 5(a) in a smaller frequency range. The excitability of these modes is

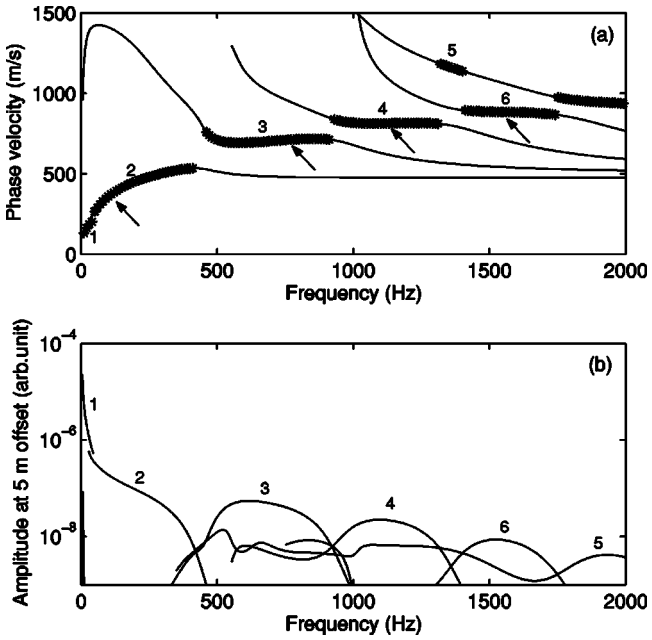

FIG. 6. (a) The first six modes from the reference model with dominating surface displacements at 5 m offset from the source marked with crosses. The arrows correspond to the locations of the mode shapes in Fig. 7. (b) The relative magnitude of surface displacements of each mode at 5-m offset from the source.

plotted in Fig. 5(b), showing that each mode will be excited with larger displacements at the surface within certain frequency bands. Figure 5(c) shows a similar behavior for the minima in leakage. However, frequencies with maximum excitability and minimum leakage are not fully correlated for each mode. For example, the third mode shows a maximum excitability at 495 Hz and a minimum leakage at 715 Hz, marked with circles in Figs. 5(b) and (c). This indicates that the dominating mode of propagation at a point on the surface at a chosen distance from the source will be dependent on a combination of the excitability and the amount of leakage, hence also the distance (x) from the source. Geometric spreading and intrinsic material attenuation will also reduce the amplitude as a function of distance from the source. Nevertheless, these latter two factors should remain constant for each frequency, so we can determine which mode is dominating surface displacements at a certain distance from the source and frequency from E and κ by using

$$U(x,\omega) = E^* e^{-(\kappa x/\lambda)}, \tag{11}$$

where U is the relative amount of surface displacement at a certain distance from the source. In Fig. 6(a) the dispersion curves with maximum U for each frequency at 5 m distance from the source are marked with crosses. Figure 6(b) shows the amount of displacement of each mode at this point on the surface; the actual amplitudes of the displacement shown here are arbitrary, what is significant is the relative values when comparing different modes and different frequencies. The pattern of the crosses reveals the same phenomenon as was experienced in the measured phase velocity spectrum [Fig. 1(b)]. It seems therefore that the existence of the observed branches of dispersion curves can be theoretically explained from the excitability and leakage of each mode.

C. Mode shapes

To further clarify the generation mechanism of the branches of dispersion curves predicted for the three-layer reference model, mode shapes are studied next. The mode shapes show how displacements or stresses vary as a function of depth (x_2) and can be used to study which layer or layers are affected by a particular mode and frequency. The mode shape is also calculated for a few wavelengths in the direction of propagation (x_1) to further illustrate the type of wave motion, although the distribution is known to be sinusoidal (modulated by an exponential decay in the cases of attenuating waves). In Figs. 7(a)–(d) mode shapes corresponding to the second, third, fourth, and sixth mode branches in Fig. 6(a) are plotted. Note that the grid form of display is used simply to show the shape; the sizes of the grid elements have no significance. Also, the plots only show an arbitrarily limited depth of the half-space.

The top layer shows the typical antisymmetric type of particle motion in all four figures. This agrees well with the earlier findings that the dominating type of wave propagation in this system is closely related with the A0 Lamb wave in a free plate [Fig. 1(a)]. The second layer also shows a mode shape similar to the mode shape of Lamb waves in a free plate (Graff, 1975) in all four cases. At the lowest branch the mode shape [Fig. 7(a)] can be identified as a fundamental mode which has a quasi-antisymmetric mode shape; since the layer is not free it is strictly not a Lamb wave mode shape but it is very similar. At the next higher branch [Fig. 7(b)] the second layer shows a fundamental mode which has a quasi-symmetric mode shape. In the next branch [Fig. 7(c)] the mode shape is quasi-antisymmetric. Finally, at the fourth branch (mode number 6) the mode shape [Fig. 7(d)] is back to symmetric and shows the particle motion of the first higher mode. Consequently, the branches correspond to successive higher modes of quasi-Lamb waves in the second layer. Since all phase velocities are higher than the shear wave velocity of the lower half-space, energy is leaking down into the lower velocity half-space in all four cases. This can be seen quite clearly by the mode shapes in the half-space which are in the form of radiating wavefronts.

The observed behavior can be explained from a physical examination of the continuity of both stresses and displacements along the layer boundaries. The stiff top layer, with its high bulk wave velocity material, carries most energy and propagates with a mode shape close to the A0 Lamb wave. Continuity across the layer boundaries forces the second layer to share the same frequency and wave number as the top layer. Since this second layer has a lower bulk wave velocity than the top layer, higher modes are generated to match the mode shape of the faster top layer. Hence, the generation mechanism of the observed branches at lower frequencies can be explained as a superposition of quasi-Lamb waves in the top and second layer. This can be seen in Fig. 8, which shows Lamb waves corresponding to the top (subscript 1) and second (subscript 2) layers as free plates, together with the crosses from Fig. 6. The free plate Lamb wave dispersion curves of the top and second layers intersect close to the corresponding mode shapes of each branch (exemplified with one circle in Fig. 8), e.g., the antisymmetric

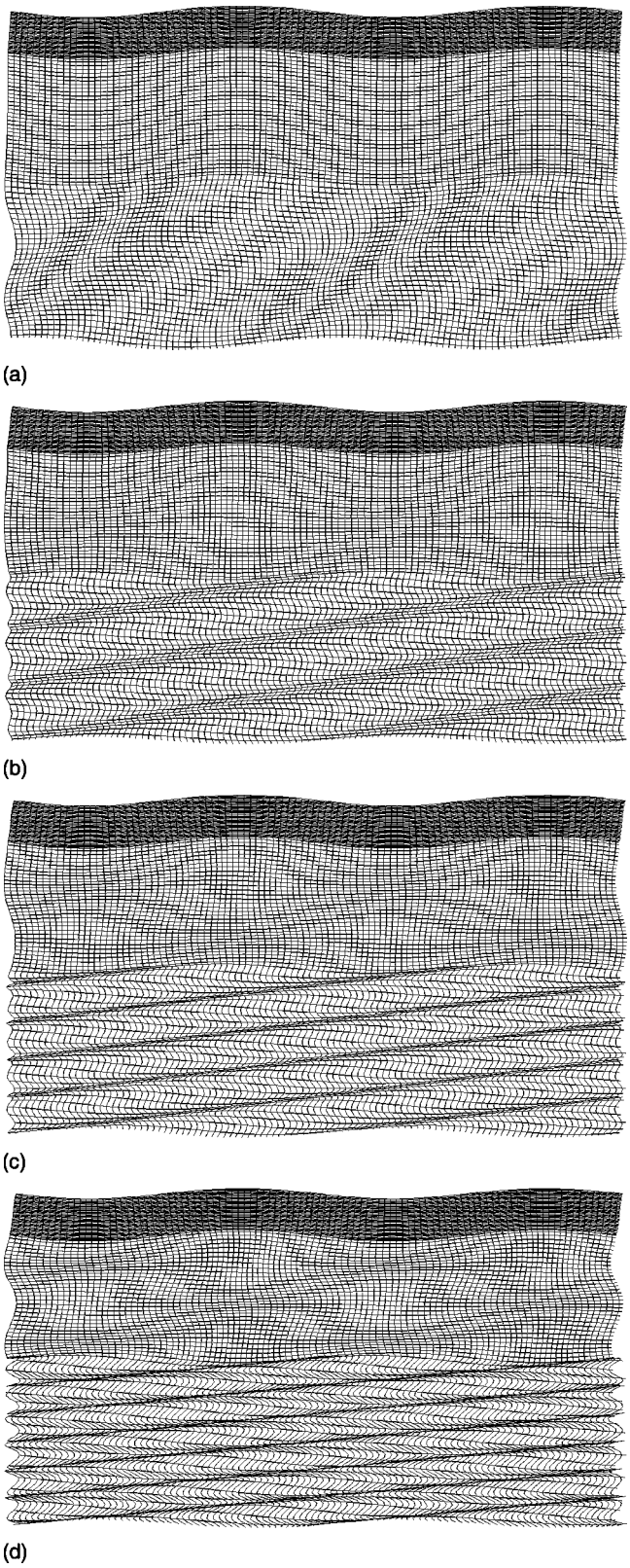

FIG. 7. Representative mode shapes of the four first branches marked with arrows in Fig. 6(a).

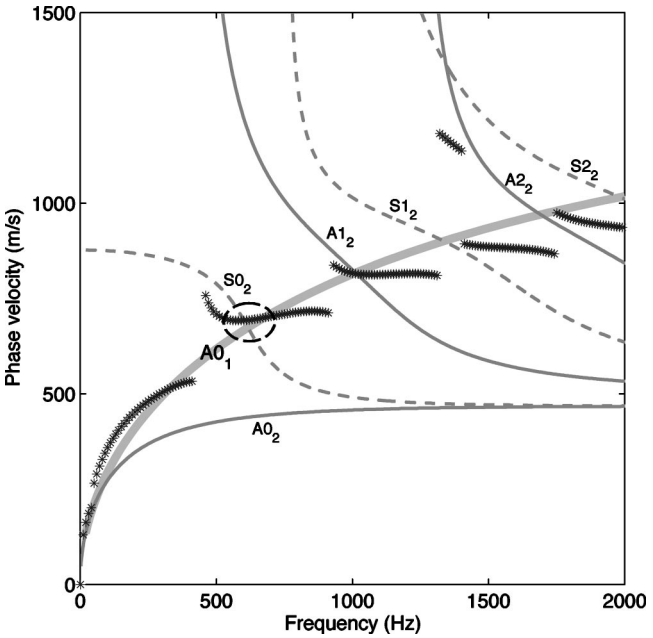

FIG. 8. Superposition of Lamb waves calculated from the (1) first and (2) second layer as free plates. (*) crosses mark the branches with dominating surface displacements at 5 m offset.

mode of the top layer $A0_1$ intersects with the symmetric mode of the second layer $S0_2$ within the second branch whose mode shape is illustrated in Fig. 7(b).

It should be noted that the mode shape is not constant but varies with frequency and phase velocity along each dispersion curve. By studying the change in mode shape along each dispersion curve it can be found that at frequencies when there is maximum surface displacements [Fig. 6(a)], there are large and smoothly varying normal (x_2) displacements over the interface between the first and second layers. At these peaks in surface displacement [Fig. 6(a)], the mode shapes in the first and second layers match, effectively resulting in dominating surface displacements. At higher and lower frequencies along the dispersion curve the mode shape shows a more abrupt change over the layer interface. This can be seen in Fig. 9 where the normal displacement is plotted as a function of depth at different frequencies along the fourth mode. The frequency is varied from 1000 to 2000 Hz in 200-Hz increments. At 1000 Hz the normal displacement varies smoothly over the interface between the first and second layers. At higher frequencies a more abrupt change develops. At phase velocities where higher mode dispersion curves drop below the main trend of the A0 mode in the corresponding free top layer, displacements at the layer interface between the first and second layers approach zero and the normal stress over the layer interface increases. At this stage there is no longer any possible harmonic wave motion in the top layer. Wave motion within the second layer then approaches the asymptotic solution of a clamped-free plate (Simonetti, 2004).

D. Parametric study

So far all the dispersion curves have been calculated from the properties of the fixed reference layer model (Table I). It could be debated that some of the results above are only valid for this specific layer model. Also, it is of practical interest to study how the measurable branches are related to

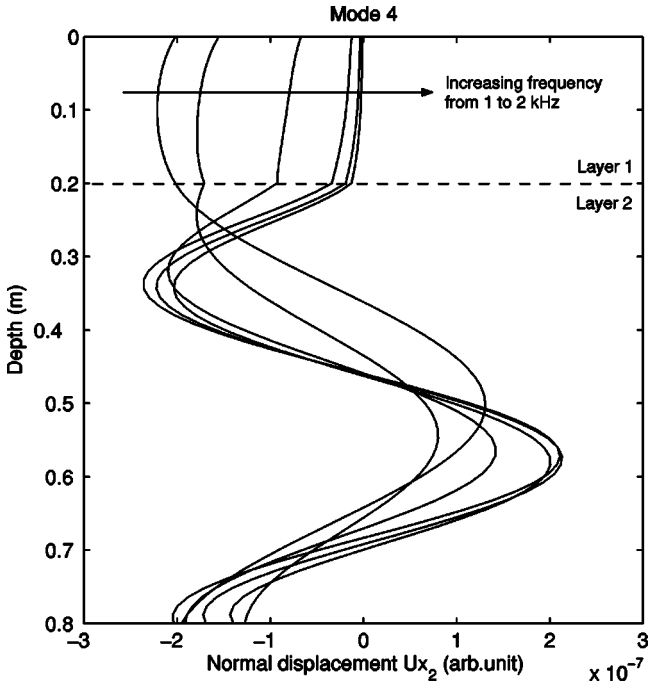

FIG. 9. Normal displacement (x_2) at different freqeuncies along the fourth mode of the reference model (Fig. 5).

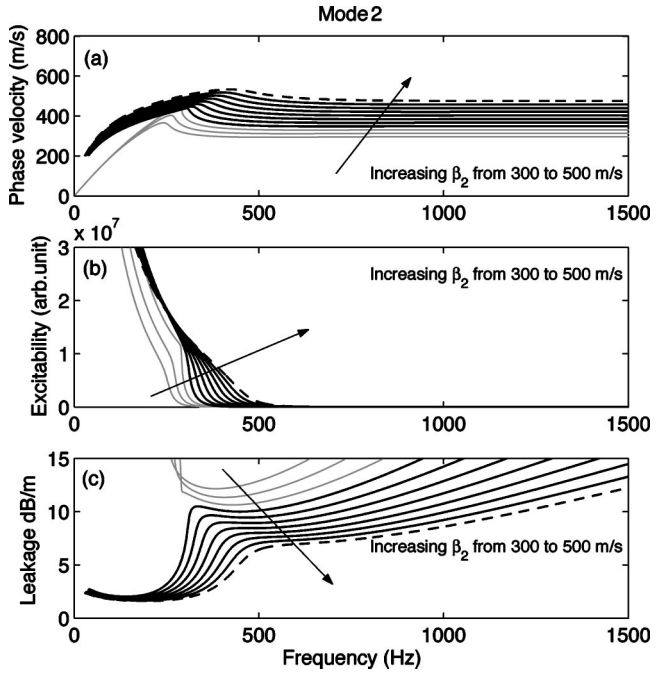

FIG. 10. Parametric study on the second mode when the shear wave velocity of the second layer is varied from 300 to 500 m/s in 20-m/s increments. The dotted line represents the reference case and gray dispersion curves mark the anomalous behavior of these modes.

different properties of the three-layer model. This motivates a parametric study on the low-frequency modes studied above.

The fundamental mode [labeled 1 in Fig. 5(a)] is very similar to the fundamental mode of the two-layer system. It has been concluded in previous studies on a two-layer model with one stiff (fast) layer on a lower velocity half-space that this mode is limited by the Rayleigh wave and the longitudinal or shear wave velocity of the lower velocity half-space depending on the velocity contrast (Vidale, 1964; Jones and Thrower, 1965; Zinin *et al.*, 1997). This cutoff behavior can be explained from the coupling between the high velocity layer and the half-space; the half-space will not support any modes propagating faster than the bulk wave velocities of the half-space (Nayfeh and Chimenti, 1984). Therefore we start with the second mode in this parametric study, which is unique for this three-layer system.

1. The second mode

The shear wave velocity of the second layer has been varied from 300 to 500 m/s in 20-m/s increments, keeping all other layer properties fixed. The resulting dispersion curves are plotted in Fig. 10. Note that the 500 m/s reference case corresponds to the results already shown (dotted line). Dispersion curves corresponding to the three lowest shear wave velocities (300–340 m/s) are colored gray since they deviate from the main trend of all the other curves. As expected the phase velocity increases with increasing shear wave velocity of the second layer [Fig. 10(a)]. However, the phase velocity of the gray dispersion curves is very much lower than the reference case in the low-frequency range where this mode was previously shown to dominate the surface displacements [Fig. 6(a)]. The excitability in Fig. 10(b) is also drastically reduced for these curves, but the main difference can be observed in the amount of leakage [Fig. 10(c)]. The gray dispersion curves all show a very large amount of attenuation due to leakage. Thus Figs. 10(b) and (c) indicate that this mode may not be measurable when the shear wave velocity of the second layer drops below 360 m/s.

2. The third mode

Figure 11 shows a similar parametric study on the third mode. This figure also reveals a deviation in the dispersion curves corresponding to the lowest shear wave velocities of the second layer (gray curves). Here the three gray dispersion curves seem to follow the pattern of the deviating gray dispersion curves from Fig. 10, indicating that this third mode actually covers both the second and the third branch observed for the reference layer model (Fig. 6). A similar mode jumping or mode coupling phenomenon was discovered by Yapura and Kinra (1995) in a bilayered plate.

3. The fourth mode

In Fig. 12 dispersion curves of the fourth mode are plotted for different shear wave velocities of both the first (β_1) [Fig. 12(a)] and the second (β_2) layer [Fig. 12(b)]. The fourth mode is clearly more sensitive to β_2 compared to β_1. But here it is interesting to see that a change in β_1 shifts the profile of the dispersion curve in one direction indicated with an arrow in Fig. 12(a), while a change in β_2 shifts it in another direction [Fig. 12(b)]. This indicates that both parameters may be detectable even at these relatively low frequencies if the shape of the measurable branch corresponding to this mode can be accurately detected.

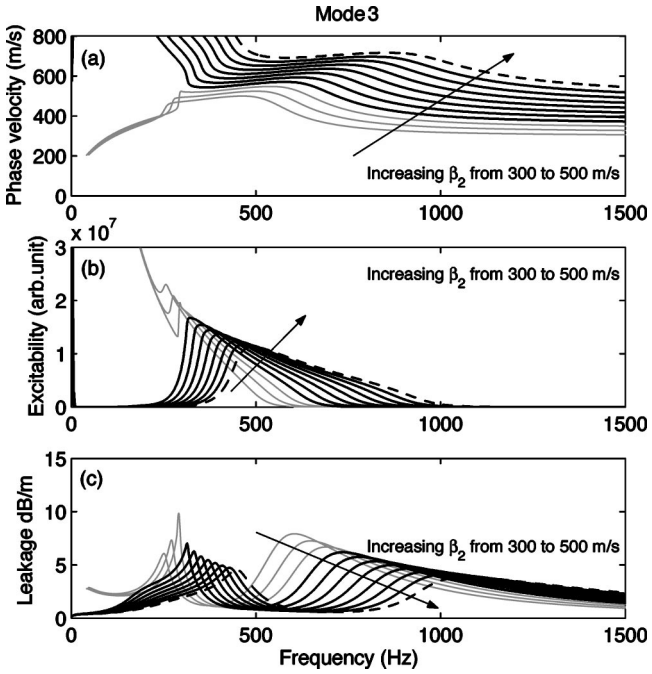

FIG. 11. Parametric study on the third mode when the shear wave velocity of the second layer is varied from 300 to 500 m/s in 20-m/s increments. The dotted line represents the reference case and gray dispersion curves mark the anomalous behavior of these modes.

E. Longitudinal waves in the top layer

In all sections above the focus has been on the individual branches of dispersion curves following the main trend of the A0 mode of the top layer as a free plate [Fig. 1(a)]. But in Fig. 1(a) there is a also a visible dispersion curve at about 3800 m/s matching the S0 Lamb wave mode of the top layer as a free plate. The limited frequency range of the visible portion of this mode [Fig. 1(a)] can be explained from the difference in excitability between the second and third modes in Fig. 4 (Ryden and Park, 2004). A closer study on the individual dispersion curves in Fig. 3, dominating surface displacements, and mode shapes, reveals a similar phenomenon as the findings along the A0 trend.

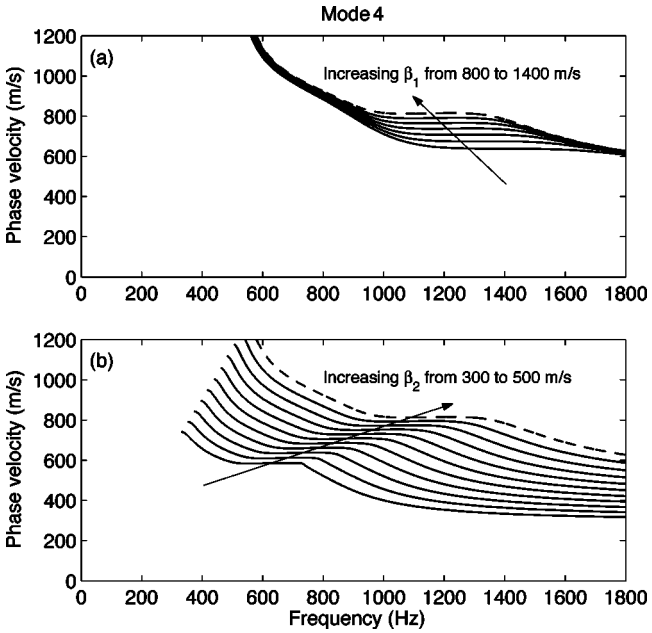

FIG. 12. Parametric study on the fourth mode when the shear wave velocity of the (a) second layer is varied from 300 to 500 m/s in 20-m/s increments, and the (b) first layer is varied from 800 to 1400 m/s in 100-m/s increments. Dotted line shows the reference case from Table I.

V. PRACTICAL CONSEQUENCIES IN APPLICATIONS TO PAVEMENTS

It is usually stated that the measured surface waves on a pavement profile are dominated by Rayleigh type of waves. But in this study it has been shown that wave propagation in this type of layered half-space is related to more general characteristics of guided waves in plates, and the Rayleigh type of waves can only be found at the asymptotes of very high (here >20 kHz) or very low (here <10 Hz) frequencies. These findings can possibly explain some of the reported difficulties and lack of sensitivity with the conventional approach of surface wave testing of pavements. In this section we examine some such observations.

A. Field testing

In the conventional field setup the wrapped phase difference between two receivers located a known distance (D) apart is measured. Spatial aliasing occurs when the phase difference exceeds half a wavelength (180°), resulting in a 360° cycle in the wrapped phase difference spectrum. The wrapped phase spectrum must be correctly unwrapped before a measured dispersion curve is calculated by using

$$c(f) = \frac{D 2\pi f}{\Delta\phi}, \tag{12}$$

where $\Delta\phi$ is the unwrapped phase difference in radians. Several researchers have reported on difficulties associated with the phase unwrapping process. Al-Hunaidi (1992) found that the wrapped phase difference spectrum measured over a pavement surface contained a spurious cycle that could not be explained. However, he observed that the most realistic measurement of phase velocity is obtained if this cycle is not unwrapped. This phenomenon may be explained from the branches of the dispersion curves studied in this paper. Let us consider the first jump at 220 Hz from the first to the second branch in Fig. 1(b). The phase velocity changes abruptly from 300 to 700 m/s. By rearranging Eq. (12) the corresponding wrapped phase spectrum from the dispersion curves in Fig. 1(b) can be obtained [Fig. 13(a)]. Here a typical receiver spacing of 2.0 m is chosen to sample these wavelengths (Heisey *et al.*, 1982). It is interesting to see that the abrupt jump in phase velocity almost creates an additional 360° cycle in the wrapped phase spectrum [marked as number 2 in Fig. 13(a)]. A longer receiver spacing or a greater phase velocity difference should actually produce a phase difference jump of more than 360°. If this additional cycle is included in the phase unwrapping process, the resulting dispersion curve will be erroneous, continuous, and smooth as indicated by the dotted line in Fig. 13(b). This indicates that the measured wrapped phase difference between two receivers is not a feasible approach to obtain a measured dispersion curve in this case.

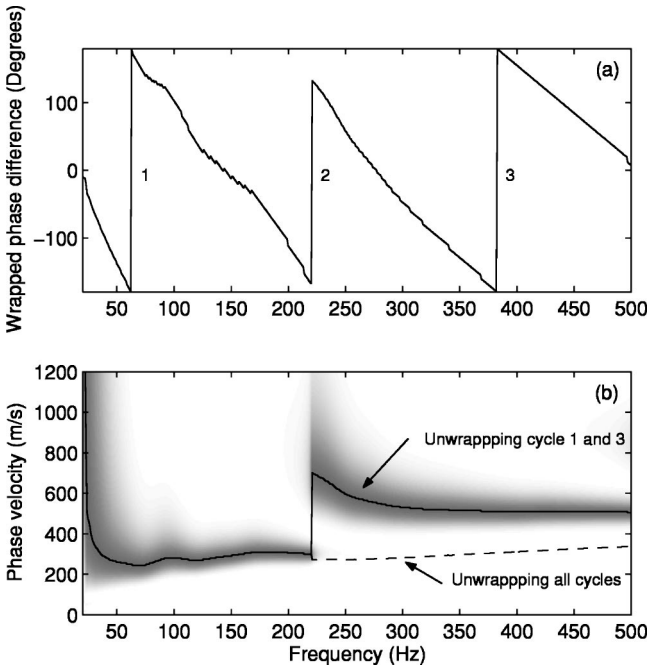

FIG. 13. (a) Wrapped phase spectrum calculated from the original data used for Fig. 1 with 2.0-m receiver spacing. The second cycle should not be unwrapped since it is created by the jump between the first and second branches at 220 Hz. (b) The effect on the dispersion curve if the second cycle is unwrapped before the dispersion curve is calculated.

Fluctuations in the measured dispersion curve have often been assumed to originate from reflections of body waves from the bottom of the asphalt layer or from horizontal boundaries and possible cracks in the pavement (Sheu *et al.*, 1988; Roesset *et al.*, 1990). However, since there are so many modes of propagation in this type of layered structure (Fig. 3), fluctuations caused by mode jumping should reasonably be expected.

B. Inversion of layer properties

Another issue is the Rayleigh wave assumption of wave propagation. Since in practice the measured dispersion curve is often analyzed from the Rayleigh wave perspective, some aspects of this procedure may be questioned. For example many sublayers (~10) are often used for the evaluation of a layer profile from the measured dispersion curve. From the Rayleigh wave perspective this resolution may be justified since the data contains measured phase velocities at many different wavelengths sampling different depths from the surface. But the analysis of the reference layer model used in this study gives another picture of the wavelength-depth relation. In the reference model, all higher modes starting from the first cutoff frequency of the fundamental mode (50 Hz or 4 m wavelength) correspond to leaky guided waves trapped in the first and second layers. Consequently all wavelengths from about 0.2 m (thickness of the top layer) to about 4.0 m sample the same depth but with different modes of propagation. This explains why the wavelength cannot be directly related to the depth in this kind of layer system. This also implies that it may not be possible to evaluate more layers than the main layers of the construction, i.e., three or four layers.

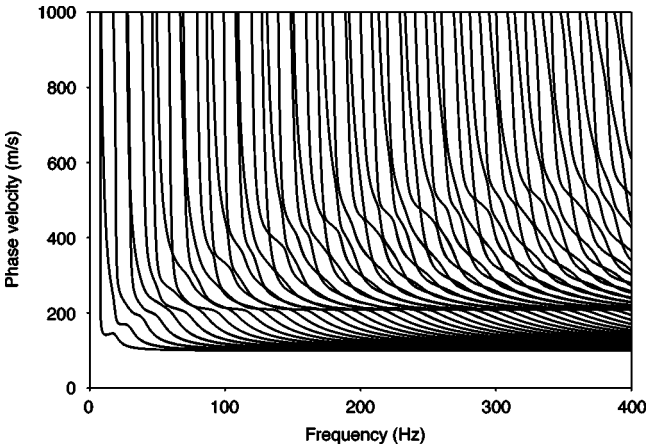

FIG. 14. Influence from a high velocity half-space at 5 m depth from the second layer in the reference layer model.

Another assumption that may have to be reconsidered is the use of a high velocity half-space to avoid tracing dispersion curves in the complex wave number domain. From the Rayleigh wave theory this may seem like a reasonable approximation, i.e., deep layers should only affect low frequencies. However, modal solutions correspond to standing waves in the thickness direction and, since no material damping is included, a high velocity half-space at deeper depths will influence modal solutions at higher frequencies, too. This is exemplified here (Fig. 14) by adding one more layer to the reference model (Table I), resulting in a new half-space with the same properties as the top layer. The thickness of the third layer, which was previously defined as a half-space, is now set to 5 m. Dispersion curves of this system are plotted in Fig. 14. Over the frequency range from 0 to 400 Hz, where the original reference model only showed three possible modes [Figs. 3 and 5(a)], there are now almost 100 modes.

As stated in the background on surface wave testing of pavements (Sec. II), many difficulties with the conventional approach have been assumed to originate from the influence of higher modes of propagation. In the light of Figs. 3 and 14 this seems quite realistic and it may be questioned if this kind of layered system can be represented with only one continuous dispersion curve. For example, it has been widely reported that results from surface wave testing of pavements are not very sensitivity to the properties of the embedded second layer (Aouad, 1993; Roesset *et al.*, 1990). This problem can be explained from the branches of dispersion curves that are difficult to resolve with the conventional method. If only one continuous dispersion curve without branches is used, this ''apparent'' dispersion curve will only be sensitive to the top and bottom layers. Figure 12 can explain more details on this topic. If the fourth mode is not resolved as a discrete branch, a change in shear wave velocity of the second layer will not be noticeable since the profiles of dispersion curves of this individual mode move in the same direction as the A0 mode of the top layer as a free plate. This direction is indicated with an arrow in Fig. 12(a). However, in Fig. 12(b) the arrow points in the direction normal to the A0 dispersion curve of the top layer as a free plate. So even

if a change in shear wave velocity of the second layer shows a higher relative sensitivity on the fourth mode, this change will be masked by the main trend of the A0 dispersion curve if this branch is not individually resolved in the measurements. The same holds for all the other higher modes following the trend of the A0 mode of the equivalent free top layer.

On the other hand, if the branches at lower frequencies are resolved, there is a potential for improved sensitivity to the embedded second layer. The instabilities which have been experienced with the partial derivatives approach for the inversion, when the apparent dispersion curve jumps between modes (Foti *et al.*, 2003), may actually be the promise for an improved surface wave method. Since a change in cutoff frequencies of the branches of the dispersion curves may hold more information on the structural properties than just the change in phase velocities, this information should preferably be included for the evaluation of the pavement layer properties. This could be done by using the complete phase velocity spectrum for the inversion of layer properties. Alternatively, the presented correlation between branches of dispersion curves and Lamb waves in the equivalent free layers may form the framework of a new simplified technique for the evaluation of pavement layer properties. Since the branches are sensitive to both the shear wave velocity of the top and second layers (Fig. 12) this implies that a lower frequency range than normally utilized in surface wave testing of pavements may be used. A lower frequency range has two major practical advantages: the measurement equipment could be simplified and the evaluated properties of materials (viscoelastic properties of the asphalt layer) should be closer to the frequency range of interest in pavement design, i.e., traffic loading.

VI. CONCLUSIONS

Wave propagation in a three-layered half-space with large velocity contrasts and decreasing velocity with depth has been investigated. Results show that it is only at the very high and very low frequency limits where wave propagation can be related to Rayleigh type of waves. Instead leaky guided waves dominate most of the frequency range that is suitable for nondestructive characterization of material properties.

A point source on the surface will generate a dominating quasi-antisymmetric Lamb wave in the high velocity top layer. This mode drives the complete system, and continuity across the boundaries generates higher modes in the embedded second layer. The interaction of leaky Lamb waves in the first two layers creates branches (portions) of dispersion curves measurable at the surface. In the lower frequency range these branches of dispersion curves can be individually resolved in practice, by using multichannel processing techniques. At higher frequencies there are theoretically substantially more modes than previously anticipated. All high-frequency branches merge together to form the dispersion curves corresponding to a stiff plate on a lower velocity half-space.

Several reported difficulties associated with surface wave testing of pavements can be explained from the presented theory. Abrupt jumps in phase velocity between branches of dispersion curves can create abrupt jumps in the measured wrapped phase spectrum also. These jumps can explain the reported difficulties in the phase unwrapping of the measured data and the cause of fluctuations in the measured dispersion curve.

It is concluded that future inversion techniques should be based on the complete phase velocity spectrum. With this approach not only phase velocities but also the overall pattern of branches of dispersion curves can be utilized. This holds the potential for a refined nondestructive testing technique for pavements.

ACKNOWLEDGMENTS

We would like to give our sincere thanks to Peab Sverige AB, VINNOVA, and the Swedish National Road Administration for financing this project. We also thank Dr. Choon B. Park, Kansas Geological Survey, and Dr. Peter Ulriksen, Lund University, for many helpful discussions.

Abraham, O., Pedersen, H., Hevin, G., Kergadallan, X., and Cote, Ph. (**2000**). ''The use of surface waves for non-destructive testing of concrete structures,'' Insight **42**(7), 444–446.

Akhlaghi, B. T., and Cogill, W. H. (**1994**). ''Application of the free plate analogy to a single-layered pavement system,'' Insight **36**, 514–518.

Al-Hunaidi, M. O. (**1992**). ''Difficulties with phase spectrum unwrapping in spectral analysis of surface waves nondestructive testing of pavements,'' Can. Geotech. J. **29**, 506–511.

Aouad, M. F. (**1993**). ''Evaluation of flexible pavements and subgrades using the spectral-analysis-of-surface-waves (SASW) method,'' Ph.D. thesis, Univ. of Texas at Austin, Texas.

Beaty, K. S., and Schmitt, D. R. (**2003**). ''Repeatability of multimode Rayleigh-wave dispersion studies,'' Geophysics **68**(3), 782–790.

Cheng, A., Murray, T. W., and Achenbach, J. D. (**2001**). ''Simulation of laser-generated ultrasonic waves in layered plates,'' J. Acoust. Soc. Am. **110**(2), 848–855.

Disperse (**2001**). ''A system for generating dispersion curves,'' User's manual version 2.0.11. Software version 2.0.15e. www.ndt.imperial.ac.uk.

Foinquinos, R., Roesset, J. M., and Stokoe, K. H. (**1995**). ''Response of pavement systems to dynamic loads imposed by nondestructive tests,'' Transp. Res. Rec. **1504**, 57–67.

Forbriger, T. (**2003**). ''Inversion of shallow-seismic wavefields part 1: Wavefield transformation,'' Geophys. J. Int. **153**, 719–734.

Foti, S. (**2000**). ''Multistation methods for geotechnical characterization using surface waves,'' Ph.D. thesis, Politecnico di Torino, Italy.

Foti, S., Sambuelli, L., Socco, V. L., and Strobbia, C. (**2003**). ''Experiments of joint acquisition of seismic refraction and surface wave data,'' Near Surface Geophys. **1**, 119–129.

Gabriels, P., Snider, R., and Nolet, G. (**1987**). ''In situ measurements of shear-wave velocity in sediments with higher-mode Rayleigh waves,'' Geophys. Prospect. **35**, 187–196.

Ganji, V., Gucunski, N., and Nazarian, S. (**1998**). ''Automated inversion procedure for spectral analysis of surface waves,'' J. Geotech. Geoenviron. Eng. **124**, 757–770.

Graff, K. E. (**1975**). *Wave Motion in Elastic Solids* (Oxford U.P., London).

Gucunski, N., and Woods, R. D. (**1992**). ''Numerical simulation of the SASW test,'' Soil Dyn. Earthquake Eng. **11**, 213–227.

Gucunski, N., Abdallah, I. N., and Nazarian, S. (**2000**). ''ANN backcalculation of pavement profiles from the SASW test,'' in Geotechnical Special Publication (ASCE) No. 98, *Pavement subgrade unbound materials, and nondestructive testing*, pp. 31–50.

Haskell, N. A. (**1953**). ''The dispersion of surface waves on multilayered media,'' Bull. Seismol. Soc. Am. **43**, 17–34.

Heisey, J. S., Stokoe, K. H., and Meyer, A. H. (**1982**). ''Moduli of pavement systems from spectral analysis of surface waves,'' Transp. Res. Rec. **852**, 22–31.

Hunaidi, O. (**1998**). ''Evolution-based genetic algorithms for analysis of non-destructive surface wave tests on pavements,'' NDT&E Int. **31**, 273–280.

Inazaki, T., and Xinglin, L. (**2003**). ''High-frequency seismic measurements using a piezoelectric type accelerometer array,'' in Proceedings of the Symposium on the Application of Geophysics to Engineering and Environmental Problems (SAGEEP 2003), San Antonio, TX, 6–10 April, CD-Rom, seis04.

Jones, R. (**1955**). ''A vibration method for measuring the thickness of concrete road slabs in situ,'' Mag. Concrete Res. **7**(20), 97–102.

Jones, R. (**1962**). ''Surface wave technique for measuring the elastic properties and thickness of roads: Theoretical development,'' Br. J. Appl. Phys. **13**, 21–29.

Jones, R., and Thrower, E. N. (**1965**). ''An analysis of waves in a two-layer composite plate and its application to surface wave propagation experiments on roads,'' J. Sound Vib. **2**(3), 328–335.

Knopoff, L. (**1964**). ''A matrix method for elastic wave problems,'' Bull. Seismol. Soc. Am. **54**, 431–438.

Lamb, H. (**1917**). ''On waves in an elastic plate,'' Proc. R. Soc. **93**, 114–128.

Laperre, J., and Thys, W. (**1993**). ''Experimental and theoretical study of Lamb wave dispersion in aluminium/polymer bilayers,'' J. Acoust. Soc. Am. **94**, 268–278.

Lee, Y. C., and Cheng, S. W. (**2001**). ''Measuring Lamb wave dispersion curves of a bilayered plate and its application on material characterization of coating,'' IEEE Trans. Ultrason. Ferroelectr. Freq. Control **48**(3), 830–837.

Lefeuvre, O., Zinin, P., and Briggs, G. A. D. (**1998**). ''Leaky surface waves propagating on a fast on slow system and the implications for material characterization,'' Ultrasonics **36**, 229–232.

Lefeuvre, O., Kolosov, O. V., Every, A. G., Briggs, G. A. D., and Tsukahara, Y. (**2000**). ''Elastic measurements of layered nanocomposite materials by Brillouin spectroscopy,'' Ultrasonics **38**, 459–465.

Long, R., Cawley, P., and Lowe, M. (**2003**). ''Acoustic wave propagation in buried iron water pipes,'' Proc. R. Soc. London, Ser. A **459**, 2749–2770.

Lowe, M. J. S. (**1995**). ''Matrix techniques for modeling ultrasonic waves in multilayered media,'' IEEE Trans. Ultrason. Ferroelectr. Freq. Control **42**, 525–542.

Lowe, M. J. S., and Cawley, P. (**1995a**). ''Comparison of the modal properties of a stiff layer embedded in a solid medium with the minima of the plane-wave reflection coefficient,'' J. Acoust. Soc. Am. **97**, 1625–1637.

Lowe, M. J. S., and Cawley, P. (**1995b**). ''The influence of the modal properties of a stiff layer embedded in a solid medium on the field generated in the layer by a finite-sized transducer,'' J. Acoust. Soc. Am. **97**, 1638–1649.

Martincek, G. (**1994**). *Dynamics of Pavement Structures* (E&FN Spon and Ister Science, London).

Nayfeh, A. H., and Chimenti, D. E. (**1984**). ''Reflection of finite acoustic beams from loaded and stiffened half-spaces,'' J. Acoust. Soc. Am. **75**, 1360–1368.

Nazarian, S. (**1984**). ''In situ determination of soil deposits and pavement systems by spectral analysis of surface waves method,'' Ph.D. thesis, Univ. of Texas at Austin, Texas.

O'Neill, A. (**2003**). ''Full-waveform reflectivety for modelling, inversion and appraisal of seismic surface wave dispersion in shallow site investigation,'' Ph.D. thesis, Univ. of Western Australia, Australia.

Park, C. B., Miller, R. D., and Xia, J. (**1998**). ''Imaging dispersion curves of surface waves on multi-channel records,'' Technical Program with Biographies, SEG, 68th Annual Meeting, New Orleans, Louisiana, pp. 1377–1380.

Park, C. B., Miller, R. D., and Xia, J. (**1999**). ''Multichannel analysis of surface waves,'' Geophysics **64**, 800–808.

Parra, J. O., and Xu, P. (**1994**). ''Dispersion and attenuation of acoustic guided waves in layered fluid-filled porous media,'' J. Acoust. Soc. Am. **95**, 91–98.

Pavlakovic, B., Lowe, M., Alleyne, D., and Cawley, P. (**1997**). ''Disperse a general purpose program for creating dispersion curves,'' Rev. Prog. Quant. Nondestr. Eval. **16**, 185–192.

Picket, G. (**1945**). ''Dynamic testing of pavements,'' J. Am. Concr. Inst. **16**(5), 473–489.

Press, F., and Dobrin, M. B. (**1956**). ''Seismic wave studies over a high-speed surface layer,'' Geophysics **XXI**(2), 285–298.

Randall, M. J. (**1967**). ''Fast programs for layered half-space problems,'' Bull. Seismol. Soc. Am. **57**, 1299–1315.

Roesset, J. M., Chang, D. W., Stokoe, K. H., and Auoad, M. (**1990**). ''Modulus and thickness of the pavement surface layer from SASW tests,'' Transp. Res. Rec. **1260**, 53–63.

Ryden, N., and Park, C. B. (**2004**). ''Surface waves in inversely dispersive media,'' Near Surface Geophysics, **2**(4), 187–197.

Ryden, N., Park, C. B., Ulriksen, P., and Miller R. D. (**2002**). ''Branching of dispersion curve in surface wave testing of pavements,'' in Proceedings of the Symposium on the Application of Geophysics to Engineering and Environmental Problems (SAGEEP 2002), Las Vegas, NV, 10–14 February, 12SE17.

Ryden, N., Park, C. B., Ulriksen, P., and Miller, R. D. (**2004**). ''A multimodal approach to seismic pavement testing,'' J. Geotech. Geoenviron. Eng. **130**, 636–645.

Ryden, N., Ulriksen, P., Park, C. B., Miller, R. D., Xia, J., and Ivanov, J. (**2001**). ''High frequency MASW for non-destructive testing of pavements-accelerometer approach,'' in Proceedings of the Symposium on the Application of Geophysics to Engineering and Environmental Problems (SAGEEP 2001), Denver, CO, RBA-5.

Sheu, J. C., Stokoe, K. H., and Roesset, J. M. (**1988**). ''Effect of reflected waves in SASW testing of pavements,'' Transp. Res. Rec. **1196**, 51–56.

Shull, P. J., Chimenti, D. E., and Datta, S. K. (**1994**). ''Elastic guided waves and the Floquet concept in periodically layered plates,'' J. Acoust. Soc. Am. **95**, 99–108.

Shuvalov, A. L., and Every, A. G. (**2002**). ''Characteristic features of the velocity dispersion of surface acoustic waves in anistropic coated solids,'' Ultrasonics **40**, 939–942.

Simonetti, F. (**2004**). ''Lamb wave propagation in elastic plates coated with viscoelastic materials,'' submitted to J. Acoust. Soc. Am.

Stokoe, K. H., Wright, G. W., James, A. B., and Jose, M. R. (**1994**). ''Characterization of geotechnical sites by SASW method,'' in *Geophysical Characterization of Sites*, ISSMFE Technical Committee #10, edited by R. D. Woods (Oxford, New Delhi).

Stoneley, R. (**1924**). ''Elastic waves at the surface of separation of two solids,'' Proc. R. Soc. **106**, 416–428.

Thomson, W. T. (**1950**). ''Transmission of elastic waves through a stratified solid medium,'' J. Appl. Phys. **21**, 89–93.

Tokimatsu, K., Tamura, S., and Kojima, H. (**1992**). ''Effects of multiple modes on Rayleigh wave dispersion characteristics,'' J. Geotech. Eng. **118**, 1529–1543.

Vidale, R. F. (**1964**). ''The dispersion of stress waves in layered media overlaying a half space of lesser acoustic rigidity,'' Ph.D. thesis, Univ. of Wisconsin.

Wilcox, P. (**2004**). ''Modeling the excitation of Lamb and SH waves by point and line sources,'' Review of Progress in Quantitative NDE, edited by D. O. Thompson and D. E. Chimenti (American Institute of Physics, New York), Vol. 23, 206–213

Wu, H., Wang, S., Abdallah, I., and Nazarian, S. (**2002**). ''A rapid approach to interpretation of SASW results,'' in Proceedings of the BCRA 2002, Lissabon, Portugal, pp. 761–770.

Xia, J., Miller, R. D., and Park, C. B. (**1999**). ''Estimation of near-surface shear-wave velocity by inversion of Rayleigh wave,'' Geophysics **64**, 691–700.

Yapura, C. L., and Kinra, V. K. (**1995**). ''Guided waves in a fluid-solid bilayer,'' Wave Motion **21**, 35–46.

Zhang, B., and Lu, L. (**2003**). ''Rayleigh wave detection of low-velocity layers in a stratified half-space,'' Acoust. Phys. **49**(5), 516–528.

Zinin, P., Lefeuvre, O., Briggs, G. A. D., Zeller, B. D., Cawley, P., Kinloch, A. J., and Thompson, G. E. (**1997**). ''Anomalous behaviour of leaky surface waves for stiffening layer near cutoff,'' J. Appl. Phys. **82**(3), 1031–1035.

Paper V

Inversion of Surface Waves using Phase Velocity Spectra

Ryden, N. and Park, C.B.†*

**Lund Institute of Technology, Lund University, Sweden*
†Kansas Geological Survey, Kansas University, USA

ABSTRACT

We describe a surface wave inversion technique especially developed for non-destructive testing of pavements. Data acquisition and processing utilize key concepts of the Multichannel Analysis of Surface Waves (MASW) method. The inversion of a vertical shear wave velocity profile is implemented on the full phase velocity spectrum, instead of discrete dispersion curves, using the Fast Simulated Annealing (FSA) algorithm. The main benefit is that the raw field data can be automatically processed and inverted without any subjective user input to identify discrete dispersion curves, while properly accounting for the interference of different modes and types of waves. The viscoelastic properties of the asphalt layer can also be included to produce the asphalt stiffness as a function of frequency, a mastercurve. The proposed approach is demonstrated on both synthetic and field data. The mastercurve inverted from the field data is compared to laboratory results obtained from core samples from the asphalt layer, while the inverted parameters of the underlying layers are compared to values obtained in the field during the construction of each layer. The same inversion approach can also be applied to surface-wave testing at soil sites and in the field of ultrasonic testing of composite materials.

INTRODUCTION

Non-destructive testing (NDT) of pavements based on surface waves hold the potential to obtain both the thickness and stiffness properties of the different layers in a pavement construction. With an efficient NDT technique these properties can be mapped as a function of time and space, providing a valuable tool in pavement design and management. Since the early studies by Jones (1962) and Vidale (1964), surface wave methods have been recognized as a promising approach for seismic/acoustic NDT of pavements. The introduction of the Spectral Analysis of Surface Waves (SASW) method (Heisey et al., 1982; Nazarian, 1984; Stokoe et al., 1994) has resulted in a widespread use of the method, and field protocols for pavement design and maintenance based on seismic methods are now being developed (Haegeman, 2002; Abdallah et al., 2003; Ekdahl et al., 2004). The evaluation of the top layer thickness and stiffness has proved to be most efficient and accurate (Roesset et al., 1990; Akhlaghi and Cogill, 1994). The inversion of deeper embedded layers has been the most challenging part in surface wave testing of pavements (Ganji et al., 1998; Gucunski et al., 2000). The embedded second layer (base) underneath the asphalt layer has been especially difficult to resolve (Aouad, 1993; Wu et al., 2002).

Recent studies by Ryden et al. (2004) and Ryden and Lowe (2004) showed that guided wave propagation in pavement structures is more complicated than previously addressed, particularly with the issue of multiple modes of leaky waves with large variations in excitability between different modes. Traditional surface wave methods based on a single composite dispersion curve may, therefore, not be sufficient to adequately resolve the

dispersion properties from pavement systems. On the other hand, the multi-channel approach has proved to be capable of separating different modes of surface waves (Ryden et al., 2004; Park et al., 1999). With surface wave testing on pavements, however, a true multi-channel approach would become expensive with many (usually more than 24) accelerometers. Instead, a synthetic source array can be used to record high-frequency multichannel-equivalent data with only one source (small hammer) and one receiver (accelerometer). The receiver is fixed at a surface point and receives signals *u(t)* from several hammer impacts at incremental offsets (*x*) (Ryden et al., 2001; 2004). All recorded signals are then compiled to make an equivalent multichannel record *u(x,t)* for dispersion analysis. A schematic description of the field set-up is shown in Figure 1.

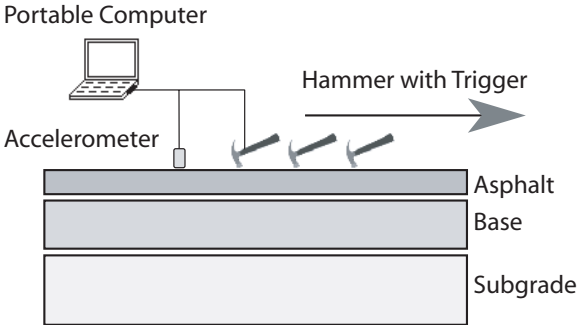

Figure 1. Schematic illustration of the field set-up and data acquisition using only one receiver and one source.

Inversion of surface wave dispersion curves is a nonunique and nonlinear inverse problem, where a direct solution is not possible. Nonunique means that different layer models may match the measured data equally well. Nonlinear means that small changes in the data can correspond to large changes in the layer model and vice versa. The conventional inversion technique for surface wave methods is usually based on a linearized damped least squares solution, driven by partial derivatives of each inverted parameter (Jacobian matrix) (Menke, 1989; Xia et al., 1999). The multimodal nature of surface wave data from pavements (Ryden and Park, 2004; Ryden and Lowe, 2004) makes the partial derivatives approach difficult because the measurable apparent dispersion curve "jumps" between mode branches and the partial derivatives are not sufficiently stable (Foti et al., 2003). When discrete dispersion curves are inverted, the correct mode number identification also becomes a critical and difficult task (Socco et al., 2002; Zhang and Chan, 2003). Forbriger (2003) presented a gradient-based inversion procedure of the complete wavefield spectrum, to solve the problems with mode number identification. A general problem with linearized gradient-based inversion techniques applied to nonlinear and nonunique problems is that the solution is often dependent on the starting model and may not always converge to the global minimum of the objective function (Sen and Stoffa, 1995). In the case of pavement systems, the problem is further complicated by largely variable parameter sensitivities and correlated parameters. These difficulties are the main motivation of the present study.

We describe a new procedure for the inversion of surface wave data. This procedure is based on the complete phase velocity spectrum rather than discrete dispersion curves. A global optimization technique, Fast Simulated Annealing (FSA), is implemented for the inversion algorithm. With this procedure, data reduction and the extraction of an experimental dispersion curve is avoided. Consequently, the complete procedure from data collection to evaluation of layer properties becomes fully automatic and objective. This study was initiated by the complicated nature of wave propagation in pavement structures. However, the same

procedure can be used for the inversion of surface wave data from soil sites, or in the field of ultrasonic testing of composite plates and coatings.

PHASE VELOCITY SPECTRA

Figure 2 shows an example of a typical phase velocity spectrum recorded over a pavement system. The grayscale image shows amplitudes as a function of frequency and phase velocity. Over the full-frequency range (Figure 2a) most energy is concentrated along the fundamental mode anti-symmetric Lamb wave (A0) dispersion curve corresponding to the top layer acting as a free plate (black solid line) (Ryden and Park, 2004). Figure 2b shows the visible mode branches at lower frequencies. The pattern of these mode branches is a function of the pavement layer properties (Ryden and Lowe, 2004).

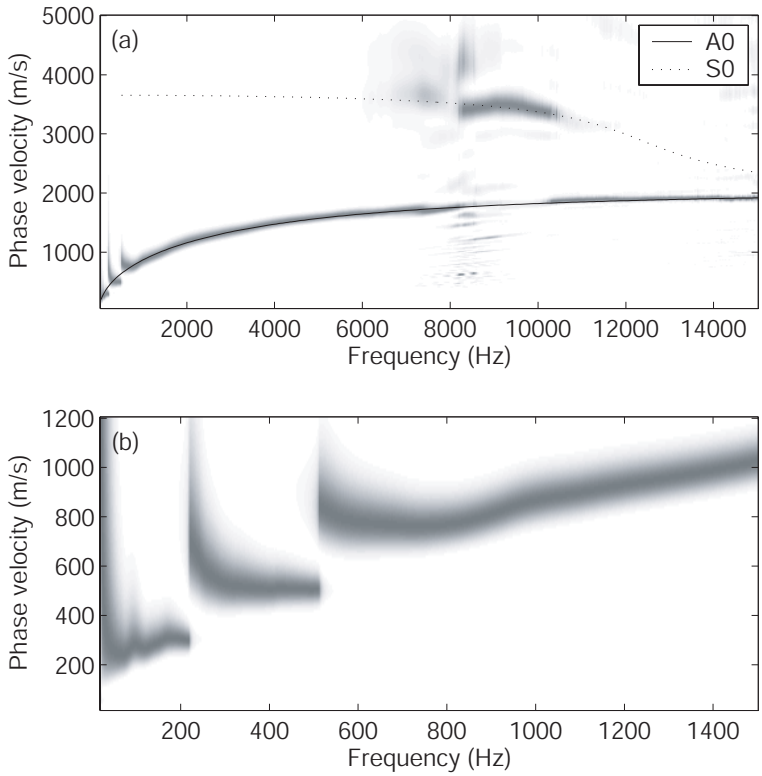

Figure 2. (a) Gray shading corresponds to the measured phase velocity spectrum from a three-layer pavement construction. Predicted Lamb wave dispersion curves from the top layer as a free plate are superimposed as solid (A0) and dotted (S0) lines. (b) The same measured data set displayed in a lower frequency and phase velocity range showing branches of dispersion curves.

Measured phase velocity spectrum

The measured phase velocity spectrum is obtained automatically from multichannel surface wave data by using the plane wave transformation technique by Park et al. (1998; 1999). The multichannel equivalent record compiled from measurements at different offsets, *u(x,t)*, is automatically and objectively transformed to the frequency-phase velocity domain by using

$$S(\omega, c_T) = \int e^{-i(\omega/c_T)x} U(x,\omega)dx \qquad (1)$$

where, $U(x,\omega)$ is the normalized complex spectrum obtained from the Fourier transformation of $u(x,t)$, ω is the angular frequency, and c_T is the testing phase velocity. $S(\omega,c_T)$ is the slant stack amplitude for each ω and c_T, which can be viewed as the coherency in linear arrival pattern along the offset range for that specific combination of ω and c_T. When c_T is equal to the true phase velocity of each frequency component there will be a maximum in $S(\omega,c_T)$. Calculating $S(\omega,c_T)$ over the frequency and phase velocity range of interest generates the phase velocity spectrum where dispersion curves can be identified as high amplitude bands. It should be noted that $U(x,\omega)$ is normalized in both the x and ω dimension so that all amplitudes at different frequencies and distances has unit amplitude. This processing scheme has shown to give better resolution in phase velocity compared to the conventional *f-k* and τ-*p* transformation (Beaty and Schmitt, 2002; Moro et al., 2003), particularly when a limited number of traces are used (Moro et al., 2003). A detailed parametric examination of equation 1 on its resolution in response to its parameters is presented in Park et al. (2001).

Theoretical phase velocity spectrum

The theoretical phase velocity spectrum (forward model) is calculated from a known layer model (**m**) and the field set-up geometry. The forward model should ideally mimic the field set up and measured response as close as possible to generate a phase velocity spectrum that is directly comparable to the measured replica. Therefore, the receiver and source locations are also included in the forward model so that superposition of different modes of propagation can be accounted for.

The first step in the forward model is to find the resonant wavenumbers *(k)* (modes) at the surface of a known layer model (**m**) resulting from a vertical load at the surface. The stiffness matrix approach by Kausel and Roesset (1981) is implemented for this calculation. The stiffness matrix approach relates loads *(p)* and displacements *(U)* at the layer interfaces in the frequency-wavenumber *(ω-k)* domain. The basic equations originate from the transfer matrix method (Haskell, 1950; Thomson, 1953) but are rearranged to be expressed in loads instead of partial wave amplitudes. All layer equations are omitted here but can be found along with more details in; Kausel and Roesset (1981), Gucunski and Woods (1992), and Gucunski and Maher (2000). The stiffness matrix method is usually implemented along with complex bulk wave velocities where the complex part is addressed as material damping *(D)*. With this approach k is always complex and there is less risk for numerical instabilities. Alternatively, a small damping coefficient can be added as a complex component of each k. With this approach a reasonable amount of leakage into the half-space can be implicitly accounted for (Ryden and Lowe, 2004). When all layer matrices are assembled, vertical amplitudes at the surface *(U)* can be calculated for each frequency *(ω)* and wavenumber *(k)* of interest. By scanning through a range of testing phase velocities *(c_T)* at each frequency, resonant peaks can be extracted along with their relative amplitude ratios. Figure 3a shows the surface response from a vertical unit load in the U-c_T domain at 760 Hz calculated from the reference layer model in Table 1. Two resonant phase velocities (or wavenumbers $k=\omega/c$) can be identified with a relative amplitude ratio of 0.85. It should be noted that these resonant wavenumbers are not necessarily the fundamental and first higher mode. An exact mode number identification is not necessary, since the inversion is based on the phase velocity spectrum instead of discrete dispersion curves.

In the next step the extracted modes, $U_{pred}(\omega,k)$, are superimposed over the same offset range as used for the measured data. The Hankel function is used instead of the plane wave approximation to account for cylindrical spreading. This will introduce a non-linear phase shift at near offsets and thereby to a certain degree account for the near field effect (Zywicki,

1999). The relative phase lag at each offset can now be calculated and expressed with a complex spectrum as

$$U_{pred}(x,\omega) = qR\int_0^\infty J_1(kR)J_0(kx)U_{pred}(\omega,k)dk \qquad (2)$$

where R represents the radius of the source point, q is the load intensity, and J_0 and J_1 are Bessel functions of the first kind of orders 0 and 1, respectively. In this application R and q can be omitted because the radius of the source point is much smaller than the wavelengths of interest and amplitudes are normalized in the subsequent processing of $U_{pred}(x,\omega)$. It should also be noted that the initial phase at zero offset is assumed to approach zero for all frequencies. The resulting phase angle as a function of offset is plotted in Figure 3b. The superimposition of two different phase velocities at the same frequency creates a non-linear phase-offset pattern. This non-linear phase offset curve is typical in surface wave testing of pavements and was noticed by Van der Poel (1951) over fifty years ago.

In the final step of the forward model the theoretical complex spectrum obtained from equation 2 is transformed to the frequency-phase velocity domain by using equation 1. Now a predicted phase velocity spectrum $S_{pred}(\omega,c_T,\mathbf{m})$ is generated which can be directly compared to the observed replica $S_{obs}(\omega,c_T)$ obtained from the measured field data. Figure 3c shows this phase velocity spectrum at 760 Hz. The difference between Figure 3a and Figure 3c is important for the subsequent inversion procedure. Figure 3c is offset dependent and includes modal superimposition effects that are not present in Figure 3a.

TABLE 1: Reference layer model with inverted values in parentheses.

Layer	V_S (m/s)	ν	ρ (kg/m^3)	h (m)
1	1400.0 (1401.5)	0.350	2000.0	0.220 (0.224)
2	300.0 (303.0)	0.350 (0.349)	2000.0	0.400 (0.404)
3	100.0 (103.4)	0.350	2000.0	∞

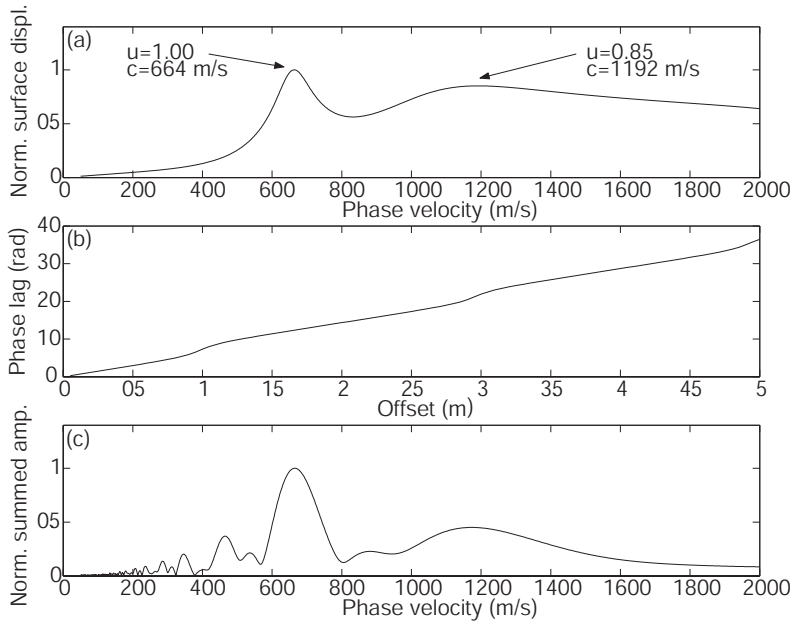

Figure 3. (a) Surface displacement at 760 Hz from a vertical unit load at the surface showing two different modes of propagation (peaks). (b) The resulting phase-offset curve and the typical step like behavior created by the interference of two different modes. (c) The corresponding summed amplitude spectrum generated from the MASW transformation technique.

SENSITIVITY ANALYSIS OF LAYER PARAMETERS

The predicted phase velocity spectrum is compared to the observed phase velocity spectrum through the objective function

$$M(\mathbf{m}) = \left(1 - \frac{\sum_{i=1}^{M}\sum_{j=1}^{N}\left|\mathbf{S}_{ij\,obs}\right| * \left|S_{ij\,pred}\right|}{\sum_{i=1}^{M}\sum_{j=1}^{N}\left|S_{ij\,obs}\right|^2} \right) \tag{3}$$

where M represents the mismatch between the two phase velocity spectra. M can be a value between 0 and 1 where 0 represents a perfect match. The value of M is to be minimized in the subsequent inversion procedure. In this study amplitudes in both the phase velocity spectra are raised to the power of 3 to suppress low amplitudes and increase the sharpness of the main amplitude bands (dispersion curves).

It is essential to find out which parameters in the layer model have a noticeable influence on the phase velocity spectrum. Therefore a sensitivity analysis is first presented before the inversion algorithm is further described. The layer model in Table 1 represents a reference pavement layer model. Each parameter value is perturbated ± 10% compared to the true value. The corresponding mean M value of the two perturbations of each parameter is presented in Figure 4. This plot can be viewed as a sensitivity analysis of each parameter in the reference layer model. In this case the sensitivity of each parameter will be influenced by a number of parameters such as the specific reference layer model, frequency range, phase velocity range, and offset range. The frequency range and frequency sampling (e.g. linear, logarithmic, or other) will have the largest influence on the ΔM value. In general a denser sampling and higher maximum frequency will result in larger sensitivities. However, in practice, real data is always contaminated with noise and there will be a maximum frequency above which mode branches cannot be individually resolved (e.g., at about 1000 Hz in Figure 1b). In this sensitivity example the minimum and maximum frequencies are 60 and 1000 Hz, respectively, with a linear sampling of 100 values. The modeled offset range is 0.05 m to 5.00 m with a station separation of 0.05 m. Figure 4 shows that the thickness and shear wave velocity of each layer are the most sensitive parameters. However, Poisson's ratio of the second layer also shows a significant sensitivity. It should be noted that the top layer properties show a noticeable influence on the phase velocity spectrum although relatively low frequencies are used compared to the conventional frequency range (50-30000 Hz) usually used in surface wave testing of pavements.

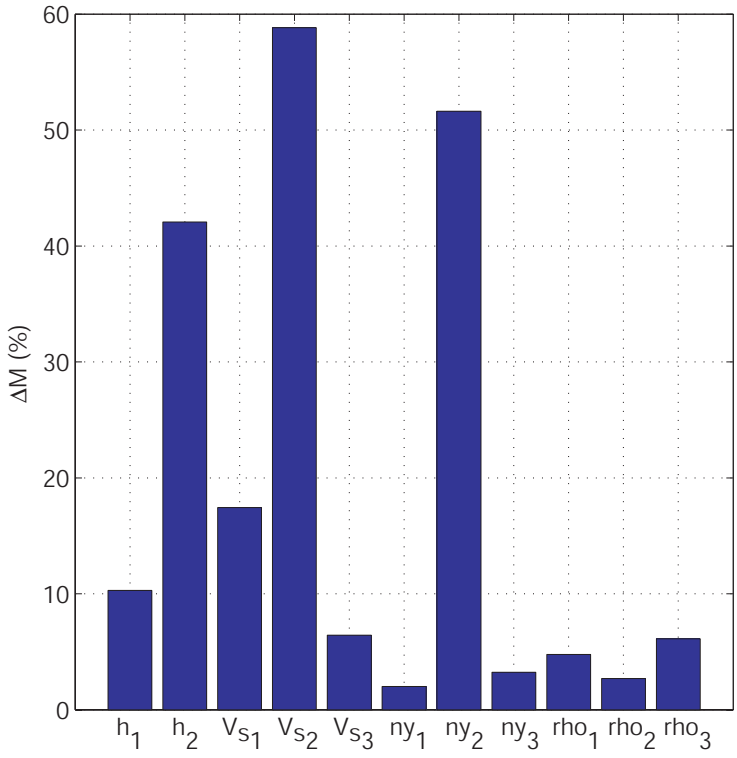

Figure 4. Sensitivity analysis of the reference layer model presented in Table 1. Each parameter is perturbated ± 10% and the bars represent the corresponding mean mismatch from each parameter.

Based on this sensitivity analysis, it can be concluded that both the thickness and the shear wave velocity of each layer should be meaningful to estimate through the inversion procedure. However, further difficulties can arise from correlated parameters and/or many local minima within the parameter space. The shape of the *M* function for each parameter reveals some of these difficulties. The one-dimensional (1-D) *M* functions are calculated by scanning through a range of parameter values while keeping all other layer parameters fixed at the true values of the reference layer model. This type of plot is presented in Figure 5 for the six most sensitive parameters from Figure 4. Unfortunately this type of plot only gives a 1-D picture of the complete multidimensional parameter space. In Figure 6, 2-D *M* functions of selected parameters are plotted. Suddenly some of the features that make the inversion of pavement layer properties a challenging task become visible i.e., local minima and correlated parameters. These features are typical for this problem and show why a global optimisation technique is necessary for the inversion of surface wave data containing multiple mode branches.

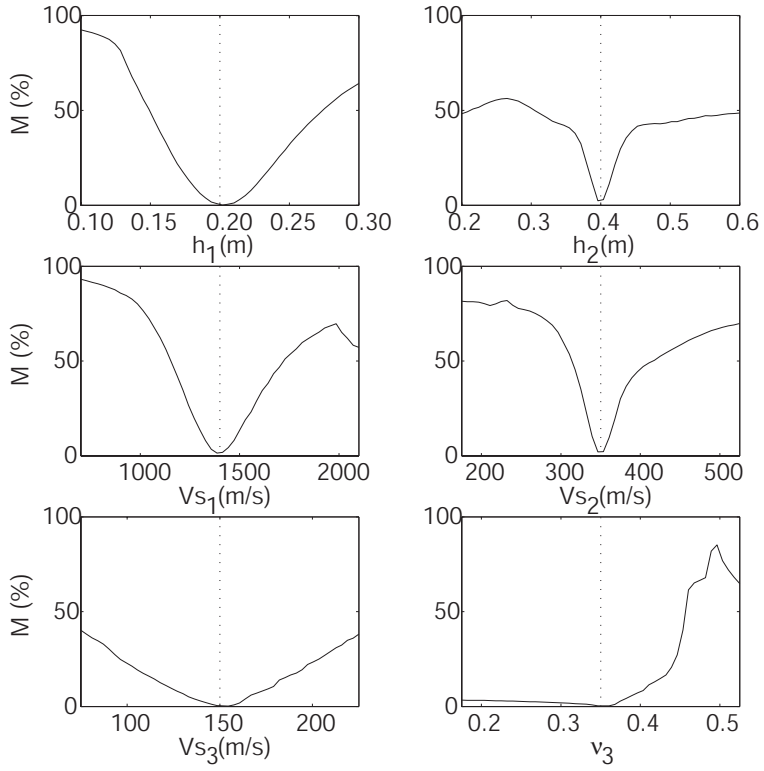

Figure 5. 1-D cross sections of the parameter space showing the variation in sensitivity of different parameters of the layer model. The dotted line corresponds to the true value of each parameter (Table 1).

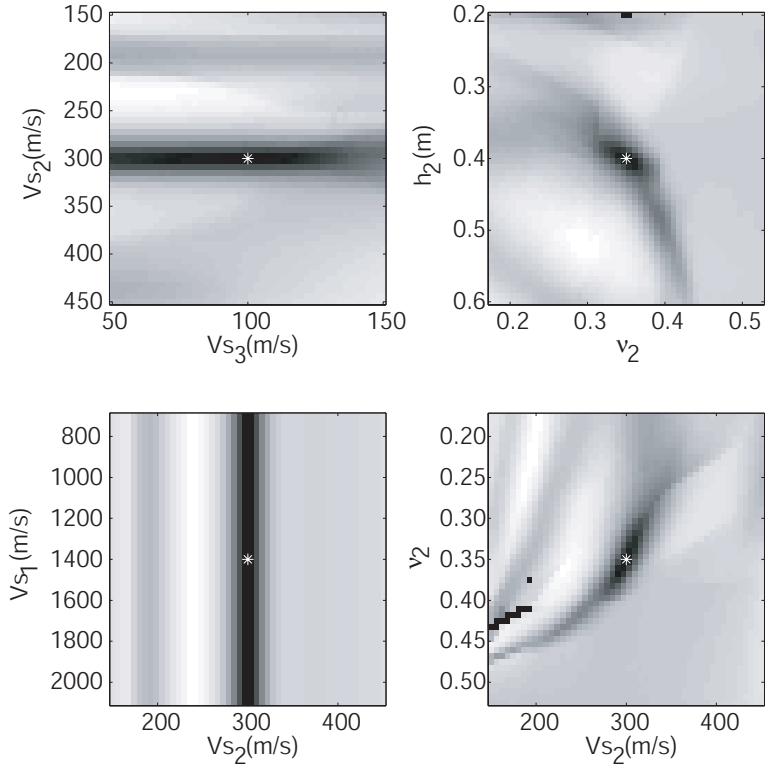

Figure 6. 2-D cross sections of the parameter space gray scaled with respect to the mismatch (*M*) value. Dark gray color corresponds to low *M* values and the white cross shows the true parameter values.

INVERSION BY FAST SIMULATED ANNEALING

The goal of the inversion procedure is to find a layer model whose corresponding phase velocity spectrum matches the measured spectrum best. This case represents the global minimum of the objective function (equation 3). A number of search strategies for this type of problem have been presented (Mosegaard and Sambridge, 2002). A straightforward approach is to define reasonable upper and lower bounds for each parameter to invert for and then simply scan through all trial layer models ($\mathbf{m_i}$) in the search for the global minimum. If each parameter is divided into N intervals and there are S number of parameters to invert for, the complete parameter space can be divided into N^S trial layer models. Unfortunately this approach quickly becomes impractical for large numbers of N and S. This is the main motivation to use statistical search strategies instead. Simulated Annealing (SA) is a global direct Monte Carlo method (Kirkpatrick et al., 1983; Laarhoven and Aarts, 1987) that was especially developed to find the global minimum of challenging functions with many local minima. The method has been applied to surface wave inversion in previous studies where discrete continuous dispersion curves have been successfully matched (Martínez et al., 2000; Beaty et al., 2002; Rambod and Gucunski, 2003). Now we apply the SA concept to the inversion of phase velocity spectra in place of discrete dispersion curves.

Simulated annealing

The basic concept of the simulated annealing method is to perform a random walk in the multidimensional parameter space with the intention of finding the global minimum of the objective function (equation 3). This process originates from the natural optimization process of thermodynamic annealing in crystalline solids (Laarhoven and Aarts, 1987). The search strategy involves two control parameters, an initial temperature *(T_0)* with the same unit as the objective function, and a cooling parameter *(a)*. Each iteration *(j)* involves a random perturbation of each parameter in **m** followed by a forward model and mismatch calculation. The initial model is randomly drawn from the predefined interval (Δm_l) of each parameter *(l)*. If the calculated mismatch is smaller than that for the previously accepted model, the new model is always accepted as a transition *(i)*. However, if the mismatch is larger than it was for the previous model, the new model may also be accepted if

$$r < e^{-\Delta M / T} \tag{4}$$

where r is a random number from 0 to 1, ΔM is the mismatch difference between the current and the previously accepted model, and T is the current temperature that is decreased with the number of accepted transitions *(i)* according to the employed cooling schedule. This second chance of acceptance (known as the Metropolis criterion) is the key concept of the SA algorithm, and can make the search escape from a local minimum and move on in the search for the global minimum. Figure 7 shows an outline of the SA algorithm used in this study. It should be noted that, compared to matrix-based inversion techniques, the SA algorithm is not directly dependent on the type of forward model or objective function used, which provides some flexibility in the definition of the type.

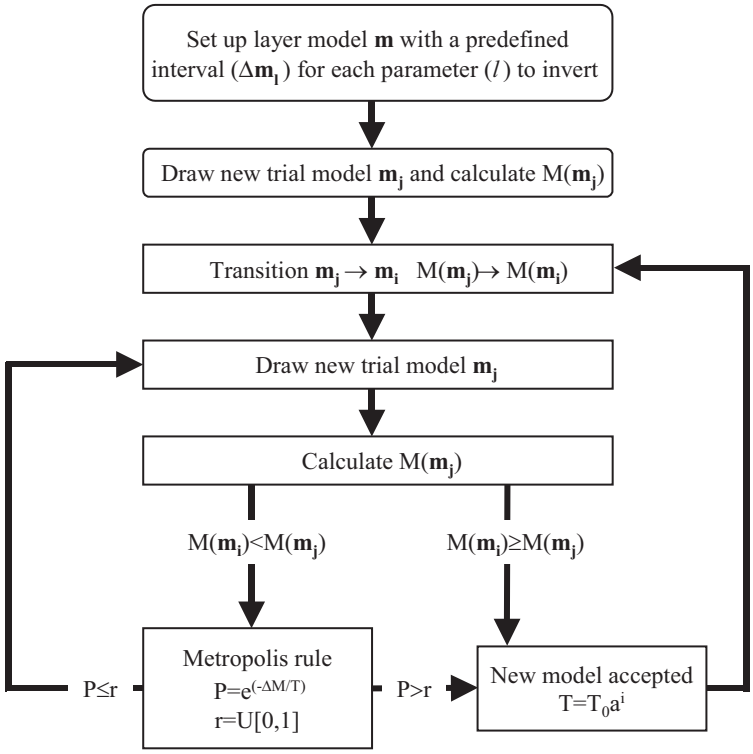

Figure 7. Schematic flow chart of the simulated annealing algorithm. Index *i* represents the number of accepted transitions and index *j* represents the total number of iterations.

The cooling schedule and the perturbation size are the most important parameters to optimize for each specific SA application. A commonly used cooling schedule is the exponential

$$T = T_0 a^i \tag{5}$$

where the cooling parameter *(a)* is a number smaller than one. Initially the temperature should be set high enough so that many iterations (*j*), about 90% according to Dosso et al. (2001), are accepted as transitions (*i*). Then, after a preset number of transitions, the temperature is gradually reduced according to the cooling parameter. The effect of *a* makes the probability of equation 4 decrease with the number of accepted transitions so that the algorithm eventually converges to a minimum. If the control parameters *a* and T_0, whose values are usually application dependent, are properly set for the specific application, there should be a good chance of finding the global minimum. However, there is no guarantee that the global minimum has been found. Several researchers have presented techniques for finding the optimum cooling schedule (Andresen and Gordon, 1994; Basu and Frazer, 1990; Hoffmann and Salamon, 1990).

The difference between standard SA and Fast Simulated Annealing (FSA) (Szu and Hartley, 1987) lies in the way the new models are randomly perturbated for each new iteration. If the search range (Δm_l) assigned to each parameter to invert is too large, it will waste a lot of time at low temperatures where large perturbations are not likely. Therefore the FSA method involves a temperature-scaled Cauchy distribution of the perturbation of each parameter (Sen and Stoffa, 1995). The Cauchy distribution has a narrow central peak and heavy tails, providing concentrated local sampling in combination with occasional large

perturbations. After each accepted transition, each parameter (m_l) is perturbated to obtain a new testing value (m'_l) according to

$$m'_l = m_l + \Delta m_l (T / T_0)(\eta_1 \tan(\eta_2 \pi / 2)) \quad (6)$$

where η_1 and η_2 are uniform random variables on [-1,1], and Δm_l are the predefined search interval for each parameter (l). With the approach presented herein all parameters are perturbated at once after each iteration (j); standard SA algorithms typically perturb one parameter at a time and cycle through all parameters (Laarhoven and Aarts, 1987). Perturbating all parameters at once is more effective for problems with correlated parameters (Dosso et al., 2001).

SYNTHETIC DATA TEST

The presented inversion procedure is first demonstrated on synthetic data from the reference layer model (Table 1). The FSA schedule was set up with five transitions per temperature, and an exponential cooling schedule with T_0=30 and a=0.99. Parameter values and corresponding M values from all iterations used for the inversion are plotted in Figure 8. The predefined search range of each parameter is equal to the x-axis range in Figure 8. The dotted lines indicate the true values from Table 1. This figure shows how the FSA algorithm searches through the given range of parameter values and finally converges towards the true values. The width of the peak of all dots in Figure 8 indicates the multidimensional sensitivity of each parameter. It should be noted that the distribution shape of all dots in Figure 8 includes the multidimensional sensitivity of each parameter while Figure 5 only shows a 1-D picture of the parameter space.

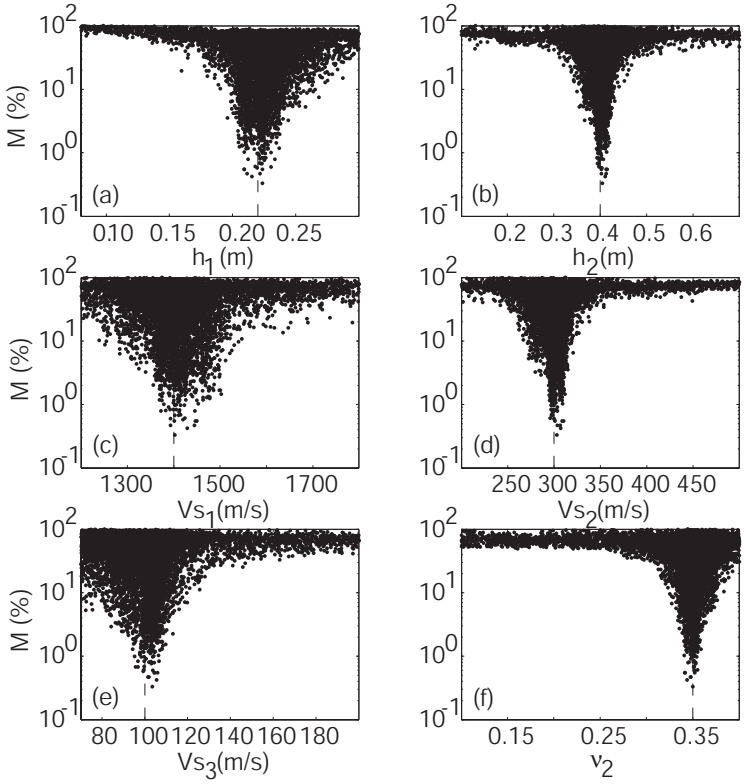

Figure 8. Each dot indicates the mismatch as a function of parameter value from the inversion of the synthetic data test.

The inversion algorithm was set up to stop after 700 transitions or an M value lower than 0.400%. In this example an M value of 0.327% was reached after 457 transitions and 9095 iterations. The target and best matching phase velocity spectrum is plotted in Figure 9. The inversion of this synthetic data test could have been continued to run for even lower M values, possibly resulting in even closer inverted parameter values. However, in practice real data is contaminated with noise and these small variations in the M value may not be realistic.

The final inverted parameter values are given in parentheses in Table 1. These values represent the dots with the lowest M values from Figure 8. The shear wave velocity of the half-space (V_{S3}) shows the largest deviation from the true value with an error of 3.4%. The other five parameters are all well resolved within about 1% of the true values. It should be noted that the thickness of the second layer (h_2) shows a sharp peak in Figure 8b, which indicates that this parameter is well resolved although this is the layer parameter that has been the most difficult to invert with the conventional methods.

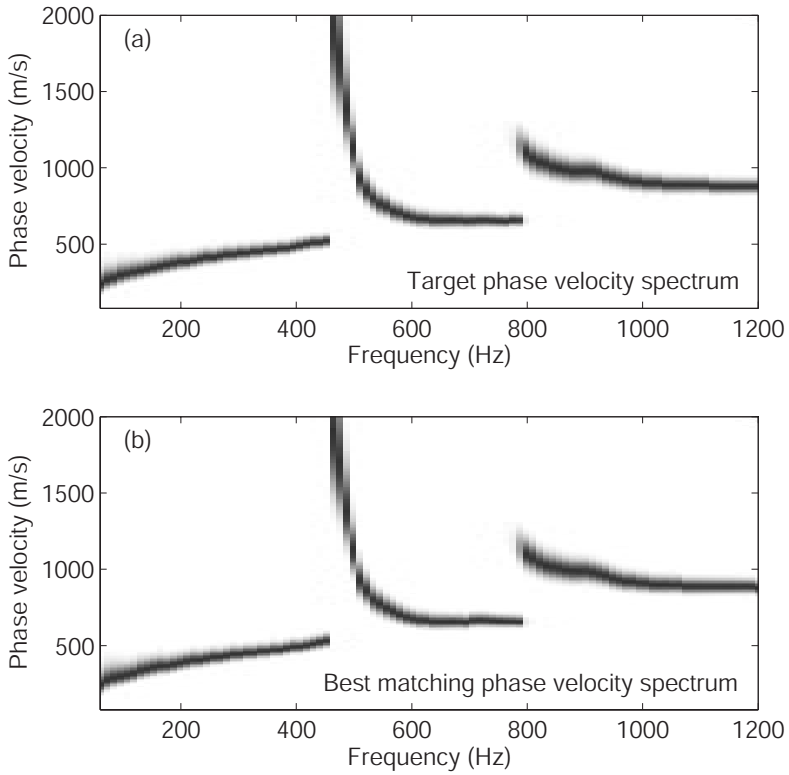

Figure 9. (a) Target phase velocity spectrum corresponding to the layer model in Table 1. (b) Best matching phase velocity spectrum from the inversion test on synthetic data.

FIELD DATA TEST

The presented inversion procedure is tested on real field data from a pavement construction site in Malmoe, Sweden. The given layering at the test site is presented in Table 2. Accurate in-situ reference shear wave velocities from the embedded layers in a pavement construction are difficult to obtain. In an attempt to get the best possible reference data, measurements were taken on top of each layer during the construction of the pavement. Data from the top of the subgrade (clay till) is shown as an example in Figure 10. The best matching P-wave velocity is indicated with a dotted line in Figure 10a. At this site the clay till layer is known to be more than five meters thick and homogeneous. As seen in both Figures

10a and 10b, high frequency (100-500 Hz) surface waves are almost non-dispersive with a velocity of about 200 m/s. The best matching V_P velocity, the given thickness, and the measured bulk density of each layer is presented in Table 2. Shear wave velocities in Table 2 are estimated from measurements on top of each layer based on the non-dispersive asymptotic surface wave velocity (V_R) at wavelengths shorter than the thickness of the top layer (Nazarian et al., 1999)

$$V_S = V_R\left(1.13 - 0.16\nu\right) \tag{7}$$

Equation 7 indicates that Poisson's ratio (ν) has an insignificant influence when V_S is calculated from V_R. It is therefore possible to estimate ν from V_S and V_P by using

$$\nu = \frac{0.5\left(V_P / V_S\right)^2 - 1}{\left(V_P / V_S\right)^2 - 1} \tag{8}$$

Calculated ν values of each layer are presented in Table 2. Poisson's ratio of the second layer (base) is here only 0.11. This is in agreement with laboratory acoustic measurements on granular materials (Santamarina et al., 2001). The asphalt material is viscoelastic and this property by itself makes the seismic wave propagation become dispersive. This dipersiveness becomes significant at high temperatures or for low frequencies. Core samples of the asphalt layer were taken in the same section and tested in the laboratory. These measurements and the laboratory tests were carried out to get the best possible reference data for comparison with the results obtained from the inversion of all layers in the final pavement construction.

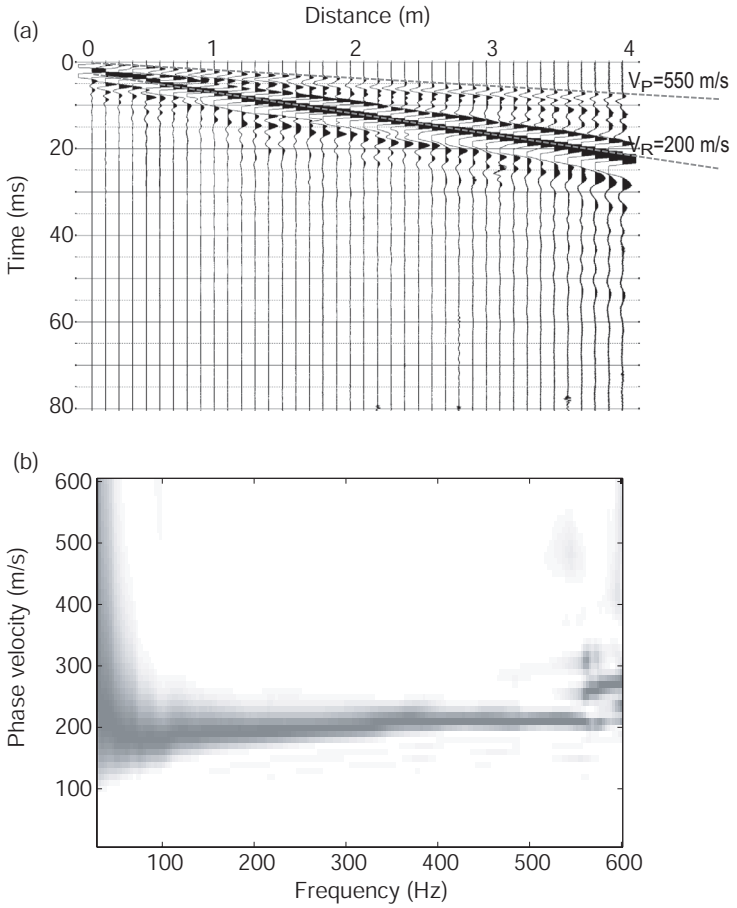

Figure 10. Recorded field data on top of the subgrade in (a) time-offset domain and (b) frequency-phase velocity domain.

TABLE 2: Pavement construction with measured properties on the top of each layer. Results from the inversion of the data collected on top of the final construction are given in parenthesis.

Layer	h (m)	ν	ρ (kg/m^3)	V_P (m/s)	V_S (m/s)
1. Asphalt	0.130 (0.129)	0.30	2400		$880f^{-0.059*}$ ($882f^{-0.070}$)
2. Base	0.300 (0.308)	0.11	2300	540 (560)	350 (371)
3. Stab. subgr.	0.200 (0.203)	0.20	2100	520 (600)	320 (368)
4. Subgrade	>5.000	0.41	2100	550 (492)	213 (192)

* **Obtained from laboratory test on core samples.**

Field data were acquired with only one accelerometer (receiver) and a small hammer (source) in the manner previously described (Ryden et al., 2001; 2004) with offsets changing from 0.50 m to 5.00 m in 0.05 m increments, using the equipment described in Ryden et al. (2002). A 40 ms record length and 200 kHz sampling rate were used. The initial 0.50 m offset was used to reduce the near field effect at low frequencies. At each offset, recordings from 4 impacts delivered with a source-coupling device (a spike) were vertically stacked to result in one time series (one trace). The asphalt temperature was 13°C. The compiled multichannel record is presented in Figure 11 and the corresponding phase velocity spectrum is shown in Figure 12a. Three distinct mode branches are observed in the frequency range from 50 to 600 Hz.

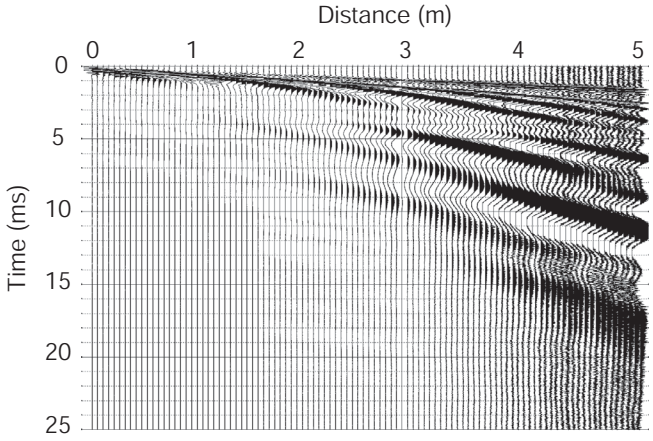

Figure 11. Recorded field data on top of the final pavement construction.

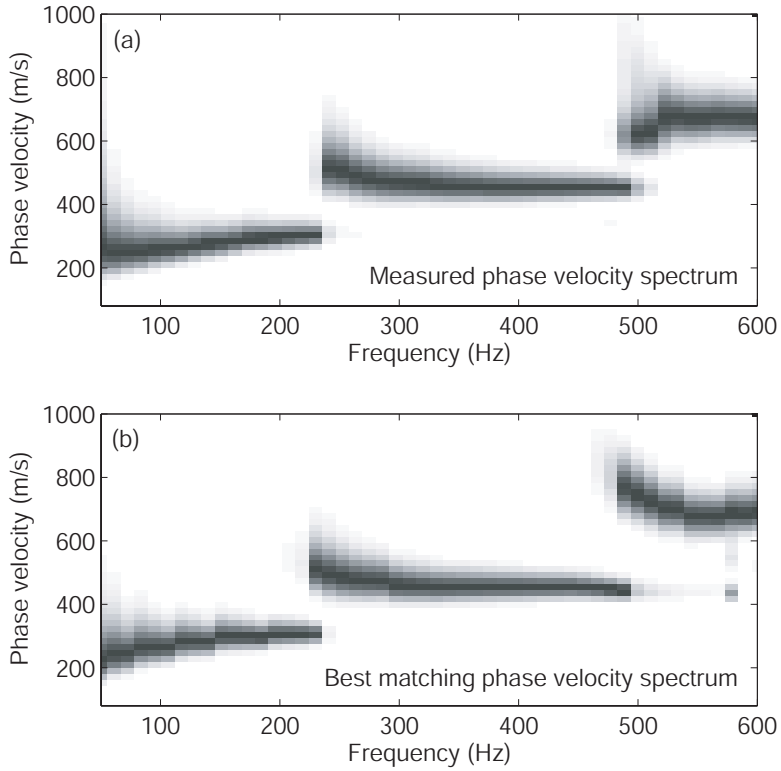

Figure 12. (a) Transformed phase velocity spectrum from the recorded data in Fig. 10. (b) Corresponding best matching phase velocity spectrum from the inversion.

To account for the viscoelastic properties, the shear wave velocity of the asphalt layer was expressed during the inversion as a power function of frequency

$$V_S(f) = b_1 f^{b_2} \tag{9}$$

where b_1 and b_2 are coefficients to be determined through the inversion procedure. The dynamic E-modulus of the asphalt layer is usually represented by a "mastercurve" showing the dynamic modulus as a function of frequency at a reference temperature. Figure 13a shows the laboratory mastercurve at 13°C obtained from the frequency sweep test (Nilsson, 2003) made on core samples from the asphalt layer. Within the inversion frequency range (50 to 600 Hz) the dynamic modulus frequency relation is known to be close to linear in a log-log scale (Aouad, 1993), which motivates the chosen format of equation 9. The subsequent inversion then tried to solve for the viscoelastic constants (b_1 and b_2), rather than for a constant shear wave velocity, by assuming a constant Poisson's ratio within this frequency range. The E-modulus is related to V_S through

$$E = 2(\rho V_S^2)(1+\nu) \tag{10}$$

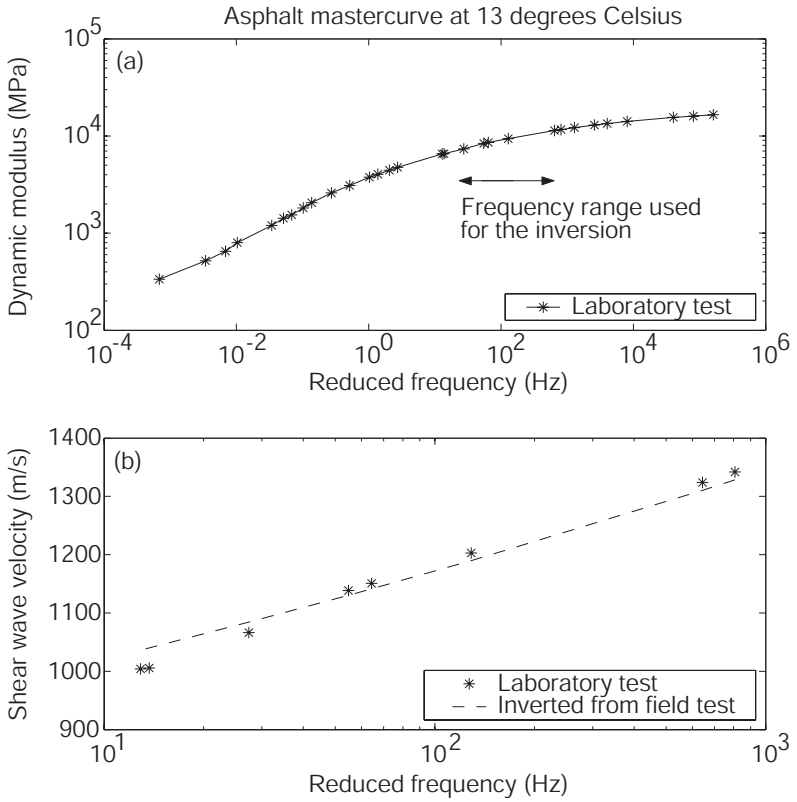

Figure 13. (a) Laboratory mastercurve showing the dynamic modulus of the asphalt layer as a function of frequency. (b) Corresponding laboratory and inverted shear wave velocity within the frequency range used for the inversion.

The inversion algorithm was set up with the same settings used for the synthetic data example. The best matching theoretical phase velocity spectrum from the inversion is plotted in Figure 12b. The corresponding layer model is presented in Table 2 where the parameters from the inversion are given in parentheses. Values of inversion parameters and their corresponding mismatch *(M)* values from all iterations are plotted in Figure 14 within the predefined search range of each parameter (x-axis). The inversion scheme was run for 800 transitions using a total of 9106 trial layer models. The total computational time was 3 hours on a 2 GHz PC.

Inverted parameters (Table 2), corresponding to an *M* value of 9.1%, agree quite well with the reference data also given in Table 2. Layer thicknesses are well resolved within 1% error of the given thicknesses. The shear wave velocity of the asphalt layer also agrees well with the results obtained from the laboratory test (Figure 13b). This indicates that the design E-modulus at 30 Hz can be obtained directly from the inverted shear wave velocity of the asphalt layer. The shear wave velocities of the base (371 m/s) and the stabilized subgrade (368 m/s) are slightly higher than the reference values. This may be explained from the higher confining pressure and the time difference (1-2 months) between the measurements on each layer and the final measurements on the top asphalt layer. Granular materials like the base layer and stabilized soils are affected by ageing and a higher shear wave velocity should therefore be expected (Santamarina et al., 2001). The inverted shear wave velocity of the unstabilized subgrade (192 m/s) is also quite close to the reference value of 213 m/s from Table 2.

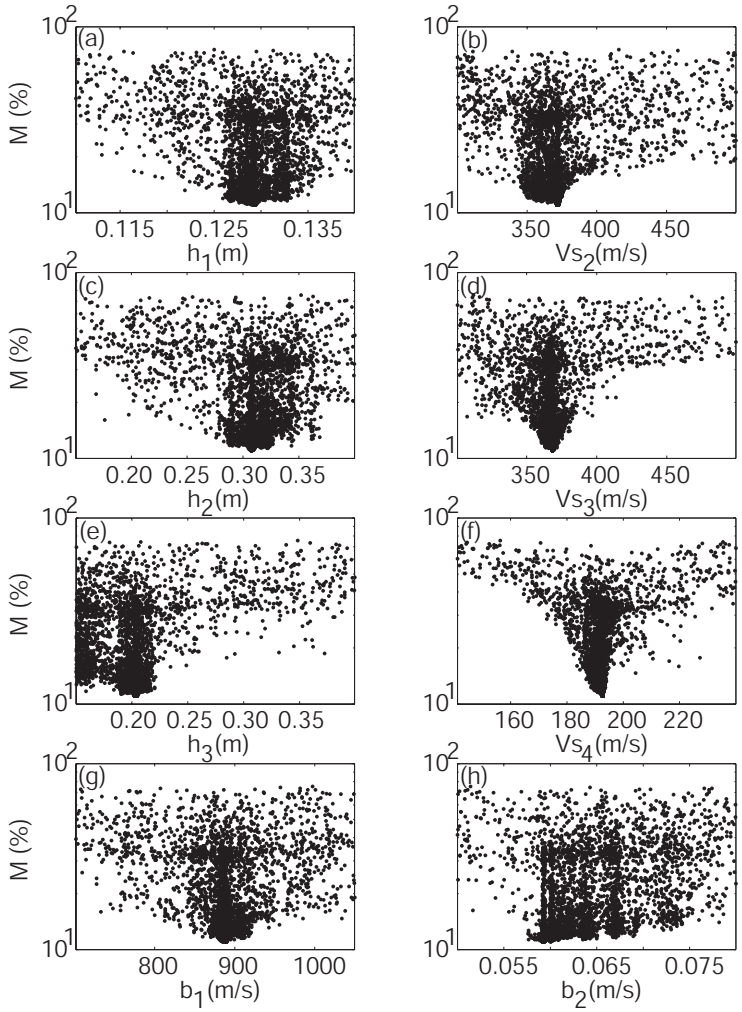

Figure 14. Mismatch (*M*) as a function of parameter value from all iterations used in the FSA inversion of the field data example. The spread of the dots indicates the multidimensional sensitivity for each inverted parameter.

DISCUSSION

The proposed method has been focused on the inversion utilizing the phase velocity spectrum only, with the objective function solely defined by the characteristics of the phase velocity spectrum. However, this function can be completely user defined and optimized for each specific application. For example, higher frequencies and first arrival velocities can be included in the objective function for surface wave testing of pavements. This will introduce some additional constraints on the properties of the top layer. Other future developments may include some quantification of the uncertainty of the inverted parameter values.

While this study has been focused on the inversion of pavement layer properties the same procedure can be used for the inversion of surface wave data from any type of layered half-space or plate. Other applications may include inversion of surface wave data from soil sites or in the field of ultrasonic testing of composite plates and coatings.

CONCLUSIONS

One of the main benefits from the presented approach is that the raw field data can be automatically processed and inverted without any subjective user input, and by properly accounting for the interference of different modes and types of waves. This is a significant advantage when surface wave data involves multiple modes of propagation. The main disadvantage at this point is the long computational time required for the inversion process.

The viscoelastic properties of the asphalt layer have been included in the forward model, resulting in an inverted "mastercurve", that shows the asphalt stiffness as a function of frequency. With this procedure the asphalt design modulus at 30 Hz can be estimated directly from surface wave tests without any further reduction factor.

It seems that the resolution of the base layer (which has been a challenging task with traditional methods) can be improved with the presented method. This improvement in resolution is obtained through the utilization of the full phase velocity spectrum in the inversion method. In addition, compared to the conventional approach where only one apparent dispersion curve is used, this utilization is believed to reduce the amount of non-uniqueness.

ACKNOWLEDGEMENTS

We would like to give our sincere thanks to Peab Sverige AB, VINNOVA, and the Swedish National Road Administration for financing this project. We also thank Professor Nenad Gucunski at Rutgers University for his assistance with the stiffness matrix method. The help from Mary Brohammer with the preparation of this manuscript is also greatly appreciated.

REFERENCES

Abdallah, I., Yuan, D., and Nazarian, S., 2003, Validation of software developed for determining design modulus from seismic testing: Research Report 1780-5, Center for Highway Materials Research, the University of Texas at El Paso, TX.

Akhlaghi, B. T., and Cogill, W. H., 1994, Application of the free plate analogy to a single-layered pavement system: INSIGHT, **36**, 514-518.

Andresen, B., and Gordon, J. M., 1994, Constant thermodynamic speed for minimizing entropy production in thermodynamic processes and simulated annealing: *Physical Review E,* **50**, 4346-4351.

Aouad, M. F., 1993, Evaluation of Flexible Pavements and Subgrades Using the Spectral-Analysis-of-Surface-Waves (SASW) Method: PhD thesis, Univ. of Texas at Austin, Texas.

Basu, A., and Frazer, L. N., 1990, Rapid determination of the critical temperature in simulated annealing inversion: *Science* **249**, 1409-1412.

Beaty, K. S., Schmitt, D. R., and Sacchi, M., 2002, Simulated annealing inversion of multimode Rayleigh wave dispersion curves for geological structure: *Geophysical Journal International*, **151**, 622-631.

Dosso, S. E., Wilmut, M. J., and Lapinski, A-L. S., 2001, An adaptive-hybrid algorithm for geoacoustic inversion: *IEEE Journal of Oceanic Engineering*, **26**, 324-336.

Ekdahl, U., Bengtsson, P. E., and Ryden, N., 2004, A new framework for analytical pavement design based on systematic control during construction work: Proceedings of the 14th Nordic Geotechnical Meeting (NGM 2004), Ystad, Sweden, May 19-21.

Forbriger, T., 2003, Inversion of shallow-seismic wavefields part 2: Inferring subsurface properties from wavefield transforms: *Geophysical Journal International*, **153**, 719-734.

Foti, S., Sambuelli, L., Socco, V. L., and Strobbia, C., 2003, Experiments of joint acquisition of seismic refraction and surface wave data: *Near Surface Geophysics*, **1**, 119-129.

Ganji, V., Gucunski, N., and Nazarian, S., 1998, Automated inversion procedure for spectral analysis of surface waves: *Journal of Geotechnical and Geoenvironmental Engineering*, ASCE, **124**, 757-770.

Gucunski, N., and Maher, A., 2000, Evaluation of the dynamic response of pavements and other layered systems using the stiffness matrix approach: Proceedings 79th Annual Meeting, Transportation Research Board, Washington D.C. Paper No. 00-0134.

Gucunski, N., Abdallah, I. N., and Nazarian, S., 2000, ANN backcalculation of pavement profiles from the SASW test: In Geotechnical Special Publication (ASCE) No. 98, Pavement subgrade unbound materials, and nondestructive testing, 31-50.

Gucunski, N., and Woods, R. D., 1992, Numerical simulation of the SASW test: *Soil Dynamics and Earthquake Engineering*, **11**, 213-227.

Haegeman, W., 2002, In situ assessment of stiffness of a road sand embankment: Proceedings of the BCRA 2002, Lissabon, Portugal. 629-635.

Haskell, N. A., 1953, The dispersion of surface waves on multilayered media: *Bulletin of the Seismological Society of America*, **43**, 17-34.

Heisey, J. S., Stokoe, K. H., and Meyer, A. H., 1982, Moduli of pavement systems from spectral analysis of surface waves: *Transportation Research Record*, **852**, 22-31.

Hoffmann, K. H., and Salamon, P., 1990, The optimal simulated annealing schedule for a simple model: *Journal of Physics A: Mathematical and General*, **23**, 3511-3523.

Jones, R., 1962, Surface wave technique for measuring the elastic properties and thickness of roads: Theoretical development: *British Journal of Applied Physics*, **13**, 21-29.

Kausel, E., and Roesset, J. M., 1981, Stiffness matrices for layered soils: *Bulletin of the Seismological Society of America*, **71**, 1743-1761.

Laarhoven, P. J. M., and Aarts, E. H. L., 1987, Simulated Annealing: Theory and Applications: Kluwer Academic Publishers. The Netherlands.

Martínez, M. D., Lana, X., Olarte, J., Badal, J., and Canas, J. A., 2000, Inversion of Rayleigh wave phase and group velocities by simulating annealing: *Physics of the Earth and Planetary Interiors*, **122**, 3-17.

Menke, W. 1989, Geophysical data analysis: discrete inverse theory: Revised edition, Academic Press. New York.

Moro, G. D., Pipan, M., Forte, E., Finetti, I., 2003, Determination of Rayleigh wave dispersion curves for near surface applications in unconsolidated sediments: Expanded Abstract, Society of Exploration Geophysicists. 1247-1250.

Mosegaard, K., and Sambridge, M., 2002, Monte Carlo analysis of inverse problems: *Inverse Problems* **18**, R29-R54.

Nazarian, S., 1984, In situ determination of soil deposits and pavement systems by spectral analysis of surface waves method: PhD thesis, Univ. of Texas at Austin, Texas.

Nilsson, R., 2003, Fatigue of asphalt mixes – theory of viscoelasticity and continuum damage mechanics applied to uniaxial fatigue data from laboratory tests: PhD thesis, Univ. of Lund, Sweden.

Park, C. B., Miller, R. D., and Xia, J., 2001, Offset and resolution of dispersion curve in multichannel analysis of surface waves (MASW): Proceedings of the Symposium on the Application of Geophysics to Engineering and Environmental Problems (SAGEEP 2001), Denver, Colorado, March 4-7.

Park, C. B., Miller, R. D., and Xia, J., 1999, Multichannel analysis of surface waves: *Geophysics*, **64**, 800-808.

Park, C. B., Miller, R. D., and Xia, J., 1998, Imaging dispersion curves of surface waves on multi-channel records: Technical Program with biographies, SEG, 68th Annual Meeting, New Orleans, Louisiana, 1377-1380.

Rambod, H., and Gucunski, N., 2003, Inversion of SASW dispersion curve using numerical simulation: Proceedings of the Symposium on the Application of Geophysics to Engineering and Environmental Problems (SAGEEP 2003), San Antonio, Texas, SUR-01.

Roësset, J. M., Chang, D. W., Stokoe II, K. H., and Auoad, M., 1990, Modulus and thickness of the pavement surface layer from SASW tests: *Transportation Research Record*, **1260**, 53-63.

Ryden, N., and Lowe M. J. S., 2004, Guided Wave Propagation in Three-layer Pavement Structures: in review.

Ryden, N., and Park, C. B., 2004, Surface waves in inversely dispersive media: in review.

Ryden, N., Park, C. B., Ulriksen, P. and Miller, R. D., 2004, Multimodal approach to seismic pavement testing: *Journal of Geotechnical and Geoenvironmental Engineering*, ASCE, **130**, 636-645.

Ryden, N., Ulriksen, P., Park, C. B., and Miller, R. D., 2002, Portable seismic acquisition system (PSAS) for pavement MASW: Proceedings of the Symposium on the Application of Geophysics to Engineering and Environmental Problems (SAGEEP 2002), Las Vegas, NV, February 10-14, 13IDA7.

Ryden, N., Ulriksen, P., Park, C. B., Miller, R. D., Xia, J., and Ivanov, J., 2001, High frequency MASW for non-destructive testing of pavements-accelerometer approach: Proceedings of the Symposium on the Application of Geophysics to Engineering and Environmental Problems (SAGEEP 2001), Denver, Colorado, RBA-5.

Santamarina, J. C., Klein, K. A., and Fam, M. A., 2001, Soils and waves, John Wiley & Sons.

Sen, M., and Stoffa, P. L., 1995, Global Optimization Methods in Geophysical Inversion: Elsevier.

Socco, L. V., Strobbia, C., and Foti, S., 2002, Multimodal interpretation of surface wave data: Proceedings of the 8th European Meeting of Environmental and Engineering Geophysics (EEGS-ES 2002), Environmental and Engineering Geophysical Society European Section, Annual Meeting, Aveiro, Portugal, 21-25.

Stokoe II, K. H., Wright, S. G., Bay, J. A., and Roësset, J. M., 1994, Characterization of geotechnical sites by SASW method: in Geophysical characterization of sites. ISSMFE Technical Committee #10, edited by R.D. Woods, Oxford Publishers, New Delhi.

Szu, H., and Hartley, R., 1987, Fast simulated annealing: *Physics Letters A*, **122**, 157-162.

Thomson, W. T., 1950, Transmission of elastic waves through a stratified solid medium: *Journal of Applied Physics*, **21**, 89-93.

Van der Poel, C., 1951, Dynamic testing of road constructions: *Journal of Applied Chemistry*, **1**, 281-290.

Vidale, R. F., 1964, The dispersion of stress waves in layered media overlaying a half space of lesser acoustic rigidity: PhD thesis, Univ. of Wisconsin.

Wu, H., Wang, S., Abdallah, I., and Nazarian, S., 2002, A rapid approach to interpretation of SASW results: Proceedings of the BCRA 2002, Lissabon, Portugal. 761-770.

Xia, J., Miller, R. D., and Park, C. B., 1999, Estimation of near-surface shear-wave velocity by inversion of Rayleigh wave: *Geophysics*, **64**, 691.

Zhang, S. X., and Chan, L. S., 2003, Possible effects of misidentified mode number on Rayleigh wave inversion: *Journal of Applied Geophysics*, **53**, 17-29.

Zywicki, D. J., 1999, Advanced signal processing methods applied to engineering analysis of seismic surface waves: Ph.D. thesis. Georgia Institute of Technology.